Innovation of Chemistry & Materials for Sustainability

https://insuf.org/journal/icms

Open-access, Peer-reviewed

Photo Credit: Dr. Madhumita Mandal

Editor-in-Chief
Prof. Dr. Susanta Banerjee

02

About the Journal

The Journal *Innovation of Chemistry & Materials for Sustainability* is a comprehensive publication that focuses on the latest research and developments in the field of sustainable chemistry and materials science. This journal provides a platform for scientists, researchers, and industry professionals to share their findings and innovations that contribute to a more sustainable future. Covering a wide range of topics such as green chemistry, renewable materials, and eco-friendly processes, this journal is a valuable resource for those working towards a more sustainable world.

Aims & Scope

Introducing the scope of the new journal, Innovation of Chemistry & Materials for Sustainability (ICMS) will cover all topics related to chemistry and materials in the widest possible sense, but there should be a sustainable chemistry aspect for successful submissions. ICMS publishes original papers, short communications and perspectives, and review articles in all areas of chemistry and materials for a safer and cleaner future. Interdisciplinary contributions are encouraged, encompassing a wide range of topics including, but not limited to, the following:

- Catalysis (homogeneous, heterogeneous and bio-catalysis)
- Green chemistry for sustainable processing routes (microwaves, ultrasounds, photochemistry, electrochemistry, flow chemistry, etc.)
- Lipid valorization – Biorefining
- Polymers: Synthetic polymers and elastomers, polymer membranes/ composites/ fibres, responsive/ functional polymers, nano structured polymers, biocompatible and biodegradable polymers
- Innovation of chemistry and materials for sustainable agriculture & pharmaceutical practices
- Bio-based chemicals, fuels, materials
- Renewable energy sources (wind, solar) and storage,
- CO_2 capture, utilization and carbon neutrality
- Chemistry and materials for circular economy
- Nano-materials for energy generation, water treatment, and environmental remediation.

Journal Particulars

Innovation of Chemistry & Materials for Sustainability

Editors & Editorial Board

Publication Ethics

The **Innovation of Chemistry & Materials for Sustainability (ICMS)** is dedicated to maintaining the utmost integrity in publication ethics. Submissions to the journal must consist of original contributions. The submitting author bears the responsibility of securing agreement from all co-authors and obtaining necessary consent from sponsors before submitting an article. Authors are accountable for the content of their articles, with ultimate responsibility resting on them rather than on the Editors or the Publisher.

Similarly, the **ICMS** pledges to conduct thorough and unbiased double-blind peer reviews of submitted works for publication, ensuring fairness and objectivity. Our intention is to avoid any conflicts of interest between our editorial and review staff and the materials under review.

Responsibilities of Editors

Publication decision: The responsibility of determining which articles submitted to the journal should be published lies with the editor. These decisions should always be influenced by the validation and importance of the work to researchers and readers. The editor may take direction from the journal's advisory board policies and must adhere to legal obligations concerning issues like defamation, copyright violation, and plagiarism.

Fair play: An editor ought to assess manuscripts based on their intellectual merit, free from consideration of the authors' race, gender, sexual orientation, religious beliefs, ethnic circumstantial, citizenship, or political convictions.

Confidentiality: Confidentiality must be maintained by the editor and all editorial/reviewer personnel, refraining from exposing any details regarding a submitted manuscript to individuals other than the corresponding author, reviewers, advisory board members, and the publisher, as deemed necessary.

Disclosure and Conflict of Interest: Information or insights gained through peer review are measured advantaged and must be preserved confidentially, without manipulation for personal gain. Editors are assigned to guarantee that all contributors disclose any appropriate challenging interests, and corrections should be issued if such conflicts come to light post-publication. If necessary, further measures such as retractions or expressions of concern may be implemented.

Participation and Collaboration in Investigations: An editor is anticipated to promptly address ethical complaints related to a submitted manuscript or published paper, in collaboration with the publisher. These actions typically comprise reaching out to the author to measure the complaint, considering the claims made, and potentially extending communication to relevant institutions and research entities. If the complaint is validated, corrective actions such as issuing a correction, retraction, expression of concern, or other appropriate measures may be taken. It's indispensable to thoroughly examine all reported instances of unethical publishing behavior, regardless of when they come to light, even if it's years after publication.

Responsibilities of Reviewers

Participation in Editorial Decision: Reviewers should decline invitations to review manuscripts if they have an evident conflict of interest and disclose the nature of the conflict. Conflict of interest refers to circumstances that could potentially lead to an unfair evaluation of the manuscript. Editors may intentionally select reviewers with particular perspectives to ensure a balanced assessment. Reviewers with suspicions regarding conflicts of interest are encouraged to seek clarification from the Editor.

Confidentiality: Confidentiality must be endorsed by reviewers regarding the manuscripts they assess. It is improper to utilize data from these manuscripts prior to their publication. Equally improper is the sharing of this data with colleagues or reproducing the manuscript for any reason. If reviewers desire to utilize information from a manuscript accepted for publication, they should request the Editor to communicate with the author(s) for permission.

Objectivity Criteria: Reviewers who accept the task of evaluating a manuscript are expected to obey to the designated timeframe for completing their reviews. In the event that meeting this deadline becomes unfeasible, reviewers are encouraged to promptly notify the editorial office. They should request guidance regarding whether to decline the review or appeal an extension for a specified duration.

Acknowledgement of Source: Reviewers who are unable to complete a manuscript review within the designated timeframe should respectfully decline the request. It is mandatory upon reviewers to approach both the author and the manuscript with professionalism and courtesy. In cases where reviewers protect any bias towards the researchers or the research, they should withdraw from participating in the review process. Similarly, if there exists a conflict of interest with the research or its sponsors, reviewers are responsible for disclosing this information to the editors.

Responsibilities of Authors

Reporting guidelines: Authors reporting original research must provide a precise description of their methodology and impartially discuss its implications. Accurate representation of essential data is imperative, with papers containing ample detail and references for replication. Deliberate misrepresentation is unethical and intolerable.

Data availability and retention: Authors may be requested to submit raw data for editorial review and should be willing to grant public access where possible. Additionally, authors should commit to retaining such data for a reasonable period post-publication.

Ensuring Originality and Avoiding Plagiarism: Authors must assurance the creation of entirely unique content. Any utilization of others' work or words should be properly recognized through citation or quotation. Plagiarism displays in various ways, such as bestowing someone else's paper as one's own, reproducing significant portions of another's work without acknowledgment, or appropriating research findings from others. Engaging in any form of plagiarism is unethical in publishing and is not accepted.

Authors may be mandatory to confirm that their manuscript has not been concurrently submitted to another journal for review. Such practices waste the time of editors and peer reviewers and can potentially harm the integrity of the research by appearing in multiple publications simultaneously. The submitting author embraces the responsibility of ensuring that all co-authors and sponsors have agreed to the submission before sending the paper.

Acknowledgement of Sources: It is crucial to appropriately acknowledge the contributions of others. Authors are grateful to reference influential publications that have influenced their work. Confidential information obtained through private exchanges, whether through conversation, correspondence, or discussions with third parties, should not be utilized or disclosed without categorical written consent from the source. Similarly, information acquired during the provision of confidential services, such as manuscript reviewing or grant evaluation, should not be hired without obtaining explicit written permission from the relevant author involved in these services.

Authorship of the Paper: Authorship ought to be reserved for individuals who have substantially contributed to the conception, design, implementation, or interpretation of the study being described. Those who have made striking contributions should be credited as co-authors. In cases where others have been involved in significant aspects of the research project, they should be acknowledged or listed as contributors. The corresponding author is responsible for ensuring that all relevant co-authors are included in the article and that no irrelevant/guest co-authors are included. Additionally, the corresponding author must ensure that all co-authors have reviewed and approved the final version of the paper and have consented to its submission for publication.

Hazards and Human or Animal Integrity: If the work involves the use of chemicals, procedures, or equipment with inherent unusual hazards, the author must explicitly describe these in the manuscript. Authors conducting research involving experimental animals and human subjects should obtain approval from the relevant Ethical committee in agreement with the "Principles of Laboratory Animal Care." The Method section of the manuscript should include a statement confirming approval for the investigation and the acquisition of informed consent.

Disclosure and Conflicts of Interest: Authors must divulge any financial or significant conflicts of interest in their manuscript that could potentially disturb the findings or understanding of their work. Additionally, they should provide transparency regarding all sources of financial assistance for the project.

Fundamental errors in published works: If an author identifies a remarkable error or inaccuracy in their published work, they are forced to promptly notify the journal editor or publisher and collaborate with them to retract or rectify the paper. In the event that the editor or publisher becomes aware through a third party that a published work contains a significant error, it is the author's responsibility to swiftly retract or amend the paper, or present evidence to the editor affirming the accuracy of the original paper.

Responsibilities of the Publisher

We are dedicated to confirming that editorial decisions remain uninfluenced by advertising or any other commercial revenue.

Plagiarism Policy

The Innovation of Chemistry & Materials for Sustainability (ICMS) serves as a platform for both national and international researchers operating within similar fields. In the current digital landscape, plagiarism has transitioned into an online phenomenon. It has been observed that numerous individuals and researchers are illicitly appropriating the work of others and presenting it as their own in various journals. As a response, the ICMS is dedicated to publishing only original, high-quality research and vehemently discourages all forms of plagiarism.

Any individual or researcher found engaging in plagiarism risks being blacklisted and permanently barred from publishing their work in our journals. Additionally, the respective head of departments and the affiliated university of the plagiarist will be promptly notified, emphasizing the necessity for serious action to be taken against such misconduct.

Instructions for Authors

Manuscript submission

Authors are requested to review the submission instructions before sending their articles. It ensures a smooth review process. The journal template is readily accessible on our website. Authors should adhere to the formatting guidelines specified in the template. For convenience, we encourage authors to submit their articles through our online platform. This facilitates faster processing and tracking of submissions. Should you encounter any difficulties or have inquiries, please don't hesitate to reach out to us via email support-icms@insuf.org; me-icms@insuf.org

We are committed to assisting you throughout the submission process. The approval of a manuscript is subject to meeting the requirements of the *Innovation of Chemistry and Materials for Sustainability* (ICMS).

Authors are requested to follow the instructions before submitting the article. The template of the journal is available in the website. Authors are advised to submit the article online. Please contact us (support-icms@insuf.org; me-icms@insuf.org) if you find any complication.

The author details instruction is mentioned bellow.

Manuscript Preparation
Length and Word Count
- For a full–length article should be within 4000 words (10-12 pages, including Figures, References, Footnotes, Caption, Tables etc.)
- Short communication should be within 2500 words (4-6 pages), excluding references, footnotes, caption, tables, etc.
- The review article should be within 12000 words, including references, footnotes, caption, tables.
- Conference proceedings should be within 3000 words (6-8 pages)
- Book reviews should be within 2500 words (4-6 pages)
- Guest Editorials (by invitation only) should be within 1200 words (maximum)

Please contact us (support-icms@insuf.org) if you need further clarification/ guidance/ support.

Language and Style

All manuscripts must adhere to high standards of English proficiency. Papers with substandard language will be returned automatically for revision prior to review. Authors are encouraged to use either British or U.S. English consistently throughout their work. ICMS endeavors to adhere to the scientific terminology outlined by IUPAC guidelines and utilizes SI units wherever applicable. Before submitting, it falls on the author to guarantee that the scientific content is both accurate and comprehensible to the referees. Please contact us (support-icms@insuf.org) if any doubt.

The format should be following manner:
Title of article: Open Sans (align to left), 16 font size and bold;
Author's name: Open Sans (Center text), 11 font size and normal;
Affiliation/s: Open Sans (Center text), 8 font size and normal;
Abstract title (Open Sans; align to left; 11 font size bold): **Abstract text** in Open Sans (Justify text), 8 font size and normal; Single paragraph within 200 words
Keywords title (Open Sans; align to left; 11 font size bold): Keywords text in Open Sans (align to left), 8 font size and italic; 3-5 keywords.
Introduction title (Open Sans; align to left; 11 font size bold; 1st order heading): Main text in Open Sans (Justify text), 8.5 font size and normal;
Results and Discussion title section (Open Sans; align to left; 11 font size bold; 1st order heading): Main text in Open Sans (Justify text), 8.5 font size and normal;
Results and Discussion title sub section (Open Sans; align to left; 8.5 font size bold; 2nd order heading): Main text in Open Sans (Justify text), 8.5 font size and normal;
Conclusions title section (Open Sans; align to left; 11 font size bold; 1st order heading): Main text in Open Sans (Justify text), 8.5 font size and normal;

Experimental title section (Open Sans; align to left; 11 font size bold; 1st order heading): Main text in Open Sans (Justify text), 8.5 font size and normal;

Experimental title sub section (Open Sans; align to left; 8.5 font size bold; 2nd order heading): Main text in Open Sans (Justify text), 8.5 font size and normal;

Supporting Information title section (Open Sans; align to left; 11 font size bold; 1st order heading): Main text in Open Sans (Justify text), 8.5 font size and normal;

Author Contribution Declaration title section (Open Sans; align to left; 11 font size bold; 1st order heading): Main text in Open Sans (Justify text), 8.5 font size and normal;

Data Availability Declaration title section (Open Sans; align to left; 11 font size bold; 1st order heading): Main text in Open Sans (Justify text), 8.5 font size and normal;

Acknowledgements title section (Open Sans; align to left; 11 font size bold; 1st order heading): Main text in Open Sans (Justify text), 8.5 font size and normal;

References title section (Open Sans; align to left; 11 font size bold; 1st order heading): Main text in Open Sans (Justify text), 7 font size and normal;

Cover Letter

ICMS suggests that authors provide a cover letter along with their submitted manuscripts, as it aids editors or referees in comprehending the significance of the work. Please suggest **four potential referees** who are familiar with your work.

Please adhere to the following order of presentation:

Author name and affiliation: The author(s) should comprise the full first and last names. In cases where there are multiple authors, it should be clearly stated who will handle correspondence regarding the paper, designated as the corresponding author, and denoted with a single asterisk (*) in superscript. Additional authors and their corresponding addresses should be indicated with superscripts a, b, c, etc. The corresponding author's contact information, including email address, full postal address, telephone number, and fax number, should be provided.
Author's Name:
Open Sans (Centered text), 11 font size, normal
Affiliation/s:
Open Sans (Centered text), 8 font size, normal

Abstract: The abstract must succinctly encapsulate the article by outlining the addressed questions and highlighting the study's key findings. It should not function as an introduction or include references. This section should comprise a single paragraph, approximately 200 words in length, providing a pertinent overview of the work.
Abstract title:
Open Sans; align to left; 11 font size bold
Abstract text:
Open Sans (Justify text), 8 font size and normal; Single paragraph within 200 words.

Keywords: Immediately following the abstract, include 3-5 concise keywords. It should be included 80 characters including spaces. These keywords aid in indexing the article for readers. Keywords like "keyword1, keyword2, keyword3," etc., are recommended.
Keywords title (Open Sans; align to left; 11 font size bold): Keywords text in Open Sans (align to left), 8 font size and italic.

Introduction: The article encompasses its scientific significance, historical context, relevance to other fields, and its objectives.
Introduction title (Open Sans; align to left; 11 font size bold; 1st order heading): Main text in Open Sans (Justify text), 8.5 font size and normal;

Material and Methods: The writing should contain enough detail for others to replicate the author(s)'s work.
Material and Methods title section (Open Sans; align to left; 11 font size bold; 1st order heading): Main text in Open Sans (Justify text), 8.5 font size and normal;
Material and Methods title sub section (Open Sans; align to left; 8.5 font size bold; 2nd order heading): Main text in Open Sans (Justify text), 8.5 font size and normal.

Results and Discussion: This section can either be integrated or maintained as distinct, and can also be subdivided further if necessary. Technical details should be avoided in this section.

Results and Discussion title section (Open Sans; align to left; 11 font size bold; 1st order heading): Main text in Open Sans (Justify text), 8.5 font size and normal;

Results and Discussion title sub section (Open Sans; align to left; 8.5 font size bold; 2nd order heading): Main text in Open Sans (Justify text), 8.5 font size and normal.

Conclusion: Compose the final statement for the article, encapsulating the paper's key conclusions succinctly.

Conclusions title section (Open Sans; align to left; 11 font size bold; 1st order heading): Main text in Open Sans (Justify text), 8.5 font size and normal

Acknowledgments: Recognize the individuals, grants, funds, and other contributors who significantly influence the content of this article. Funding organizations should be identified by their full names.

It's essential to adhere to research integrity by acknowledging your funding agencies and any infrastructural or personal assistance received during manuscript preparation.

References: References ought to be sequentially numbered, such as 1, 2, 3, 4, and so forth. In the text, references must be indicated by consecutive superscript numbers, like (e.g., [1] or [1, 2, 3]). References title section (Open Sans; align to left; 11 font size bold; 1st order heading): Main text in Open Sans (Justify text), 7 font size and normal. The reference list should be arranged in the order of their initial mention in the text and formatted accordingly.

(1) For article: (a) F. (Firstname initial) M. (Middlename initial) Surname (Lastname), F. (Firstname initial) M. (Middlename initial) Surname (Lastname), F. (Firstname initial) M. (Middlename initial) Surname (Lastname). Title of the article. *Journal Name (Abbreviated).* **Year,** *Volume*, first page. Mention DOI link here (b) F. (Firstname initial) M. (Middlename initial) Surname (Lastname), F. (Firstname initial) M. (Middlename initial) Surname (Lastname), F. (Firstname initial) M. (Middlename initial) Surname (Lastname). Title of the article. *Journal Name (Abbreviated).* **Year,** *Volume,* first page. Mention DOI link here.
(2) For book: (a) Editors name in *Title of book*, Vol. X (Eds.: S. K. Sinha, A. B. Madan, S. K. Ghosh, S. Shukla), Cambridge, **Year**, *Ch.X*, page range. Mention DOI link here. (b) A. Engel, *Title of book*, Publishers, Oxford, **Year**, *Ch.X*, pp. 215-310. Mention DOI link here
(3) (a) F. (Firstname initial) M. (Middlename initial) Surname (Lastname), F. (Firstname initial) M. (Middlename initial) Surname (Lastname), F. (Firstname initial) M. (Middlename initial) Surname (Lastname). Title of the article. *arXiv preprint (Abbreviated)* **Year,** Mention DOI link here
(4) For Crystal Information: Deposition numbers (CCDC numbers) xxxxxx (for **X**), yyyyyy (for **Y**), and zzzzzz (for **Z**) contain the supplementary crystallographic data for this paper.

Tables and Figures

Tables and figures need to be integrated within the text. Each table should have a concise descriptive title positioned above it, accompanied by a clear legend, and any footnotes should be appropriately marked below. Refrain from using vertical lines. Tables and figures should be sequentially numbered as they appear in the text, labeled as Table 1, Table 2, etc., for tables, and Fig. 1, Fig. 2, etc., for figures. Figures must be fully labeled, considering potential size adjustments. Captions should be double-spaced.

If there are images, tables, photographs, diagrams, graphs, etc., in the article that have been published elsewhere (such as in books, journals, conference presentations, etc.), the author is accountable for acquiring permission from the original author, publisher, or copyright holder to reproduce the material.

Equations

Each equation should be displayed on a separate line, with appropriate punctuation placed before and after it. All equations must be sequentially numbered, with the number of the equation placed near the right-hand margin. Avoid using bars above or below letters, and refrain from using subscripts on subscripts. Sufficient space must be allocated for marking superior and inferior letters or numbers. Overcrowded equations can result in compositional errors. When referencing equations in the text, use the following format: "Equation (5) follows from substituting Eqs. (2) and (3) into Eq. (4)."

Nomenclature

The nomenclature ought to adhere to present American standards. Whenever feasible, writers should employ systematic designations that align with those utilized by the Chemical Abstracts Service or IUPAC.

External Review

The process of external review commences when the editor dispatches the manuscript for evaluation. Upon receiving the reports, the editor deliberates based on the recommendations and the manuscript's revision history, then notifies the author of the decision via a decision letter.

Decisions for initial submissions are as follows:

- Manuscripts with negative or inadequately supportive reviews will be declined.
- In all other cases, including mixed reviews, the manuscript will be returned for revision with guidance for resubmission.
- Authors are required to accompany resubmissions with a cover letter summarizing revisions and addressing the editor's and/or reviewers' concerns. Resubmitted manuscripts typically undergo re-evaluation by previous reviewers and occasionally new ones.

Revised Manuscript

Authors are expected to submit a revised manuscript within 10 days for minor changes and within 3 weeks for major revisions. Failure to meet these deadlines will result in the manuscript being considered withdrawn, and any subsequent submissions will be treated as new contributions. Authors may request additional time from the editor if necessary.

After acceptance:

Copyright Policy

Innovation of Chemistry & Materials for Sustainability (ICMS) typically does not accept articles that have previously appeared in a similar form, regardless of language. Please confirm that your submission is not under consideration for publication elsewhere. Authors must be willing to transfer copyright to **ICMS** and **Insuf Publications (OPC) Pvt. Ltd**, and all authors must agree to submit the paper to ICMS. If the article includes previously published images, tables, photographs, diagrams, or graphs, authors are responsible for obtaining permission from the original copyright holders.

To share your article after it has been published in ICMS, please refer to our Open Access policy.

Copyright transfer: Authors will be requested to assign copyright of the article to the publisher, guaranteeing the broadest protection and dissemination of information in accordance with copyright laws.

Proof reading: The corresponding author will be provided with a proof and is expected to return it to the publisher within three days of receipt. Only typos errors should be corrected; any other alterations will be reviewed and amended, as late corrections cannot be accommodated. The final proof must be approved by the corresponding author(s). Failure to obtain approval may result in the withdrawal of the article from publication.

Correction and Retraction Policy:

Corrections

Corrections are issued when the accuracy of published information significantly impacts the publication record. These corrections are included in the following release under the section titled "Corrections and Addendum".

Retractions

Retractions occur when the primary conclusion of a paper is significantly compromised. Readers are advised to initially reach out to the original paper's authors and subsequently inform the journal, attaching any correspondence exchanged with the authors. The editor will seek feedback from reviewers. Retraction of the article may be warranted in instances of multiple submissions, plagiarism, or fraudulent data usage.

Impact Factor

This journal, launched in June 2024, will undergo annual evaluation of its impact factor by various indexing agencies in 2025, with routine updates provided here.

Year	Impact Factor
2025	XXXX (Available in 2026)

Policy on Ethics and Governance

The Innovation of Chemistry & Materials for Sustainability (ICMS) adheres to globally acknowledged ethical standards for scientific publishing.

Authorship

This journal invites submissions from academics and industry researchers across all fields outlined in our "Aims & Scope". The corresponding author is required to list all co-authors and contributors, with the agreement of each author to be named and to submit the article to this journal.

To receive authorship credit, one must satisfy three fundamental criteria:

- Significant involvement in formulating the study's conception and design, gathering and analyzing data, and interpreting findings
- Drafting or refining the article to ensure intellectual coherence
- Providing scientific endorsement for the final iteration

People engaged in a research project who don't meet the journal's authorship requirements can be acknowledged in the Acknowledgements section. This may include those who offered advice, provided research facilities, oversaw the department, or secured financial support.

The author's affiliation must accurately reflect their status at the time of completing the work. For instance, if an author was affiliated with a different company, university, or institution when the work was done, that should be indicated as their affiliation. If an author's affiliation has since changed, their current affiliation can be noted as " Current address...".

All eligible authors must be included on the list, with no restriction on the number of authors per paper. The order of authors is not specified by us.

Authors seeking publication in this journal must possess appropriate qualifications and be prepared to furnish evidence upon request. This may include one or more of the following:

- Proof of present or previous association with an institution (such as a university, research institute, or company).
- Membership in an acknowledged national or international scientific organization.
- Confirmation of a documented publication history in respected scientific journals.
- The corresponding author must possess an ORCID identifier

The author(s) designated as corresponding should furnish at least one institutional email address that has been authenticated for our documentation.

Acknowledgements

Please reflect mentioning any individuals, organizations, or departments that have contributed to the project through data provision, equipment support, services (such as analytical services), image sharing, funding, or inspiring discussions. However, they may not qualify as co-authors for the paper. All individuals named in the Acknowledgements must provide consent to be mentioned.

Copyright holders should be acknowledged beside the corresponding image or data they provided.

Innovation of *Chemistry & Materials* for *Sustainability*

Peer review policy

All articles will undergo assessment by referees, also referred to as peer reviewers, to evaluate the scientific merit and suitability for publication. Referees are chosen from a global pool of proficient scientists with recent contributions in the pertinent field(s). The *Innovation of Chemistry & Materials for Sustainability* (ICMS) typically engages single-blind peer review. This entails that referees are responsive of the authors' identities, while the referees' reports remain anonymous.

At the Editor's discretion, double-blind peer review may be applied instead of single-blind review. In this approach, the referees are uninformed of the authors' identities. Every effort will be made to secrete authors' identities, although thorough privacy cannot be guaranteed.

Referees suggested by the author

Authors are welcome to suggest potential referees upon submission within cover letter. Additionally, if there are any referees the authors feel should not be approached due to potential conflicts of interest, they should inform the Editor. However, the final choice of referees will be at the decision of the Editor.

It's important to note that providing inaccurate information, such as suggesting referees with false identities or contact details, will lead to rejection of the manuscript.

*For any inquiry/complain regarding policy on ICMS research ethics, please contact research ethics and integrity team (Email: integrity-icms@insuf.org)

Article Processing Charges

What is the rationale behind ICMS requiring authors to pay publication fees?

All original research papers published by *Innovation of Chemistry & Materials for Sustainability* (ICMS) are immediately and permanently accessible online at no cost upon publication. We ensure that neither university libraries nor individual readers will ever need to purchase a subscription or pay any pay-per-view fees to access articles in the electronic format of any journal. Consequently, ICMS does not generate revenue from electronic subscriptions or pay-per-view fees.

However, the online publication process does incur expenses, including the setup and maintenance of publication infrastructure, ongoing journal operations, manuscript processing through peer review, editing, publishing, maintaining scholarly records, and archiving. To offset these costs, ICMS levies publication fees, also known as Article Processing Charges (APCs), from authors. Subscription charges are applicable only for the printed version of the journal. APCs are payable upon acceptance of a manuscript for publication.

Journal Title	Regular APC*
Innovation of Chemistry & Materials for Sustainability (ICMS)	$150 (Rs. 12000/-)

*Authors from Low-Income Countries receive APC reductions. There is no APC for invited article.

*For any inquiry, please feel free to contact us,

Email: gargiagarwala@gmail.com; me-icms@insuf.org

Contact Nos.: +919933060646; +918902278875

Note: ICMS does not require Article Submission Charges, also referred to as Submission Fees, which are typically payable upon manuscript submission. Additionally, ICMS does not impose charges based on the number of pages, inclusion of colour figures, or any other items that other publishers often levy fees for.

It's worth noting that ICMS's standard Article Processing Charges (APC) are notably below average. Despite this, ICMS remains committed to enhancing the quality of both authorship and readership experiences through various means, such as:

- **Providing detailed article-level metrics** to track the reach and impact of individual publications.
- **Covering production expenses**, including copyediting, typesetting, formatting, and assigning **Digital Object Identifiers** (DOIs).
- **Maintaining and hosting the journal's website** to ensure continuous online access to articles.
- **Calculating journal performance indicators**, such as the two-year Google-based Journal Impact Factor (2-GJIF).
- **Archiving articles on Porch** to guarantee long-term digital preservation and accessibility.
- **Facilitating indexing and discoverability** by submitting articles to multiple databases and search engines.
- **Supporting administrative functions**, including staff compensation, IT infrastructure, and author services.
- **Managing the editorial and peer review process**, which includes coordinating reviewers, handling revisions, and ensuring editorial quality and decision-making integrity.

Authors should also consider the cost-effectiveness or value for money of publishing Open Access with ICMS, which the organization believes it excels at. However, further research is necessary to fully understand this aspect.

SUBSCRIPTION INFORMATION

Subscription type: Library/ Institution/ Industry/ Personal

Name: Mr./Ms./Dr/Prof: ……………………………………………….. Designation: ………………….……………….

Organization: ……………….............................…….. Address for Communication: ………………………….

City: …………………………………………. State: …………………………………… PIN: …………………

Tel. (off.): ……………………………….. (Mobile): …………………………….. (Resi.): …………………………

Email: …………………………………………………..

Date: ……………. Signature of Subscriber: ……………………….

Innovation of Chemistry & Materials for Sustainability

SUBSCRIPTION FORM

(*Innovation of Chemistry & Materials for Sustainability*)

No. of Years	Subscription Charges*
1st Year	$500 (Rs.30000/-)
2nd Year	$800 (Rs.50000/-)
3rd Year	$1000 (Rs.70000/-)
4th Year	$1200 (Rs.90000/-)
5th Year	$1500 (Rs.110000/-)

Mode of Payment

Subscriptions must be paid in advance, with all rates covering postage and taxes. We kindly ask subscribers to include payment with their order when possible. Issues will be sent only upon receipt of payment. Payments can be made via online transfer, and the details should be sent to the director of INSUF PUBLICATIONS (OPC) PVT. LTD. (Email: gargiagarwala@gmail.com) or Managing Editor, ICMS (Email: me-icms@insuf.org) or Editor, ICMS (Email: editor-icms@insuf.org).

Payment Details:

Beneficiary Name: **Insuf Publications (OPC) Private Limited**

Bank Name: **HDFC Bank**; Branch Name: **Kestopur**; Bank Account No.: **50200097905680** (Current Account)

RTGS/NEFT IFSC Code: **HDFC0002492**; Branch Address: **HDFC Bank LTD, Akashdeep Apartments, 3AC-232,1 Prafulla Kanan, Kolkata – 700101, West Bengal, INDIA**.

You can also place your journal orders using the following methods:

1. Email your order to me-icms@insuf.org, editor-icms@insuf.org, or gargiagarwala@gmail.com.

2. To order by phone, call us at +91-9933060646 or +91-8902278875.

3. For orders via regular mail, please send your complete subscription information and payment details to:

Director,

Insuf Publications (OPC) Pvt. Ltd.

Address: BD51, Gitanjali Apartment, FL 5B, Rabindra Pally, Prafulla Kanan, Kolkata-700101, West Bengal, INDIA.

Contact: +919933060646; +918902278875. Email: gargiagarwala@gmail.com; me-icms@insuf.org Website: https://insuf.org/

Table of Content

Note: You can visit our website https://insuf.org/journal/icms to access these articles.

We invite you to submit your valuable article for the July-December 2025 issue of our open access journal.

Note: Please be aware that there are no Article Processing Charges (APC) for this issue also. Additionally, we will never take APC for invited review articles.

Editorial

Academia and Industry: An Essential Alliance for a Sustainable Future

Bikram Keshari Agrawalla[a]* , and Susanta Banerjee[b]*

[a]Roche Diagnostics GmbH, Penzberg, DE-82377, Germany.
[b]Materials Science Centre, Indian Institute of Technology Kharagpur, Kharagpur - 721302, India.
*Correspondence: bikram.keshari_agrawalla@roche.com; susanta@matsc.iitkgp.ac.in

For centuries, the collaboration between academia and industry has driven mutual progress, with academic innovations transforming into products and services through industrial channels. This symbiotic relationship has empowered both sectors to achieve their goals, fueling academic research to address real-world challenges and inspiring groundbreaking solutions. Industry, in turn, gains access to cutting-edge technologies and a highly skilled workforce. Through this partnership, technological advancement, entrepreneurship, and workforce development are accelerated.[1] Now, the time has come for this influential alliance to transform to collaborative ecosystem, where the mutual benefit combines harmoniously with broader positive impacts on the surrounding environment or community. Both academia and industry must embrace sustainability as a core principle in guiding innovation and practices. By combining their strengths, they can optimize resources, minimize waste, and create more environmentally friendly solutions. In doing so, academia and industry can help shape a sustainable future that benefits laboratories, the environment, and society as a whole.[2]

1. Academia's Responsibility

A. Research and Knowledge Creation

Institutions, scholars and academics must prioritize environmental, social, and economic sustainability in their research efforts. This includes integrating sustainability principles into curricula, fostering interdisciplinary collaborations, and promoting innovations that address global challenges like climate change, biodiversity loss, and socio-economic inequality.[3] Moreover, academia has the responsibility to ensure that research outcomes contribute meaningfully to the public good and are effectively communicated to policymakers and the wider public. Universities should also set a leading example by embedding sustainable practices into their operations, such as reducing carbon footprints, conserving resources, and supporting the development of green technologies.[4] By emphasizing the interconnectedness of ecological, social, and economic systems, academia can guide sustainable development and inspire responsible decision-making. Ultimately, academia must embody the values of responsible stewardship, advancing knowledge that benefits both society and the planet.

B. Education and Capacity Building

Academia holds a significant responsibility in advancing sustainability through education and capacity-building. Universities and educational institutions are key in preparing students with the knowledge and skills necessary to address global sustainability challenges. This involves integrating sustainability principles across various disciplines, fostering critical thinking, and cultivating a deep understanding of the interconnectedness of environmental, social, and economic systems.[5] Additionally, academia must support research that drives innovative solutions to urgent issues such as climate change and resource depletion. Educational institutions should also empower communities through lifelong learning initiatives, equipping professionals and policymakers to adopt and implement sustainable practices.[6] By promoting sustainability literacy, fostering a sense of global citizenship, and creating an

environment where sustainability is central to decision-making, academia can drive transformative change. Ultimately, education has the power to prepare future leaders to build a sustainable and equitable future for all.

Bikram Keshari Agrawalla has been with Roche Diagnostics GmbH since 2018, serving in the Department of Protein Chemistry-I within the Division of Rare Reagent Development. His work focuses on advancing immunoassay performance and enhancing diagnostic detection limits. Prior to joining Roche, Bikram gained three years of postdoctoral research experience at Ulm University and the Max Planck Institute for Polymer Research in Mainz. He earned his PhD in Chemistry from the National University of Singapore in 2015 and completed his master's degree at the National Institute of Pharmaceutical Education and Research (NIPER), Kolkata, in 2009. With a strong background in both academia and industry, Bikram has contributed to numerous high-impact publications and patents in his field.

Susanta Banerjee has been with the Indian Institute of Technology Kharagpur for over 19 years. He previously served as the head of the Materials Science Centre from May 2014 to May 2017 and is currently the Institute Chair Professor and Chairperson of Central Research Facility. Prior joining to IIT Kharagpur, he spent 14 years as a Scientist at DRDO and the GE India Technology Centre in Bangalore. He has been awarded the prestigious AvH fellowship from Germany and is a fellow of the WAST. Prof. Banerjee has supervised more than 30 doctoral and 45 master's theses in polymer and materials science and engineering. He has led numerous innovative projects at DRDO, GEITC, and IIT-Kharagpur, driven by his commitment to endorse future sustainability.

C. Bridging Theory and Practice

The responsibilities of bridging theory and practice to advance sustainability lays both on academics and industry. While academic research provides valuable theoretical frameworks, it is essential for institutions to ensure that this knowledge is effectively applied in real-world contexts.[7] Universities must encourage collaboration among researchers, practitioners, policymakers, and local communities to develop practical solutions for sustainability challenges. This includes supporting interdisciplinary research that combines scientific, economic, and social perspectives to tackle critical issues such as climate change, resource management, and social equity.[8] Academia can also form partnerships with industries, governments, and NGOs to implement sustainable practices across various sectors. Additionally, incorporating experiential learning opportunities, such as internships, field projects, and community-based research, into curricula helps students gain practical skills and knowledge. By bridging the gap between theory and practice, academia can drive impactful, evidence-based initiatives that contribute to a sustainable and equitable future.

D. Promoting Ethical Standards and Long-Term Thinking

Advancing ethical standards and promoting long-term thinking in sustainability is one of the pillar of education institutions. By integrating ethics into sustainability research and education, academic institutions ensure that decisions and actions prioritize social equity, environmental stewardship, and justice.[9] Researchers are encouraged to consider the broader impact of their work, ensuring that innovations do not exploit or harm vulnerable communities or ecosystems. Additionally,

Agrawalla and Banerjee

Innov. Chem. Mater. Sustain. **2025**, 2(1), 001-004

academia must emphasize the importance of long-term thinking, guiding students and professionals to prioritize the needs of future generations when addressing present-day challenges. This involves questioning short-term solutions and fostering a mindset that values enduring sustainability over immediate gains. Institutions should lead by example, embedding ethical practices into their operations, research funding, and collaborations. By promoting ethical decision-making and encouraging long-term perspectives, academia can ensure that sustainability efforts are responsible, inclusive, and aligned with the overarching goal of creating a just and resilient future for all.

2. Industry's Responsibility for Sustainability

A. Innovation in Green Technologies

Industry's role in advancing sustainability through innovation in green technologies is paramount. As major contributors to environmental impact, industries must prioritize the development and adoption of technologies that reduce resource consumption, minimize waste, and lower carbon emissions.[10] By investing in renewable energy, energy-efficient solutions, and sustainable manufacturing processes, businesses can lead the transition to a more sustainable economy. Industry leaders should also foster a culture of research and development to create products and services with a smaller environmental footprint. Ultimately, by driving innovation in green technologies, industries can make a significant contribution to the global effort to combat climate change and ensure a sustainable future for generations to come.

B. Operational Sustainability

Industries have a major obligation to adopt sustainable operational practices to reduce their environmental impact and support the long-term ecological health of the planet. This involves optimizing resource use, minimizing waste, and lowering energy consumption across all business activities.[11] By re-optimizing existing processes with environmentally friendly solutions, companies can develop more sustainable products. Additionally, businesses must implement sustainable supply chain practices, such as responsibly sourcing raw materials, reducing carbon emissions, and promoting ethical labor standards. Industries should also adopt energy-efficient technologies, prioritize renewable energy, and work toward achieving zero-waste objectives. Water conservation and pollution control are equally vital in preserving natural resources. Transparent reporting on sustainability initiatives and progress promotes accountability and encourages continuous improvement. By embedding sustainability into their core operations, industries not only reduce their environmental footprint but also build long-term resilience, enhance their reputation, and increase profitability.

C. Circular Economy and Waste Reduction

Industries play an essential task in advancing sustainability by adopting circular economy principles and waste reduction practices. In a circular economy, companies design products with longevity, reusability, and recyclability in mind, minimizing waste and reducing dependence on raw materials.[12] Industries are responsible for shifting from traditional linear models of production and consumption to circular systems, where resources are continually reused, refurbished, or recycled. This approach requires rethinking product design, incorporating modular components, and using sustainable materials. Waste reduction strategies, such as minimizing packaging, optimizing production processes, and recycling industrial by-products, are essential for mitigating environmental impact. Additionally, companies can invest in closed-loop systems that allow waste to be reused within the production cycle. By embracing these practices, industries not only conserve natural resources but also reduce pollution and decrease landfill waste. Ultimately, industries' commitment to circular economy principles is vital for creating a sustainable, resource-efficient future.

D. Corporate Social Responsibility (CSR)

Industries have a critical accountability to advance sustainability through Corporate Social Responsibility (CSR). CSR involves incorporating ethical practices into business models to ensure positive social, environmental, and economic outcomes.[13] Companies must address critical issues such as climate change, fair labor practices, community development, and responsible sourcing. By adopting sustainable business practices, industries can reduce their environmental impact, support local communities, and enhance overall societal well-being. CSR initiatives should prioritize transparency, accountability, and active engagement with stakeholders, including employees, consumers, and local communities. Furthermore, companies should invest in education, healthcare, and social equity programs to improve quality of life and promote economic stability. Through strategic investments and partnerships, businesses can contribute to long-term environmental and social sustainability. Ultimately, CSR enables companies to align their growth with broader societal goals, ensuring their operations not only generate profits but also contribute to a more sustainable and equitable world.

3. Bridges between Industry and Academia

A. Innovation Hubs and Research Centers

Collaboration between industry and academia within innovation hubs and research centers is crucial for advancing sustainability. These partnerships combine academic research expertise with industry's practical knowledge, enabling the development of sustainable technologies and solutions.[14] Academia contributes cutting-edge scientific insights and drives innovation through interdisciplinary research, while industries offer real-world challenges and provide the means for implementation. Innovation hubs and research centers act as collaborative spaces where researchers, students, and industry professionals work together to address pressing issues such as climate change, renewable energy, and waste management. This collaboration accelerates the commercialization of sustainable innovations, ensuring that research remains relevant and impactful. Additionally, it fosters the exchange of knowledge, skills, and resources, helping to cultivate a new generation of sustainability-focused professionals. By providing a platform for diverse stakeholders to collaborate, innovation hubs and research centers play a vital role in driving transformative change, promoting responsible practices, and ensuring the development of sustainable solutions to global environmental, economic, and social challenges.

B. Public-Private Partnerships (PPPs)

Public-Private Partnerships (PPPs) combine the strengths of both sectors to tackle complex sustainability challenges, including climate change, resource management, and social equity.[15] Academia contributes through research, innovation, and data-driven solutions, while industry offers practical experience, funding, and the ability to scale sustainable technologies. These partnerships promote the development and implementation of sustainable practices and policies, benefiting both communities and the environment. PPPs also encourage knowledge sharing, capacity building, and the creation of new job opportunities in emerging green industries. Furthermore, they align public goals with private sector capabilities, fostering a balanced approach to sustainability. By collaborating through PPPs, industry and academia can pursue common objectives, driving innovation, reducing environmental impact, and enhancing long-term social and economic well-being. The success of these partnerships relies

Agrawalla and Banerjee

Innov. Chem. Mater. Sustain. **2025**, *2*(1), 001-004

on mutual trust, effective communication, and shared accountability to ensure lasting impact.

C. Data Sharing and Open Access

Data sharing and open access are essential for building trust and strengthening partnerships between industry and academia. The exchange of data between these sectors enables more informed decision-making and the creation of sustainable solutions.[16] Academia provides valuable research findings, while industry offers real-world data, ensuring that solutions are based on both scientific insights and practical knowledge. Open access platforms further facilitate the sharing of crucial information, allowing researchers, policymakers, and industry professionals to freely access and utilize data for sustainable innovations. This collaborative approach speeds up the development of technologies, strategies, and policies that address global challenges like climate change, resource depletion, and environmental degradation. By promoting transparency and collaboration, data sharing and open access foster cross-sector partnerships, boost innovation, and ensure that sustainable solutions are scalable and widely adopted. Ultimately, this approach amplifies the collective impact of academia and industry in driving a more sustainable and equitable future.

D. Systems Thinking

Collaboration between industry and academia for sustainability through systems thinking involves recognizing the interconnections between environmental, social, and economic factors. Systems thinking enables both sectors to understand the broader implications of sustainability challenges and solutions, emphasizing the importance of holistic, long-term strategies.[17] Academia provides the theoretical framework and research tools to analyze complex systems, while industry offers practical insights and real-world applications. By collaborating, both sectors can develop sustainable innovations that address various dimensions of challenges such as climate change, resource depletion, and social inequality. This approach promotes interdisciplinary research, fosters cross-sector dialogue, and encourages solutions that consider the entire lifecycle of products and processes.[18] Systems thinking also supports the design of circular economies, where waste and resource consumption are minimized, and long-term impacts are prioritized. Ultimately, this collaboration strengthens sustainability efforts by ensuring that solutions are comprehensive, effective, and adaptable to evolving global conditions.

E. Systematic Framework for EHS, ESG Management

International Organization for Standardisation (ISO) certification provides a clear and organized approach to managing environmental, health, and safety (EHS) issues, helping both industry and academia work towards sustainability. It encourages continuous improvement, efficiency, and responsibility, making sure organizations follow global governance standards for sustainability.[19]

In industry, certifications like ISO 14001 (Environmental Management) and ISO 45001 (Health and Safety) help companies reduce their impact on the environment and keep employees safe. These standards guide businesses in cutting waste, saving energy, and reducing risks, while ensuring a safe working environment. By following these guidelines, companies show their commitment to sustainability and improve their operations, helping create a more sustainable future. In universities, ISO 14001 helps manage environmental impact by promoting waste reduction and energy savings. ISO 45001 ensures that campuses are safe and healthy for students, staff, and faculty. ISO 9001 (Quality Management) ensures high-quality research and academic programs, making sustainability research stronger and more impactful. By adopting ISO standards, universities can innovate and run more sustainably by using resources wisely and reducing waste.

Ultimately, a structured framework like ISO certification in both sectors strengthens the shared commitment to sustainability, guiding organizations and institutions toward a more efficient and ethical future for all.

Challenges and Barriers to Sustainability

Challenges and barriers to sustainability involve a variety of economic, political, social, and environmental factors that impede progress toward sustainable development.[20] These obstacles include financial limitations, political instability, weak regulations, public resistance, and a lack of awareness. Overcoming these challenges demands coordinated efforts across sectors, with an emphasis on policy reform, education, and promoting innovation. Tackling these issues is essential to achieving long-term environmental protection, social equity, and economic stability for future generations. While the importance of sustainability is widely acknowledged, both industry and academia face challenges in fulfilling their respective responsibilities.

A. Economic Constraints

Economic constraints present significant challenges to achieving sustainability. Limited financial resources often prevent organizations, especially in developing regions, from investing in sustainable technologies and practices. The high upfront costs associated with renewable energy, eco-friendly infrastructure, and sustainable supply chains may discourage businesses and governments from adopting green solutions. Additionally, economic pressures frequently prioritize short-term profits over long-term sustainability goals, resulting in the continued use of unsustainable practices. Smaller businesses, in particular, may struggle with the financial burden of implementing sustainable initiatives, creating disparities in the adoption of green technologies. Moreover, economic constraints can limit funding for research and innovation in sustainability, hindering the development of new solutions. These challenges are further exacerbated by global economic inequalities, where wealthier nations and corporations are better positioned to lead sustainability efforts, leaving poorer regions behind.[21] Overcoming these barriers requires policy incentives, international cooperation, and investment in green technologies to make sustainability financially viable and accessible to all.

B. Political and Regulatory Barriers

Political and regulatory barriers pose significant challenges to achieving sustainability. In many regions, inconsistent or weak environmental policies hinder progress toward sustainable practices. Governments may prioritize short-term economic growth over long-term environmental objectives, leading to delays or compromises in regulatory measures. Political instability and a lack of political will can further prevent the implementation of sustainable policies. Additionally, regulatory frameworks may be outdated or insufficient to address emerging environmental issues such as climate change or resource depletion.[21,22] In some cases, industries may lobby against stringent regulations to protect their profits, resulting in weaker enforcement of environmental standards. Moreover, the lack of international coordination and the varying political agendas of different countries can create obstacles to global sustainability efforts. Overcoming these challenges requires strong political commitment, alignment of policies with sustainability goals, and the enforcement of regulations that promote sustainable development while balancing the interests of all stakeholders. Effective governance and global collaboration are critical to addressing these barriers.

C. Public Perception and Resistance to Change

Public perception and resistance to change are significant barriers to sustainability. Many individuals remain unaware of the urgency of environmental issues or underestimate the long-term consequences of unsustainable practices.[23] This

lack of awareness often leads to apathy or resistance to adopting sustainable behaviors. Additionally, people may prioritize immediate convenience or economic benefits over long-term sustainability goals. Cultural norms, misinformation, and concerns about economic disruption can also contribute to resistance to sustainable changes, such as transitioning to renewable energy or embracing new technologies. Industries and governments frequently face challenges in convincing the public to support policies that may initially seem costly or inconvenient. Overcoming these barriers requires education, transparent communication, and efforts to highlight the benefits of sustainability, such as job creation, improved health, and economic resilience. Shifting public perception involves addressing concerns, offering practical solutions, and emphasizing the collective responsibility to protect the environment for future generations.

6. Conclusion

In conclusion, the collaboration between academia and industry is crucial for shaping a sustainable future. Academia fosters innovation, research, and education, cultivating the right mindset, while industry brings the resources, technologies, and practical expertise required to transform sustainable solutions into reality. By joining forces, these sectors can advocate for policy changes, co-develop advanced green technologies, and implement sustainable practices. To ensure that sustainability becomes a lasting reality—where scientific advancement, environmental stewardship, and social well-being are intertwined-the partnership between academia and industry is indispensable. This facilitative mutualism holds the key to creating a sustainable planet for both society and future generations.

Author Contribution Declaration

We are equally contributed to finalize the editorial.

Data Availability Declaration

There are no new data was created.

Notes

References

1. A. Chausson, E. A. Welden, M. S. Melanidis, E. Gray, M. Hirons, N. Seddon. Going beyond market-based mechanisms to finance nature-based solutions and foster sustainable futures. *PLOS Clim.* **2023**, *2*, e0000169. https://doi.org/10.1371/journal.pclm.0000169
2. K. F. Mulder. Innovation for sustainable development: from environmental design to transition management. *Sustain Sci.* **2007**, 2, 253. https://doi.org/10.1007/s11625-007-0036-7
3. P. Duran. Universities: Getting ready for the Sustainable Development Goals (SDGs). United Nations. Academic Impact. https://www.un.org/en/academic-impact/universities-getting-ready-sdgs
4. G. H. Brundtland. *Our common future. Oxford University Press.* **1987**
5. S. Giarola, A. Kell, S. Sechi, M. Carboni, A. Dall-Orsoletta, P. Leone, A. Hawkes. Sustainability Education: Capacity Building Using the MUSE Model. *Energies.* **2023**, *16*, 5500. https://doi.org/10.3390/en16145500
6. H. V. Weenen. Towards a vision of a sustainable university, *IJSHE*, **2000**, *1*, 20. https://doi.org/10.1108/1467630010307075
7. D. Tilbury. Education for sustainable development: An expert review of processes and learning. *UNESCO.* **2011**. https://unesdoc.unesco.org/ark:/48223/pf0000191442
8. M. Singer-Brodowski. The potential of transformative learning for sustainability transitions: moving beyond formal learning environments. *Environ Dev Sustain.* **2023**. https://doi.org/10.1007/s10668-022-02444-x
9. R. Torelli. Sustainability, responsibility and ethics: different concepts for a single path, *Soc. Responsib. J.* **2021**, *17*, 719. https://doi.org/10.1108/SRJ-03-2020-0081
10. M. Shahzad, Y. Qu, S. Rehman, A. U. Zafar. Adoption of green innovation technology to accelerate sustainable development among manufacturing industry, *Journal of Innovation & Knowledge.* **2022**, *7*, 100231. https://doi.org/10.1016/j.jik.2022.100231
11. P. H. Walker, P. S. Seuring, P. J. Sarkis, P. R. Klassen. Sustainable operations management: recent trends and future directions, *International J. Oper. Prod. Manag.*, **2014**, *34*, 5. https://doi.org/10.1108/IJOPM-12-2013-0557
12. M. Möslinger, G. Ulpiani, N. Vetters. Circular economy and waste management to empower a climate-neutral urban future, *J. Clean. Prod.*, **2023**, *421*, 138454. https://doi.org/10.1016/j.jclepro.2023.138454
13. A. McWilliams, D. Siegel. Corporate Social Responsibility: A Theory of the Firm Perspective. *AMR*, **2001**, 26, 117. https://doi.org/10.2307/259398
14. N. Carbonara, R. Pellegrino. The role of public private partnerships in fostering innovation. *CM&E,* **2020**, *38*, 140. https://doi.org/10.1080/01446193.2019.1610184
15. Z. Cheng, H. Wang, W. Xiong, D. Zhu, L. Cheng. Public–private partnership as a driver of sustainable development: toward a conceptual framework of sustainability-oriented PPP. *Environ. Dev. Sustain.*, **2021**, *23*, 1043. https://doi.org/10.1007/s10668-019-00576-1
16. S. M. Alexander, K. Jones, N. J. Bennett, A. Budden, M. Cox, M. Crosas, E. T. Game, J. Geary, R. D. Hardy, J. T. Johnson, S. Karcher, N. Motzer, J. Pittman, H. Randell, J. A. Silva, P. P. Silva, C. Strasser, C. Strawhacker, A. Stuhl, N. Weber. Qualitative data sharing and synthesis for sustainability science. *Nat. Sustain.*, **2020**, *3*, 81. https://doi.org/10.1038/s41893-019-0434-8
17. N. Voulvoulis, T. Giakoumis, C. Hunt, V. Kioupi, N. Petrou, I. Souliotis, C. Vaghela, W. W. Rosely . Systems thinking as a paradigm shift for sustainability transformation. *GEC*, **2022**, *75*, 102544. https://doi.org/10.1016/j.gloenvcha.2022.102544
18. T. Rebs, M. Brandenburg, S. Seuring. System dynamics modeling for sustainable supply chain management: A literature review and systems thinking approach. *J. Clean. Prod.*, **2019,** *208*, 1265. https://doi.org/10.1016/j.jclepro.2018.10.100
19. (a) J. M. S. Lira, E. G. Salgado, L. A. Beijo, C. E. S. Da Silva. Shedding light on the diffusion of ISO 14001 across Africa, Asia and Oceania. *J. Clean. Prod.*, **2021**, *289*, 125724. https://doi.org/10.1016/j.jclepro.2020.125724. (b) ISO 45001: 2018- Occupational health and safety management systems– requirements with guidance for use. International Organization for Standardization, Geneva, Switzerland. **2018**. (c) J. Priede. Implementation of Quality Management System ISO 9001 in the World and Its Strategic Necessity. *Procedia Soc. Behav. Sci.*, **2012**, *58*, 1466. https://doi.org/10.1016/j.sbspro.2012.09.1133
20. C. S. Dutra, U. Rohan, R. Branco, C. K. Chinelli, A. Jose V. B. de Araujo, C. A. P. Soares. Barriers and Challenges to the Sustainability Requirements Implementation in Public Procurement of Engineering Works and Services. *Open J. Civ. Eng.*, **2017**, *7*, 1. https://doi.org/10.4236/ojce.2017.71001
21. N. Blampied. Economic growth, environmental constraints and convergence: The declining growth premium for developing economies. *Ecol. Econ.,* **2021**, *181*, 106919. https://doi.org/10.1016/j.ecolecon.2020.106919
22. D. Misleh, J. Dziumla, M. De La Garza, E. Guenther. Sustainability against the logics of the state: Political and institutional barriers in the Chilean infrastructure sector, *EIST*, **2024**, *51*, 100842. https://doi.org/10.1016/j.eist.2024.100842
23. R. Lozano. Resistance to Sustainability Change in Organisations and Strategies to Overcome It. *In: Organisational Change Management for Sustainability. Strategies for Sustainability*. Springer, Cham. **2024**, 129. https://doi.org/10.1007/978-3-031-59622-3_8

REVIEW ARTICLE

Siphonochilus aethiopicus: A Comprehensive Review of its Therapeutic Application for Alleviating Symptoms of Allergic and Infectious Respiratory Diseases

Schalk van Rooyen[a] ⓘD , and Gerda Fouche[b]* ⓘD

[a]Laeveld Agrochem, 410 Rigel Ave, Pretoria, South Africa.
[b]Department of Chemistry, Faculty of Natural and Agricultural Sciences, University of Pretoria, Pretoria, South Africa.
*Correspondence: gerda.fouche@up.ac.za; foucheg51@gmail.com

Dedicated to Hans Vahrmejier who taught me the beauty of medicinal plants.

Abstract: *Siphonochilus aethiopicus*, is a medicinal plant traditionally used in South Africa to treat respiratory and inflammatory conditions. The plant species is endangered due to overharvesting, necessitating conservation and cultivation efforts. Scientific studies on *S. aethiopicus* led to the identification of key bioactive compounds, primarily furanoterpenoids, with demonstrated anti-inflammatory, bronchodilatory, and immunomodulatory effects. Laboratory and animal studies confirm its effectiveness in treating asthma and allergic airway diseases. Preclinical studies demonstrate the plant's effectiveness in models of allergic airway diseases, supporting its role in complementary medicine. This review consolidates ethnopharmacological knowledge, phytochemical composition and pharmacological properties related to *S. aethiopicus*, highlighting its potential therapeutic applications.

Keywords: *Siphonochilus aethiopicus, furanoterpenoids, respiratory diseases, phytochemistry*

Contents

Schalk van Rooyen is a technical consultant at Laeveld Agrochem in Pretoria, South Africa and guest scientific speaker at high schools and private colleges and on television programs from time to time. He is also a qualified nutritional consultant and independent researcher in the fields of natural product chemistry, biology and biochemistry with a special focus on human disease mechanisms and the specific therapeutic functioning of marker molecules and extracts of medicinal plants on a cellular level.

Dr. Gerda Fouche is a scientist with more than 30 years of experience. She served as the Scientific Innovation Leader for the Natural Product Group at the CSIR Biosciences, where her responsibilities included group administrative functions, leadership, mentoring, and effective management of large projects. The research projects focused on the discovery and development of drug and natural product leads derived from the biodiversity of South Africa. Currently, she is an Extraordinary Lecturer in the Department of Chemistry, Faculty of Natural and Agricultural Sciences at the University of Pretoria. Her research focuses on the organic chemistry of medicinal plants. This work involves the purification, isolation, and structural elucidation of active constituents present in these medicinal plants.

1. Introduction

Medicinal plants have been essential to traditional healing practices across worldwide, and their therapeutic significance continues to gain recognition in modern pharmacology.[1] In Africa, diverse plant species are employed as natural remedies against various ailments, which are often passed down through generations of traditional healers.[2] One such plant is *Siphonochilus aethiopicus* (Schweinf.) B. L. Burtt (British taxonomist that originally described the species), a plant species from the Zingiberaceae (ginger) family, renowned for its healing properties. *Siphonochilus aethiopicus* is unique to the African continent and has been used for centuries to alleviate respiratory conditions, inflammation, and various other ailments.[3] Geographically, it is widely distributed across Mozambique, Zimbabwe, and South Africa and in parts of Senegal, Ethiopia, and Malawi. Even the specific epithet of the scientific name points to the plant being primarily originated from southern Africa.

The traditional knowledge surrounding *S. aethiopicus* has motivated scientific groups, leading to delve into its phytochemical composition and pharmacological activities.[4] Studies have shown that furanoterpenoids, one of the key bioactive constituents, is responsible for the plant's anti-inflammatory, bronchodilatory, and antimicrobial effects.[5] These findings support its traditional uses and indicate potential therapeutic applications in modern medicine.

Other research into the plant's biological activity and its constituents revealed the presence of a new identified diarylheptanoid, 2,3-diacetoxy-7-(3'',4''-dihydroxy-5''-methoxyphenyl)-1-(4'-hydroxy-3'-methoxyphenyl)-5-heptene with significant antiplasmodial activity against *Plasmodium falciparum*, the causative species of cerebral malaria.[6] Potent anti-leishmanial activity was also established for this diarylheptanoid.[7] Further phytochemical investigation yielded the presence of a novel eudesmane sesquiterpenoid (2, Figure

2) from the rhizomes of the plant, which undoubtedly contributes to its biological activity.[8]

Despite its well-documented medicinal value, *S. aethiopicus* faces serious conservation threats due to overharvesting and habitat destruction.[9] The increasing demand for the plant in both local and global markets has led to its near-extinction in the wild. As a result, efforts are underway to cultivate and sustainably manage its growth to ensure its continued availability for medicinal use. Several research initiatives have focused on optimizing cultivation methods, including tissue culture propagation, to reduce the pressure on wild populations,[10] although there are some concerns regarding the chemistry of cultivated plants that are not exposed to their normal environmentral pressures.

Given the growing interest in natural remedies for respiratory and inflammatory diseases, there is a pressing need to bridge traditional knowledge with scientific validation.[11] This review intends to provide a comprehensive overview of the ethnopharmacological uses, phytochemistry and pharmacological properties of *S. aethiopicus.* By consolidating available research, this review emphasizes the potential for developing pharmaceutical and nutraceutical products based on *S. aethiopicus.*

2. Review Methodology

Information was gathered by searching for pertinent literature on *S. aethiopicus.* This review encompassed abstracts, full-text articles, MSc and PhD theses, research outputs, and books to provide succinct and comprehensive information about the plant's phytochemistry, indigenous medicinal uses, and pharmacological characteristics. Several online databases and search engines were also utilized, including ScienceDirect, Scopus, Google Scholar, Web of Science, PubMed, CAB Abstracts, SciFinder, and MEDLINE. Keywords used in the literature search included *Siphonochilus aethiopicus*, Zingiberaceae, siphonochilone, Natal ginger, medicinal plants, ginger, plant parts used, biological activity and indigenous knowledge. Only publications in the English language were considered for this review.

3. Ethnomedicinal Uses

Many plant species within the Zingiberaceae family are frequently used as flavouring agents, spices and medicines because of their distinctive taste and health benefits.[12] The roots and rhizomes of *S. aethiopicus* are widely employed in traditional African medicine. The fresh rhizomes have a potent ginger aroma and are chewed to alleviate nasal congestion and treat coughs, asthma, flu, colds and several other ailments and cultural practices.[13] Traditionally, the Zulu people of South Africa use the plant for safeguard against lightning and snakes[12]. Chewing the fresh leaves and a decoction of the rhizomes are used for menstrual pain relief.[14]

In parts of East Africa and Senegal, *S. aethiopicus* rhizomes and roots are utilized to treat stomach infections, diarrhoea, and internal parasites, including schistosomiasis, and as a spice.[15] Traditionally, the combination of roots and rhizomes is used to treat hysteria and alleviate dysmenorrhea.[16] In Benin, a water decoction of the rhizomes and roots is used for treating endometriosis and female infertility.[17] In Swaziland (Kingdom of Eswatini), this plant species is used as a remedy for malaria and to relieve menstrual pain.[18] In Africa, various ethnic groups utilize *S. aethiopicus* for colds, coughs, asthma, pain-related conditions, headaches, and respiratory problems.[19] The published literature indicates a prevalent pattern in the traditional practice of *S. aethiopicus* rhizomes and roots, against respiratory problems (including cough, influenza), pain, and malaria across the different African regions where this plant is found.

4. Phytochemistry

The key chemical components of the plant species are sesquiterpenoids of the furanoid type and diarylheptanoids.[20] Organic extracts of *S. aethiopicus* prepared by extraction of the dried, ground roots and rhizomes of the plant mainly consist of a mixture of furanoterpenoids. HPLC UV/MS data identified the major constituent in both the diethyl ether and ethanol extracts as 4,4a,5,8a,9-tetrahydro-3,5,8a-trimethylnaptho[2,3-b]furan-8-one, also named as siphonochilone (Figure 1,2).[21] The major furanoterpenoid was purified from the diethyl ether extract of the plant *via* fractionation of the diethyl ether extract. Flash chromatography with silica gel was used, eluting with increasing polarity of a 5% ethyl acetate/hexane solution to 100% ethyl acetate.[21] The structure of the furanoterpenoid was confirmed using NMR and mass spectrometry.[21,22] Another method of obtaining the furanterpenoid is *via* steam distillation of the fresh rhizomes of the plant. The rhizomes are sliced and placed in a suitable vessel for steam distillation. This process produces a clear distillate containing crystals of the pure compound, which is retrieved after filtration, washing with cold water, and drying in a desiccator overnight.[21]
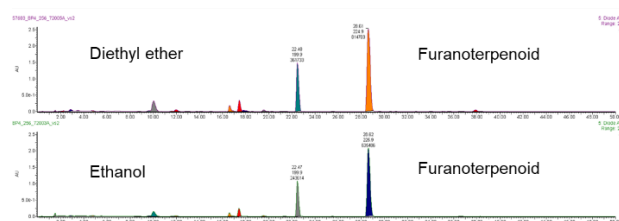
Figure 1. *HPLC UV chromatograms of the diethyl ether and ethanol extracts [Represented with permission from Ref [21].*
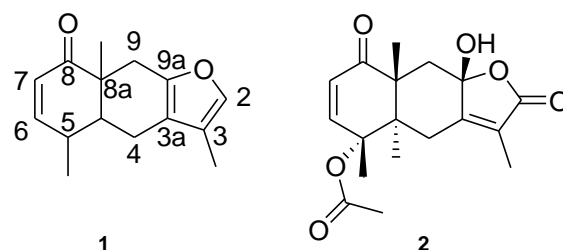
Figure 2. *Chemical structures of compounds isolated from Siphonochilus aethiopicus [Represented with permission from Ref [21].*

Other compounds were also isolated by Igoli[16] and Lategan[23] namely, epi-curzerenone, furanodienone, 16-oxo-8(17),12E-labdadiene-15-oic acid, 15-hydroxy-8(17), 12E-labdadiene-16-al, 8(17),12E-labdadiene-15,16-dial, 2-hydroxy-4aαH-3,5α,8αβ-trimethyl-4,4α,8α,9-tetrahydro-naphtho[2,3β]-furan-8(5H) and 8,12-epoxy-1(10),4,7,11-germacratetraen-6-one. Viljoen *et al.*[24] identified seventy compounds in the essential oil obtained by hydrodistillation of the roots of the plant. Siphonochilone was shown to be the major compound, comprising over 20%, and could be taxonomically significant for this plant species. The other key compounds identified in the roots included cis-alloocimene, 1,8-cineole, terpinen-4-ol, (E)-β-ocimene, kessane, sabinene, and β-pinene.

The traditional preparation involved inhalation of the vapours from the steaming of *S. aethiopicus* rhizomes as a decongestant and for treating asthma.[25] Evidence was found by Naude *et al.*[26] that eucalyptol was the major component in the vapour phase of hot water infusions prepared from fresh and dried rhizomes. The authors observed a considerable reduction of eucalyptol and other compounds in the dried rhizomes. These results support the use of *S. aethiopicus* as a

decongestant, offering additional scientific support for the anecdotal claims of its effectiveness against coughs, flu, colds and allergic asthma.

5. Pharmacological Properties

5.1 *In vitro* biological assays

The aqueous extract, the diethyl ether extract, and the purified furanoterpenoid compound of *S. aethiopicus* were evaluated using the histamine receptor binding assay, the glucocorticoid receptor binding assay, and the phosphodiesterase IV inhibition assay at a single dose concentration and the data are shown in Table 1.[21] Dose-response studies were conducted for the diethyl ether extract and the furanoterpenoid compound only, as the water extract did not show any activity. The results are given in Table 2. The diethyl ether extract demonstrated good efficacy in both the glucocorticoid receptor binding assay (IC_{50} of 12.9 µg/ml) as well as the phosphodiesterase IV enzyme assay (IC_{50} of 26.6 µg/ml), suggesting that the plant may function similarly to corticosteroids in the treatment of allergies and asthma. The purified compound (Figure 2) demonstrated activity comparable to that of the diethyl ether extract.

These results showed that the diethyl ether extract and purified compound of *S. aethiopicus* have notable activity *in vitro* in systems associated with anti-inflammatory and anti-allergic effects.

Table 1. *Bioassay results of extracts and purified compound (1), furanoterpenoid*

Sample	PDE IV[a] %	Glu %[b]	H$_1$ %[c]
Ether	70	104	60
Water	15	11	-
Compound	78	91	80

a: PDE IV (Phosphodiesterase Inhibition. b: Glu (Glucocorticoid Inhibition). c: H$_1$ (Histamine Inhibition). Testing was conducted using the sample at a concentration of 100 µg/ml.

Table 2. *Bioassay results of the diethyl ether extract and compound (1), furanoterpenoid.*

Sample	Bioassay	IC$_{50}$ (µg/ml)	K$_i$ (µg/ml)	n$_H$
Ether	PDE IV	26.6	-	-
Ether	Glu	12.9	6.92	1.48
Ether	H1	89.0	42.50	1.75
Compound	PDE IV	43.6	-	-
Compound	Glu	11.4	6.12	0.91
Compound	H1	56.5	27.00	2.05

n$_H$: Hill coefficient. K$_i$: Inhibition constant. IC$_{50}$: Inhibition concentration. Reference compound data: Phosphodiesterase PDE IV: 4-(3-Butoxy-4-methoxybenzyl)-2-imidazolidinone, IC$_{50}$ = 1.10 µM. Glucocorticoid: Dexamethasone, IC$_{50}$ = 4.10 nM. Histimine H$_1$: Pyrilamine, IC$_{50}$ = 3.30 nM.

In chronic inflammatory diseases, including rheumatoid arthritis, asthma, psoriasis, and inflammatory bowel diseases, several cytokines recruit activated immune and inflammatory cells to the site of lesions, thereby amplifying and perpetuating the inflammatory state. Transcription factors are essential in regulating immune and inflammatory responses, and nuclear factor-κB (NF-κB) is a particularly important and widespread transcription factor. NF-κB serves as a central mediator of the human immune response, regulating the transcription of a range of pro-inflammatory and inflammatory mediators such as the cytokines, interleukin-2, -1, -8 and TNF-α, as well as genes that encode nitric oxide synthase, cyclo-oxygenase II, cell adhesion molecules, immunoreceptors, or acute phase proteins. NF-κB acts as a master regulator of inflammation, making it a promising target for drug development. The diethyl ether extract was assessed for its anti-inflammatory properties in the NF-κB transcription assay where significant inhibition was observed with an estimated IC_{50} of 14.3 µg/mL and no cytotoxicity was observed at concentrations up to 100 µg/mL.[21] Cyclosporin A served as the reference compound in this assay (IC_{50} of 0.0608 µM). These results indicated that the diethyl ether extract effectively inhibited NF-κB, consequently reducing the release of various pro-inflammatory and inflammatory mediators involved in the inflammatory pathway of asthma.

Numerous cytokines are recognized as mediators of inflammation and play a role in the development of asthma. When an allergen, for instance, is inhaled, bronchial epithelial cells become activated and produce specific pro-inflammatory cytokines (interleukins, abbreviated IL), particularly the chemokine IL-8. We showed that extracts of *S. aethiopicus* exhibited substantial suppression of IL-8 with the stimulation of PMA compared to the positive control.[25] Evidence also linked NF-κB activation to improved IL-8 production, which recruits specific immune cells called neutrophils (and other granulocytes) to the site of disruption/infection.[27] Manna and Ramesh[28] showed that NF-κB, which regulated IL-8 expression, was also induced further by this chemokine. The interrelationship between NF-κB and IL-8 indicates that they are closely connected and play a significant role in inflammation and immune responses associated with allergic airway reactions. It is highly probable that *S. aethiopicus* exerts its actions on IL-8 and other cytokines through its observed inhibition of NF-κB.

5.2 *In vivo* biological assays

Upon inhalation of a causative agent such as an allergen, bronchial epithelial cells are activated and release specific pro-inflammatory cytokines. To evaluate the efficacy of *S. aethiopicus* against allergic inflammation *in vivo*, mice were sensitized and exposed to the allergen ovalbumin while simultaneously receiving *S. aethiopicus* extracts (diethyl ether or ethanol) or the purified furanoterpenoid compound.[21] Airway hyperreactivity, assessed through whole body plethysmography, was heightened in ovalbumin-sensitized mice challenged with methacholine when compared to naïve controls, and there was no substantial reduction observed in any group following the administration of S. aethiopicus extracts (Figure 3). Results showed that *S. aethiopicus* extracts exhibited anti-inflammatory properties in the lung. When given intraperitoneally, the diethyl ether extract of *S. aethiopicus* reduced allergic inflammation in the lungs similarly to the dexamethasone control. This was observed by a significant decrease in the percentage of eosinophils in the bronchoalveolar lavage fluid (see Figure 3) and a reduction in immune cell infiltration around the airways and blood vessels (Figure 4). Oral administration of the powdered plant material and diethyl ether or ethanol extract also led to a significant reduction in eosinophil counts in the bronchoalveolar lavage fluid, along with a decrease in lung inflammation (Figure 3). Although neutrophils were found in lower numbers compared to eosinophils in the bronchoalveolar lavage fluid, their counts were also significantly diminished by intraperitoneal administration of dexamethasone or the diethyl ether extract.
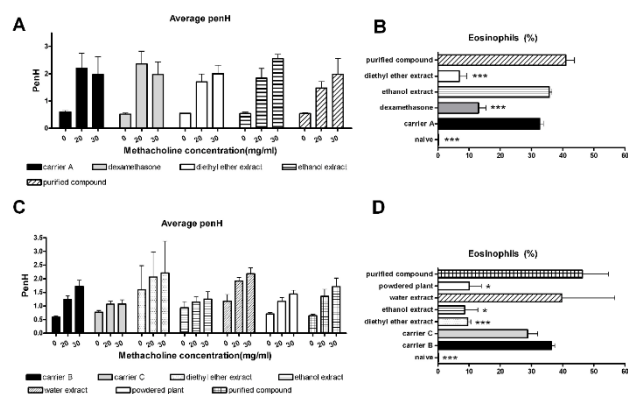
Figure 3. *Influence of S. aethiopicus on airway hyperreactivity and eosinophils in bronchoalveolar lavage fluid. Mice were sensitized and challenged with ovalbumin and treated with S. aethiopicus or control solutions intraperitoneally (A, B) or orally (C, D) twice daily for 3 days and 1 hour before methacholine challenge. A, C. PenH value as a measure of airway hyperreactivity. B, D. Percentage of eosinophils in the bronchoalveolar lavage fluid after challenge. Significance was calculated in comparison to the correlating carrier controls. *, P<0.05; ***, P<0.001. [Represented with permission from Ref [21].*
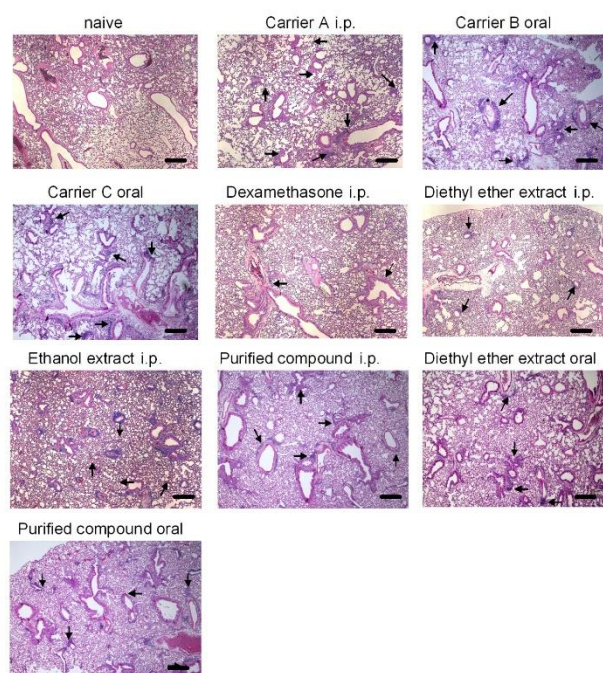
Figure 4. *Effect of S. aethiopicus on airway inflammation. Mice were sensitized and challenged with ovalbumin and treated with S. aethiopicus or control solutions twice daily for 3 days and 1 hour before methacholine challenge. Lung tissue sections were stained with haemotoxylin and eosin and examined at 100x magnification. Cellular inflammation around airways and blood vessels is indicated by black arrows. Scale bar = 200μm. [Represented with permission from Ref [21].*

The ethanol extract of *S. aethiopicus* was also assessed in a different *in vivo* animal model to evaluate its anti-asthmatic and anti-allergic/inflammatory properties. Ethanol and diethyl ether extracts of the plant were prepared and chemical constituents were analyzed using HPLC MS instrumentation. The extract was suspended in 1% ETOH/PEG solution. The test substance at a dose of 1000 mg/kg was given orally once daily for 6 consecutive days, one hour before the challenge of ovalbumin. The results of the anti-asthmatic activity are summarized in Figure 5, indicating that the ethanol extract (coded as BP4-256-72015A) demonstrated enhanced Penh values in the OVA-sensitized mice assay.
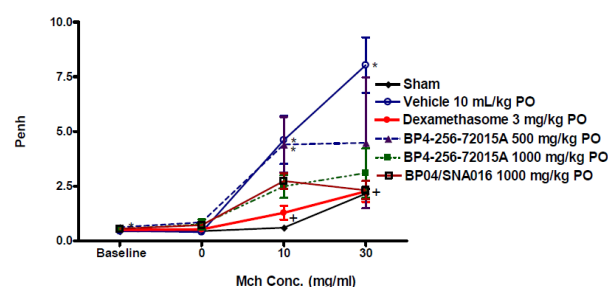
Figure 5. *Anti-asthmatic measurements [Represented with permission from Ref [21].*

Bronchoalveolar lavage fluid (BALF) samples were analyzed, and significant inhibition was observed in total WBC, lymphocytes, and eosinophils versus respective sham controls (Figure 6). One-way ANOVA, with subsequent Dunnett's test was performed to access the comparison between sham control, vehicle control, and test compound-treated groups (P<0.05 is considered significant).

The ethanol extract significantly suppressed the increase of inflammatory cells in bronchoalveolar lavage fluid (BALF) when measured in an *in vivo* anti-asthmatic ovalbumin-sensitized mice assay. In conclusion, biological assays performed on the extracts of *S. aethiopicus* and the purified furanoterpenoid compound demonstrated beneficial effects in the *in vitro* histamine H1, glucocorticoid receptor binding, phosphodiesterase IV, and NF-κB assays, indicating that this plant has anti-inflammatory, anti-allergic, immune and bronchodilatory effects. When the extracts were further tested *in vivo*, significant anti-inflammatory effects were observed, and the inflammatory cells were also significantly suppressed in BALF.

6. Toxicology

6.1 *In vitro* cytotoxicity, mutagenicity, and cardiac toxicity

The cytotoxicity of the diethyl ether extract, obtained from the liquid-liquid partitioning of the aqueous extract of the rhizomes was determined on Chinese Hamster Ovarian (CHO) cells using the MTT colorimetric assay. Emetine dihydrochloride (IC$_{50}$ 0.07 μg/ml) was used as the standard reference compound and an IC$_{50}$ value of 48.5 μg/ml was determined for the diethyl ether extract. The ethanol extract was evaluated against a cytotoxicity panel and genetic toxicity tests were also conducted, focusing on bacterial cytotoxicity and the Ames test. Four different bacterial strains were used; TA1537–S9, TA1535–S9, TA100–S9 and TA98–S9. No cytotoxicity was observed for concentrations up to 125 μg/ml.

The Ames test, which was performed using *Salmonella typhimurium*, is a commonly employed bacterial assay for identifying compounds capable of inducing gene mutations. This assay has a strong predictive value in relation to rodent carcinogenicity tests. The standard Ames test typically involves five strains of *Salmonella* that have pre-existing mutations preventing the bacteria from synthesizing the essential amino
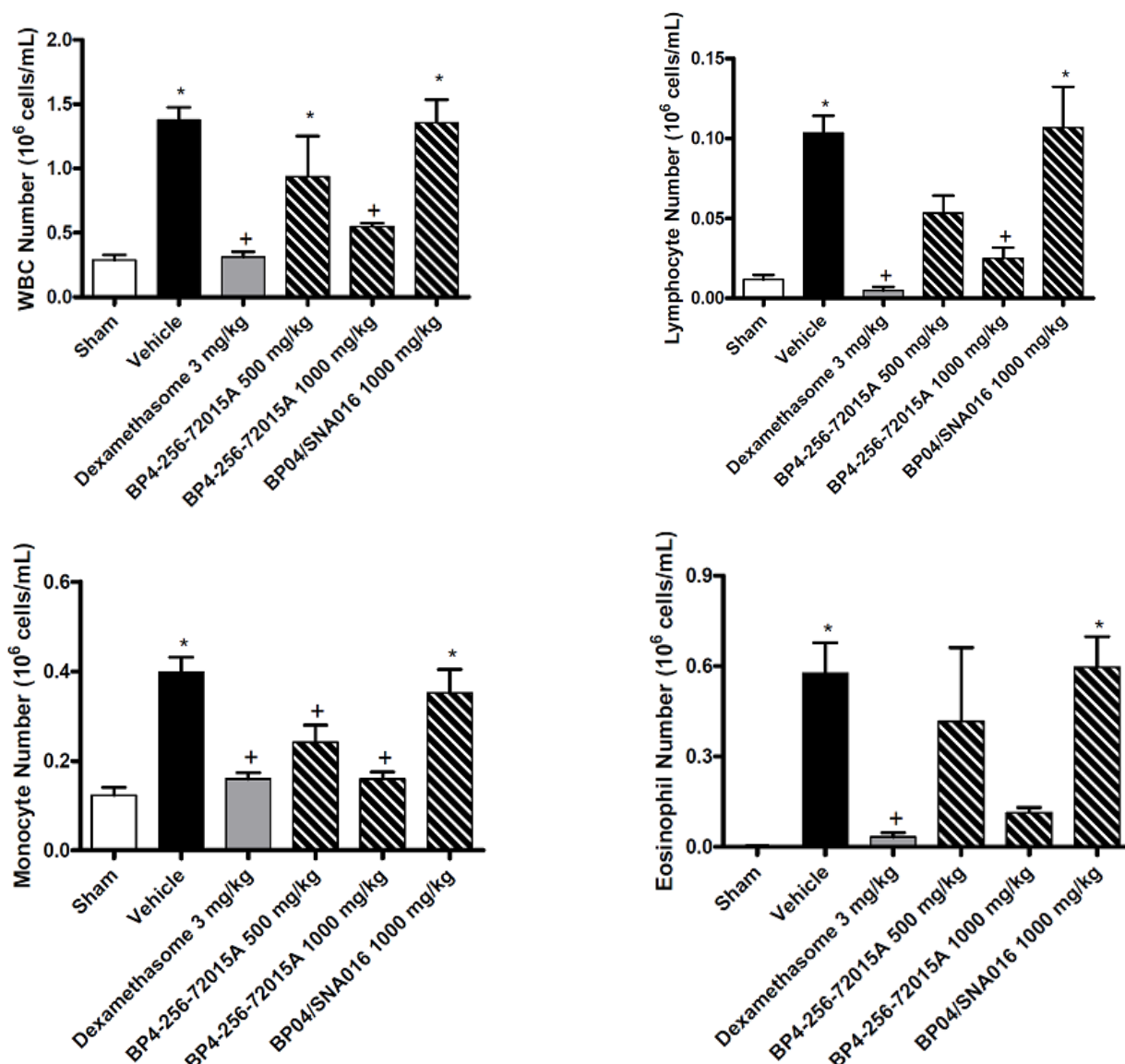
Figure 6. *Anti-allergic and inflammatory measurements BP4-256-72015A: ethanol extract; BP04/SNA016: dry, ground plant material. [Represented with permission from Ref [21].*

acid histidine, rendering them unable to grow in a histidine-free medium. The *Salmonella* strains used have different mutations in various genes in the histidine operon and are designed to be responsive to mutagenic compounds that act through different mechanisms. No cytotoxicity was observed in the Ames test for the ethanol extract up to a concentration of 125 µg/ml. A cardiac toxicity test (hERG, automated patch-clamp) was also conducted. Patch-clamp is an electrophysiological technique performed on cells recombinantly expressing the channel of interest (in this case hERG) and capable of detecting any change in its physiological properties. An IC_{50} of 50 µg/ml was obtained.

6.2 *In vivo* acute toxicological evaluation

Two separate acute *in vivo* toxicological studies were conducted. The first study assessed the acute oral toxicity of a diethyl ether extract of the plant in Sprague Dawely rats and was carried out according to Guideline 420 (fixed dose procedure). The diethyl ether extract was sequentially administered to three rats until signs of evident toxicity were observed. From the results of the study no evident toxicological

symptoms were recorded during the sighting study at the 300-2000 mg/kg dosage levels. There was also no evident effect of the substance on the weight of the animals. The diethyl ether extract was classified in category 5 of the Global Harmonized System for chemicals.

The objective of the second study was to characterize the toxicity of the ethanol extract as well as finely, ground plant material of *S. aethiopicus* in rats following a single oral dose. The *in vivo* toxicology study consisted of two Phases according to the Food and Drug Administration's International Conference on Harmonization (ICH) and the Organisation for Economic Co-operation and Development (OECD) guidelines. Animals were dosed with either the crude plant extract or the ethanol extract dissolved in propylene glycol and 5% ethanol. The animals were dosed in two sub-groups of three animals each, two days apart, and monitored for 14 full days. Following the monitoring period, the animals were terminated by an isoflurane overdose and submitted for gross necropsy.

Histological evaluation from the acute toxicity study did not demonstrate any specific morphological pathology. From the

observed clinical signs, the most prominent effect was mild sleepiness that was induced within about 15 to 30 minutes from dose administration. This clinical effect was resolved within 5-6 hours post-drug administration. Based on the clinical signs of sedation and recovery in the absence of pathology or weight related effects, these clinical signs are assigned to sedative-like effects induced by dosing. While it is possible that the extract produced this mild sedative effect, it is more likely that these clinical signs were a result of the 5% alcohol solvent. The clinical signs seen are very similar to the signs seen by Chuck *et al.*[29] in which rats were exposed to various concentrations of ethanol and evaluated over a period of 30 minutes. In this study, most of the animals demonstrated some form of depression within 5 minutes of administration. The major difference between this study and that of Chuck *et al.*,[29] was that the effects seen were minor at 0.25 mg/kg. For this study, the animals received approximately 0.8ml of a 5% ethanol solution which converts to approximately 0.160 mg/kg. There were no histological findings to indicate toxic tissue damage. Based on the reversible clinical signs of mild sedation that lasted approximately 6 hours, normal habitus for > 99% of the study, absence of weight-related effects, and lack of gross pathological changes the product is believed to have a LD_{50} of > 5000 mg/kg when administered by the oral route (category 5).

6.3 *In vivo* sub-chronic toxicological evaluation

The objective of this study was to further characterize the toxicity of the plant species in rats following repeated oral dosages. The study consisted of a follow-up Phase 3 according to the Food and Drug Administration's International Conference on Harmonization (ICH) and the Organisation for Economic Co-operation and Development (OECD) guidelines. Data was obtained in 80 rats over a three-month period at three different dosages administered, namely 3, 30 and 300 mg/kg. A repeated dose 90-day oral toxicity study in rodents as per OECD guideline 408 was followed. 40 female and 40 male outbred rats of 6-8 weeks were used at the start of the study, 10 animals of each sex per dosage group. The *S. aethiopicus* ethanol extract was dissolved in 1% ethanol and polyethylene glycol (PEG) for oral administration. The following monitoring parameters were included in the study: Individual Habitus, Cage feed intake, Change in weight, Basic ophthalmology, Terminal clinical pathology, Terminal haematology, Full pathology, Full histopathology, Actual and relative organ weights and Terminal urine analysis.

No significant changes were evident on clinical signs, necropsy, histopathology or clinical pathology when the groups were evaluated independent of sex. When evaluated by sex, the animals had minor changes evident in some of the organ weight parameters, especially testicular weight, albeit in the absence of histopathological changes. Based on the results, it is assumed that the product is non-toxic. However, based on the organ weights and urine analysis, there appeared to be a physiological effect which may be due to the pharmacodynamics mechanisms of the extract viz steroid-like mechanism coupled with the ability to interfere with smooth muscle functionality.

7. Conclusion

Siphonochilus aethiopicus as one of the most commonly used medicinal plants in South Africa, holds significant promise in complementary medicine for treating respiratory and inflammatory conditions. Traditionally, it is primarily used for mild asthma, colds, influenza, and sinus issues. Preparations include both cold and hot infusions of the rhizomes and roots,

steaming the rhizomes and inhaling the vapour, as well as chewing on the fresh rhizomes. Unlike many other widely used international medicinal plants e.g. *Ginko biloba* and *Echinacea*, there is currently no scientifically validated product based on *S. aethiopicus* on the market both locally and internationally. Only a few South African medicinal plants are now on international markets (e.g. Devil's Claw and *Pelargonium*); these plants have been extensively researched internationally and their claims scientifically validated.

Literature studies on *S. aethiopicus* provided anecdotal information but little scientifically assessed biological data. Scientific research conducted on *S. aethiopicus* led to the identification of extracts/compound (s) from the plant that can be developed for the management of allergic diseases, infectious respiratory diseases, and asthma. Biological assaying of the extracts of the plant and the purified non-steroidal metabolite showed a very interesting pharmacological profile supporting the beneficial effects of the plant extract in allergic and infectious respiratory diseases. The plant extract and/or the purified non-steroidal metabolite showed activity in the glucocorticoid receptor binding, histamine receptor binding, and phosphodiesterase IV inhibition assays. All these systems have a crucial role in respiratory diseases and inflammation and support a soothing and supporting effect in the treatment of allergic and infectious respiratory diseases. These activities were also supported by activities on IL-8, 5-lipoxygenase and nuclear factor-κB assays. The organic extracts and dried ground plant material demonstrated reduced infiltration of inflammatory cells in the lung tissue of animals and lowered production of inflammatory mediators in these animal models of asthma.

The plant extract of this widely used medicinal plant has been tested both *in vitro* and *in vivo* for toxicity. *In vitro* cytotoxicity studies in Chinese Hamster Ovarian (CHO) cells showed that the cytotoxicity (IC_{50}) of the diethyl ether extract using the MTT colorimetric assay is 48.5 µg/ml. The *in vivo* acute toxicity studies in rats have been completed using the diethyl ether and ethanol extracts as well as the finely, ground plant material and are based on OECD (The Organisation for Economic Cooperation and Development) Guideline 420 (fixed dose procedure) and Guideline 423 (single dose procedure). The results are encouraging, as the oral administration of organic extracts and ground plant material to rats exhibited no visible signs of toxicity. Additionally, histological evaluations revealed no specific morphological abnormalities or noticeable weight differences at the test concentrations of 300-2000 mg/kg. Based on the absence of toxicity at the limit dose of 2000 mg/kg, the finely ground rhizomes as well as the diethyl ether and ethanol extracts are considered category 5 compounds, according to OECD guideline 423.

Based on research results, data, and the conservation status of the plant, it is evident that commercial quantities of plant material can be supplied more cost-effectively and sustainably by using cultivation sites rather than harvesting from the wild. Areas in the Limpopo, Mpumalanga, and KwaZulu-Natal provinces should be identified as potential cultivation sites. *Siphonochilus aethiopicus* is well adapted to the climates of these provinces and is relatively easy to cultivate, as it grows from cuttings of the rhizomes during the winter when they are dormant. The plant may also be propagated from seeds, although this process may take up to a year for germination. Tissue culture is another method for propagating the plant. Cultivation is a critical aspect of any future development program for this species, which is critically threatened in the wild. Collectively, these findings demonstrate the beneficial properties of *S. aethiopicus* in alleviating symptoms associated with allergic and infectious respiratory diseases, providing scientific evidence that supports its traditional use and inclusion in complementary medicine products. Further research should focus on clinical trials to establish standardized dosing and assess long-term safety. Sustainable

Gerda and Schalk

REVIEW ARTICLE

Innov. Chem. Mater. Sustain. **2025**, *2*(1), 005-011

cultivation remains a priority to ensure its availability for medicinal use, as extensive harvesting has led to near extinction in its natural habitat.

Author Contribution Declaration

Schalk van Rooyen: engaged in editing, data curation and writing.

Gerda Fouche: engaged in data curation, writing, conceptualization and editing.

Data Availability Declaration

New data were included for the toxicology evaluation of the extracts and purified compound, furanoterpenoid of *S. aethiopicus*.

References

1. C. W. Holzapfel, W. Marais, P. L. Wessels, B. Van Wyk. Furanoterpenoids from *Siphonochilus aethiopicus. Phytochemistry*, **2002**, *59*, 405. https://doi.org/10.1016/S0031-9422(01)00402-2
2. M. Mander. The marketing of indigenous medicinal plants in South Africa: A case study in KwaZulu-Natal. **1998**, http://www.fao.org/3/w9195e/w9195e.pdf
3. B. Van Wyk, B. Van Oudtshoorn, N. Gericke. Medicinal Plants of South Africa. Briza Publications, **2009**, Pretoria, p. 274. https://doi.org/10.1365/s10337-010-1583-0
4. A. B. Cunningham. African medicinal plants: Setting priorities at the interface between conservation and primary healthcare. People and Plants Working Paper, **1993**, *1*, 1. https://docslib.org/doc/11109930/african-medicinal-plants-setting-priorities-at-the-interface-between-conservation-and-primary-health-care
5. A. Hutchings, A. H. Scott, G. Lewis, A. Cunningham. Zulu Medicinal Plants: An Inventory. Univ. Natal Press, **1996**, Pietermaritzburg. ISBN 0-86980-893-1.
6. N. P. Igoli, N. F. Al-Tannak, I. C. Ezenyi, A. I. Gray, J. O. Igoli. Antiplasmodial activity of a novel diarylheptanoid from *Siphonochilus aethiopicus. Nat. Prod. Res.*, **2020**, *35*, 5588. https://doi-org.uplib.idm.oclc.org/10.1080/14786419.2020.1799358
7. I. Ezenyi, E. Madan, J. Singhal, R. Jain, A. Chakrabarti, G. D. Ghousepeer, R. P. Pandey, N. Igoli, J. Igoli, S. Singh. Screening of traditional medicinal plant extracts and compounds identifies a potent anti-leishmanial diarylheptanoid from *Siphonochilus aethiopicus. J. Biomol. Struct. Dyn.*, **2024**, *42*, 2449. https://doi.org/10.1080/07391102.2023.2212779
8. A. Ortigosa-Palomo, D. Fuentes-Ríos, F. Quiñonero, M. C. Melguizo, R. Ortiz, J. M. López-Romero, J. Prados. Evaluation of cytotoxic effect of siphonochilone from African ginger: an *in vitro* analysis. *Environ. Toxicol.* **2024**; *39*, 4333. https://doi.org/10.1002/tox.24308
9. M. E. Light, L. J. McGaw, T. Rabe, S. G. Sparg, M. B. Taylor, D. G. Erasmus, A. K. Jäger, J. van Staden, J. N. Eloff. Investigation of the biological activities of *Siphonochilus aethiopicus* and the effect of seasonal senescence. *S. Afr. J. Bot.*, **2002**, *68*, 55. https://doi.org/10.1016/S0254-6299(16)30455-0
10. R. A. Street, G. Prinsloo. Commercially important medicinal plants of South Africa: A review. *J. Ethnopharmacol.*, **2013**, *148*, 678. https://doi.org/10.1155/2013/205048
11. A. P. Dold, M. L. Cocks. The trade in medicinal plants in the Eastern Cape Province, South Africa. *S. Afr. J. Sci.*, **2002**, *98*, 589. https://journals.co.za/doi/abs/10.10520/EJC97419
12. N. R. Crouch, M. C. Lötter, S. Krynauw, C. Pottas-Bircher. *Siphonochilus aethiopicus* (Zingiberaceae), the prized indungulu of the Zulu—an overview. *Herbertia*, **2000**, *55*, 115.
13. V. Steenkamp, H. Grimmer, M. Semano, M. Gulumian. Anti-oxidant and genotoxic properties of South African herbal extracts. *Mutation Research*, **2005**, *581*, 35. https://api.semanticscholar.org/CorpusID:1300374.
14. K. Lindsey, A. K. Jäger, D. M. Raidoo, J. van Staden. Screening of plants used by Southern African traditional healers in the treatment of dysmenorrhoea for prostaglandin-synthesis inhibitors and uterine relaxing activity. *J. Ethnopharmacol.*, **1999**, *64*, 9. https://doi.org/10.1016/s0378-8741(98)00097-x.
15. H. M. Burkill. The Useful Plants of West Tropical Africa, vol. 5. Families S–Z. Royal Botanic Gardens, Kew, **2000**. ISBN:190034713X.
16. N. P. Igoli, Z. A. Obanu, A. I. Gray, C. C. Clements. Bioactive diterpenes and sesquiterpenes from the rhizomes of wild ginger (*Siphonochilus aethiopicus* (Schweinf) B.L. Burtt). *Afr. J. Tradit., Complementary Altern. Med.*, **2012**, *9*, 88. https://doi.org/10.4314/ajtcam.v9i1.13
17. J. P. Noudogbessi, H. Yedomonhan, G. A. Alitonou, P. Chalard, G. Figueredo, E. Adjalian, F. Avlessi, J. C. Chalchat, D. C. Sohounhloué. Physical characteristics and chemical compositions of the essential oils extracted from different parts of *Siphonochilus aethiopicus* (Schweinf.) B.L. Burtt (Zingiberaceae) harvested in Benin. *J. Chem. Pharmaceut. Res.*, **2012**, *4*, 4845. https://hal.science/hal-00950238v1/file/Noudogbessi2013.pdf
18. J. Watt, M. Breyer-Brandwijk. The Medicinal and Poisonous Plants of Southern and Eastern Africa. Livingstone, London, UK, **1962**. https://doi.org/10.2307/4113816
19. S. A. Adebayo, S. O. Amoo, S. N. Mokgehle, A. O. Aremu. Ethnomedicinal uses, biological activities, phytochemistry and conservation of African ginger (*Siphonochilus aethiopicus*): A commercially important and endangered medicinal plant. *J. Ethnopharmacol.*, **2021**, *266*, 113459. https://doi.org/10.1016/j.jep.2020.113459
20. B. -E. Van Wyk, B. Van Oudtshoorn, N. Gericke. Medicinal plants of South Africa. Revised and expanded edition. Briza Publications, Pretoria, **2009**. ISBN: 9781875093373.
21. G. Fouche, N. Nieuwenhuizen, V. Maharaj, S. van Rooyen, N. Harding, R. Nthambeleni, J. Jayakumar, F. Kirstein, B. Emedi, P. Meoni. Investigation of *in vitro* and *in vivo* anti-asthmatic properties of *Siphonochilus aethiopicus. J. Ethnopharmacol.*, **2011**, *133*, 843. https://doi.org/10.1016/j.jep.2010.11.014
22. C. W. Holzapfel, W. Maraisa, P. L. Wessels, B. -E. van Wyk. Furanoterpenoids from *Siphonochilus aethiopicus. Phytochemistry*, **2002**, *59*, 405. https://doi.org/10.1016/s0031-9422(01)00402-2
23. C. A. Lategan, W. E. Campbell, T. Seaman, J. Peter, P. J. Smith. The bioactivity of novel furanoterpenoids isolated from *Siphonochilus aethiopicus. J. Ethnopharmacol.*, **2009**, *121*, 92. https://doi.org/10.1016/j.jep.2008.10.007
24. A. M. Viljoen, B. Demirci, K. H. C. Bas¸e, B. -E. Van Wyk. Essential oil composition of the roots and rhizomes of *Siphonochilus aethiopicus. South Afr. J. Bot.*, **2002**, *68*, 115. https://doi.org/10.1016/S0254-6299(16)30467-7
25. G. Fouche, S. van Rooyen, T. Faleschini. *Siphonochilus aethiopicus*, a traditional remedy for the treatment of allergic asthma. *Int. J. Gen. Med.*, **2013**, *3*, e6. https://api.semanticscholar.org/CorpusID:55860467
26. Y. Naude, R. Makuwa, V. Maharaj. Investigating volatile compounds in the vapour phase of (1) a hot water infusion of rhizomes, and (2) rhizomes of *Siphonochilus aethiopicus* using head space solid phase microextraction and gas chromatography with time of flight mass spectrometry. *South Afr. J. Bot.*, **2016**, *106*, 144. https://doi.org/10.1016/j.sajb.2016.07.006
27. R. E. Simone, M. Russo, A. Catalano, G. Monego, K. Froehlich, V. Boehm, P. Palozza. Lycopene inhibits NF-KB-mediated IL-8 expression and alters redox and PPARγ signaling in cigarette smoke-stimulated macrophages. *PLoS One*, **2011**, *6*, 1. https://doi.org/10.1371/journal.pone.0019652
28. S. K. Manna, G. T. Ramesh. Interleukin-8 induces nuclear transcription factor-KB through a TRAF-6 dependent pathway. *J. Biol. Chem.*, **2005**, *280*, 7010. https://doi.org/10.1074/jbc.M410994200
29. T. L. Chuck, P. J. McLaughlin, M. N. Arizzi-LaFrance, J. D. Salamone, M. Correa. Comparison between multiple behavioral effects of peripheral ethanol administration in rats: Sedation, ataxia, and bradykinesia. *Life Sciences*, **2006**, *79*, 154. https://doi.org/10.1016/j.lfs.2005.05.045

REVIEW ARTICLE

Theranostic Potential of Quantum Dots: From Imaging to Therapy

Pratibha Chahal[a] , Ajit Kumar[a] , and Avinash Singh[a]*

[a] Department of Chemistry, SRM University Delhi-NCR, Sonepat, Haryana, 131029, India
*Correspondence: avinash.s@srmuniversity.ac.in

Abstract: The combination of nano-biotechnology advances the biomedical field, opening up groundbreaking opportunities for disease diagnosis, monitoring and treatment. Quantum dots (QDs) are at the leading edge of this innovation, known for their exceptional physicochemical qualities and customizable optoelectronic features. These luminous nanoparticles have become invaluable in theranostics by offering a unique combination of diagnostic and therapeutic capabilities. This review offers a comprehensive analysis of QDs, emphasizing their cytotoxicity, imaging potential, and applications in targeted drug delivery, photothermal therapy (PTT), and photodynamic therapy (PDT). By assessing their potential and limitations, we aim to harness QDs to reshape precision medicine and drive advancements in healthcare.
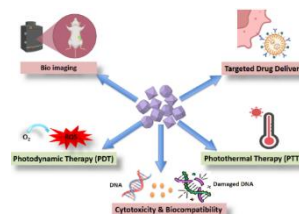
Keywords: *QDs, theranostic, toxicity*

Contents

1. Introduction

Semiconductor quantum dots (QDs) have continued to captivate the scientific community in recent decades, with their unique optoelectronic properties and versatility making them a prime candidate for a wide range of applications, including theranostics.[1,2] Theranostics, derived from the words "therapeutics" and "diagnostics," is an innovative field that combines diagnostic and therapeutic functionalities into a single nanoplatform, ushering in a new era of personalized medicine[3]. In oncology, QDs have shown immense promise as theranostic agents. Their tunable emission spectra, high photostability, and ability to be functionalized with targeting moieties have made them valuable tools for cancer detection, imaging, and treatment.[3] For instance, QDs have been utilized for the simultaneous diagnosis and monitoring of tumour response to chemotherapy, allowing for timely adjustments to the treatment regimen.[4] Furthermore, the development of multifunctional quantum dot-based nanocomposites has paved the way for the integration of both imaging and therapeutic capabilities. By combining QDs with drug-delivery systems or photosensitizers, these nanoplatforms can provide a comprehensive approach to cancer management, enabling early detection, targeted drug delivery, and photo-induced tumour ablation.[5] QDs have various applications (fig.1) in fields like photothermal therapy (PTT),[6] chemotherapy,[7] and photodynamic therapy (PDT),[8] along with techniques such as photoacoustic imaging (PAI),[9] fluorescence imaging,[10] biosensing,[11] and magnetic resonance imaging (MRI).[12]

Pratibha Chahal graduated from Maharshi Dayanand University in Rohtak in 2020 with a master's degree in chemistry, specialising in physical chemistry. She demonstrated academic excellence by being eligible for national and state-level exams such as the CTET (2023), HTET (2022), and Net JRF (2022). She is now working with Dr. Avinash Singh at SRM University in Delhi-NCR, Sonepat, to complete her PhD. Her areas of interest are nanotechnology and semiconductor QDs.

Dr. Ajit Kumar is currently working as a Professor and Head of the Department of Chemistry, SRM University Delhi-NCR, Sonepat Haryana. He obtained his Ph.D. degree from Faculty of Medical Sciences, University of Delhi in 2006. His research interest is post translational modifications of proteins and related biological implications. He has been credited to unravel acetyl transferase function of calreticulin, a Ca binding protein and has extensively studied aflatoxin-B1 induced genotoxicity and carcinogenicity

Dr. Avinash Singh received his PhD from the Radiation & Photochemistry Division of the Bhabha Atomic Research Centre in Mumbai, India, in 2018. He had previously completed his BSc (Hons) and MSc in Chemistry at Banaras Hindu University. He is currently employed with SRM University Delhi-NCR, Sonepat, as an Assistant Professor in the Chemistry Department. His research areas of interest are photochemistry, radiation chemistry, and semiconductor nanomaterials.
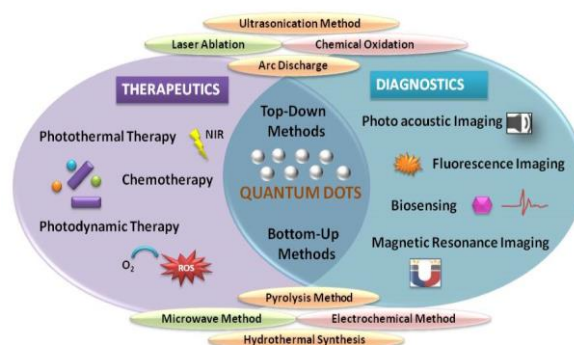
Figure 1: *Theranostic applications of QDs along with various synthetic methods*

Table 1: *QDs with their sizes, synthetic methods, capping agents and theranostic applications*

QD Type	Size (nm)	Synthetic Method	Capping Agent	Theranostic Applications
CdSe QDs	3.5–5.8	Wet chemical method	Trioctylphosphine (TOP) and oleic acid (OA)	ROS-mediated apoptosis, fluorescence imaging, gastric cancer therapy
CdZnSe QDs	21 ± 7	Hot injection	Gallic acid/Alginate	Drug delivery (BA, C2), enhanced fluorescence imaging
CQDs (Orange Juice)	~12	Hydrothermal	—	ROS-induced apoptosis in HCT-116 cells, bioimaging
CQDs (Hibiscus)	~ 12	Microwave-assisted	Hibiscus *rosa-sinensis* leaf extract	Wound healing, anti-inflammatory, antimicrobial
CQDs (Gandha Prasarini)	2-3.5	Hydrothermal	*Gandha Prasarini* leaves	Fluorescent tartrazine sensing, antibacterial activity
CQDs	~2–10	Hydrothermal	Intrinsic N-containing functional groups	NIR-triggered PTT in HeLa and MCF7 cells
GQDs	~1–10	Green/microwave/top-down	Poly-L-lysine, Au nanostars	Brain cancer therapy, immune modulation, PDT, PTT, radiotracer imaging
AIS QDs	< 8	One-step aqueous	2MPA, PEI/2MPA	ALA-based PDT, colon cancer therapy, fluorescence imaging
SiQDs@DMSNs	140–300	One-pot synthesis	DMSNs	Bioimaging, anti-counterfeiting, fluorescence stability
Chiral SiQDs	~2–10 (core) ~10–20 (hydrodynamic size)	Hydrothermal	KYF peptide	ONOO⁻ detection in inflammation and cancer diagnostics
CuInSe$_2$@ZnS:Mn QDs	~71 (DLS), ~5–10 (core)	Hot injection	ZnS shell	NIR-II/MRI imaging, PTT, immune activation, anti-tumor therapy

Recent advancements in the field of quantum dot-based theranostics have also extended beyond oncology, with potential applications in other disease areas, such as neurological disorders and cardiovascular diseases.[13] Mazahir *et al.*[14] reviewed the theranostic potential of bioinspired QDs (BQDs) in cancer treatment, highlighting their superior solubility, low toxicity, biocompatibility, and targeted action. They emphasized BQDs' unique features like photoluminescence, photothermal effect, singlet oxygen and H_2S generation, while also addressing existing challenges in their clinical application. Ho *et al.*[15] summarized the theranostic potential of QDs as multifunctional platforms for imaging and drug delivery while noting existing challenges.

The synthesis of QDs is generally categorized into two primary strategies: the top-down[16] and bottom-up[17] approaches. In the top-down method,[18] breaks down larger bulk materials into nanoscale QDs using techniques like laser ablation, chemical oxidation, arc discharge or ultra-sonic method. Though effective, this method often involves high costs and complex setups. The bottom-up method,[19] on the other hand, builds QDs from smaller precursors using simpler, cost-effective methods like, hydrothermal synthesis, electrochemical method, combustion or microwave irradiation. This method is not only cost-effective and scalable but also offers the flexibility needed for various real-world applications, from advanced drug delivery systems to cutting-edge diagnostic tools, contributing to its increasing popularity in both research and industry. The theranostic applications of the QDs depend upon its material, particle size, capping agents used and the method of synthesis (see table-1).

After synthesis, QDs are characterized using techniques such as high-resolution transmission electron microscopy (HRTEM) for morphology, selected area electron diffraction (SAED) and X-ray diffraction (XRD) for crystallinity, UV-Vis and photoluminescence (PL) spectroscopy for optical properties, and Fourier-transform infrared spectroscopy (FTIR) for surface functional group, ensuring their quality and functionality for biomedical applications[20]. When comparing the toxicity levels of semiconductor QDs, binary QDs stand out as the most hazardous. This stems from their composition, which often includes toxic heavy metals like Lead (Pb), Cadmium (Cd), and Mercury (Hg). The harmful effects of these elements on both health and the environment restrict the use of binary QDs, particularly in biomedicine and consumer products.[21,22] In contrast, ternary QDs, often made from less harmful elements like Copper (Cu), Indium (In), and Sulfur (S) or Selenium (Se), for example, $CuInS_2$[23] and CdZnSe[24] show much lower toxicity. Their advantageous properties make them viable alternatives to traditional binary QDs, enabling use in various fields without the risks associated with heavy metals[10] and have piqued interest for their adjustable optical characteristics and reduced toxicity, which makes them highly compatible with biological applications like drug delivery and imaging.[25] The toxicity of quaternary QDs can fluctuate based on their elemental composition. While some may exhibit low toxicity, akin to ternary QDs, the incorporation of specific metals could raise potential health risks. Nonetheless, many quaternary QDs are crafted to boost performance while keeping toxicity at a minimum.[26] Because of their safer profile, ternary QDs are frequently chosen for sensitive applications, highlighting a movement towards more sustainable materials in nanotechnology.

2. Toxicity of Semiconductor QDs

The possible cytotoxicity of semiconductor QDs remains a significant issue, and understanding the underlying mechanisms is essential for their safe and effective application in theranostic. One of the primary mechanisms of QD-induced cytotoxicity is

generating reactive oxygen species (ROS).[27] Semiconductor QDs, particularly those composed of heavy metal elements, can undergo photocatalytic reactions, producing superoxide radicals, hydroxyl radicals and hydrogen peroxide. These ROS can generate oxidative stress within cells, causing damage to cellular macromolecules (fig. 2), such as DNA, proteins, and lipids, ultimately leading to cell death. The interaction of QDs with cell membranes plays a role in their toxicity. Smaller QDs can enter cells more readily, accumulate in organelles, and interfere with regular cellular functions. Additionally, QD exposure can induce inflammatory reactions in tissues, worsening tissue damage and increasing overall toxicity. Carbon-based,[28] silicon-based,[29,30] and biomolecule-based ternary I-III-VI QDs have emerged as promising alternatives with reduced toxicity profiles. These novel designs aim to preserve the desirable optical and semiconductor properties of QDs while mitigating their inherent toxicity. Some strategies are used to control the toxicity of QDs including core/shell structure,[31] surface modification,[32] biomolecule,[33] and green synthesis methods.[34]
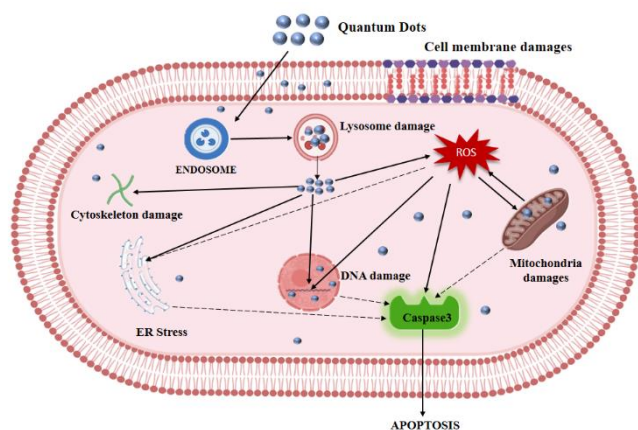
Figure 2: *The mechanism of cytotoxicity of Quantum Dots*

3. Cadmium-based QDs

Cadmium-based QDs are recognized for their excellent photoluminescence and therapeutic properties, making them useful in nanotheranostic applications. Nonetheless, their application is frequently constrained by safety issues, mainly stemming from the release of (Cd^{2+}).[35] Multimodal nanoparticles combining GZCIS/ZnS QDs, mesoporous silica, and gold nanoparticles are designed as targeted therapeutic carriers for colorectal cancer (CRC). These nanoparticles, which carry the chemotherapy drug epirubicin and are engineered to specifically target CRC cells, exhibit selective cytotoxicity towards cancer cells and enhanced anti-tumour effects in animal studies. This approach offers the potential for more effective cancer treatment and imaging with reduced side effects.[7] Bimodal nanoprobes were developed by combining CdTe QDs with thiolated GdDOTA complexes for optical and MRI imaging. These nanoprobes showed enhanced fluorescence and improved MRI contrast, with r1 values 69% higher than clinical GdDOTA, making them promising for imaging applications.[36] Huong *et al.*[37] synthesized CdSe QDs, sized 3.5-5.8 nm with strong emission peaks from 585-630 nm using the wet chemical method. Cytotoxicity tests on HepG2 liver cancer cells revealed cell cycle arrest in S and G0/G1 phases and apoptosis induced by ROS generation. Among three QDs sizes, CdSe2 (4.7nm) showed the strongest anti-cancer activity against AGS stomach cancer cells as compared to CdSe1 (3.5nm) and CdSe3 (5.4nm), with effective concentrations between 5 and 20 µg/mL, offering potential for gastric cancer therapy.

4. Carbon QDs

Carbon QDs (CQDs), known for their outstanding optical properties, high quantum yield, strong absorption, low toxicity, and excellent biocompatibility, hold great potential for cancer treatment in various applications, including targeted drug delivery to cancer cells, tumour imaging, and therapies like PTT and PDT.[38] Recent developments in green synthesis have attracted considerable attention for producing low-cost and environmentally friendly CQDs, addressing issues of toxicity and avoiding the use of harmful chemicals.[39,40] Natural resources such as waste biomass,[41,42] bamboo leaves,[43,44] orange juice,[45] lemon juice,[46] microorganism,[47] milk,[48] tulsi leaves,[49] red lentils,[50] aloe vera,[51] almond resin,[52] egg,[53] turmeric[54] and neem leaves[55] etc. have been explored for eco-friendly synthesis of CQDs. CQDs were prepared from orange juice through a hydrothermal synthesis approach and combined with silver nanoparticles to form CQD/Ag heterostructures, which exhibit strong photoluminescence, low toxicity to healthy cells, effective cellular uptake, bioimaging capability, and significant anticancer effects in human colorectal cancer (HCT 116) cells at 6 µg/mL through a ROS-mediated mitochondrial apoptosis pathway involving Akt (RAC-α serine/threonine-protein kinase).[56] Additionally, the bio-fabricated CQDs from Mesosphaerum suaveolens using microwave-assisted approach extracts demonstrated anticancer activity against MDA-MB-231 breast cancer cells at a concentration of 6 µg/mL, showcasing their potential for cancer treatment and as a theranostic agent for cancer diagnosis and therapy.[57] Using the microwave-assisted method, CQDs extracted from *Hibiscus rosa-sinensis* leaves showed strong fluorescence, wound healing, anti-inflammatory properties, and effectiveness against *K. pneumoniae* and *B. Cereus* bacteria. They inhibited COX-2 and regulated inflammatory cytokines, with excellent biocompatibility, making them promising for therapeutic applications in wound healing and infection treatment.[58] Activated carbon nanoparticles (ANs) from coconut shells, loaded with gadodiamide (Gd@PANs), efficiently generate hydroxyl radicals for chemodynamic therapy (CDT) in cancer cells and

exhibit 45.20% photothermal conversion efficiency for PTT. They also enable T1-MRI imaging, combining diagnosis and treatment.[12] N,S-doped CDs derived from Gandha Prasarini leaves exhibited green fluorescence and detected tartrazine with a 0.18 µM detection limit and 92–110.2% recovery in honey and soft drinks. They also showed strong antibacterial effects against harmful bacteria by damaging their membranes, without harming human red blood cells, highlighting their dual role in both diagnostics and therapy, making them promising for biomedical applications such as bacterial infection treatment and targeted detection.[59] CQDs synthesized from citric acid with urea and ammonium fluoride showed strong NIR emission at 808 nm. The ammonium fluoride-based CDs (MF) had better NIR absorption and photothermal efficiency, effectively killing HeLa and MCF7 cancer cells under NIR irradiation, while both types displayed excellent biocompatibility and caused no toxicity or tissue damage in mice, indicating their potential for NIR-triggered cancer treatment.[60] However, high-purity CDs were synthesized from graphite via pulse electrolysis, with a concentration of 500 µg/mL showed a photothermal conversion efficiency of 64.3% under NIR irradiation, raising the temperature to 82.2°C. The CDs were absorbed by HepG2 cells, decomposed H_2O_2, and induced apoptosis. In vivo studies indicated their potential in PAI and guiding tumour treatment, making them a promising tool for cancer diagnosis and therapy.[9] Curcumin-based carbon nanodots as discussed by Rai *et al.*[61] are small, water-soluble, biocompatible, and effective against pathogenic microbes. They can be used for early diagnosis, bioimaging, and as carriers for antimicrobial drugs. Wu *et al.*[62] developed curcumin-quaternized CQDs (Q-CQDs) with stronger antibacterial properties than natural curcumin. The Q-CQDs damage bacterial membranes, generate ROS, and lead to bacterial death. In mouse wound infection models, they reduced bacterial growth, decreased inflammation, and enhanced healing. These findings suggest that Q-CQDs could be an effective antibacterial agent for treating infections and promoting wound healing. C_5N_5 QDs with piezoelectric effects demonstrated efficient H_2O_2 production at a rate of 918.4 µM/h, with a 2.6% efficiency in converting solar energy into chemical energy under low light conditions (0.1 sun). It enabled effective sono-photochemodynamic cancer therapy by producing reactive intermediates essential for tumour treatment and supporting diagnostic imaging[63]. Broccoli-based carbon QDs (BCQDs), synthesized using a simple hydrothermal process, demonstrate significant promise as a PDT agent. These BCQDs effectively produce singlet oxygen ($^1O_2$) when exposed to 660 nm light and trigger germline apoptosis in *C. elegans* via the cep-1/p53 pathway. This research positions BCQDs as an effective PDT agent and presents *C. elegans* as a useful model for rapid PDT assessment.[8] Liu *et al.*[6] derived CDs from osmanthus fragrans fruits demonstrated great biocompatibility, 46.7% photothermal conversion efficiency under 808 nm light, and effective cell killing in HeLa cells, indicating their potential for PTT. Rutin-loaded CDs (R-CDs) effectively killed *methicillin-resistant Staphylococcus aureus* (MRSA) at a MIC of 32 µg/mL, causing membrane damage and exhibiting strong antibacterial effects in a mouse model. They also showed good biocompatibility, indicating their potential as an alternative to traditional antibiotics.[64] Khan *et al.*[65] developed blue-emitting CDs (Du-CDs) from *Diaporthe unshiuensis* YSP3 extract, which displayed strong antimicrobial activity against bacteria and fungi at low MICs. Du-CDs also prevented biofilm formation, damage cell membranes, and supported wound healing in a mouse model, highlighting their potential as an effective and biocompatible antimicrobial agent. Mg/N-doped CQDs were synthesized with an impressive quantum yield of 89.44%, and modified with hyaluronic acid and folic acid to specifically target cancer cell delivery of epirubicin (CQD-FA-HA-EPI). In vitro studies demonstrated enhanced toxicity and cellular uptake in 4T1 and MCF-7 cell lines. Additionally, in vivo experiments with breast cancer mouse models showed a significant reduction in tumour size and minimal organ damage, indicating the potential of CQD-FA-HA as an effective multifunctional drug delivery system.[66]

5. Graphene QDs

Graphene QDs represent a distinctive type of carbon nanomaterial, defined by their quasi-zero-dimensional structure and derived from graphene, which preserves its planar configuration. The quasi-zero-dimensional structure of GQDs means they are small graphene segments with an extensive surface area relative to their volume, offering excellent chemical reactivity and biocompatibility. Their strong photoluminescence and tunable emission make them highly appropriate for bioimaging, drug delivery, and biological molecule detection.[67] These biocompatible nanoparticles are capable of crossing the blood-brain barrier, offering promising potential for the treatment of brain diseases like glioblastoma,[68] Parkinson's disease,[69] and Alzheimer's disease.[70] Moreover, GQDs boosted the efficacy of chemotherapy even at subtherapeutic levels, including 1 µM doxorubicin and 100 µg/mL temozolomide, by enhancing drug delivery and reducing tumour growth in 3D glioblastoma models.[71] In contrast, CQDs are produced from a wide range of carbon sources, including organic substances and carbon soot, typically leading to a more amorphous structure. These differences in their origins and structural characteristics result in notable variations in their properties, with GQDs offering better electrical conductivity and stability compared to CQDs.[72] Deng *et al.*[73] studied the toxicity of four types of GQDs on zebrafish embryos. A-GQDs led to developmental problems, such as reduced survival, heartbeat rates, and more malformations at concentrations of 100 and

200µg/mL. mRNA analysis revealed that all GQDs influenced ion channels, with A-GQDs particularly disrupting the coagulation pathway. Xia *et al.*[74] introduce a technique to enhance cancer treatment by using GQDs to deliver microRNA155 (miR) to monocytes. This strategy helps bypass the tumour's immune defences by reprogramming harmful immune cells into those that target the tumour, improving tumour eradication. A novel fluorescence-based method has been developed for detecting *Carcinoembryonic Antigen (CEA)* using poly-l-lysine-functionalized GQDs (PLL-GQDs) made from peanut shell waste. This eco-friendly technique offers a high sensitivity limit of detection 1.19pg/mL and 98.32% accuracy in real samples, with potential applications in bioimaging and therapy.[75] Tehrani *et al.*[76] created ^{99m}Tc-labeled GQDs for glioma tumour detection. The GQDs demonstrated stability with a radiochemical yield above 97% and efficiently targeted tumour sites in animal models. Scintigraphy imaging revealed notable accumulation in both glioma tumours and organs such as the kidneys, indicating their potential as a radiotracer for glioma diagnosis. Soleimany *et al.*[77] developed a nanohybrid combining riboflavin-conjugated GQDs (Rf-N,S-GQDs) and thiolated chitosan-coated gold nanostars (AuNS-TCS) for dual PDT and PTT. Utilizing a single low-power laser (200 mW·cm^{-2}, 760 nm), the system demonstrated increased singlet oxygen production, efficient thermal effects, and enhanced tumour destruction compared to standalone treatments. Its notable effectiveness in 3D tumour models emphasizes its potential for treating solid tumours and progressing toward clinical applications. Lung cancer, a leading cause of death, faces challenges in early detection and treatment. GQDs show promise in therapies like photolytic therapy, hyperthermia therapy, and drug delivery, offering the potential for improved lung cancer management.[78] Ku *et al.*[79] investigated three types of GQDs on breast cancer cells such as MCF-7, MDA-MB-231, T-47D, and BT-474, at concentrations ranging from 2.5 to 40 µg/L. All GQDs reduced cell viability, with ortho-GQDs specifically inducing arrest in the G2/M phase of cell division. Treatment also led to an increase in the apoptotic proteins p21 (1.41-fold) and p27 (4.75-fold). These GQDs show potential for treating estrogen receptor-positive breast cancer. Organotin (IV) complexes are effective in cancer therapy but are limited by their poor water solubility. To address this, nitrogen-doped GQDs were modified with organotin-based compounds and 4-formylbenzoic acid (FBA). The resulting NGQDs-FBA-Sn system demonstrated significant toxicity against breast cancer cells (MDA-MB-231), with IC$_{50}$ value of 0.10 µM (Sn2) and 0.41 µM (Sn1), while showing minimal effect on non-cancerous HEK293T cells (IC$_{50}$ of 0.27µM and 0.87 µM respectively). Additionally, the system allowed for fluorescence imaging, suggesting efficient cellular uptake and drug release.[80] Khose *et al.*[81] synthesized N-GQDs from discarded materials like arjuna bark and melamine sponge using microwave treatment and used for bio-imaging of MDA-MB-231 breast cancer cells, successfully

staining them in blue fluorescence. The N-GQDs also showed fluorescence quenching in the presence of H$_2$O$_2$, allowing toxin detection. With 70% cell survival at a concentration of approximately 1.8 mg/ml, the N-GQDs showed high biocompatibility, highlighting their potential for imaging and sensing applications in cancer studies. The incorporation of GQDs into polycaprolactone (PCL) scaffolds significantly enhanced mechanical strength and bioactivity, with 3 wt% showing optimal performance, suggesting their potential for theranostic use in tissue regeneration[11]. Najafi *et al.*[82] developed a pH-responsive drug delivery system by combining Agarose, GQDs, and α-Fe$_2$O$_3$ in a hydrogel nanocomposite for the controlled release of the highly effective anti-cancer compound Quercetin. The nanoparticles measured an average size of 279.04 nm and had a zeta potential of 52.8 mV. Incorporating α-Fe$_2$O$_3$ improved the drug loading and encapsulation efficiencies to 47% and 86.25%, respectively. In vitro testing on HepG2 cells demonstrated enhanced anticancer activity, suggesting the system's promising potential for cancer therapy. Zhang *et al.*[10] introduced a new treatment for liposarcoma using graphene quantum dot-based nanoprobes. The nanoprobes, made of gadolinium (Gd^{3+}), IR820 dye, and a heat shock protein inhibitor (17-AAG), enhance mild photothermal therapy and enable effective T1-MRI and near-infrared fluorescence imaging. In vivo studies revealed that the nanoprobes had low toxicity, were efficiently excreted, and lowered heat shock protein expression in tumour cells, improving the therapeutic effect.

6. Silver QDs

Silver-based QDs, such as Ag$_2$S, Ag$_2$Se, Ag$_2$Te, have shown significant potential in theranostic applications due to their unique optical properties and biocompatibility. These QDs emit in the second near-infrared window (NIR-II, 900-1700nm), which allows for deeper tissue penetration and reduced background fluorescence, making them ideal for bioimaging and therapeutic applications.[83] Ag$_2$S QDs combined with ALA and Cetuximab achieved over 80% cell death in colorectal cancer cells using only 0.17 mM ALA. When paired with 5-fluorouracil (5FU), the treatment resulted in nearly complete cell death at 0.35 mM ALA and 15 µg/mL 5FU. The QDs also improved photothermal therapy and reduced the required dose of methotrexate from 10 µg/mL to 0.21 µg/mL for targeted killing of cancer cells. This approach is being studied for more effective treatments, including for breast cancer.[84] Silver–indium–sulfide QDs (AIS QDs) were produced using a simple method, achieving high quantum yields and long-lasting stability. Cationic (AIS-PEI/2MPA) and anionic (AIS-2MPA) QDs, when loaded with 5-aminolevulinic acid (ALA), enhanced PDT in colon

cancer cells by increasing ROS production, leading to significant cell death. The cationic AIS QDs notably reduced the IC50 for ALA to 0.01 mM, demonstrating AIS-2MPA's potential as a promising theranostic agent for drug delivery and imaging.[85]

7. Alloy QDs

Alloy QDs can be engineered to reduce the toxicity associated with heavy metals in traditional QDs. This is particularly significant for clinical applications where ensuring biocompatibility is a critical requirement. For example, CdZnSeS QDs were prepared using the hot injection method, with a quantum yield of 85% were stabilized in gallic acid/alginate matrices. These QD-based carriers, loaded with anticancer drugs such as ceranib-2 (C2) and betulinic acid (BA), demonstrated enhanced therapeutic efficiency. In vitro results revealed that BA-loaded carriers achieved an IC50 of 8.76µg/mL for HL-60 cells, a threefold improvement over free BA, while C2-loaded carriers displayed IC50 values of 2.24µg/mL for HL-60 and 7.37µg/mL for PC-3 cells, showcasing their potential for advanced cancer therapies.[86] $CuInSe_2$@ZnS:Mn QDs were developed with high near-infrared (NIR)-II fluorescence efficiency (31.2%) and MRI contrast, enabling accurate detection of small metastases in 4T1 breast cancer tumours. These QDs showed a tendency to accumulate in tumours, and upon exposure to NIR light, they produced heat and radicals that destroyed cancer cells and triggered an immune response. This method successfully prevented tumour regrowth in 80% of mice.[87]

8. Silicon QDs

Silicon QDs (SiQDs) are becoming promising theranostic agents because of their unique features, such as biocompatibility, adjustable photoluminescence, and capability for multimodal imaging and therapy. Traditional SiQDs encounter issues such as complicated preparation, inconsistent quality, low water solubility, and aggregation-caused quenching (ACQ), which lowers their brightness. However, their key benefit is biocompatibility, as silicon is less toxic than QDs made from heavy metals, reducing potential in vivo risks.[88] SiQDs are being increasingly used to develop high-performance fluorescent biosensors for detecting chemical and biological substances. These biosensors leverage the unique photoluminescent properties of SiQDs, which offer excellent optical stability and biocompatibility. Recent developments include the creation of water-soluble SiQDs and the development of biosensors that display photoluminescence variations in response to analytes.[89] Huang *et al.*[90] introduced SiQDs@DMSNs, a novel fluorescent material consisting of SiQDs encapsulated within dendritic mesoporous silica (DMSNs), with particle sizes ranging from 140 to 300 nm. These particles emitted blue light under UV exposure, with sodium salicylate (NaSAL) playing a key role in their formation. SiQDs@DMSNs exhibited strong fluorescence, high water solubility, stability, and successfully avoided ACQ. They are suitable for

applications in biosensors, nanomedicine, imaging, fingerprint identification, and anti-counterfeiting. Chiral SiQDs-(K/P) ox were developed for the precise detection of ONOO⁻, a molecule involved in inflammation and cancer. These SiQDs, created through a one-step hydrothermal method with KYF as a precursor, have a broad emission range (380–700 nm) and peak at 490 nm. SiQDs-(K/D-P)ox demonstrates a high quantum yield (47.66%), while SiQDs-(K/L-P)ox offers a long fluorescence lifetime (27.219 µs) and strong biocompatibility. SiQDs-(K/L-P)ox can effectively detect ONOO– in cells via fluorescence quenching, making it a valuable tool for detecting inflammation in cancer cells.[91] Moreover, Pei *et al.*[92] developed SiQDs that emit blue fluorescence and have antibacterial activity. The SiQDs inhibited the growth of *E. coli* (0.45 mg/mL) and *S. aureus* (0.25 mg/mL) by damaging their cell walls. A fluorescence sensor for tetracycline (TC) detection had a limit of 0.0006µmol/L and a range of 0.001 to 0.010 µmol/L. The sensor successfully detected TC in honey with nearly 100% recovery. A fluorescent probe, SiQDs@PDA, was created by attaching dopamine to silicon QDs, emitting at 530 nm with a quantum yield of 44.7%. This probe can interact with various molecules and was employed to selectively label and image gram-positive and gram-negative bacteria, along with their biofilms. Due to the distinctive properties of the SiQDs@PDA is highly resistant to photobleaching, making it a valuable tool for studying microbial research.[93] Liang *et al.*[94] focused on enhancing the optical properties of SiQDs and CQDs by encapsulating them in polyhedral oligomeric silsesquioxanes (POSS). The resulting green-emitting POSS-G-CNDs, red-emitting POSS-R-CNDs, and blue-emitting POSS-SiQDs showed excellent luminescence, biocompatibility, and the ability to penetrate cell membranes. This makes them highly suitable for multicolour intracellular imaging and offers potential applications in clinical diagnostics and bioimaging. Researchers have made significant progress in synthesizing multi-emissive SiQDs, which can emit multiple colours depending on the excitation wavelength. This property is particularly useful for biological and analytical applications, as it allows for more precise and versatile detection methods. These SiQDs exhibit low toxicity to cells, high luminous efficiency, and strong resistance to photobleaching.[95]

9. Conclusion

This review provides information on the emerging theranostic potential of QDs, emphasizing their unique optical tunability, diverse synthesis strategies, biomedical applications, and the critical challenges associated with toxicity. While Cd-based QDs have demonstrated considerable promise, their clinical translation is hindered by toxicity concerns

related to their composition, surface coatings, and administration routes. Studies with other QDs like CQDs, GQDs, and silicon QDs are actively focusing on developing biocompatible surface coatings and using naturally sourced, less toxic materials to reduce toxicity. Another limitation is the lack of robust clinical data on the long-term safety and efficacy of theranostic systems. Extensive preclinical and clinical trials are necessary to establish the safety and clinical utility of these nanomaterials before they can be widely adopted in the clinic. Ongoing research efforts are focused on enhancing biocompatibility and reducing the toxicity of QD systems, improving tumour targeting strategies, and establishing robust clinical data on their safety and efficacy. The future looks bright for multifunctional QDs that can both diagnose and treat diseases simultaneously, with artificial intelligence (AI) playing an important role in their development. AI enhances QDs by optimizing their synthesis, predicting toxicity, improving imaging accuracy, and enabling targeted drug delivery. This combination of AI and QDs is expected to change personalized medicine, making treatments safer, more effective, and specially designed for each patient. As these advancements continue, the theranostic applications of semiconductor QDs are poised to have a transformative impact on managing cancer and other diseases. As we advance these technologies and accumulate clinical data, the theranostic capabilities of semiconductor QDs are set to revolutionize the field of medicine. The combination of AI with eco-friendly, biocompatible QDs will pave the way for groundbreaking healthcare solutions, tackling both disease management challenges and promoting environmental sustainability.

Author Contribution Declaration

Miss Pratibha Chahal has conducted the literature survey, designed the images and written the manuscript. Dr. Ajit Kumar has given suggestion regarding the theranostic applications and has done the proofreading and editing. Dr. Avinash Singh has prepared the manuscript draft, designed the images and performed the proof reading. Attention! The authors have no financial conflict of interest to declare.

Data Availability Declaration

In this review, no new data was created or analyzed, and no primary research findings or software were used.

Acknowledgements

References

1. C. Zhu, Z. Chen, S. Gao, Ban L. Goh, I. B. Samsudin, K. W. Lwe, Y. Wu, X. Su. Recent advances in non-toxic quantum dots and their biomedical applications. *Prog. Nat. Sci.: Mater. Int.* **2019**, *29*, 628. https://doi.org/10.1016/j.pnsc.2019.11.007

2. R. M. Abdelgalil, S. N. Khattab, S. Ebrahim, K. A. Elkhodairy, M. Teleb, A. A. Bekhit, M. A. Sallam and A. O. Elzoghby. Engineered sericin-tagged layered double hydroxides for combined delivery of pemetrexed and ZnO quantum dots as biocompatible cancer nanotheranostics. *ACS Omega* **2023**, *8,* 5655. https://doi.org/10.1021/acsomega.2c07128

3. C. T Matea, T. Mocan, F. Tabaran, T. Pop, O. Mosteanu, C. Puia, C. Lancu, L. Mocan. Quantum dots in imaging, drug delivery and sensor applications. *Int. J. Nanomed.* **2017**, *12*, 5421. https://doi.org/10.2147/ijn.s138624

4. L. He, L. Zeng, X. Mai, C. Shi, L. Luo, T. Chen. Nucleolin-targeted selenium nanocomposites with enhanced theranostic efficacy to antagonize glioblastoma. *J. Mater. Chem. B* **2017**, *5*, 3024. https://doi.org/10.1039/C6TB03365B

5. N. S. Kulkarni, Y. Guererro, N. Gupta, A. Muth, V. Gupta. Exploring potential of quantum dots as dual modality for cancer therapy and diagnosis. *J. Drug Del. Sci. Tech* **2019**, *49*, 352. https://doi.org/10.1016/j.jddst.2018.12.010

6. S. Liu, H. Cui, J. Huang, B. Tian, J. Bao. Osmanthus-derived carbon dots for cell imaging and NIR photothermal therapy. *Mater. Lett.* **2024**, *377*, 137347. https://doi.org/10.1016/j.matlet.2024.137347

7. A. Abrishami, A. R. Bahrami, S. Nekooei, A. Sh. Saljooghi, M. M. Matin. Hybridized quantum dot, silica, and gold nanoparticles for targeted chemo-radiotherapy in colorectal cancer theranostics. *Commun. Biol.* **2024**, *7*, 393. https://doi.org/10.1038/s42003-024-06043-6

8. S. M. Elsherbiny, C. Shao, A. Acheampong, M. A. Khalifa, C. Liu, Q. Huang. Green synthesis of broccoli-derived carbon quantum dots as effective photosensitizers for the PDT effect testified in the model of mutant caenorhabditis elegans. *Biomater. Sci.* **2022**, *10*, 2857. https://doi.org/10.1039/D2BM00274D

9. S. Liu, J. Wang, X. Wang, Y. Guo, S. Guan, T. Zhang. Nucleus-targeted carbon dots as peroxidise nanozyme for photoacoustic imaging and phototherapy of tumour. *Colloids Surf. B Biointerfaces* **2024**, *239*, 113950. https://doi.org/10.1016/j.colsurfb.2024.113950

10. J. Zhang, P. Fan, Y. Shi, X. Huang, C. Shi, W. Ye, H. Tong, F. Shan, Z. Zhang. Near-infrared-mediated self-assembly of graphene quantum dot-based nanoprobes to silence heat shock protein expression for mild photothermal therapy in liposarcoma. A*CS Appl. Nano Mater.* **2023**, *6*, 16276. https://doi.org/10.1021/acsanm.3c02387

11. D. Meng, Y.-Hou, D. Kurniawan, R.-J. Weng, W.-H. Chiang, W. Wang. 3D-printed graphene and graphene quantum dot-reinforced polycaprolactone scaffolds for bone-tissue engineering. *ACS Appl. Nano Mater.* **2024**, *7*, 1245. https://doi.org/10.1021/acsanm.3c05225

12. G. Wu, B. Jiang, L. Zhou, A. Wang, S. Wei. Coconut-shell-derived activity carbon for NIR photo-activated synergistic photothermal-chemodynamic cancer therapy. *J. Mater. Chem. B* **2021**, *9*, 2447. https://doi.org/10.1039/D0TB02782K

13. Y. Hu, X. Wang, Y. Niu, K. He, and M. Tang. Application of quantum dots in brain diseases and

their neurotoxic mechanism. *Nanoscale Adv.* **2024**, *6*, 3733 https://doi.org/10.1039/D4NA00028E

14. F. Mazahir, R. Sharma, A. K. Yadav. Bioinspired theranostic quantum dots: paving the road to a new paradigm for cancer diagnosis and therapeutics. *Drug Discov. Today* **2023**, *28*, 103822 https://doi.org/10.1016/j.drudis.2023.103822

15. Y.-P. Ho and K. W. Leong. Quantum dot-based theranostics. *Nanoscale* **2010**, *2*, 60. https://doi.org/10.1039/B9NR00178F

16. Z. Chen, C. Zhao, X. Zhou, L. Xiao, Z. Li, Y. Zhang. A review of top-down strategies for the production of quantum-sized materials. *Small science* **2023**, *3*, 2300086 https://doi.org/10.1002/smsc.202300086

17. L. Shi, B. Wang, S. Lu. Efficient bottom-up synthesis of graphene quantum dots at an atomically precise level. *Matter* **2023**, *6*, 728. https://doi.org/10.1016/j.matt.2023.01.003

18. S. Yalshetti, B. Thokchom, S. M. Bhavi, S. R. Singh, S. R. Patil, B. P. Harini, M. Sillanpaa, J. G. Manjunatha, B. S. Srinath, R. B. Yarajarla. Microwave-assisted synthesis, characterization and in vivo biomedical applications of hibiscus rosa-sinensis linn.-mediated carbon quantum dots. *Sci Rep* **2024**, *14*, 9915. https://doi.org/10.1038/s41598-024-60726-y

19. P. Chahal, A. Goel, A. Singh. Recent development and challenges in metal chalcogenide dots: from material design strategies to applications. *Innov. Chem. Mater. Sustain.* **2024**, *1*, 30. https://doi.org/10.63654/icms.2024.01030

20. P. G. Balkanloo, K. M. Sharifi, and A. P. Marjani. Graphene quantum dots: synthesis, characterization, and application in wastewater treatment: a review. *Mater. Adv.* **2023**, *4*, 4272. https://doi.org/10.1039/D3MA00372H

21. X. Lin and T. Chen. A review of in vivo toxicity of quantum dots in animal models. *Int. J. Nanomed.* **2023**, *18*, 8143. https://doi.org/10.2147/IJN.S434842

22. O. A. Aladesuyi, T. C. Lebepe, R. Maluleke, and O. S. Oluwafemi. Biological applications of ternary quantum dots: a review. *Nanotechnol. Rev.* **2022**, *11*, 2304. https://doi.org/10.1515/ntrev-2022-0136

23. J. Ning, Z. Duan, S. V. Kershaw and A. L. Rogach. Phase-controlled growth of $CuInS_2$ shells to realize colloidal $CuInSe_2/CuInS_2$ core/shell nanostructures. *ACS Nano* **2020**, *14*, 11799. https://doi.org/10.1021/acsnano.0c04660

24. G. Mao, G. Wu, M. Chen, C. Yan, J. Tang, Y. Ma and X.-E. Zhang. Synthesis of dual-emitting CdZnSe/Mn:ZnS quantum dots for sensing the pH change in live cells. *Anal. Chem.* **2022**, *94*, 6665. https://doi.org/10.1021/acs.analchem.1c04811

25. B. M. May, M. F. Bambo, S. S. Hosseini, U. Sidwaba, E. N. Nxumalo, and A. K. Mishra. A review on I-III-VI ternary quantum dots for fluorescence detection of heavy metals ions in water: optical properties, synthesis and application. *RSC Adv.* **2022**, *12*, 11216. https://doi.org/10.1039/D1RA08660J

26. N. I.-Rodriguez, R. Munoz, J. A. Rodriguez, R. A. V.-Garcia, and M. Reyes. Integration of ternary I-III-VI quantum dots in light-emitting diodes. *Front. Chem.* **2023**, *11*, 1106778. https://doi.org/10.3389/fchem.2023.1106778

27. S. Nikazar, V. S. Sivasankarapillai, A. Rahdar, S. Gasmi, P S Anumol, M. S. Shanavas. Revisiting the cytotoxicity of quantum dots: an in-depth overview. *Biophys Rev* **2020**, *19*, 703. https://doi.org/10.1007/s12551-020-00653-0

28. A. Nair, J. T. Haponiuk, S. Thomas, S. Gopi. Natural carbon-based quantum dots and their applications in drug delivery: a review. *Biomed Pharmacother* **2020**, *132*, 110834. https://doi.org/10.1016/j.biopha.2020.110834

29. B. J. Furey, B. J. Stacy, T. Shah, R. M. Barba-Barba, R. Carriles, A. Bernal, B. S. Mendoza, B. A. Korgel and M. C. Downer. Two-photon excitation spectroscopy of silicon quantum dots and ramifications for bio-imaging. *ACS Nano* **2022**, *16*, 6023. https://doi.org/10.1021/acsnano.1c11428

30. A. Guleria, S. Neogy, D. K. Maurya, and S. Adhikari. Blue light-emitting Si quantum dots with mesoporous and amorphous features: origin of photoluminescence and potential applications. *J. Phys. Chem. C* **2017**, *121*, 24302. https://doi.org/10.1021/acs.jpcc.7b07283

31. W. A. A. Mohamed, H. A. E.-Gawad, S. Mekkey, H. Galal, H. Handal, H. Mousa, and A. Labib. Quantum dots synthetization and future prospect applications. *Nanotechnology Reviews* **2021**, *10*, 1926. https://doi.org/10.1515/ntrev-2021-0118

32. L. Hu, C. Zhang, G. Zeng, G. Chen, J. Wan, Z. Guo, H. Wu, Z. Yu, Y. Zhou, J. Liu. Metal-based quantum dots: synthesis, surface modification, transport and fate in aquatic environments and toxicity to microorganisms. *RCS Adv.* **2016**, *6*, 78595. https://doi.org/10.1039/C6RA13016J

33. A. Singh, A. Guleria, A. Kumar, S. Neogy, M. C. Rath. Saccharide capped CdSe quantum dots grown via electron beam irradiation. *Mater. Chem. Phy.* **2017**, *199*, 609. https://doi.org/10.1016/j.matchemphys.2017.07.062

34. L. J. Desmond, A. N. Phan and P. Gentile. Critical overview on the green synthesis of carbon quantum dots and their application for cancer therapy. *Environ. Sci.: Nano* **2021**, *8*, 848. https://doi.org/10.1039/D1EN00017A

35. D. Mo, L. Hu, G. Zeng, G. Chen, J. Wan, Z. Yu, Z. Huang, K. He, C. Zhang, M. Cheng. Cadmium-containing quantum dots: properties, applications, and toxicity. *Appl Microbiol Biotechnol* **2017**, *101*, 2713. https://doi.org/10.1007/s00253-017-8140-9

36. G. M. Albuquerque, R. M. Melo, S. D. Coiado, G. A. L. Pereira, G. Pereira. Nanoprobes based on quantum dots and Gd (III) complexes for dual optical and magnetic resonance imaging. *Mater. Lett.* **2024**, *371*, 136921. https://doi.org/10.1016/j.matlet.2024.136921

37. L. T. T. Huong, N. P. Hung, N. T. Ha, N. T. Luyen, N. T. Hien, N. X. Ca, N. T. M. Thuy. Chemically synthesized CdSe quantum dots induce apoptosis in AGS gastric cancer cells via ROS generation. *Nanoscale Adv.* **2025**, *7*, 572. https://doi.org/10.1039/D4NA00795F

38. P. Bhatia, T. Chaira, L. K. Gupta. Therapeutic applications of carbon quantum dots (CQDs): a review. *J. Inorg. Organomet. Polym* **2024**, 1574. https://doi.org/10.1007/s10904-024-03510-9

39. S. Sahana, A. Gautam, R. Singh, S. Chandel. A recent update on development, synthesis methods, properties and application of natural products derived carbon dots. *Nat. Prod. Bioprospect* **2023**, *13*, 51. https://doi.org/10.1007/s13659-023-00415-x

40. J. Dhariwal, G. K. Rao, D. Vaya. Recent advancements towards the green synthesis of carbon quantum dots as an innovative and eco-friendly solution for metal ion sensing and monitoring. *RCS Sustain.* **2024**, *2*, 11. https://doi.org/10.1039/D3SU00375B

41. S. Pandiyan, L. Arumugam, S. P. Srirengan, R. Pitchan, P. Sevugan, K. Kannan, G. Pitchan, T. A. Hegde, V. Gandhirajan. Biocompatible carbon quantum dots derived from sugarcane industrial wastes for effective nonlinear optical behavior and antimicrobial activity applications. *ACS Omega* **2020**, *5*, 30363. https://doi.org/10.1021/acsomega.0c03290

42. A. Kundu, B. Maity, S. Basu. Orange pomace-derived fluorescent carbon quantum dots: detection of dual analytes in the nanomolar range. *ACS Omega* **2023**, *8*, 22178. https://doi.org/10.1021/acsomega.3c02474

43. X. Yang, D. Wang, N. Luo, M. Feng, X. Peng, X. Liao. Green synthesis of fluorescent N,S-carbon dots from bamboo leaf and the interaction with nitrophenol compounds. *Spectrochim. Acta A Mol. Biomol. Spectrosc.* **2020**, *239*, 118462 https://doi.org/10.1016/j.saa.2020.118462

44. M. Z. Fahmi, A. Haris, A. J. Permana, D. L. N. Wibowo, B. Purwanto, Y. L. Nikmah, A. Idris. Bamboo leaf-based carvon dots for efficient tumour imaging and therapy. *RCS Adv.* **2018**, *8*, 38376. https://doi.org/10.1039/C8RA07944G

45. K. Kasirajan, M. Karunakaran, H. K. Choi. Synthesis of environmentally-friendly carbon quantum dots from orange juice for selective detection of Fe^{+3} ions, antibacterial activity, and bio-imaging applications. *J. Environ. Chem. Eng.* **2024**, *12*, 113535 https://doi.org/10.1016/j.jece.2024.113535

46. M. He, H. Wang, Y. Kong, Y. Xiao, W. Xu. Material and optical properties of fluorescent carbon quantum dots fabricated from lemon juice via hydrothermal reaction. *Nanoscale Res. Lett.* **2018**, *13*, 175 https://doi.org/10.1186/s11671-018-2581-7

47. S. A. Kousheh, M. Moradi, H. Tajik, R. Molaei. Preparation of antimicrobial/ultraviolet protective bacterial nanocellulose film with carbon dots synthesized from lactic acid bacteria. *Int. J. Biol. Macromol.* **2020**, *155*, 216. https://doi.org/10.1016/j.ijbiomac.2020.03.230

48. A. Kumar, I. Kumar, A. K. Gathania. Synthesis characterization and potential sensing application of carbon dots synthesis via the hydrothermal treatment of cow milk. *Sci. Rep.* **2022**, *12*, 22495 https://doi.org/10.1038/s41598-022-26906-4

49. K. Doshi, A. A. Mungray. Bio-route synthesis of carbon quantum dots from tulsi leaves and its application as a draw solution in forward osmosis. *J. Environ. Chem. Eng.* **2020**, *8*, 104174 https://doi.org/10.1016/j.jece.2020.104174

50. Z. M. S. H. Khan, R. S. Rahman, Shumaila, S. Islam, M. Zulfequar. Hydrothermal treatment of red lentils for the synthesis of fluorescent carbon quantum dots and its application for sensing Fe^{+3}. *Opt. Mater.* **2019**, *91*, 386. http://dx.doi.org/10.1016/j.optmat.2019.03.054

51. J. P. Malavika, C. Shobana, M. Ragupathi, P. Kumar, Y. S. Lee, M. Govarthanan, R. K. Selvan. A sustainable green synthesis of functionalized biocompatible carbon quntum dots from aloe barbadensis miller and its multifunctional applications. *Environ. Res.* **2021**, *200*, 111414 https://doi.org/10.1016/j.envres.2021.111414

52. P. K. Praseetha, R. I. J. Litany, H. M. Alharbi, A. A. Khojah, S. Akash, M. Bourhia, A. A. Mengistie, G. A. Shazly. Green synthesis of highly fluorescent carbon quantum dots from almond resin for advanced theranostics in biomedical applications. *Sci. Rep.* **2024**, *14*, 24435. https://doi.org/10.1038/s41598-024-75333-0

53. R. Zhong, C. Peng, L. Chen, N. Yu, Z. Chen. Egg white-mediated green synthesis of CuS quantum dots as a biocompatible and efficient 980 nm laser-driven photothermal agent. *RCS Adv.* **2016**, *6*, 40480. https://doi.org/10.1039/C5RA26801J

54. H. Yan, P. Li, F. Wen, Q. Guo, W. Su. Green synthesis of carbon quantum dots from turmeric holds promise as novel photosensitizer for in vitro photodynamic antimicrobial activity. *J. Mater. Res. Technol.* **2023**, *22*, 17. https://doi.org/10.1016/j.jmrt.2022.11.090

55. G. Gedda, Sri A. Sankaranarayanan, C. L. Putta, K. K. Gudimella, A. K. Rengan, W. M. Girma. Green synthesis of multi-functional carbon dots from medicinal plant leaves for antimicrobial, antioxidant, and bioimaging applications. *Sci. Rep.* **2023**, *13*, 6371 https://doi.org/10.1038/s41598-023-33652-8

56. S. Mishra, K. Das, S. Chatterjee, P. Sahoo, S. Kundu, M. Pal, A. Bhaumik, C. K. Ghosh. Facile and green synthesis of novel fluorescent carbon quantum dots and their silver heterostructure: an in vitro anticancer activity and imaging on colorectal carcinoma. *ACS Omega* **2023**, *8*, 4566. https://doi.org/10.1021/acsomega.2c04964

57. P. Kumar, A. Ravichandran, S. Durgadevi, V. Manikandan, K. S. Song, D. Prabhu, J. Jeyakanthan, D. Thirumurugan, G. Muthusamy. Microwave-assisted green synthesis of CQDs from mesosphaerum suaveolens extract: photocatalytic degradation and anticancer activity. *Waste Biomass Valor* **2024**, *15*, 6539. https://doi.org/10.1007/s12649-024-02643-9

58. S. Yalshetti, B. Thokchom, S. M. Bhavi, S. R. Singh, S. R. Patil, B. P. Harini, M. Sillanpaa, J. G. Manjunatha, B. S. Srinath, R. B. Yarajarla. Microwave-assisted synthesis, characterization and in vitro biomedical applications of hibiscus rosa-sinensis linn.-mediated carbon quantum dots. *Sci. Rep.* **2024**, *14*, 9915 https://doi.org/10.1038/s41598-024-60726-y

59. T. Mohanta, H. G. Behuria, S. K. Sahu, A. K. Jena, S. Sahu. Green synthesis of N,S-doped carbon dots for tartrazine detection and their antibacterial activity. *Analyst* **2023**, *148*, 5597. https://doi.org/10.1039/D3AN01609A

60. Y. Jin, H. Qiao, Y. Zhang, Y. He, S. Xie, Y. Gu, F. Lin. Facile microwave hydrothermal synthesis of citric acid-derived carbon dots for photothermal therapy of cancers under NIR irradiation. Carbon Lett. **2024**, 2233. https://doi.org/10.1007/s42823-024-00830-1

61. M. Rai, A. P. Ingle, G. Toros, J. Prokisch. Assessing the efficacy of carbon nanodots derived from curcumin on infectious diseases. *Expert Rev Anti Infect Ther* **2024**, *22*, 1107. https://doi.org/10.1080/14787210.2024.2409401

62. L. Wu, Y. Gao, C. Zhao, D. Huang, W. Chen, X. Lin, A. Liu, L. Lin. Synthesis of curcumin-quaternized carbon quantum dots with enhanced broad-spectrum antibacterial activity for promoting infected wound healing. *Biomater. Adv.* **2022**, *133*, 112608 https://doi.org/10.1016/j.msec.2021.112608

63. J. Ma, C. Peng, X. Peng, S. Liang, Z. Zhou, K. Wu, R. Chen, S. Liu, Y. Shen, H. Ma, Y. Zhang. H_2O_2 photosynthesis from H_2O and O_2 under weak light by carbon nitrides with the piezoelectric effect. *J. Am. Chem. Soc.* **2024**, *146*, 21147. https://doi.org/10.1021/jacs.4c07170

64. F. Lang, Q. Zhao, Z. Sun, M. Zhong, L. Xiong, Z. Hao. Rutin-loaded carbon dots for management of methicillin-resistant staphylococcus *ACS Appl. Nano Mater.* **2024**, *7*, 10902. https://doi.org/10.1021/acsanm.3c05774

Singh *et al.*

REVIEW ARTICLE

Innov. Chem. Mater. Sustain. **2025**, 2(1), 012-022

65. B. Khan, J. Zhang, S. Durrani, H. Wang, A. Nawaz, F. Durrani, Y. Ye, F.-G. Wu, F. Lin. Carbo-dots-mediated improvement of antimicrobial activity of natural products. *ACS Appl. Mater. Interfaces* **2024**, *16*, 47257. https://doi.org/10.1021/acsami.4c09689

66. N. Ziaee, N. Farhadian, K. Abnous, M. M. Matin, A. Khoshnood, E. Yaghoobi. Dual targeting of Mg/N doped-carbon quantum dots with folic and hyaluronic acid for targeted drug delivery and cell imaging. *Biomed. Pharmacother.* **2023**, *164*, 114971 https://doi.org/10.1016/j.biopha.2023.114971

67. A. Kalluri, B. Dharmadhikari, D. Debnath, P. Patra, C. V. Kumar. Advances in structural modifications and properties of graphene quantum dots for biomedical applications. *ACS Omega* **2023**, *8*, 21358. https://doi.org/10.1021/acsomega.2c08183

68. G. Perini, V. Palmieri, G. Ciasca, M. D'Ascenzo, J. Gervasoni, A. Primiano, M. Rinaldi, D. Fioretti, C. Prampolini, F. Tiberio, W. Lattanzi, O. Parolini, M. D. Spirito, M. Papi. Graphene quantum dots' surface chemistry modulates the sensitivity of glioblastoma cells to chemotherapeutics. *Int. J. Mol. Sci.* **2020**, *21,* 6301 https://doi.org/10.3390/ijms21176301

69. P. Kaliyaperumal, S. Renganathan, K. Arumugam, B. R. Aremu. Engineered graphene quantum dot nanocomposite triggers –synuclein defibrillation: therapeutics against Parkinson's disease. *Nanomed.: Nanotechnol. Biol. Med.* **2023**, *47*, 102608 https://doi.org/10.1016/j.nano.2022.102608

70. K. Tak, R. Sharma, V. Dave, S. Jain, and S. Sharma. Clitoria ternatea mediated synthesis of graphene quantum dots for the treatment of alzheimer's disease. *ACS Chem. Neurosci.* **2020**, *11,* 3741. https://doi.org/10.1021/acschemneuro.0c00273

71. G. Perini, V. Palmieri, G. Friggeri, A. Augello, M. D. Spirito, M. Papi. Carboxylated graphene quantum dots-mediated photothermal therapy enhances drug-membrane permeability, ROS production, and the immune system recruitment on 3D glioblastoma models. *Cancer Nano* **2023**, *14*, 393. https://doi.org/10.1186/s12645-023-00168-9

72. S. Tajik, Z. Dourandish, K. Zhang, H. Beitollahi, Q. Van Le, H. W. Jang, M. Shokouhimehr. Carbon and graphene quantum dots: a review on syntheses, characterization, biological and sensing applications for neurotransmitter determination. *RSC Adv.* **2020**, *10,* 15406. https://doi.org/10.1039/D0RA00799D

73. S. Deng, E. Zhang, Y. Wang, Y. Zhao, Z. Yang, B. Zheng, X. Mu, X. Deng, H. Shen, H. Rong, D. Pei. In vivo toxicity assessment of four types of graphene quantum dots (GQDs) using mRNA sequencing. *Toxicol. Lett.* **2022**, *363*, 55. https://doi.org/10.1016/j.toxlet.2022.05.006

74. Q. Xia, Y. Tang, W. Li, T. Liang, Y. Zhou, J. Liu, F. Liu. Surface-engineered monocyte immunotherapy combined graphene dots effective against solid tumour targets. *Int. J. Nanomed.* **2023**, *18*, 2127. https://doi.org/10.2147/IJN.S404486

75. R. S. Tade, P. O. Patil. Fabrication of poly-L-lysine-functionalized graphene quantum dots for the label-free fluorescent-based detection of carcinoembryonic antigen. *ACS Biomater. Sci. Eng.* **2022**, *8*, 470. https://doi.org/10.1021/acsbiomaterials.1c01087

76. M. M. Tehrani, M. Erfani, M. Amiri, M. Goudarzi. Technetium-99m radiolabeling of graphene quantum dots (GQDs) as a new probe for glioblastoma tumour imaging. Int. J. Radiat. Biol. **2024**, *101*, 65. https://doi.org/10.1080/09553002.2024.2404460

77. A. Soleimany, S. Khoee, S. Dias, B. Sarmento. Exploring low-power single-pulsed laser-triggered two-photon photodynamic/photothermal combination therapy using a gold nanostar/graphene quantum dot nanohybrid. *ACS Appl. Mater. Interfaces* **2023**, *15*, 20811. https://doi.org/10.1021/acsami.3c03578

78. R. S. Tade, M. P. More, S. N. Nangare, P. O. Patil. Graphene quantum dots (GQDs) nanoarchitectonics for theranostic application in lung cancer. *J. Drug Target.* **2022**, *30*, 269. https://doi.org/10.1080/1061186X.2021.1987442

79. T.-H. Ku, W.-T. Shen, C.-T. Hsieh, G. S. Chen, W.-C. Shia. Specific forms of graphene quatum dots induce apoptosis and cell cycle arrest in breast cancer cells. *Int. J. Mol. Sci.* **2023**, *24*, 4046 https://doi.org/10.3390/ijms24044046

80. I. J. Gomez, K. O.-Paredes, J. M. M.-Arriaga, N. Pizurova, M. Filice, L. Zajickova, S. Prashar, S. G.-Ruiz. Organotin-(IV)-decorated graphene quantum dots as dual platform for molecular imaging and treatment of triple negative breast cancer. *Chem. Eur. J.* **2023**, *29*, e20231845. https://doi.org/10.1002/chem.202301845

81. R. V. Khose, P. Bangde, M. P. Bondarde, P. S. Dhumal, M. A. Bhakare, G. Chakraborty, A. K. Ray, P. Dandekar, S. Some. Waste derived approach towards wealthy fluorescent N-doped graphene quantum dots for cell imaging and H_2O_2 sensing applications. *Spectrochim. Acta A Mol. Biomol. Spectrosc* **2022**, *266*, 120453. https://doi.org/10.1016/j.saa.2021.120453

82. M. Najafi, Z. Khoddam, M. Masnavi, M. Pourmadadi, M. Abdouss. Physicochemical and in vitro characterization of agarose based nanocarriers incorporated with graphene quantum dots/α-Fe_2O_3 for targeted drug delivery of quercetin to liver cancer treatment. *Mater. Chem. Phys.* **2024**, *320*, 129333. https://doi.org/10.1016/j.matchemphys.2024.129333

83. Z. Zhang, H. Yang, M. Wang, Y. Zhang, J. Jiang, Q. Wang. NIR-II silver-based quantum dots: synthesis and applications. *Nano Res.* **2024**, *17*, 10620. https://doi.org/10.1007/s12274-024-6977-7

84. F. Y. Acar. Theranostic silver chalcogenide quantum dots in phototherapy. *Photodiagnosis Photodyn Ther* **2023**, *41*, 103397 https://doi.org/10.1016/j.pdpdt.2023.103397

85. M. Hashemkhani, M. Loizidou, A. J. MacRobert, H. Y. Acar. One-step aqueous synthesis of anionic and cationic $AgInS_2$ quantum dots and their utility in improving the efficacy of ALA-based photodynamic therapy. *Inorg. Chem.* **2022**, *61*, 2846. https://doi.org/10.1021/acs.inorgchem.1c03298

86. E. Tan, P. T. Snee, F. D.-Kalindemirtas. An investigation of quantum dot theranostic probes for prostate and leukemia cancer cells using a CdZnSeS QD-based nanoformulation. *J. Colloid Interface Sci.* **2024**, *675*, 1032. https://doi.org/10.1016/j.jcis.2024.07.075

87. Y. Li, P Zhang, W. Tang, K. J. Mchugh, S. V. Kershaw, M. Jiao, X. Huang, S. Kalytchuk, C. F. Perkinson, S. Yue, Y. Qiao, L. Zhu, L. Jing, M. Gao, B. Han. Bright, magnetic NIR-II quantum dot probe for sensitive dual-modality imaging and intensive combination therapy of cancer. *ACS Nano* **2022**, *16*, 8076. https://doi.org/10.1021/acsnano.2c01153

88. V. S. Sivasankarapillai, J. Jose, M. S. Shanavas, A. Marathakam, Md. S. Uddin, B. Mathew. Silicon quantum dots: promising theranostics probes for

the future. *Curr. Drug Targets*, **2019**, *20*, 1255. http://dx.doi.org/10.2174/13894501206661904051523 15

89. Y. Zhang, N. Cai, V. Chan. Recent advances in silicon quantum dot-based fluorescent biosensors. *Biosensors*, **2023**, *13*, 311. https://doi.org/10.3390/bios13030311

90. Y. Huang, Y. Zhang, Z. Dai, R. Miao, H. Chen. One-pot synthesis quantum dots-based fluorescent nanomaterial and its application. *ACS Appl. Mater. Interfaces*, **2024**, *16*, 37513. https://doi.org/10.1021/acsami.4c05117

91. J. Zhou, Y. Du, Q. Wang, R. Zhao, S. Liu, W. Li, S. Gai, H. Ding, D. Yang, P. Yang. Chiral melanin-like particle-inspired fluorescent silicon quanum dots for sensitively detecting inflammation in cells. *ACS Appl. Nano Mater.*, **2023**, *6*, 15969. https://doi.org/10.1021/acsanm.3c02904

92. S. Pei, X. Hou, Y. Chi, W. Sun, F. Chen, K. Luo, S. Chai. Facile synthesis of highly efficient fluorescent silicon quantum dots used for highly sensitive sensor of tetracycline in honey samples and antibacterial agent. *Food Chem.* **2025**, *467*, 141844. https://doi.org/10.1016/j.foodchem.2024.141844

93. J. Lin, L. Xu, Y. Zheng, D. Wu, J. Yue. Imitation-mussel fluorescent silicon quantum dots for selective labelling and imaging of bacteria and biofilms. *Front. Bioeng. Biotechnol.* **2022**, *10*, 1. https://doi.org/10.3389/fbioe.2022.971682

94. H. Liang, F. Wu, R. Xia, W. Wu, S. Li, P. Di, M. Yang. Polyhedral oligomeric silsesquioxane (POSS)-silicon/carbon quantum dots nanocomposites for cell imaging. *RCS Adv.* **2024**, *14*, 25301. https://doi.org/10.1039/D4RA02987A

95. P. Chowdhury, D. Roy. Multi-emissive silicon quantum dots: synthesis, characteristics and their biological and analytical relevance. *Bull. Mater. Sci.* **2022**, *45*, 143. https://doi.org/10.1007/s12034-022-02706-4

RESEARCH ARTICLE

Network Pharmacology Approach to Evaluate the Therapeutic Effects of *Caesalpinia bonduc* (L.) Components for the Nephroprotective Activity

Hanumant U. Bhusnar[1]* , Sushil Dagadu Patil[1] , Soma Das[2] , and Laxmikant B. Borse[1]

[1]SunRise University, Bagar Rajput, Alwar, Rajasthan, 301028, India.
[2]Department of Pharmaceutical Technology, School of Health and Medical Sciences, Adamas University, Barasat -West Bengal, 700126, India.
*Correspondence: hanumantbhusnar19@gmail.com

Abstract: *Caesalpinia bonduc* (L.) (Family: Caesalpiniaceae) commonly known as Bonduc Nut and Fever Nut is the main ingredients in Hjam-hbras formulation, a single herb formulation documented in Buddha Shakamuni for treating renal diseases. *C. bonduc* seed extract is also scientifically validated for having renal protective effects but its exact mechanism by which it showed renal protective effect is still unknown. In this study, we aimed to evaluate the nephroprotective mechanism of action of *C. bonduc* seed by performing Network pharmacology analysis. ADMET property analysis reveals 21 out of 190 phytochemicals of *C. bonduc* seeds has passed the good ADMET criteria. Network pharmacology analysis identified 197 mutual common nephroprotective targets for these 21 phytochemicals. The PPI analysis discovered that AKT1, PIK3CA, SRC, PIK3R1, HSP90AA1, MAPK1, PTPN11, FYN, EGFR and STAT3 are the top 10 genes sorted by degree value. GO enrichment analysis showed various processes, functions, and cellular components involved in nephroprotection while the KEGG enrichment analysis showed the associated pathways HIF-1 signaling pathway, Thyroid hormone signaling pathway etc. involved in nephroprotection. This study provides bioinformatic insights via Network pharmacology analysis could pave the way for understanding the effectiveness of *C. bonduc* as nephropotective agent.
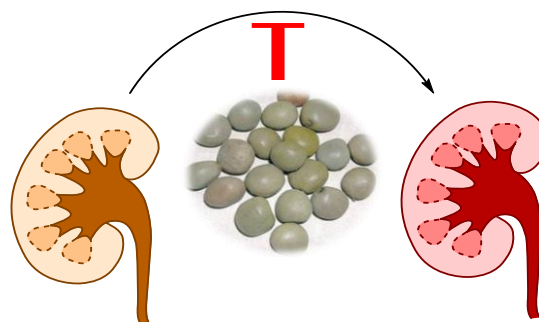
Keywords: *Caesalpinia bonduc, Hjam-hbras formulation, nephropotection, network pharmacology, renal*

Introduction

Investigating nephroprotective herbal remedies takes one into a world where the complex web of plant components interacts with the kidneys' sensitive anatomy and physiology, providing a therapeutic opportunity for the avoidance and management of kidney diseases. Herbal medicine studies have recently centered on nephroprotection, a broad concept including many measures to protect the kidneys.[1-3] Currently, Indian medicinal plants have a significant impact on the treatment of numerous disorders in India. The prominent traditional medical systems utilized in India include Ayurveda, Siddha, and Unani.[4,5] The Traditional Knowledge Digital Library (TKDL) is a repository that documents India's traditional knowledge, particularly relating medicinal and ethnobotanical plants, as well as various formulations and preparations used in Indian systems of medicine.[6] We use this library to search plants and formulation having their major role in treating alignment related to kidney.

Hjam-hbras is a therapeutic single/compound formulation whose knowledge for treating diseases of the kidney is well known since 1000 years and is found in Buddha Shakamuni documents which was retrieved from the online search in TKDL.[7] *Caesalpinia bonduc* (L.) (Synonym: *Caesalpinia bonducella*; Family: Caesalpiniaceae) commonly known as Bonduc Nut, Fever Nut and Nicker Nut is the main ingredients in Hjam-hbras formulation. *C. bonduc* is a well-known Indian medicinal plant containing several nonpolar and polar phytoconstituents that are divided in different types of phytochemicals including, flavonoid[8] terpenoids, polysaccharides, and derivatives of phenolic acids however, cassane furanoditerpenes[9,10] and diterpenes of cassane[11,12] and norcassane[11] are the most significant substances. *C. bonduc* seed extract showed renal protective effects against paracetamol intoxication.[13] Apart from this, it is also showed various therapeutic properties like antidiabetic,[14-16]

antimicrobial,[17] used for the treatment of hyperthyroidism,[18] Poly Cystic Ovary Syndrome (PCOS)[19,20] and several other complications/disorders. The presence of different phytoconstituents could be the main reasons behind its pharmacological effect mainly the nephrprotective effect. Network pharmacology analysis is a new powerful tool that could help to provide a correlation between plant secondary metabolites and disease/metabolic targets and helps us in understanding mechanism of action behind its traditional use.[21-23] Network pharmacology together with systems modeling has been successfully used to evaluate the nephroprotective mechanism of action of various traditional medicines and formulations.[23-28] Hence the main objective of our study is to decipher the nephroprotective mechanism of *C. Bonduc* seeds through network pharmacology analysis.

Results and Discussion

Analysis of phytochemicals

A total of 190 phytochemicals of *Caesalpinia bonduc* seeds had been obtained from PubMed® and Scopus based research articles. The chemical information of each of these phytochemicals was obtained from the public database like SciFinder® (https://scifinder-n.cas.org) or Pubchem (https://pubchem.ncbi.nlm.nih.gov/).

ADMET prediction

The obtained phytochemicals were then screened for their ADMET profile. A good drug candidate should always have good efficacy as well as appropriate ADMET properties at a therapeutic dosage. Additionally, compounds should not possess blood-brain barrier (BBB) penetration properties in order to avoid any CNS toxicities. Evaluation of the ADMET

S.N	Name	Molecular Weight	Caco-2	BBB	CYP1A2-inh	CYP1A2-sub	CYP2C19-inh	CYP2C19-sub	CYP2C9-inh	CYP2C9-sub	CYP2D6-sub	CYP3A4-inh	CYP3A4-sub	CL	Carcinogenicity	Genotoxic Carcinogenicity	LogP	nHA	nHD	PAINS	Lipinski
1	Rosenonolactone	316.2	-5.0	0.7	0.0	0.6	0.1	0.9	0.2	0.2	0.3	0.9	0.5	5.7	0.8	0.0	3.0	3.0	0.0	0.0	Accepted
2	Phenanthro[3,2-b]furan-1,2,4aβ(2αH)-triol, 1α,3,4,5,6,8,9,11b-octahydro-4,4,7,11bα-tetramethyl	332.2	-4.7	0.9	0.1	0.6	0.0	0.9	0.0	0.9	0.8	0.0	0.4	12.7	0.0	0.0	2.7	4.0	3.0	0.0	Accepted
3	Caesaldekarin I	334.2	-4.8	0.6	0.1	0.6	0.1	0.8	0.1	0.0	0.1	0.9	0.5	10.5	0.7	0.0	2.2	4.0	3.0	0.0	Accepted
4	δ-Cesalpin, 14-deoxy	350.2	-4.9	0.9	0.0	0.2	0.0	0.7	0.0	0.3	0.4	0.0	0.4	11.8	0.1	0.0	1.9	5.0	4.0	0.0	Accepted
5	Phenanthro[3,2-b]furan-1,2,4aβ,7 (2αH)-tetrol, 1α,3,4,5, 6,6aα ,7,11 ,11 aβ,11b-decahydro-4,4,7β,11bα-tetramethyl	350.2	-4.9	1.0	0.0	0.2	0.0	0.8	0.1	0.5	0.4	0.0	0.5	9.3	0.2	0.0	1.8	5.0	4.0	0.0	Accepted
6	Dehydrodiconiferyl alcohol	358.1	-4.8	0.4	0.1	0.7	0.0	0.8	0.1	0.7	0.8	0.5	0.8	8.8	0.3	1.0	1.8	6.0	3.0	0.0	Accepted
7	β-Caesalpin	364.2	-4.9	1.0	0.0	0.3	0.0	0.8	0.0	0.4	0.2	0.0	0.4	6.8	0.2	0.0	1.4	6.0	4.0	0.0	Accepted
8	Caesall D	374.2	-4.7	0.5	0.1	0.1	0.1	0.7	0.4	0.1	0.2	0.6	0.5	8.7	0.9	0.0	2.8	5.0	2.0	0.0	Accepted
9	Phenanthro[3,2,-b]furan-1,2,4aβ (2αH)-triol, 1α,3,4,5,6,6 aα ,7 ,11 , 11aβ,11b-decahydro-4,4,11bα-methyl-7-methylene-, 2-acetate	374.2	-4.7	0.5	0.1	0.1	0.1	0.8	0.4	0.3	0.6	0.1	0.6	10.2	0.6	0.0	2.7	5.0	2.0	0.0	Accepted
10	Norcaesalpinin E	376.2	-4.8	0.6	0.1	0.1	0.1	0.7	0.2	0.1	0.2	0.6	0.5	7.2	0.9	0.0	2.4	6.0	2.0	0.0	Accepted
11	Caesalmin B	388.2	-4.8	0.8	0.0	0.1	0.1	0.8	0.1	0.0	0.2	0.6	0.6	7.8	0.6	0.0	3.0	6.0	1.0	0.0	Accepted
12	Caesalmin E1	392.2	-4.9	0.8	0.0	0.1	0.0	0.7	0.1	0.1	0.1	0.4	0.5	7.2	0.9	0.0	2.5	6.0	3.0	0.0	Accepted
13	Phenanthro[3,2-b]furan-1,2,4aβ,7(2αH)-tetrol, 1α,3,4,5,6,6aα,7,11,11aβ,11b-decahydro-4,4,7β,11bα-tetramethyl-, 2-acetate	392.2	-4.8	0.9	0.0	0.1	0.0	0.9	0.1	0.3	0.4	0.1	0.7	6.7	0.4	0.0	2.3	6.0	3.0	0.0	Accepted
14	Caesalpinin I	402.2	-5.0	0.8	0.1	0.1	0.1	0.7	0.1	0.1	0.2	0.6	0.5	6.2	0.1	0.0	1.8	7.0	1.0	0.0	Accepted
15	Bonducellpin D	404.2	-5.0	0.7	0.1	0.1	0.0	0.6	0.0	0.2	0.4	0.4	0.4	6.2	0.3	0.0	2.1	7.0	2.0	0.0	Accepted
16	(+)-Bonducellpin C	420.2	-4.8	0.8	0.0	0.3	0.1	0.8	0.1	0.0	0.2	0.6	0.6	8.2	0.6	0.0	2.5	7.0	2.0	0.0	Accepted
17	Cassabonducin H	422.2	-4.9	0.8	0.0	0.0	0.0	0.8	0.0	0.1	0.2	0.5	0.6	7.1	0.9	0.0	2.1	7.0	3.0	0.0	Accepted
18	Caesalmin K	436.2	-5.0	0.4	0.0	0.1	0.0	0.7	0.0	0.1	0.2	0.2	0.3	5.1	0.3	0.0	1.9	8.0	3.0	0.0	Accepted
19	7-Acetoxybonducellpin C	462.2	-4.9	0.8	0.0	0.1	0.1	0.8	0.1	0.0	0.1	0.5	0.7	6.3	0.3	0.0	2.8	8.0	1.0	0.0	Accepted
20	Caesaldekarin G	364.2	-4.7	0.6	0.0	0.9	0.2	0.9	0.1	0.0	0.0	0.8	0.8	6.9	1.0	1.0	2.2	5.0	2.0	0.0	Accepted
21	δ-Cesalpin	366.2	-5.1	0.5	0.0	0.1	0.0	0.7	0.0	0.1	0.2	0.0	0.2	5.7	0.9	0.0	1.7	6.0	5.0	0.0	Accepted
			Absorption	Distribution				Metabolism						Excretion	Toxicity		Physicochemical Property			Medicinal Chemistry	

Figure 1: *ADME/Toxicity profile of the shortlisted phytochemicals from C. bonduc seeds.*

profile is, therefore, an important criterion for studying drug-like molecules to minimize their failure during the clinical stages of drug development.

Evaluation of ADMET profile is therefore the important criteria to study drug-like molecules in order to minimize their failure clinical stage of drug development. Based on the selection criteria of ADMETlab 2.0, 21 out of 190 phytochemicals of *C. bonduc* seeds were selected for target identification (**Figure 1**).

Putative protein targets for shortlisted phytochemicals

The human putative protein targets for the eligible phytochemicals were retrieved from Swiss Target Prediction (http://www.swisstargetprediction.ch), Similarity Ensemble Approach (https://sea.bkslab.org/), PharmMapper Server (https://www.lilab-ecust.cn/pharmmapper/) and SuperPred (https://prediction.charite.de/subpages/target_prediction.php) databases. A total of all the symbols/names of proteins were gathered and a total of 336 unique protein targets have been obtained after excluding the duplicate values for the particular phytochemicals was selected (**Figure 2**).

***Caesalpinia bonduc* seeds target network analysis**

Network pharmacology serves as a powerful approach for exploring and identifying drug targets. In this study through network pharmacology analysis, we have identified multiple targets & pathways that are associated with the *C. bonduc* phytochemicals and this will help us to justify their mechanism responsible for nephroprotective effect. There were 197 mutual common targets between *C. bonduc* seeds

phytochemicals targets and nephroprotective targets and these targets were considered as the potential therapeutic targets of *C. bonduc* seeds for nephroprotective activity (**Figure 3**). The STRING database (https://string-db.org/) is a used to analyze protein–protein interactions. From Protein−Protein Interaction network, 154 mutual targets (interaction score > 0.9 and except disconnected targets) with 194 nodes and 464 edges were sorted by centrality degree. Intelligent network pharmacology platform unique generate the PPI network for common targets (**Figure 4**).[29] The PPI analysis discovered that AKT1, PIK3CA, SRC, PIK3R1, HSP90AA1, MAPK1, PTPN11, FYN, EGFR and STAT3 as the

C. bonduc   **Nephroprotective**

336   197   1541
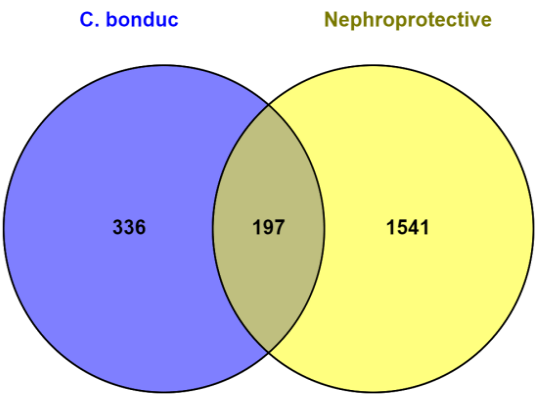
Figure 2: *Intersection of the Caesalpinia bonduc and nephroprotective-related targets. Blue and Yellow circles represent the predicted targets of Caesalpinia bonduc and nephroprotection respectively. The pale brown area reflects the common targets*

top 10 genes based on their degree values. These hub genes derived from the PPI network are illustrated in **Figure 5**. The top targets whose combined score is > 0.999 were selected for DAVID Pathway Analysis, the KEGG pathway and Gene Ontology (GO) enrichment analysis.

Gene Ontology (GO) enrichment analysis

Functional analysis of concerned genes can be possible with the help of GO analysis. It generally describes the role of selected genes in the BP-biological process (**Figure 6A**), CC-cellular component (**Figure 6B**) & MF-molecular function (**Figure 6C**). The top terms involved in the above mentioned three categories of gene ontology process i.e BP, CC & MF are represented in **Figure 6** has been developed by using ShinyGO,[30] an intuitive, graphical web application.

For *Caesalpinia bonduc* seeds, within the biological process ontology, the PPI network targets are primarily associated with process such as the transmembrane receptor protein tyrosine kinase signaling pathway, reg. of response to external stimulus, response to abiotic stimulus, cellular response to oxygen-containing compound, and reg. of phosphorylation among others. In the CC ontology, the targets are primarily located in extrinsic component on the cytoplasmic side of plasma membrane, cell body, and caveola. According to GO annotation for molecular function, the targets are mainly involved in activities such as nitric-oxide synthase regulator activity, 1-phosphatidylinositol-4-phosphate 3-kinase activity, phosphatidylinositol-4,5-bisphosphate 3-kinase activity, phosphatidylinositol-3,4-bisphosphate 5-kinase activity, 1-phosphatidylinositol-3-kinase activity, and insulin receptor substrate binding.

DAVID AND KEGG PATHWAY ANALYSIS

KEGG (Kyoto Encyclopedia of Genes and Genomes) pathway analysis along with other pathway analysis like reactome, wikipathways and Elsevier pathway collection showed that *C. bonduc* seeds have many more important pathways which are responsible for nephroprotective activity. *C. bonduc* seeds were associated with pathways like HIF-1 signaling pathway, Thyroid hormone signaling pathway,

Figure 3: *Compound – Target Network of Caesalpinia bonduc seeds*
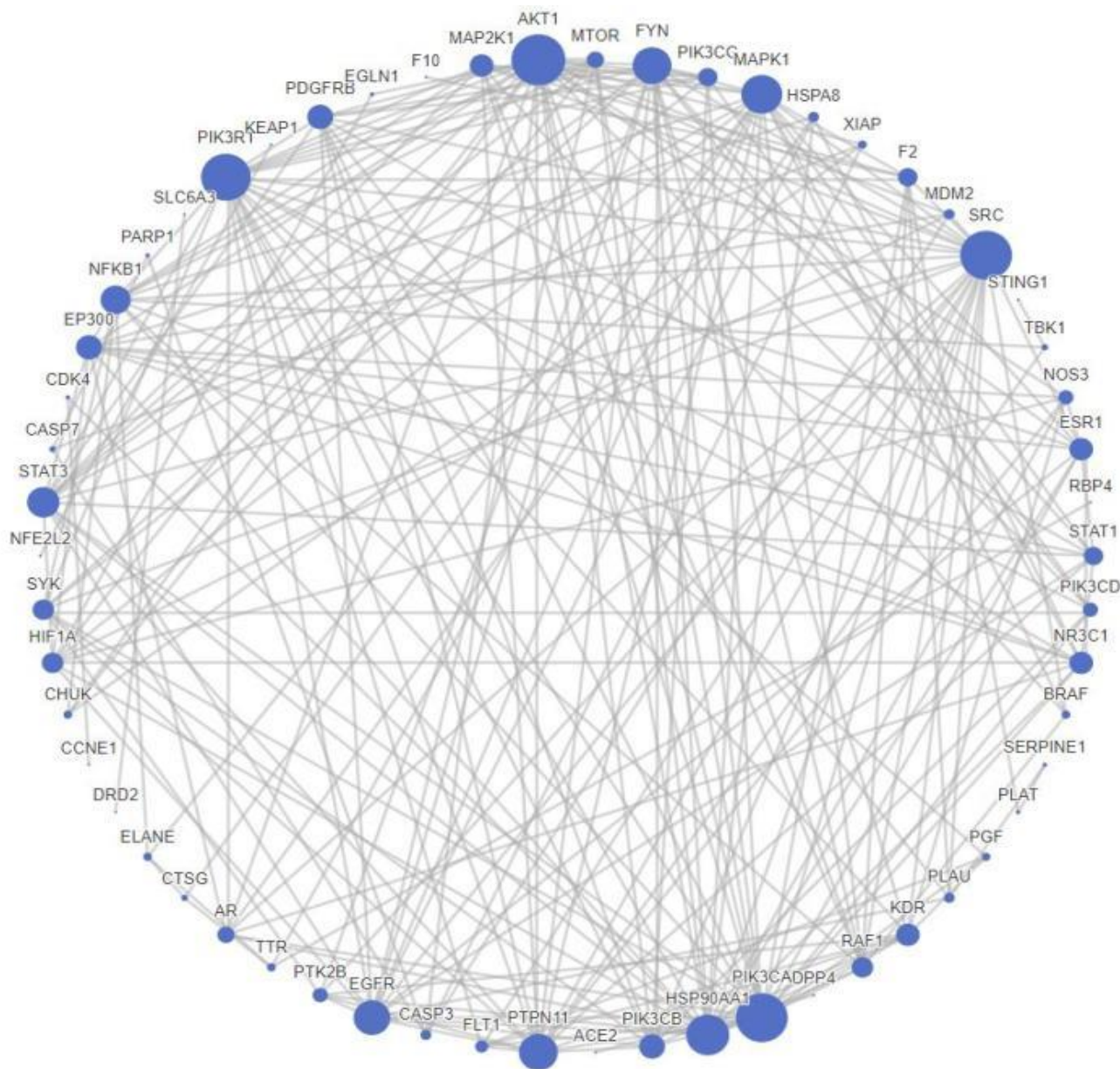
Figure 4: *PPI network for common Caesalpinia bonduc seeds targets*

Phospholipase D signaling pathway, Chemokine signaling pathways, FoxO signaling pathway etc. (**Figure 7,** developed by using ShinyGO, an intuitive, graphical web application).

Discussion

In our study we perform network pharmacological analysis which has been emerged as a reliable tool for identifying interactions and correlations between different pathways, so that to uncover the underlying mechanisms behind the nephroprotective effect of *C. bonduc* seeds. GO analysis helps us to identify pathways pathways. KEGG analysis showed that the PI3K-AKT, JAK-STAT, MAPK and Chemokine signaling pathways were significantly enriched. The PPI analysis discovered that AKT1, PIK3CA, SRC, PIK3R1, HSP90AA1, MAPK1, PTPN11, FYN, EGFR and STAT3 are the top 10 genes sorted by degree value. This study will provide research direction and reference for future clarification of the specific effective ingredients and

mechanism of action of *C. bonduc* seeds as nephropotective agent. biologicalprocesses, molecular functions and cellular components of the proteins and genes influenced during nephroprotective activity.

KEGG analysis emphasizes on the pathways which plays important role in nephroprotectiive activity. β-catenin pathway, inflammasome pathway (NF-κB/NLRP3), STAT3 signaling pathways, PI3K/Akt pathway, ROS and SO pathways are some of the important pathways which plays important role in nephroprotectiive activity.[31,32] *C. bonduc* seeds was associated with pathways like renal cell carcinoma, PI3K-AKT signaling pathway, JAK-STAT signaling pathway, MAPK signaling pathway and Chemokine signaling pathways and hence of *C. bonduc* seeds showed it's nephroprotective effect though these pathways. For the aforementioned potential pharmacological effects, clinical trials involving humans could be considered for these plants. In summary, based on our network pharmacology studies, the key bioactive ingredients

of *C. bonduc* seeds showed nephropotective action through various signaling

Materials and Methods
Study design

The phytochemical constituents found in *Caesalpinia bonduc* seeds were retrieved from published literature and databases such as PubChem (https://pubchem.ncbi.nlm.nih.gov/), and SciFinder® (https://scifinder.cas.org/).[33,34] The ADMETlab 2.0 server (https://admetmesh.scbdd.com/), a free online tool used to predict absorption, distribution, metabolism, excretion, and toxicity (ADMET) properties of these phytochemicals found in *C. bonduc* seeds.[35]

GeneCards and DisGeNET.[39,40] All targets were limited to human-specific entries. Subsequently, the targets were input into UniProt (https://www.UniProt.org/) to obtain functional annotations and standardized gene names. Cytoscape 3:2.1., the potential protein targets of phytochemicals were predicted using Swiss Target Prediction (http://www.swisstargetprediction.com/),[36] the Similarity Ensemble Method (https://sea.bkslab.org), SuperPred (https://prediction.charite.de/subpages/target_prediction.php)[3]

[7] and PharmMapper Server (http://lilab.ecust.edu.cn/pharmmapper/submit_file.php).[38] Nephroprotection-related genes were chosen from network visualization program that was used to establish relationships between target proteins and phytochemicals, resulting in the construction of a graphical interaction network.[41]

Chemical databases

Molecular weight, molecular formula, chemical structure and SMILES for the phytochemicals of *Caesalpinia bonduc* are recovered from the databases like Pubchem (https://pubchem.ncbi.nlm.nih.gov/), SciFinder® (https://scifinder-n.cas.org) or from the reported literature. [42,43]

ADMET screening

Pharmacokinetic profile of phytochemicals can be identified with the help of ADMETlab 2.0, a free online tool that is used to the ADMET and drug-likeness properties. The *Caesalpinia bonduc* phytochemicals which was obtained from various databases were screened based on the selection criteria of ADMETlab 2.0.[35]

Figure 5: *Top 10 Hub genes obtained from PPI network*

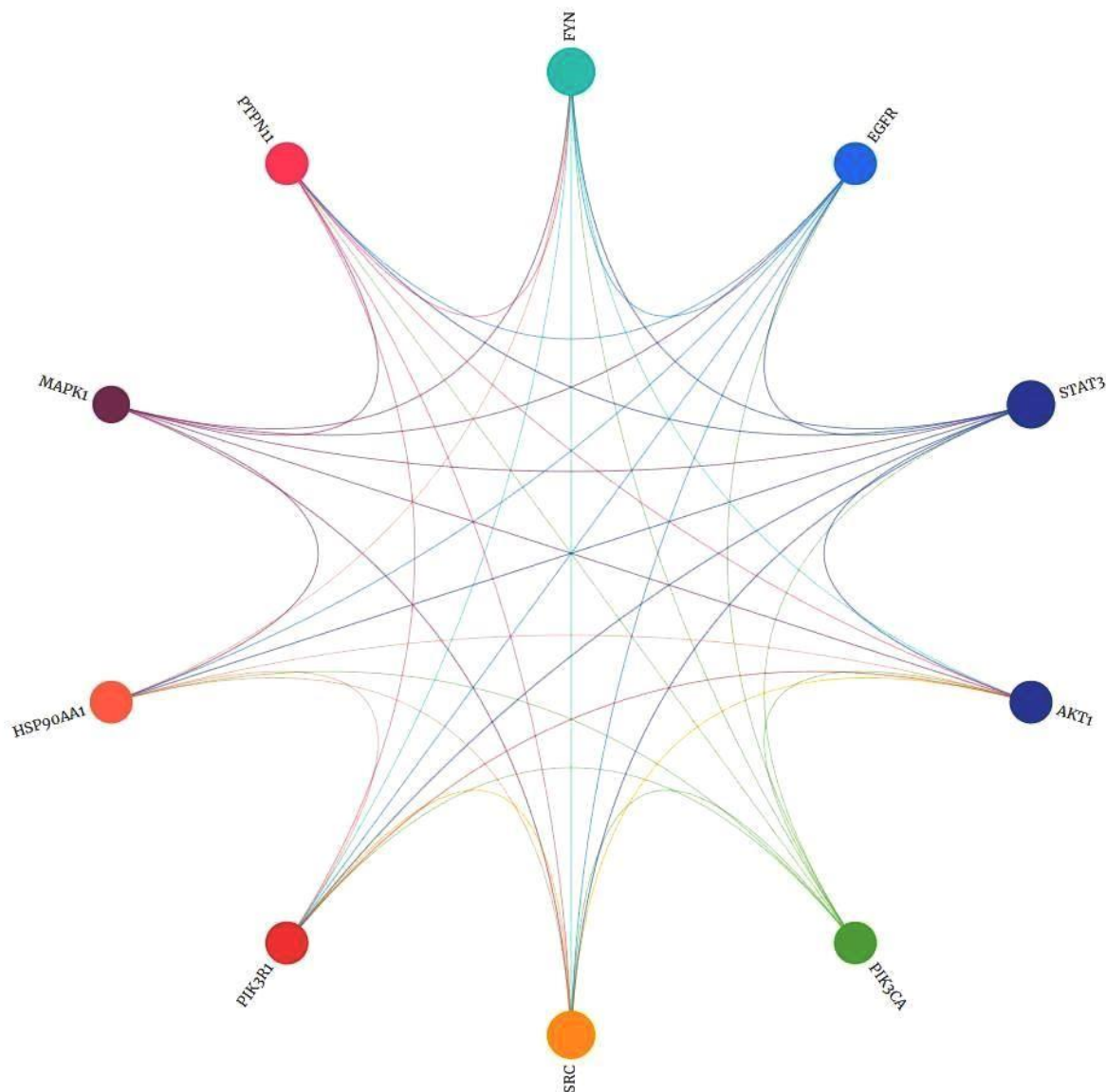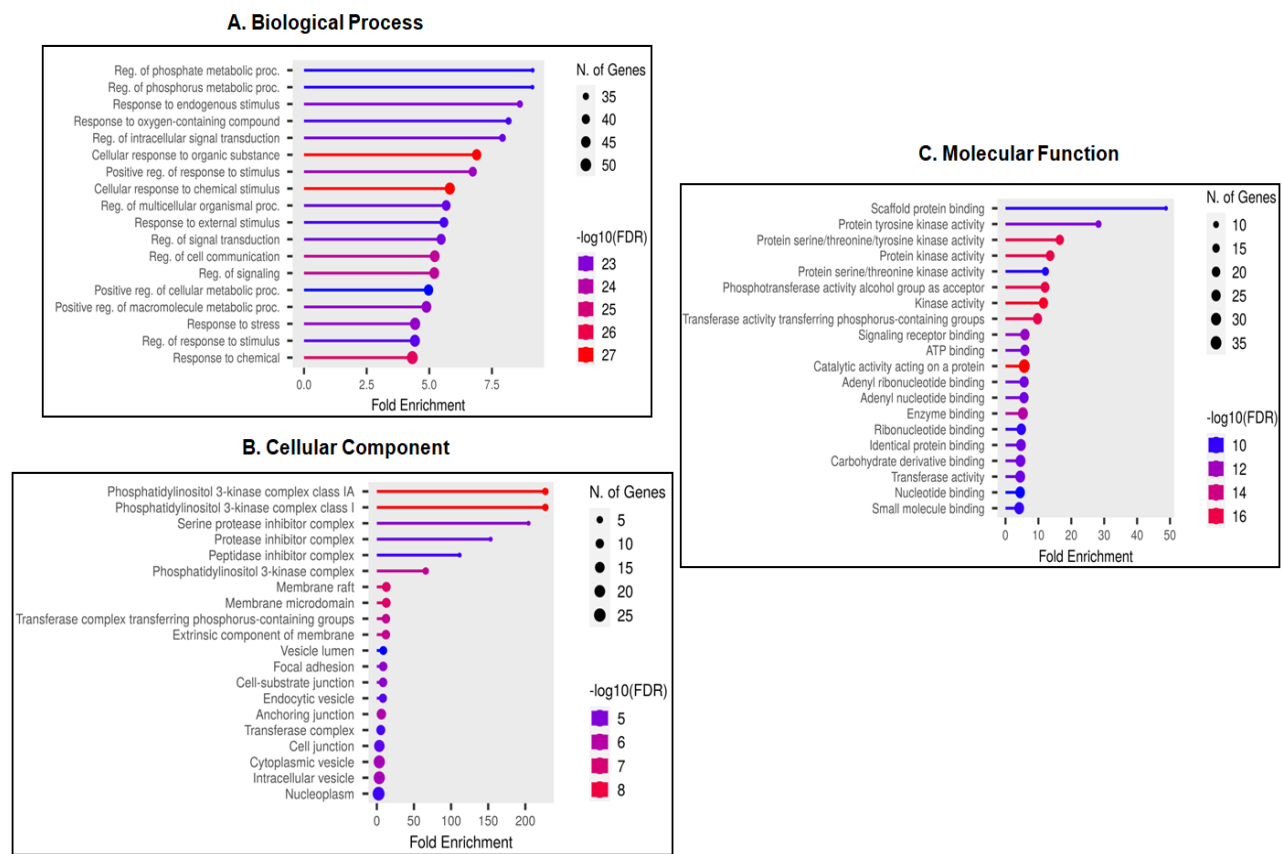**Figure 6:** *GO function analysis of Caesalpinia bonduc seeds: BP-biological process (Figure 6A), CC-cellular component (Figure 6B) & MF-molecular function (Figure 6C).*
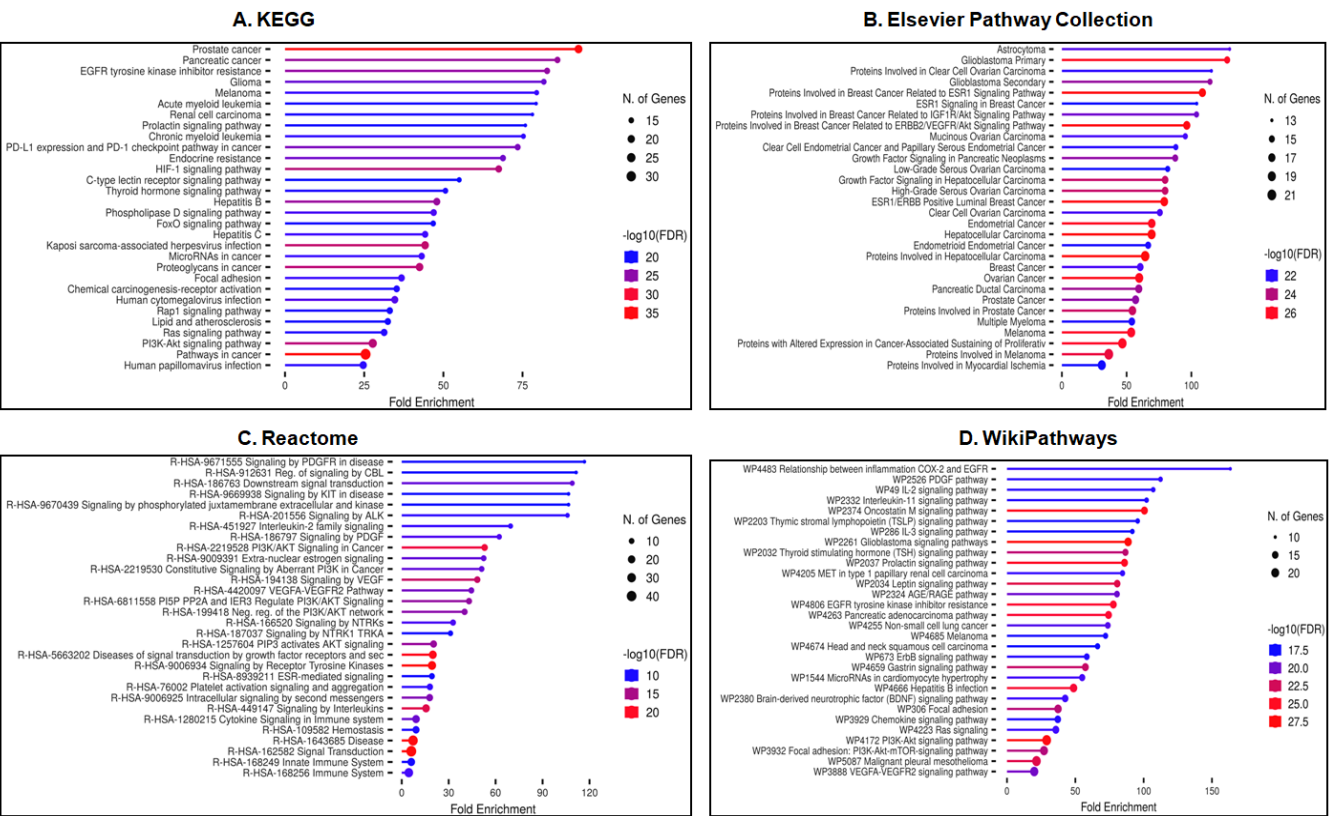

Figure 7: *Pathway enrichment analysis of Caesalpinia bonduc seeds*

Target genes prediction

The interaction between target proteins each compound was obtained from the databases like Swiss Target Prediction, Similarity Ensemble Approach, PharmMapper Server and SuperPred databases.

Identification of targets for nephroprotection

The nephroprotective targets were retrieved from databases like Gene Cards (https://www.genecards.com/), DisGeNET (https://disgenet.com/) & Mala Cards (https://www.malacards.org/).[23] The network between the target genes and active compounds has been created and visualized using the Cytoscape software. In order to shed light on the mechanism of action of specific medicinal plants, network visualizations of "compound target" network maps were created using the visualization program Cytoscape 3.2.[41] The software in particular visually integrates the network with expression profiles and connects the network to databases of functional annotations. This software was also used for network creation, editing, visualization, and analysis. In these networks each nodes represent the compounds while edges represent the interactions between the nodes.[44]

Protein-Protein interaction (PPI) network

The statistical depictions of the physical interactions between proteins within a cell are given by protein-protein interactions (PPIs). Graphs are typically used to model PPI networks, with the proteins acting as the nodes and the interacting proteins acting as the edges. The Search Tool for the Retrieval of Interacting Genes/Proteins (STRING) database (https://string-db.org/. version 11.0) was used to build the PPI network.[45] The organisms included in the database were designated as "Homo sapiens". From the PPI network, the target genes with confidence score >0.90 has been selected for further analysis.[28]

The criteria for the STRING analysis included text mining, co-expression, gene fusion, co-occurrence, databases, and interaction sources from experiments.

Gene ontology & DAVID pathway enrichment analysis

The shortlisted network's protein targets (identified by target name or UniProt id) were loaded into the DAVID (Database for annotation, Visualization, and Integrated Discovery) platform to elucidate their mode of operation (https://davidbioinformatics.nih.gov/tools.jsp).[46] DAVID is a freely accessible online bioinformatics resource that provides information on cellular components, biological functions, molecular roles, and biological pathways associated with the given genes.[47] Pathway analysis was performed on the annotated datasets corresponding to each compound's targets. Gene Ontology (GO) was used to examine the biological process and perform enrichment analysis on the gene sets.[48] Additionally, the KEGG database, which includes information on drugs, chemicals, diseases, genomes, and biological pathways, was utilized for further analysis.[49]

Conclusion

Hjam-hbras is a 1000 year old traditional formulation consisting of useful parts of *Caesalpinia bonduc* was found in traditional Buddha Shakamuni documents for treating diseases of the kidney. Network pharmacology analysis proves the effectiveness of *C. bonduc* as nephropotective agent by analyzing its ability of phytochemicals to influence diverse pathways and targets. This study provides bioinformatic insights that could pave the way for a deeper understanding of the mechanisms of action of the nephroprotection.

This comprehensive analysis not only affirms nephropotective efficacy but also lays the groundwork for further exploration into the intricate workings of this 1000 years old traditional knowledge. By elucidating the complex interplay between *C. bonduc* and the biological pathways associated with nephropotection, this study not only validates its therapeutic potential but also offers a roadmap for future research endeavors.

Author Contribution Declaration

Funding sources

Data Availability Declaration

The new data generated and analyzed is included in this article.

Acknowledgements

References

1. P. Basist, B. Parveen, S. Zahiruddin, G. Gautam, R. Parveen, M. A. Khan, A. Krishnan, M. Shahid, S. Ahmad. Potential nephroprotective phytochemicals: Mechanism and future prospects. *J Ethnopharmacol.*, **2022**, *283*, 114743. https://doi.org/10.1016/j.jep.2021.114743

2. H. Shahin D. H., R. Sultana, J. Farooq, T. Taj, U. F. Khaiser, N. S. A. Alanazi, M. K. Alshammari, M. N. Alshammari, F. H. Alsubaie, S. M. B. Asdaq, A. A. Alotaibi, A. A. Alamir, M. Imran, S. Jomah. Insights into the uses of traditional plants for diabetes nephropathy: a review. *Curr. Issues Mol. Biol.,* **2022**, *44*, 2887. https://www.mdpi.com/1467-3045/44/7/199

3. S. Chaurasia, V. S. Mahalwal, P. M. Chandrika. Ethano medicinal plants used as nephroprotective in different traditional medicine: A review. *Res. J. Pharm. Technol.*, **2021**, *14*, 1183. https://doi.org/10.5958/0974-360X.2021.00211.0

4. R. Basu, S. Dasgupta, S. N. Babu, A. Noor. Medicinal Plants in the Indian Traditional Medicine and Current Practices. *Bioprospecting of Tropical Medicinal Plants.* **2023**, 253-86. https://doi.org/10.1007/978-3-031-28780-0_9

5. A. Parveen, M. Ahmad, B. Parveen, R. Parveen, M. Iqbal. The traditional system of Unani medicine, its origin, evolution and Indianisation: A critical appraisal. *Indian J. Tradit. Knowl.*, **2022**, *21*, 511.

6. S. Panda, N. Kaur. Harnessing Traditional Tribal Knowledge Treasure in India by Unlocking the Potential of Digital Platform. *University News.*, **2023**, *2023*, 110. https://doi.org/10.5281/zenodo.10213022.

7. M. Hirwade. Protecting traditional knowledge digitally: a case study of TKDL. **2010**.

8. W. J. A. Musa, N. Bialangi, A. K. Kilo, C. J. Lamangantjo, B. Situmeang, A. M. Ibrahim. Flavonoid glycoside compound from tombili seed (Caesalpinia bonducella) and its antioxidant

activity. *Rasayan J Chem.*, **2022**, *15*, 2237. http://doi.org/10.31788/RJC.2022.1547087

9. K. Pudhom, D. Sommit, N. Suwankitti, A. Petsom. Cassane Furanoditerpenoids from the Seed Kernels of Caesalpinia bonduc from Thailand. *J Nat Prod.*, **2007**, *70*, 1542. https://doi.org/10.1021/np070330y.

10. A. N. Jadhav, N. Kaur, K. K. Bhutani. A new furanoditerpenoid marker for the distinction between the seeds of two species of Caesalpinia. *Phytochem Anal.*, **2003**, *14*, 315. https://doi.org/10.1002/pca.722.

11. T. Liu, X. Li, Z. Ning, S. Qi, H. Gao. Two new cassane-type diterpenoids from the seed kernels of Caesalpinia bonduc (Linn.) Roxb. and their anti-inflammatory activity. *Nat Prod Res.*, **2022**, *36*, 3901. https://doi.org/10.1080/14786419.2021.1896511.

12. J. Cao, Y. Xu, R. Lou, W. Shi, J. Chen, L. Gan, J. Lu, L. Lin. Cassane-Type Diterpenoids from the Seeds of Caesalpinia bonduc (L.) Roxb. *Chem Biodiversity.*, **2021**, *18*, e2100309. https://doi.org/10.1002/cbdv.202100309

13. S. Nithiyanandam, S. E. Prince. Caesalpinia bonducella mitigates oxidative damage by paracetamol intoxication in the kidney and intestine via modulating pro/anti-inflammatory and apoptotic signaling: an In vivo mechanistic insight. *3 Biotech.*, **2023**, *13*, 176. https://doi.org/10.1007/s13205-023-03601-3

14. A. K. Sachan, C. V. Rao, N. K. Sachan. Determination of antidiabetic potential in crude extract of caesalpinia bonducella wild on normal and streptozotocin induced diabetic rats. Res. *J. Pharm. Technol.*, **2020**, *13*, 857. https://doi.org/10.5958/0974-360X.2020.00162.6.

15. S. Chakrabarti, T. K. Biswas, T. Seal, B. Rokeya, L. Ali, A. K. A. Khan, N. Nahar, M. Mosihuzzaman, B. Mukherjee. Antidiabetic activity of Caesalpinia bonducella F. in chronic type 2 diabetic model in Long-Evans rats and evaluation of insulin secretagogue property of its fractions on isolated islets. *J Ethnopharmacol.*, **2005**, *97*, 117. https://doi.org/10.1016/j.jep.2004.10.025.

16. D. M. Kannur, V. I. Hukkeri, K. S. Akki. Antidiabetic activity of Caesalpinia bonducella seed extracts in rats. *Fitoterapia.* **2006**, *77*, 546. https://doi.org/10.1016/j.fitote.2006.06.013.

17. K. Simin, S. M. Khaliq-Uz-Zaman, V. U. Ahmad. Antimicrobial activity of seed extracts and bondenolide from Caesalpinia bonduc (L.) Roxb. *Phytother Res.,* **2001**, *15*, 437. https://doi.org/10.1002/ptr.756.

18. K. Raveena, T. P. Jayachandran. Evaluation of ethanol extract of Caesalpinia bonducella L. seeds on Hyperthyroidism. *J. Pharm. Sci. & Res.*, **2020**, *12*, 1420.

19. V. Kandasamy, U. Balasundaram. Caesalpinia bonduc (L.) Roxb. as a promising source of pharmacological compounds to treat Poly Cystic Ovary Syndrome (PCOS): A review. *J Ethnopharmacol.*, **2021**, *279*, 114375. https://doi.org/10.1016/j.jep.2021.114375.

20. M. Sumithra, V. Chitra, M. K. Moka, Padaleeswaran, S. Ahmed. Anti - androgenic activity of Caesalpinia bonducella in androgen-induced polycystic ovarian syndrome rats. *J Pharm Res Int.,* **2021**, *33*, 220. https://doi.org/10.9734/JPRI/2021/v33i55A33826

21. T. D. P. Rini, F. Sangande, K. Agustini, A. Bahtiar. Identification and analysis of Ardisia humilis as potential antihyperlipidemic by network pharmacology followed by molecular docking. *Res. J. Pharm. Technol.*, **2024**, *17*, 2009. https://doi.org/10.52711/0974-360X.2024.00318.

22. J. -Q, Wang, X. -X. Liu, J. -J. Zhang, Z. Shuai, C. Jiang, S. -W. Zheng, Z. Wang, D. -Y. Li, W. Li, D. -F. Shi. Amelioration of Cisplatin-Induced kidney injury by Arabinogalactan based on network pharmacology and molecular docking. *J. Funct. Foods.*, **2023**, *104*, 105504. https://doi.org/10.1016/j.jff.2023.105504.

23. S. Das, R. L Gajbhiye, N. Kumar, D. Sarkar. Multi-Targeted Prediction of the Antiviral Effect of Momordica charantia extract based on Network Pharmacology. *J. Nat. Remedies.*, **2023**, *23*, 169. https://doi.org/10.18311/jnr/2023/31430.

24. C. Jia, X. Pan, B. Wang, P. Wang, Y. Wang, R. Chen. Mechanism Prediction of Astragalus membranaceus against Cisplatin-Induced Kidney Damage by Network Pharmacology and Molecular Docking. *Evid Based Complement Alternat Med.,* **2021**, *2021*, 9516726. https://doi.org/10.1155/2021/9516726.

25. M. J. Alqahtani, S. A. Mostafa, I. A. Hussein, S. Elhawary, F. A. Mokhtar, S. Albogami, M. Tomczyk, G. E. S. Batiha, W. A. Negm. Metabolic Profiling of Jasminum grandiflorum L. Flowers and Protective Role against Cisplatin-Induced Nephrotoxicity: Network Pharmacology and In Vivo Validation. *Metabolites.,* **2022**, *12*, 792. https://doi.org/10.3390/metabo12090792.

26. X. Li, J. Shi, Y. Teng, Z. Liu. The preventative effect of Baihe Gujin Pill on cisplatin-induced acute kidney injury by activating the PI3K/AKT and suppressing the NF-κB/MAPK pathways. *J Ethnopharmacol.,* **2024**, *318*, 117071. https://doi.org/10.1016/j.jep.2023.117071.

27. Z. Liu, Y. Xu, X. Bai, L. Guo, X. Li, J. Gao, Y. Teng, P. Yu. Prediction of the mechanisms of action of Zhibai Dihaung Granule in cisplatin-induced acute kidney injury: A network pharmacology study and experimental validation. *J Ethnopharmacol.,* **2022**, *292*, 115241. https://doi.org/10.1016/j.jep.2022.115241.

28. S. Pal, M. L. Yellurkar, P. Das, V. Sai Prasanna, S. Sarkar, R. L. Gajbhiye, R. Velayutham, S. Arumugam. A network pharmacology, molecular docking and in vitro investigation of Picrorhiza kurroa extract for the treatment of diabetic nephropathy. *Journal of Biomolecular Structure and Dynamics.,* **2024**, 1. https://doi.org/10.1080/07391102.2024.2314259.

29. X. Li, Q. Tang, F. Meng, P. Du, W. Chen. INPUT: An intelligent network pharmacology platform unique for traditional Chinese medicine. *Computational and Structural Biotechnology Journal.,* **2022**, *20*, 1345. https://doi.org/10.1016/j.csbj.2022.03.006.

30. S. X. Ge, D. Jung, R. Yao. ShinyGO: a graphical gene-set enrichment tool for animals and plants. *Bioinformatics.,* **2020**, *36*, 2628. https://doi.org/10.1093/bioinformatics/btz931.

31. F. Zhang, R. Wu, Y. Liu, S. Dai, X. Xue, Y. Li, S. Gong. Nephroprotective and nephrotoxic effects of Rhubarb and their molecular mechanisms. *Biomedicine & Pharmacotherapy.*, **2023**, *160*, 114297. https://doi.org/10.1016/j.biopha.2023.114297.

32. C. -y. Fang, D. -y. Lou, L. -q. Zhou, J. -c. Wang, B. Yang, Q. -j. He, J. -j. Wang, Q. -j. Weng. Natural products: potential treatments for cisplatin-induced nephrotoxicity. *Acta Pharmacologica Sinica.,* **2021**, *42*, 1951. https://doi.org/10.1038/s41401-021-00620-9.

33. L. Zhang, X. -p. Li, J. -q. Lai, L. Zhang, editors. Bioinformatics databases for network pharmacology research of traditional chinese medicine: A systematic review. **2017** IEEE *International Conference on Bioinformatics and Biomedicine* (BIBM); **2017**: IEEE.

34. F. Noor, M. Tahir ul Qamar, U. A. Ashfaq, A. Albutti, A. S. Alwashmi, M. A. Aljasir. Network pharmacology approach for medicinal plants: review and assessment. *Pharmaceuticals.,* **2022**, *15*, 572. https://doi.org/10.3390/ph15050572.

35. G. Xiong, Z. Wu, J. Yi, L. Fu, Z. Yang, C. Hsieh, M. Yin, X. Zeng, C. Wu, A. Lu, X. Chen, T. Hou. ADMETlab 2.0: an integrated online platform for accurate and comprehensive predictions of ADMET properties. *Nucleic Acids Research.,* **2021**, *49*, W5-W14. https://doi.org/10.1093/nar/gkab255.

36. D. Gfeller, A. Grosdidier, M. Wirth, A. Daina, O. Michielin, V. Zoete. SwissTargetPrediction: a web server for target prediction of bioactive small molecules. *Nucleic Acids Research.,* **2014**, *42*, W32-W8. https://doi.org/10.1093/nar/gku293.

RESEARCH ARTICLE

37. M. -y. Liu, D. -x. Jiang, X. Zhao, L. Zhang, Y. Zhang, Z. -d. Liu, R. -z. Liu, H. -j. Li, X. -y. Rong, Y. -z. Gao. Exploration in the Mechanism of Ginsenoside Rg5 for the Treatment of Osteosarcoma by Network Pharmacology and Molecular Docking. *Orthopaedic Surgery.*, **2024**, *16,* 462. https://doi.org/10.1111/os.13971.

38. X. Liu, S. Ouyang, B. Yu, Y. Liu, K. Huang, J. Gong, S. Zheng, Z. Li, H. Li, H. Jiang. PharmMapper server: a web server for potential drug target identification using pharmacophore mapping approach. *Nucleic Acids Research.*, **2010**, *38*, W609-W14. https://doi.org/10.1093/nar/gkq300.

39. X. Xie, H. Lou, Y. Shi, G. Gan, H. Deng, X. Ma, M. Meng, X. Gao. A network pharmacological-based study of the mechanism of Liuwei Dihuang pill in the treatment of chronic kidney disease. *Medicine.*, **2023**, *102*, e33727. https://doi.org/10.1097/MD.0000000000033727.

40. L. Zhang, S. Lu, Z. Hu, M. Liao, C. Li, S. Kong. Prediction of the anti-inflammatory effects of bioactive components of a Hippocampus species-based TCM formulation on chronic kidney disease using network pharmacology. *Trop. J. Pharm. Res.,* **2021**, *20*, 2355. https://doi.org/10.4314/tjpr.v20i11.18.

41. P. Shannon, A. Markiel, O. Ozier, N. S. Baliga, J. T. Wang, D. Ramage, N. Amin, B. Schwikowski, T. Ideker. Cytoscape: a software environment for integrated models of biomolecular interaction networks. *Genome Res.*, **2003**, *13*, 2498. https://doi.org/10.1101/gr.1239303.

42. R. Zhang, X. Zhu, H. Bai, K. Ning. Network pharmacology databases for traditional Chinese medicine: review and assessment. *Front. Pharmacol.*, **2019**, *10*, 123. https://doi.org/10.3389/fphar.2019.00123.

43. J. Zhao, J. Yang, S. Tian, W. Zhang. A survey of web resources and tools for the study of TCM network pharmacology. *Quantitative Biology.*, **2019**, *7*, 17. https://doi.org/10.1007/s40484-019-0167-8.

44. P. Shannon, A. Markiel, O. Ozier, N. S. Baliga, J. T. Wang, D. Ramage, N. Amin, B. Schwikowski, T. Ideker. Cytoscape: a software environment for integrated models. *Genome Res.,* **1971**, *13*, 426. https://doi.org/10.1101/gr.1239303.

45. C. v. Mering, M. Huynen, D. Jaeggi, S. Schmidt, P. Bork, B. Snel. STRING: a database of predicted functional associations between proteins. *Nucleic Acids Research.,* **2003**, *31*, 258. doi:https://doi.org/10.1093/nar/gkg034.

46. B. T. Sherman, M. Hao, J. Qiu, X. Jiao, M. W. Baseler, H. C. Lane, T. Imamichi , W. Chang. DAVID: a web server for functional enrichment analysis and functional annotation of gene lists (2021 update). *Nucleic Acids Research.*, **2022**, *50*, W216-W21. https://doi.org/10.1093/nar/gkac194.

47. Q. Yang, S. Wang, E. Dai, S. Zhou, D. Liu, H. Liu, Q. Meng, B. Jiang, W. Jiang. Pathway enrichment analysis approach based on topological structure and updated annotation of pathway. *Briefings in Bioinformatics.*, **2019**, *20*, 168. https://doi.org/10.1093/bib/bbx091.

48. G. O. Consortium. The Gene Ontology (GO) database and informatics resource. N*ucleic Acids Research.*, **2004**, *32*, D258-D61. https://doi.org/10.1093/nar/gkh036.

49. M. Kanehisa, M. Furumichi, M. Tanabe, Y. Sato, K. Morishima. KEGG: new perspectives on genomes, pathways, diseases and drugs. *Nucleic Acids Research.*, **2017**, *45*, D353-D61. https://doi.org/10.1093/nar/gkw1092.

REVIEW ARTICLE

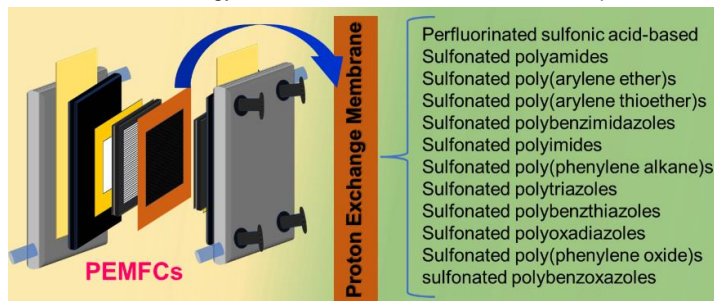# Proton Exchange Membrane Fuel Cells: A Sustainable Approach Towards Energy Generation

Bholanath Ghanti ⓘ , and Susanta Banerjee ⓘ *

Materials Science Centre, Indian Institute of Technology Kharagpur, Kharagpur 721302, India.

*Correspondence: susanta@matsc.iitkgp.ac.in

Abstract: Fuel cell technologies are on the verge of creating new milestones in energy conversion devices in the automobile, portable, and transportation sectors. This review article summarizes all types of fuel cells. Proton exchange membrane fuel cells (PEMFCs) have earned massive attention due to their high efficiency, light weight, rapid startup ability, low noise, and net-zero carbon emissions. The perfluorinated sulfonic acid-based membranes are the most utilized proton exchange membrane (PEM) materials; however, they have severe disadvantages. Henceforth, there is a noteworthy urge to develop alternative PEMs for PEMFC applications. The current research aims to design and develop alternative hydrocarbon-based membranes with improved properties and performance for PEMFC applications. This review starts with the essential components and the working principle of the PEMFC. Then, it explores the recent advances in various alternative sulfonated PEM materials for PEMFC applications, highlighting their synthetic process, PEM properties, and single-cell performances. Unlike a particular PEMFC-related topics review, this literature review emphasizes a comprehensive review of recent advances in the field of various types of hydrocarbon-based alternative sulfonated PEM materials, such as sulfonated polyamides, sulfonated poly(arylene ether)s, sulfonated poly(arylene thioether)s, sulfonated polybenzimidazoles, sulfonated polyimides, sulfonated poly(phenylene alkane)s, sulfonated polytriazoles, sulfonated polybenzothiazoles, sulfonated polyoxadiazoles, etc.

Keywords: *Fuel cell, ion exchange capacity, membrane, proton exchange membrane, sulfonated, sustainable, proton conductivity.*

Contents

Abbreviations

AFC: alkaline fuel cell; AEM: anion exchange membrane; AEMFC: anion exchange membrane fuel cell; CL: catalyst layer; CuAAC: Cu(I)-catalyzed azide-alkyne cycloaddition; DS: degree of sulfonation; DMFC: direct methanol fuel cell; DPP: diphenyl phosphite; EV: electrical vehicle; EW: equivalent weight; FC: fuel cell; GDL: gas-diffusive layer; GHG: greenhouse gas; GPC: gel permeation chromatography; HOR: hydrogen oxidation reaction; ICE: internal combustion engine; IEC: ion exchange capacity; MCFC: molten carbonate fuel cell; MEA: membrane electrode assembly; MOF: metal organic framework; ORR: oxygen reduction reaction; OCV: open circuit voltage; PC: proton conductivity; PDI: polydispersity index; PEM: proton exchange membrane; PEMFC: proton exchange membrane fuel cell; PA: phosphoric acid; PPA: polyphosphoric acid; PAFC: phosphoric acid fuel cell; PEFC: polymer electrolyte membrane fuel cell; PFSA: perfluorinated sulfonic acid; PPD: peak power density; PTFE: polytetrafluoroethylene; PY: pyridine; RH: relative humidity; ROS: reactive oxygen species; RW: residual weight; SACFC: super acid-catalyzed Friedel-Craft; SOFC: solid oxide fuel cell; SPA: sulfonated polyamide; SPAE: sulfonated poly(arylene ether); SPATE: sulfonated poly(arylene thioether); SPBI: sulfonated polybenzimidazole; SPI: sulfonated polyimide; SPPA: sulfonated poly(phenylene alkane); SPT: sulfonated polytriazole; SPBT: sulfonated polybenzthiazole; SPOD: sulfonated polyoxadiazole; SR: swelling ratio; TPP: triphenyl phosphite; WU: water uptake.

and industrialization, the rapid consumption of natural fossil fuels has led to the emission of harmful greenhouse gases

Biographical Information

Bholanath Ghanti is currently working in the Department of Materials Science Centre, Indian Institute of Technology Kharagpur, India, as a research scholar under the supervision of Prof. Susanta Banerjee. He completed his M.Sc. from the Department of Chemistry, IIT Kharagpur, India, in 2020. His current area of research interest is polymer and proton exchange membrane fuel cells.

Susanta Banerjee has been with the Indian Institute of Technology Kharagpur for over 19 years. He previously served as the head of the Materials Science Centre from May 2014 to May 2017 and is currently the Institute Chair Professor and Chairperson of Central Research Facility. Prior to joining IIT Kharagpur, he spent 14 years as a Scientist at DRDO and the GE India Technology Centre in Bangalore. He has been awarded the prestigious AvH fellowship from Germany and is a fellow of the WAST. Prof. Banerjee has supervised more than 30 doctoral and 45 master's theses in polymer and materials science and engineering. He has led numerous innovative projects at DRDO, GEITC, and IIT-Kharagpur, driven by his commitment to endorse future sustainability. He is the founding Editor-in-Chief of the journal *Innovation of Chemistry & Materials for Sustainability*.

1. Introduction

There is a never-ending need to develop eco-friendly energy conversion and storage technologies to fulfill the overwhelming demands of global energy.[1-3] Fossil fuels such as oils, coal, and natural gases are the primary sources of global energy, contributing 84% of the total consumed global energies as of 2019.[3,4] The contribution of the different energy sources in total global energy consumption is depicted in **Figure 1a**. With the exponentially growing world population
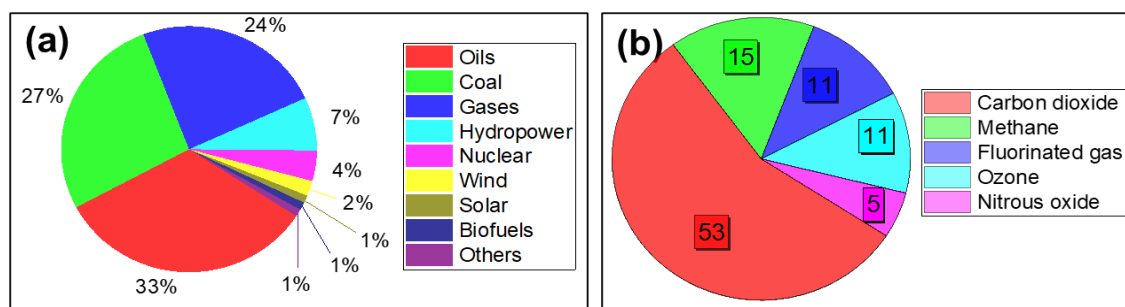
Figure 1. (a) Contribution of various energy sources in total global energy consumption,[3] and (b) Contribution of the different GHGs in global warming.[15]

(GHGs), including CO_x, SO_x, and NO_x, which play an important role in global warming, air pollution, and climate change.[5-8] Carbon dioxide (CO_2) emissions have increased by more than 40% since the Industrial Revolution.[9,10] In this decade, the rate of CO_2 emissions on the planet is 50 billion tons per year.[11,12] Since 1880, the rate of global warming increase was 0.08 ℃ per decade, but recently, it has been 0.18 ℃ per decade.[13] The Intergovernmental Panel on Climate Change (IPCC) reported that the global temperature has climbed by 1.5 °C since the Industrial Revolution.[14] So, the CO_2 emissions rate must be reduced before reaching the 2 °C mark this decade. The global warming caused by the various GHGs is shown in **Figure 1b**.[15] Thus, it is mandatory to focus on alternative renewable and sustainable energy production technology due to the high price, detrimental environmental impacts, and depletable nature of fossil fuel resources.[16-18]

Therefore, an alternative power generation source is essential to fulfill the global energy demand and solve the energy crisis issues, which causes less environmental pollution and has high efficiency and power supply capacity. Over time, internal combustion engines (ICEs) have been considered the most popular energy conversion technology in all sectors, from transportation to power suppliers.[19] However, the ICEs also have various disadvantages, such as the emission of GHGs, relatively low energy conversion efficiency, high noise, and usage of non-renewable fuels for energy conversions.[20-22] So, it is noteworthy to develop alternative green, sustainable, and renewable energy conversion technology to safeguard our society and environment by fulfilling the overwhelming social, industrial, and economic demands. In this direction, the most utilized sustainable and renewable energy conversion technologies are wind power, solar energy, biofuel, hydrothermal, geothermal, and many more.[23,24] These types of energy sources efficiently produce energy with net zero air pollution and GHGs emissions.[24,25] In the 21st century, renewable and sustainable energy production technologies have gained remarkable attention as a mainstream contributor owing to their reliability, affordability, and sustainability, but most of

these technologies are in the developing stage.[24,26,27] Among these renewable and sustainable energy production technologies, fuel cell (FC) is the most demanding and promising because of its high efficiency, silent nature, rapid start-up abilities, and net-zero carbon emission.[28-31] FC technology has achieved notable interest in energy conversion technology to serve future energy demands sustainably.

This review article provides a brief history and recent advancements in FC technology. The different types of FCs and their essential components, efficiency, limitations, and applicability are discussed. This review article emphasized the working principle, essential components, basic requirements, and commercially available proton exchange membrane (PEM) materials and mainly focused on the recent developments and endeavors in the field of alternative sulfonated proton exchange membrane fuel cells (PEMFCs), precisely, the synthesis, characterization, PEM properties, and single fuel cell applications of the recently developed hydrocarbon-based alternative sulfonated copolymer backbones [polyamides, poly(arylene ether)s, poly(arylene thioether)s, polybenzimidazoles, polyimides, poly(phenylene alkane)s, polytriazoles, polybenzothiazoles, polyoxadiazoles, etc.].

2. Fuel Cells (FCs)

2.1 Brief History

Fuel cells are electrochemical devices that directly convert the chemical energy of fuels and oxygen into electrical energy without any direct combustion reaction or emission of harmful GHGs.[32,33] It has a long history before flourishing in several applications of the current scenario. Humphry Davy laid the scientific foundation of the FC in 1801, who discovered several new metals (sodium, potassium, and alkali earth) by splitting the common compounds using a voltaic pile electrolysis.[32,34] Then, it was first designed by Christian Friedrich Schönbein in 1838.[32,35] In 1839, Sir William Robert Grove generated electricity for the first time by the electrochemical reaction between hydrogen (H_2) and oxygen (O_2) in a gas voltaic battery.[36-38] Then, the term "fuel cell" was
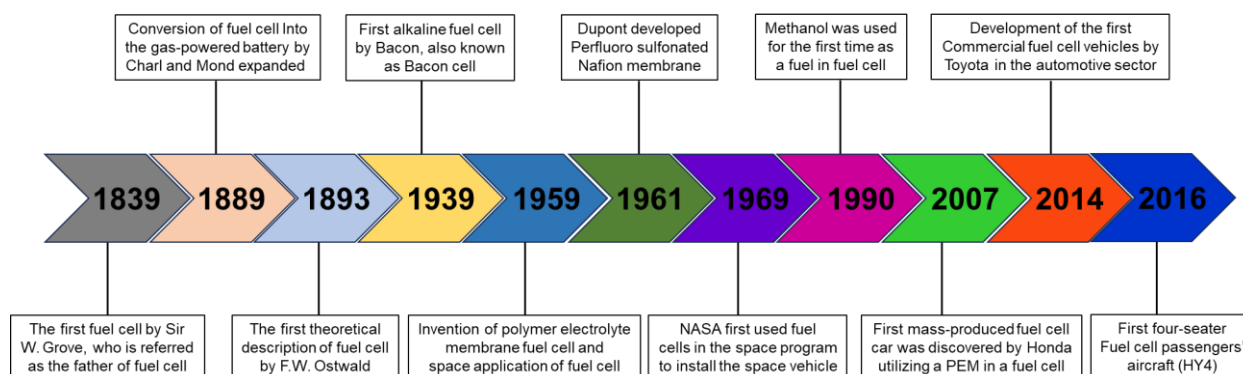
Figure 2. Chronological illustration of the significant developments in the field of FCs.[19,47]

Banerjee and Ghanti

Innov. Chem. Mater. Sustain. **2025**, 2(1), 032-073

Table 1. *Comparison of all types of FC along with their related applications.*[3,45,47,51,52]

Characteristics	PEFCs	DMFCs	AFCs	PAFCs	MCFCs	SOFCs
Operating temperature (℃)	60-100	70-130	60-250	150-210	500-700	500-1000
Primary fuel	H_2	CH_3OH	H_2	H_2	H_2, CO, CH_4	H_2, CO, CH_4
Electrolyte	Polymer membrane	Polymer membrane	30-50% of KOH solution in water	Phosphoric acid	Molten carbonate ceramic matrix	Solid oxide ceramic matrix
Catalyst	Pt and Pt/Ru	Pt and Pt/Ru	Pt	Pt	Ni	Ni, Perovskites
Conductive ion by electrolyte	H^+/HO^-	H^+	HO^-	H^+	CO_3^{2-}	O^{2-}
Efficiency (%)	40-55	40	60-70	40-50	50-60	40-60
Production power (kW)	≤25	<10	≤20	>50	>1	>200
Advantages	Low operating temperature, small size, lightweight, rapid startup	Low operating temperature, low primary fuel cost, high power density	Less expensive, rapid startup ability, and a wide range of applications	Suitable for combined heat and power (CHP), high impurity tolerance capability	Fuel variety and high-efficiency	High efficiency, fuel flexibility, suitable for CHP and hybrid/gas turbine cycle
Disadvantages	Highly sensitive to temperature, humidity, salinity, and fuel impurities	Low reaction kinetics, the fuel gas is highly toxic and flammable	Highly sensitive to CO_2 in air and fuel gas, electrolyte management (leakage issue), and electrolyte conductivity	Expensive, high startup time, and highly sensitive to sulfur	Slow response time, low gas-crossover resistivity, and low power density	High temperature, long startup time, intensive heat, and limited number of shutdowns
Applications	Vehicles and power plants	Portable applications	Submarine and space	Power plants	Power plants	Power plants

introduced for the first time by Ludwig Mond and Charles Langer in 1889, as they used coal as a fuel and obtained a current density value of 20 A/m^2 at 0.73 V.[39,40] Francis T. Bacon developed the first alkaline fuel cell (AFC) in 1932, which also known as a "Bacon cell."[41] In 1959, Willard Thomas Grubb and Leonard Niedrach designed and developed the PEMFC for the first time, which was used by NASA in the Gemini space program to provide power and drinking water to the astronauts.[42,43] Then, the interest in incorporating FC in electrical vehicles (EVs) has arisen since 1970, and finally, it was commercialized in 2007.[44-46] In this scenario, worldwide research is ongoing to commercialize the FC to fulfill global energy requirements. The major developments achieved in FC history are shown in **Figure 2**. Since 2008, FC technology has been commercialized for various types of applications.[40,47,48]

2.2 Classification, Applications, Advantages, and Disadvantages

The core components of FCs are an electrolyte, an anode (negative electrode), and a cathode (positive electrode). Depending on the electrolytes and operating temperatures, FCs are classified as alkaline fuel cells (AFCs), direct methanol fuel cells (DMFCs), molten carbonate fuel cells (MCFCs), phosphoric acid fuel cells (PAFCs), polymer electrolyte fuel cells (PEFCs), and solid oxide fuel cells (SOFCs).[3,32,44,49-50] The essential characteristics (operating temperature, electrolyte, life span, efficiency, and required fuels), limitations (advantages and disadvantages), and applications of all types of FC are compiled in **Table 1**.

In light of the aforementioned overview of FCs, it can be concluded that FC technologies will benefit from fulfilling the global energy demand and the energy crisis. FCs have various applications, advantages, and disadvantages depending on the operating temperature, efficiency, and types of electrolytes; those are illustrated as a general overview in **Figure 3**.[1,3]
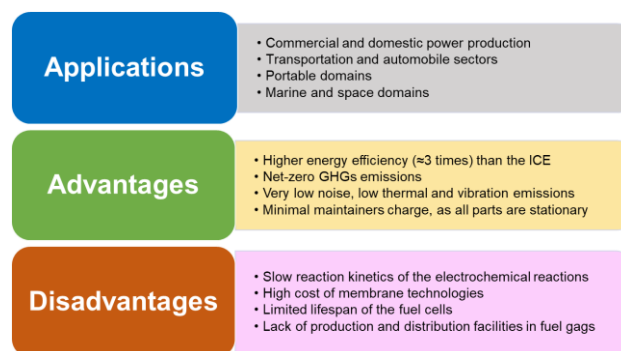
Figure 3. Vertical schematic illustration of applications, advantages, and disadvantages of fuel cell technologies.[1,3]

3. Proton Exchange Membrane Fuel Cells (PEMFCs)

3.1 Comparison and Preference

Among all types of FCs, PEFCs are the most popular, demanding, and favorable type of FC due to their high theoretical (83%) and practical (~50%) efficiencies, low processing temperature range, rapid startup capability, and minimal maintenance charge.[53,54] PEFCs are also classified as proton exchange membrane fuel cells (PEMFCs) and anion exchange membrane fuel cells (AEMFCs), depending on the
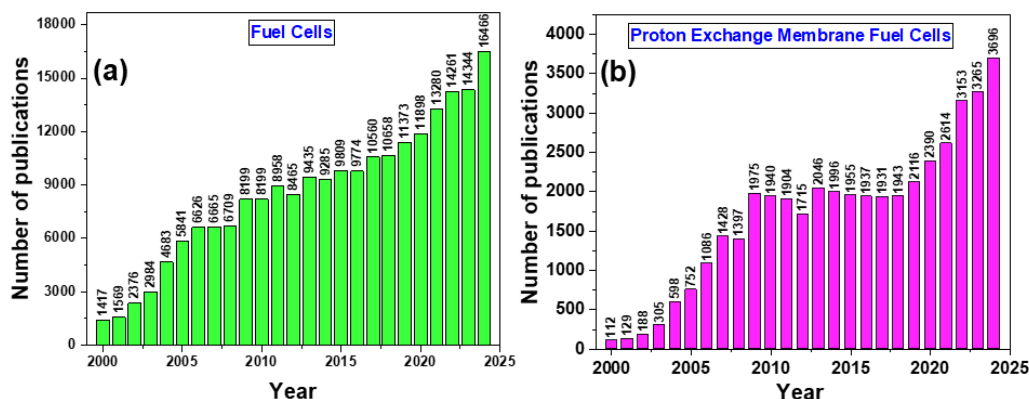
Figure 4. A figure of the year-wise number of publications in (a) FCs and (b) PEMFCs since 2000 (data obtained from Scopus by searching "Fuel Cells" and "Proton Exchange Membrane Fuel Cells").

Banerjee and Ghanti

Innov. Chem. Mater. Sustain. **2025**, 2(1), 032-073
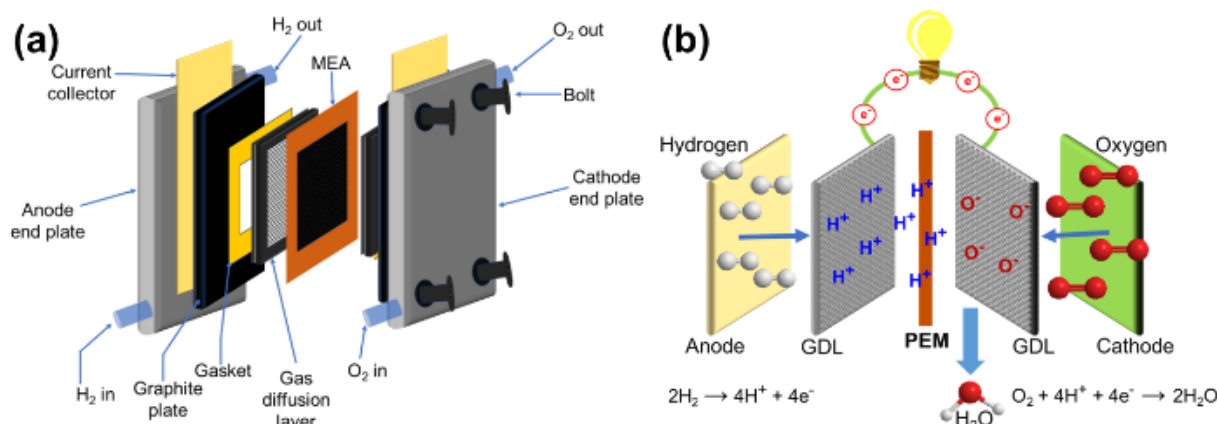
Figure 5. Schematic illustration of (a) structure and (b) working principle of PEMFCs.[81,82]

types of polymeric backbone (electrolyte).[54-57] There are some distinct differences between PEMFCs and AEMFCs. In the case of PEMFCs, the solid polymeric backbone is a cation-exchangeable negatively charged polymer backbone, whereas that of the AEMFCs is an anion-exchangeable positively charged polymeric backbone.[58-64] The basic comparison between the PEMFCs and AEMFCs is shown in **Table 2**.[58] The conductive ions are also different for PEMFCs and AEMFCs; specifically, protons (H^+ ions) are transported between the electrodes for the earlier one, in contract hydroxides (HO^- ions) are transported between the electrodes for the later one.[55] Additionally, water (H_2O) molecules are produced as a product in the cathode for PEMFCs, whereas H_2O is formed at the anode and consumed at the cathode for AEMFCs (**Table 2**).[28,55,65,66] Usually, the polymer electrolyte membranes or proton exchange membranes (PEMs) exhibited higher ionic conductivity values compared to that of the anion exchange membrane (AEM), which can be ascribed due to the intrinsic higher mobility of the protons than the hydroxide ions.[58,67] So, a high ion exchange capacity (IEC) value of the AEM is required to achieve high ionic conductivity values as exhibited by a PEM, but this may cause deterioration of the AEM's mechanical properties and dimensional stability.[58,68,69]

Table 2. *The essential components and characteristics of PEMFCs and AEMFCs.*[55,65,66]

Characteristics	PEMFCs	AEMFCs
Polymer electrolytes	Anionic polymer backbone	Cationic polymer backbone
Conductive ion	H^+	HO^-
Catalyst	Pt, Pt/C, PtCo/C, PtNi/C	Pt, PtRu, Ni alloy
Electrodes reaction	Anode: $2H_2 \rightarrow 4H^+ + 4e^-$	Anode: $2H_2 + 4HO^- \rightarrow 4H_2O + 4e^-$
	Cathode: $O_2 + 4H^+ + 4e^- \rightarrow 2H_2O$	Cathode: $O_2 + 2H_2O + 4e^- \rightarrow 4HO^-$
Availability	Readily available	Limited availability

Furthermore, AEMs may lose some of the quaternary charge-carrier sites in the AEM's backbone due to hydrolysis or elimination reactions of the hydroxide ion during the AEMFC operations that lead to the potential reduction of the IEC value and consequently, reduction in ionic conductivity value and durability of the AEMs.[58,70-73]

The PEMFCs gained remarkable global recognition as sustainable and renewable energy-producing sources because of their higher ionic conductivity and better durability

than the AEMFCs.[55,74-76] That is due to their high energy efficiency, rapid startup ability, low operating temperature, high power density, and net-zero environmental impacts.[19,28,77-80] A significant number of research on FCs and PEMFCs is ongoing in this decade, and the number of publications on FCs and PEMFCs since 2000 is depicted in **Figure 4**. **Figure 4b** shows that the research activity in the field of PEMFCs has increased substantially since 2022, which indicates the rapid growth of PEMFC-based research interest in sustainable and renewable energy generation.[81]

3.2 Structure and Working Principle

The schematic representation of a PEMFC is shown in **Figure 5a**. The essential components of a PEMFC are end plates, current collectors, graphite plates, gas diffusion plates/layers, gaskets, and membrane electrode assembly (MEA), respectively.[82,83] Among these, the MEA is the heart of the PEMFC, where electrochemical reactions occur.[84] The MEA comprises porous carbon papers, catalyst layers (CL), and PEM.[84-86] The porous carbon paper acts as a gas-diffusive layer (GDL), which helps to diffuse the fuel gases into the CLs.[84-86] The CL generally contains platinum on carbon (Pt/C), in which the hydrogen oxidation reaction (HOR) and oxygen reduction reaction (ORR) take place.[84-86] The PEM is the most vital component of the MEA, which acts as a semipermeable layer.[80,87,88] The PEM conducts the protons from the anode to the cathode, where the ORR occurs, and it resists the movement of electrons and fuel gases through it.[80,84-89] The PEM is sandwiched between the two electrodes and functions as a separator between them by preventing the crossover of the fuels.[80,84-90]

In PEMFCs, electricity is produced from the chemical energy of a fuel (H_2) via the electrochemical reaction with oxygen.[91] The schematic illustration of the working principle of a PEMFC is provided in **Figure 5b**. Initially, the anode's fuel gas (H_2) undergoes electrochemical oxidation in the CL's metal surface (Pt), producing H^+ ions and electrons.[91,92] Then, the PEM conducts these protons to the cathode via the Grotthuss and Vehicular mechanism.[28,55,93,94] The electrons flow towards the cathode through an external wire, producing electricity that powers external devices.[91,93] Finally, the electrochemical reduction reaction of O_2 occurs on the anode's CL in the presence of those received protons and electrons, and water is obtained as the product.[91,95] The electrochemical reactions, along with the overall reaction of the PEMFC, are shown below:

The HOR (anode): $2H_2 \rightarrow 4H^+ + 4e^-$.
The ORR (cathode): $O_2 + 4H^+ + 4e^- \rightarrow 2H_2O$.
The overall reaction: $2H_2 + O_2 \rightarrow 2H_2O$.
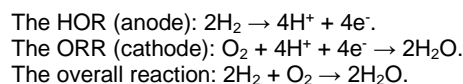
4. Proton Exchange Membrane (PEM)

4.1 Role and Criteria

The PEM is the most vital component of a PEMFC.[91,94,95] It functions as a positively charged-carrier solid electrolyte by blocking the crossover of the fuel gases between the electrodes in a PEMFC.[28,93-95] The PEM must possess the following characteristics for fruitful and efficient PEMFC operations.

❖ *Proton conductivity* (PC): A PEM must possess a high proton conductivity (σ) value for the facile H^+ ions transportation between the electrodes, reducing the internal resistance in the PEMFC.[82,96] Consequently, the PEM leads to a high efficiency and power density during the PEMFC operations.

❖ *Fuel gas resistivity*: The PEM should exhibit a high fuel resistivity for efficient PEMFC applications. If the fuel gases cross through the PEM, then this also leads to a loss of fuel and reduction of the cell voltages, and hence, the efficiency of PEMFC reduces.[82,97]

❖ *Chemical/oxidative stability*: PEMs should have high chemical or oxidative stability for long-term, durable, and efficient PEMFC applications.[82] During the real-time fuel cell operating conditions, peroxide radicals are formed due to the partial reduction of the oxygen molecules, and these reactive oxygen species (ROSs) may degrade the PEM backbone.[98,99] Therefore, the PEM should withstand a high oxidative resistance for durable and efficient PEMFC applications.

❖ *Dimensional stability*: PEMs must exhibit high dimensional stability under the PEMFC operating conditions for better water management properties and to maintain a fixed and tight interface with the CL of the MEA.[82,99]

❖ *Thermal and mechanical stabilities*: The PEM should have high thermal and mechanical stabilities to endure its durability and remain resilient during the manufacturing process of MEA.[82]

❖ *Processability and cost-effectiveness*: The PEM materials should be highly processable and cost-effective for their successful integration as a PEM in this competitive market.

4.2 Sulfonated PEMs

The PEM plays the most significant role in the proton migration process from the anode to the cathode during the PEMFC operating conditions and ensures the high power density and efficiency of the PEMFC.[3,28,45,82] The PEM usually comprises a hard hydrophobic segment and a soft hydrophilic segment[96,99,100] The hard hydrophobic part ensures its high mechanical and dimensional stabilities.[96,99,100] It also helps to form a well-segregated and interconnected hydrophobic-hydrophilic phase morphology, which is beneficial for achieving an appropriate proton conductivity value.[96,99,100] On the contrary, the hydrophilic part ensures the high proton conductivity and appropriate water absorption values of the PEM.[96,99,100] The soft hydrophilic segment of the PEM generally contains acidic functionalities or protogenic groups in the solid polymeric backbone.[101,102] The PEMs mainly contain two types of acidic groups in the PEM's backbone: sulfonic acid (-SO_3H) and phosphonic acid (-PO_3H) groups.[96,99,100,101-104] However, the sulfonic acid-containing PEMs are more employed and analyzed than the phosphonic acid-containing PEMs for the PEMFC applications.[101,102] This is mainly due to the higher acidity of the sulfonic acid-containing PEMs compared to the phosphonic acid-containing PEMs, which resulted in a higher proton conductivity value for the earlier one.[105-107] Additionally, the simplistic synthetic procedure of the sulfonic acid-containing PEMs makes them more popular and commercialized than the phosphonic acid-containing PEMs.[101,102] So, the recent studies on the sulfonic acid-containing PEMs are discussed in this review article.

4.2.1 Commercial and State-of-the-Art

The most widely used commercially available PEM material is perfluorinated sulfonic acid (PFSA) ionomer membranes, which are well-known for their outstanding ionic conductivity value and chemical and mechanical stability.[93,108-110] These PFSA-based ionomer membranes are extensively used as a solid-electrolyte separator in PEFCs and chloro-alakli electrolyzer (sodium-ion separator) since 1970.[93] The chemical structures of the commercially available PFSA-based ionomer membranes are depicted in **Figure 6**.[93,110] Generally, these PFSA-based ionomers are classified based on their equivalent weights (EW; grams of polymers per ionic group) and the side-chain length (**Figure 6**).[93,110] In 1960, DuPont developed a PFSA-based Nafion membrane as a solid separator for the chloro-alkali electrolyzer.[93,108,111,112] Nafion is an electronically neutral semicrystalline random copolymer, having a polytetrafluoroethylene (PTFE) backbone and randomly ordered with a pendant perfluorosulfonyl fluoride vinyl ether ionic side chain (**Figure 6**).[93,110] The chemical structures of a few other short side chains (Nafion is considered as a long side chain) PFSA-based ionomers, such as 3M, Aquivion (DOW SSC ionomer or Solvey specialty Polymers), Flemion (Asahi Glass), along with the reinforced composite PFSAs (W. L. Gore & Associates, Inc.) are depicted in **Figure 6**.[93,110] Among these PFSA-based ionomer membranes, DuPont Nafion membrane is considered as the state-of-the-art PEM materials.[3,28,93,94,110] Nafion membrane showed exceptionally high mechanical and dimensional stabilities due to the presence of the hydrophobic PTFE backbone.[93,110,113] The PTFE backbone and pendant perfluorosulfonyl fluoride vinyl ether group in Nafion creates a well-separated and interconnected hydrophobic and hydrophilic phase morphology.[93,110,113] As a result, the PFSA-based Nafion membrane exhibited a high PC value.[93,110,113,114] Additionally, the Nafion membranes endured high chemical stability under the PEMFC operating conditions, mainly associated with the presence of the PTFE backbone and the strong C-F bonds in Nafion's repeat unit.[93,110,113-116]
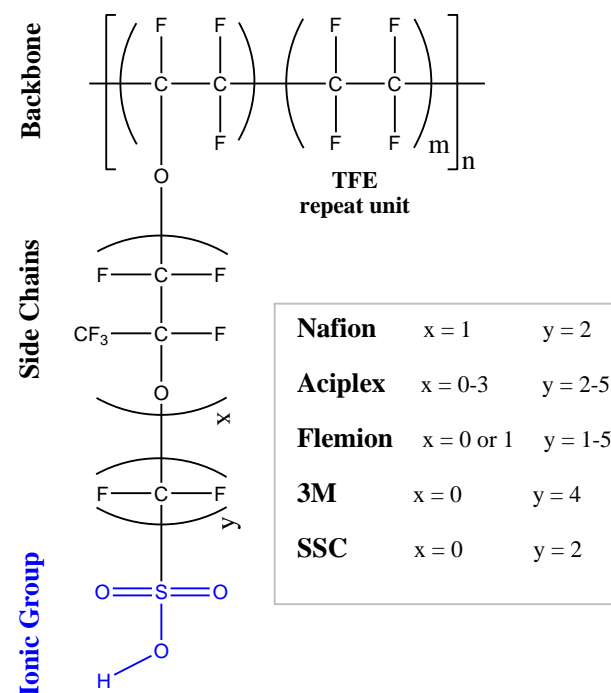
Figure 6. Chemical structures of the commercially available PFSA-based PEM materials [93,110]

Despite the aforementioned superior properties, the Nafion membrane has a few drawbacks, such as its complicated synthetic procedure, high fuel gas permeability, low operating temperature limits, deterioration of mechanical

Banerjee and Ghanti

Innov. Chem. Mater. Sustain. **2025**, 2(1), 032-073
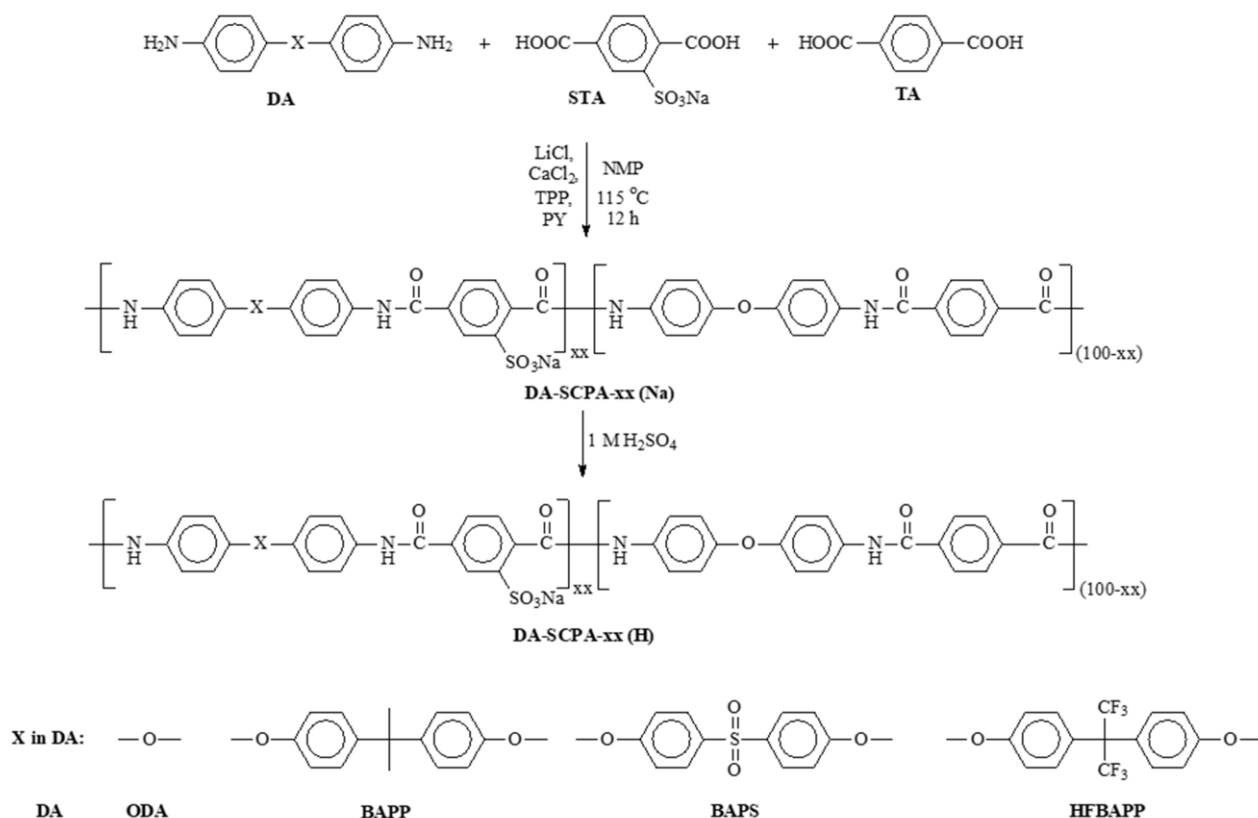
Scheme 1. The synthesis scheme of ether-containing SPAs (DA-SCPA-xx).[140]
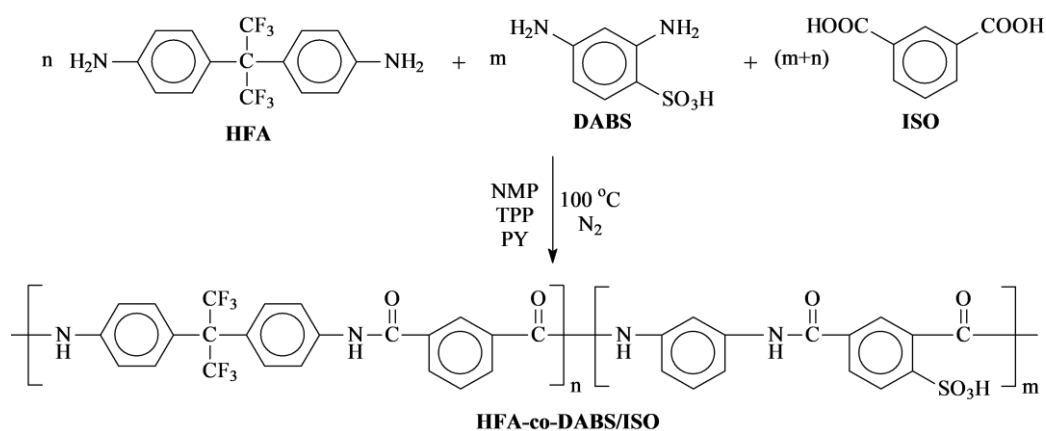
Scheme 2. The synthesis scheme of the semi-fluorinated SPAs (HFA-coDABS/ISO).[142]

stability above 80 ℃, reduction of proton conductivity values at higher temperatures and low humidity levels, and being highly expensive, simulated a golden opportunity for the global researchers to design and develop alternative PEM materials for the PEMFC applications.[28,93,110-117] Recently, aromatic hydrocarbon-based sulfonated PEM materials emerged as a promising alternative to PFSA materials due to their ease of the synthetic procedure and versatility in their structural design.[28,118-121] Recent studies revealed that the various types of aromatic hydrocarbon-based sulfonated PEMs, including polyamides, poly(arylene ether)s, polybenzimidazoles, polyimides, polyphenylenes, polytriazoles, etc., have significant PEM properties.[96,122-130]

4.2.2 Polyamides, PAs

Hydrocarbon-based aromatic sulfonated polyamides (SPAs) are a special type of high-performing engineering polymers because of their high thermal and mechanical stabilities, appropriate stability under acidic conditions, low flammability,

and excellent oxidative stability.[131-136] However, the hydrocarbon-based SPAs have very low processability due to the rigid aromatic backbone and strong interchain hydrogen bonding interactions of the SPA architecture, making them insoluble in many organic solvents.[137,138] Generally, hydrocarbon-based aromatic SPAs are synthesized by the phosphorylation polycondensation reaction between the aromatic diamines and diacids or diacid chloride in the presence of triphenyl phosphite (TPP) or diphenyl phosphite (DPP), pyridine (PY), lithium chloride (LiCl) or calcium dichloride (CaCl₂) in N-methyl-2-pyrrolidone (NMP).[137-139] Herein, the TPP/DPP and PY were used as a condensing agent by forming N-phosphonium pyridinium salts.[139] Hydrocarbon-based aromatic SPAs gained remarkable interest in PEMFC applications due to their high thermal, mechanical, and dimensional stabilities.[140,141] Here, some of the hydrocarbon-based aromatic SPAs are discussed.

JO *et al.* synthesized a set of hydrocarbon-based fluorinated and non-fluorinated SPAs with different degrees of sulfonation (DS) on the dicarbonyl aromatic ring via the phosphorylation polycondensation reaction of terephthalic acid (TA) and sulfonated terephthalic acid (STA) with different aromatic

acid-containing HFAS55 copolymer demonstrated the highest σ value of 3.3 mS/cm at 25 ℃.[142] However, the accelerated Fenton test did not explore the oxidative stability of these SPAs.

Wang *et al.* designed and synthesized a series of pendant

Table 3. *The ion exchange capacity (IEC), weight-average molecular weight (M_w), inherent viscosity (η_{inh}), water uptake (WU), oxidative stability (τ), and proton conductivity (σ) values of the SPAs.*

Polymer	IEC (meq/g)[a]	M_w (kDa)[b]	η_{inh} (dL/g)[c]	WU (%)[d]	τ (h)[e,f]	σ (mS/cm)[g]	Ref.
ODA-SPEA-40 (H)	1.05	80.8	-	17	1.8[e]	6.7	140
ODA-SPEA-50 (H)	1.33	45.5	-	23	1.7[e]	46.7	140
ODA-SPEA-60 (H)	1.56	53.2	-	24	1.6[e]	52.5	140
ODA-SPEA-70 (H)	1.83	60.3	-	32	2.0[e]	105	140
BAPP-SPEA-70 (H)	1.06	102.1	-	17	2.5[e]	8.7	140
BAPS-SPEA-70 (H)	1.11	110.4	-	10	2.8[e]	21.4	140
HFBAPP-SPEA-70 (H)	0.64	119.7	-	13	4.3[e]	1.5	140
HFAS82	0.59	-	0.27	8.5[h]	-	<0.04[i]	142
HFAS73	0.87	-	0.25	16[h]	-	0.04[i]	142
HFAS64	1.02	-	0.18	22[h]	-	0.09[i]	142
HFAS55	1.39	-	0.19	25[h]	-	3.3[i]	142
ODA-STA-TPA-90	2.22	-	1.83	65	-	158	143
ODA-STA-TPA-80	2.05	-	1.78	53	-	129	143
ODA-STA-IPA-90	2.15	-	0.79	67	-	142	143
ODA-STA-TFTPA-90	2.10	-	0.97	55	-	140	143
ODA-STA-TFTPA-80	1.94	-	0.81	48	-	117	143
ODA-STA-TFIPA-90	2.13	-	0.64	50	-	110	143
ODA-STA-GA-90	2.01	-	1.93	42	-	166	143
ODA-STA-GA-80	1.71	-	1.48	40	-	104	143
ODA-STA-SEA-90	1.85	-	0.98	42	-	100	143
ODA-STA-SEA-80	1.75	-	1.97	38	-	41	143
ODA-STA-SUA-90	1.90	-	0.91	38	-	126	143
ODA-STA-SUA-80	1.84	-	1.31	35	-	78	143
ODA-STA-HFGA-90	2.02	-	0.89	36	-	114	143
ODA-STA-HFGA-80	1.75	-	0.53	33	-	94	143
ODA-STA-PFSEA-90	1.91	-	0.82	34	-	125	143
ODA-STA-PFSEA-80	1.78	-	0.64	32	-	103	143
ODA-STA-PFSUA-90	1.90	-	0.60	37	-	111	143
ODA-STA-PFSUA-80	1.65	-	0.53	33	-	91	143
SPA-70	1.39	-	1.23	33	8.0[f]	62	144
SPA-80	1.56	-	1.61	37	6.5[f]	96	144
SPA-90	1.73	-	1.85	44	5.0[f]	127	144
SPA-100	1.89	-	2.16	52	4.5[f]	141	144
CP-1	0.79	-	0.28	9[h]	-	0.053[i]	145
CP-2	0.97	-	0.26	12[h]	-	0.054[i]	145
CP-3	1.11	-	0.24	15[h]	-	0.057[i]	145
CP-4	1.19	-	0.23	20[h]	-	0.113[i]	145
CP-5	1.30	-	0.20	27[h]	-	0.29[i]	145

[a]Theoretical IEC value, [b] weight-average molecular weight, [c] inherent viscosity values, [d] water uptake at 80 ℃, [e] starting dissolution time in Fenton's reagent at 80 ℃, [f] complete dissolution time in Fenton's reagent at 80 ℃, [g] σ values at 80 ℃, [h] WU values at 75 ℃, [i] σ values under fully hydrated state at 25 ℃, [j] proton conductivity in dry conditions.

diamines (DAs) in NMP as depicted in **Scheme 1**.[140] The calculated and titrimetric experimental IEC values of the SPAs were 0.94-1.83 and 0.99-1.80 meq/g (**Table 3**). The flexible ether-linkage containing SPAs showed good solubility in polar aprotic solvents. The weight-average molecular weight (M_w) and polydispersity index (PDI) were obtained between 45-120 kg/mol (**Table 3**) and 2.9-4.4, respectively.[140] Among all the fabricated membranes, the ODA-SPEA-70 (H) exhibited the highest water uptake (WU) value of 32% at 80 ℃ (**Table 3**).[140] The bulky trifluoromethyl (-CF$_3$) groups containing HFBAPP-SPEA-70 (H) demonstrated enhanced oxidative stability in Fenton's reagent due to the electronegative fluorine atoms in the copolymer architecture.[93,113,116] Among the SPA series, the ODA-SPEA-70 (H) membrane exhibited the highest σ value (105.1 mS/cm) at 80 ℃ under 100% relative humidity (RH), as tabulated in **Table 3**.

Aguilar-Vega *et al.* synthesized a series of semi-fluorinated SPAs with increasing DS value by the direct polycondensation reaction of isophthalic diacid (ISO) with two different aromatic diamines [4,4′-(hexafluoroisopropylidene)dianiline (HFA) and 2,4-diaminobenzenosulfonic acid (DABS)] as shown in **Scheme 2**.[142] The synthesized SPAs showed moderate inherent viscosity (η_{inh}) values between 0.18-0.27 dL/g in DMAc (**Table 3**). The SPAs (HFA-co-DABS/ISO) demonstrated high thermal stability (onset temperature was 320 ℃) and mechanical properties (tensile strength, TS: 20-34 MPa; Young's modulus, YM: 280-428 MPa, and elongation at break, EB: 9-12%).[144] The semifluoro-sulfonated copolyamides HFAS64 and HFAS55 exhibited the best water absorption properties at 75 ℃ (**Table 3**). The highest sulfonic

nitrile (-CN) group-based SPAs for the first time by the phosphorylation polyamidation reaction of 2,6-bis(4-aminophenoxy)benzonitrile with two different aromatic dicarboxylic acids (5-sulfoisophthalic acid sodium salt and terephthalic acid) as shown in **Scheme 4**.[144] The η_{inh} values of the SPA-XX copolymers were found between 1.39-2.16 dL/g, as tabulated in **Table 3**. The SPA-XX membranes exhibited the WU and swelling ratio (SR) values in the 32-52% range and 7-18% at 80 ℃, respectively (**Table 3**). The SPA-100 membrane showed the highest σ value of 141 mS/cm at 80 ℃ under fully hydrated conditions (**Table 3**). All the nitrile group bearing SPA-XX membranes demonstrated better oxidative stability values (τ ≥ 4 h, **Table 3**) in Fenton's reagent at 80 ℃, which is even higher than literature-reported SPAs having identical IEC$_w$ values.[140] Thus, the presence of the polar -CN group in the SPA-XX backbone improved the solubility, water absorption properties, and proton conductivity values.[144]

Sulub-Sulub *et al.* prepared a series of block SPAs by the polycondensation reaction of a hydrophobic block [4,4′-(hexafluoroisopropylidene)bis(p-phenyleneoxy)-dianiline, HFD] and a hydrophilic block [4,4′-Diaminobiphenyl-2,2′-disulfonic acid, DFS], as provided in **Scheme 5**.[145] The DS values of the block copolyimides were controlled by varying the mole proportion of the HFD/DFS blocks.[145] The calculated IEC and η_{inh} values of the sulfonated block copolyamides (CP-1 to -5) were between 0.6-1.38 meq/g and 0.20-0.28 dL/g, as illustrated in **Table 3**. The 10% thermal decomposition temperature ($T_{d10\%}$) of CP-1 to CP-5 block copolymers was found between 240-320 ℃.[145] Among all the sulfonated block

Banerjee and Ghanti

Innov. Chem. Mater. Sustain. **2025**, 2(1), 032-073

Scheme 3. The synthesis scheme of the various SPAs (ODA-STA-Y-XX).[143]

Scheme 4. The synthesis scheme of the pendant nitrile group-containing SPAs (SPA-XX).[144]
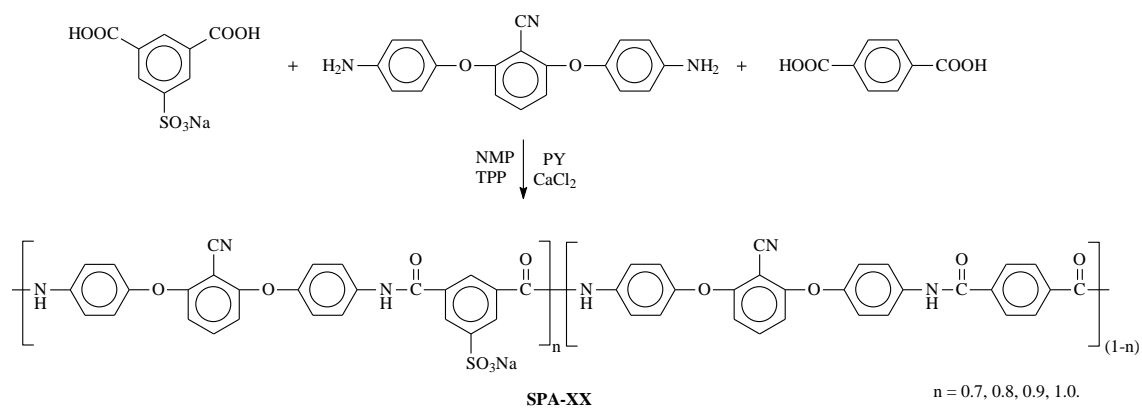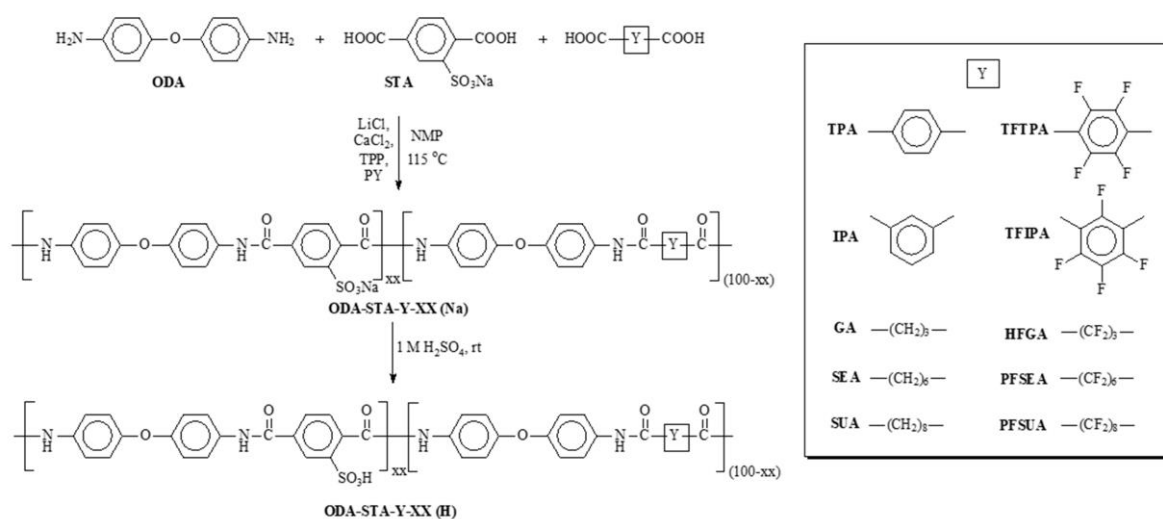
copolyamides, the CP-5 membrane demonstrated the highest water absorption value (WU: 27%) at 75 ℃ (**Table 3**). The sulfonated block copolyamides (CP-1 to CP-5) showed σ values between 0.053-0.29 mS/cm in dry conditions (**Table 3**),

Scheme 5. Synthesis scheme of the block SPAs (HFD-b-DSF).[145]

Banerjee and Ghanti

Innov. Chem. Mater. Sustain. **2025**, 2(1), 032-073
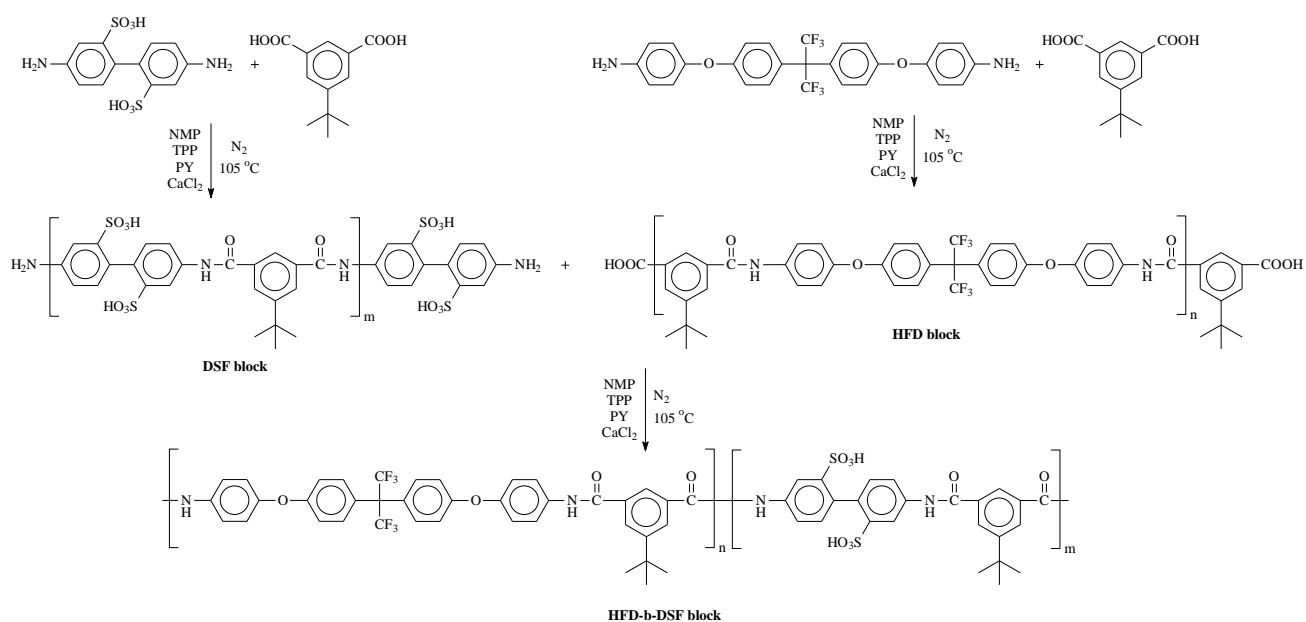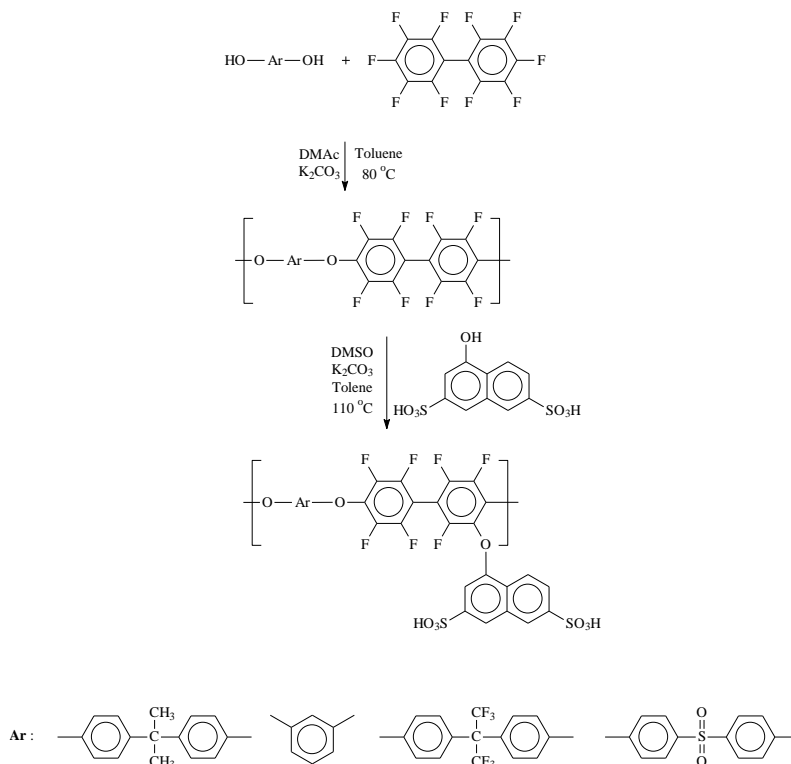
Scheme 6. The synthesis scheme of the pendant disulfonated naphthol-based SPAEs.[153]

which is lower than that of Nafion-115 under similar testing conditions.[145]

4.2.3   Poly(arylene ether)s, PAEs

Sulfonated poly(arylene ether)s (SPAEs) are one of the high-performing thermoplastic engineering materials.[65] These materials are famous for their excellent thermal and mechanical stabilities, high solubility, physical properties, and improved oxidative stabilities.[65,146-148] Generally, PAEs were prepared by the nucleophilic substitution polycondensation reaction of the activated aromatic dihalo or dinitro compounds with the bisphenoxide at high temperatures in polar aprotic solvents.[65,149] The SPAEs were synthesized either by the direct polymerization of the sulfonated comonomers or by post-sulfonation methods. The direct sulfonated polymerization

method has a few advantages, such as the quick variation of the DS values, which is not possible for the post-sulfonation method.[150,151] Though the grafting of sulfonic acid groups in the post-modification method is complex, several PEMs were still designed using this method with well-defined structures.[147,152] A few of the recent SPAEs developed for the PEMFC applications are discussed here.

Four series of pendant disulfonated naphthol-based PAEs with various sulfonic acid contents were prepared via the two-step nucleophilic-substitution reaction by Oroujzadeh *et al.*, as shown in **Scheme 6**.[153] The IEC values of these four sets of SPAEs were between 1.14-2.15 meq/g (**Table 4**). The number-average (M_n) and weight-average (M_w) molecular weights were determined by the gel permeation chromatography (GPC) analysis and obtained between 33000-65000 g/mol and
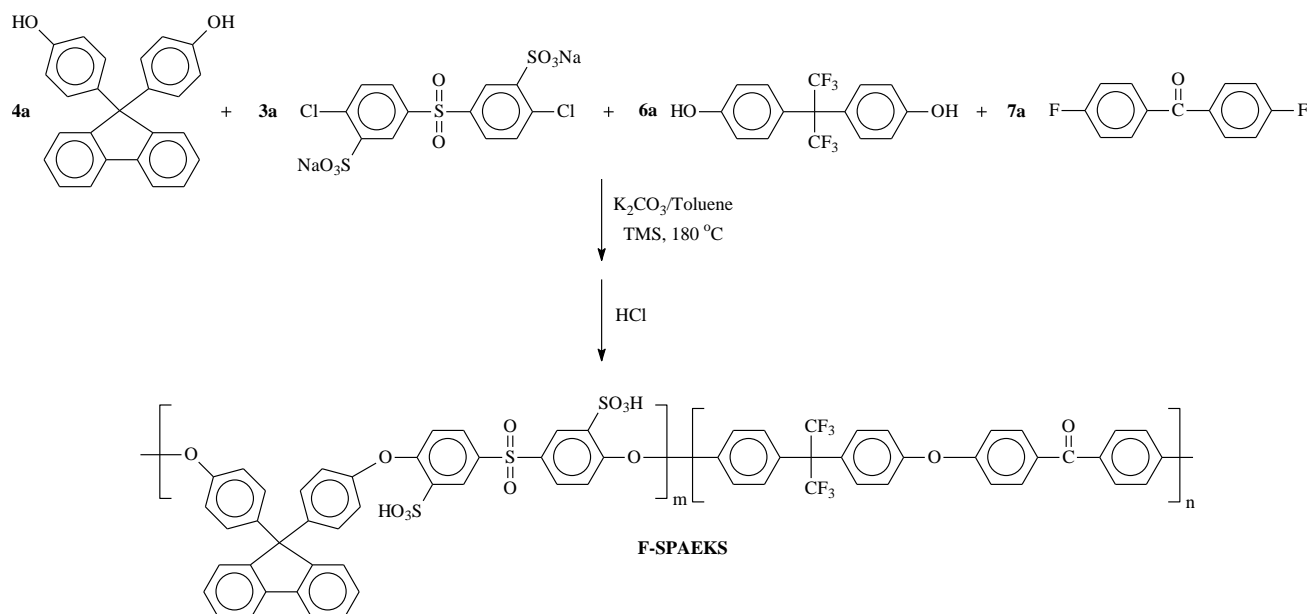
Scheme 7. The synthesis scheme of the semi-fluorinated SPAE copolymers (F-SPAEKS).[154]

97000-163000 g/mol, respectively (**Table 4**). The Dec-AF and Dec-A membranes showed lower water uptake values than the Dec-S and Dec-Res membranes at 80 ℃, as illustrated in **Table 4**.

Among all the membranes, the Dec-AF series membranes exhibited the lowest SR values at 80 ℃, indicating high dimensional stability.[153] The σ values of the SPAEs were obtained between 61-182 mS/cm and 96-217 mS/cm at 30 and 80 ℃, respectively (**Table 4**).[153] The Dec-AF series membranes had the highest oxidative stability in the Fenton reagent.[153] Among all the membranes, the Dec-AF-3 membrane demonstrated the best combined PEM properties [oxidative stability: 118 min; PC: 213 mS/cm at 80 ℃; WU: 66.3% at 80 ℃; and SR: 27% at 80 ℃].[153] Based on the overall PEM properties, the single fuel cell performances were analyzed for the Dec-A-1, Dec-A-3, and Dec-AF-3.[153] Among these three membranes, the Dec-AF-3-based MEA demonstrated the best overall single fuel cell performance with the open circuit voltage (OCV) value 1030 mV, the current density of 1130 mA/cm², and peak power density (PPD) value 336 mW/cm² at 80 ℃ and 100% RH.[153]

4 exhibited a high OCV value of 0.994 V and a maximum PPD value of 466 mW/cm² at 80℃ and 100% RH.[154] Thus, the acid-base bifunctionalized MOFs-based hybrid membrane (FSMNC-4) possessed promising properties as PEM materials. Xu *et al.* synthesized a set of PAEKS copolymers (C-PAEKS-DBS, CPD-x) by the nucleophilic polycondensation reaction, as shown in **Scheme 8**.[155] Finally, a series of pendant sulfonated SPAEKSs (CPDA-x) were synthesized by a simple double bond cross-linking reaction of hydrophilic long alkyl side chains (AMPS) with CPD-x, as depicted in **Scheme 8**.[155] The IEC values of the CPDA-x copolymers were found between 0.67-0.77 mmol/g (**Table 4**).

The CPDA-3 membrane demonstrated higher mechanical properties (TS: 52.2 MPa and YM: 1.72 GPa) than the Nafion-117 membrane.[155] Among all the membranes, the CPDA-3 membrane displayed the lowest water contact angle (40.4º), which confirmed the hydrophilic nature of this membrane.[155] The CPDA-3 membrane showed a high PC value of 77.8 mS/cm at 80 ℃ (**Table 4**) and possessed better oxidative stability [RW: 93.3%] in Fenton's reagent at 80 ℃.[155]
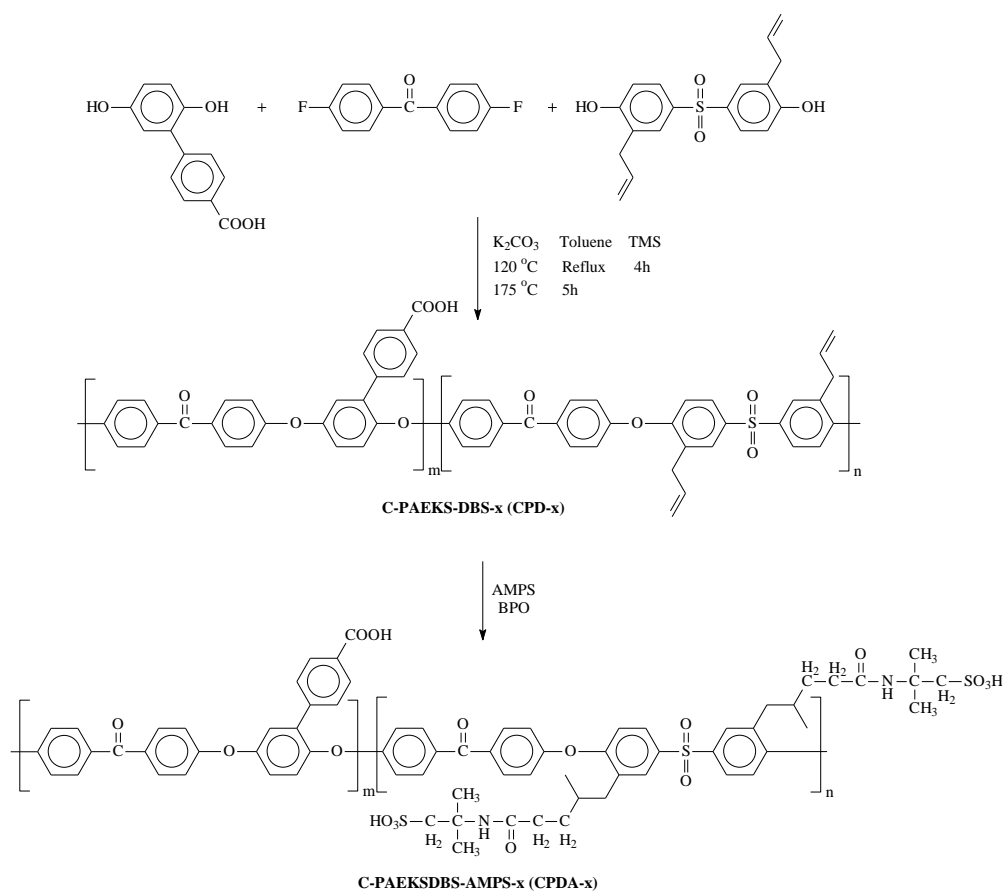
Scheme 8. The synthesis scheme of the C-PAEKSDBS-AMPS-x (CPDA-x) copolymer.[155]

A fluorenyl group containing sulfonated poly(arylene ether ketone sulfone)s (SPAEKSs), F-SPAEKS (IEC: 1.05 meq/g) was synthesized by Wang *et al.*[154] Two series of hybrid matrix membranes (FSMN-x and FSMNC-x) were fabricated by mixing two different functionalized metal organic frameworks (MOFs) (MIL-101-NH₂ and MIL-101-NH₂-COOH) with F-SPAEKS.[154] Among all the hybrid membranes, the FSMNC-4 membrane exhibited the highest WU (21.6%) and SR (9.3%) values at 80 ℃ due to its highest IEC value (1.29 meq/g, **Table 4**). The FSMNC-4 hybrid membrane showed the highest σ value (159.9 mS/cm at 80 ℃) and oxidative stability (residual weight, RW: 95.3%).[154] Also, the FSMNC-4 hybrid membrane exhibited high long-term stability, retaining more than 73% of its initial proton conductivity value even after 96 h.[154] The proton conduction-related activation energy (Eₐ) of the FSMNC-4 hybrid membrane was 7.62 kJ/mol.[154] The FSMNC-

A series of densely sulfonated poly(arylene ether sulfone ketone)s (SPAESK-x) copolymers were synthesized by the post-sulfonation of PAESK-x by Pang *et al.*, as depicted in **Scheme 9**.[156] The calculated and experimental IEC values of the SPAESK-x copolymers were found between 0.99-2.26 meq/g and 0.80-1.82 meq/g, respectively (**Table 4**). The M_w and PDI values of the SPAEKS-x copolymers were between 110-174 kg/mol and 1.56-1.62, as provided in **Table 4**. The SPAEKS-x copolymers showed high thermal stabilities (4 wt% decomposition temperature below 300 ℃) and mechanical properties (TS: 43-62 MPa and EB: 28-44%).[156] The morphological analysis of SPAESK-x membranes showed the formation of a well-separated and inter-connected phase morphology by the small-angle X-ray scattering (SAXS) and transmission electron microscopy (TEM) investigation.[156] The
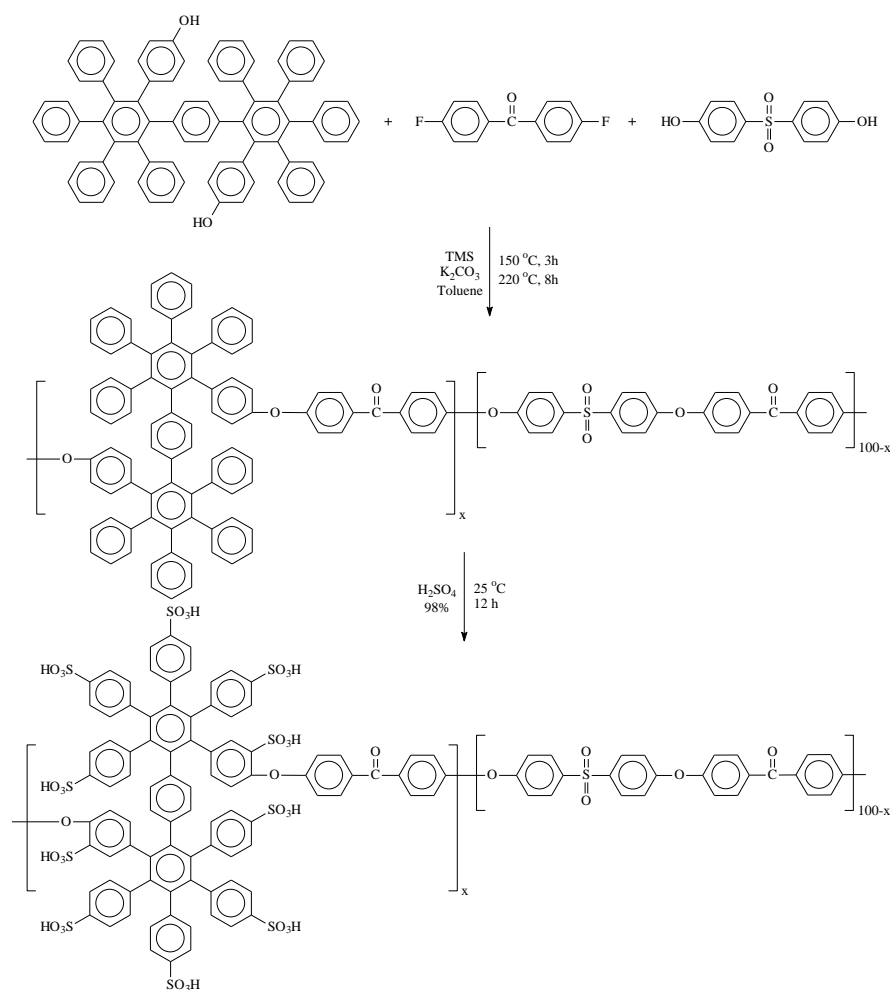
Scheme 9. The synthesis scheme of the PAESK-x and SPAESK-x copolymer.[156]

Table 4. *The IEC, M_w, thermal decomposition temperature (T_d), tensile strength (TS), Young's modulus (YM), elongation at break (EB), WU, τ, and σ values of the SPAEs*

Polymer	IEC (meq/g)[a]	M_w (kDa)[b]	T_d (°C)[c]	TS (MPa)	YM (GPa)	EB (%)	WU (%)[d]	τ (h)[e,f]	σ (mS/cm)[g]	Ref.
Dec-AF-1	1.14		320	-	-	4.8[i]	25[h]	2.06[f]	125	153
Dec-AF-2	1.31	163	235	-	-	6.2[i]	42[h]	1.93[f]	148	153
Dec-AF-3	1.65		118	45.2[i]	-	8.4[i]	66[h]	1.97[f]	213	153
Dec-S-1	1.6		344	-	-	-	43[h]	0.75[f]	213	153
Dec-S-2	1.73	105	345	-	-	-	85[h]	0.53[f]	225	153
Dec-S-3	1.81		118	-	-	-	113[h]	0.63[f]	194	153
Dec-A-1	1.28		238	-	-	3.0[i]	25[h]	1.80[f]	136	153
Dec-A-2	1.46	128	233	-	-	5.4[i]	47[h]	1.73[f]	189	153
Dec-A-3	1.79		91	44.2[i]	-	6.6[i]	70[h]	1.63[f]	217	153
Dec-Res-1	1.70		312	-	-	-	37[h]	0.35[f]	96	153
Dec-Res-2	1.81	97	306	-	-	-	58[h]	0.42[f]	160	153
Dec-Res-3	2.15		286	-	-	-	227[h]	0.32[f]	-	153
F-SPAEKS	1.05	-	-	32.3	1.84	12.7	15.0	-	89.3	154
FSMN-2	0.97	-	-	27.1	1.59	10.1	15.5	-	119.4	154
FSMN-4	0.95	-	-	34.7	1.98	8.5	16.8	-	127.6	154
FSMN-6	0.98	-	-	21.7	1.43	5.2	15.9	-	93.9	154
FSMNC-2	1.25	-	-	27.7	1.35	9.2	15.8	-	131.7	154
FSMNC-4	1.29	-	-	47.7	2.04	8.5	21.6	-	159.9	154
FSMNC-6	1.03	-	-	22.2	1.60	5.5	18.1	-	82.7	154
CPDA-1	0.67	-	-	29.0	1.20	3.1	27.9	-	52.6	155
CPDA-2	0.72	-	-	33.3	1.39	3.7	32.4	-	70.0	155
CPDA-3	0.77	-	-	52.2	1.72	4.5	33.3	-	77.8	155
SPAESK-5	0.99	174	-	63.2	-	28.6	16[j]	6.5[e]	50[j]	156
SPAESK-10	1.71	110	-	45.8	-	32.5	91[j]	4.5[e]	152[j]	156
SPAESK-15	2.26	165	-	43.7	-	43.4	147[j]	4.0[e]	182[j]	156
Am-SPAEKS	1.04	-	-	31.5	1.5	7.5	38.3	-	67.8	157
SPAEKS-CL-QP5-3%	0.88	-	-	37.5	1.4	10.5	18.4	-	70.0	157
SPAEKS-CL-QP5-5%	0.74	-	-	50.4	1.8	14.9	15.6	-	86.5	157
SPAEKS-CL-QP5-7%	0.66	-	-	44.1	1.5	11.8	14.3	-	88.1	157
SPAEKS-CL-QP5-10%	0.57	-	-	40.0	1.4	11.0	10.7	-	56.8	157
SPAEKS-CL-QP5-15%	0.49	-	-	36.3	1.1	12.3	9.7	-	38.5	157

[a] Theoretical IEC value, [b] weight-average molecular weight, [c] 10% decomposition temperature obtained from TGA analysis, [d] WU at 80 °C, [e] starting fractured time in Fenton's reagent at 80 °C, [f] complete dissolution time in Fenton's reagent at 80 °C, [g] σ values under fully hydrated state at 80 °C, [h] WU at ambient temperature, [i] mechanical properties in the dry state, [j] σ values at 100 °C.conductivity in dry conditions.

Banerjee and Ghanti

Innov. Chem. Mater. Sustain. **2025**, 2(1), 032-073

Figure 7. Schematic illustration for the synthesis of Pillararene-Cross-Linked Membranes.[157] (Reprinted with permission from (157). Copyright (2024) American Chemical Society.)

Scheme 10. The synthesis scheme of the Am-SPAEKS copolymers.[157]

Figure 8. (a-e) Water contact angle, WU, SR, stress-strain, and oxidative stability plots, and (f) oxidative stability-related images of the SPAEKS-CL-QP5-x%.[157] (Reprinted with permission from (157). Copyright (2024) American Chemical Society.)

SPAESK-15 membrane showed higher PC (181.5 mS/cm) and WU (146.5%) values than Nafion-117 at 100 ℃.[156] Also, the SPAESK-15 showed higher PPD value (370.4 mW/cm²) than the Nafion-117 (255.8 mW/cm²) in H₂/air single fuel cell performance at 80 ℃ and 90% RH.[156]

Yang *et al.* synthesized a pendant amino group functionalized SPAEKS (Am-SPAEKS), as shown in **Scheme 10**.[157] Then, a series of macrocycle-cross-linked SPAEKSs (SPAEKS-CL-BrP5) were designed and synthesized by reacting the amino groups of Am-SPAEKS with bromo-functionalized pillar[5]arene (BrP5) and finally, quaternized into the SPAEKS-CL-QP5-x%, as portrayed in **Figure 7**.[157] The gel content of the SPAEKS-CL-QP5-x% (x = 0, 3, 5, 7, 10, and 15) cross-linked copolymers gradually increases with the rise in the degree of the cross-linking.[157] The surface and cross-sectional scanning electron microscopy (SEM) investigation of the cross-linked membranes revealed a dense microstructure without voids, defects, and cracks.[157] The WU values of the cross-linked membranes at 80 ℃ reduced with the increase in the degree of cross-linking, as provided in **Table 4**. The SPAEKS-CL-QP5-x% membranes displayed higher mechanical properties (TS: 36.3-50.4 MPa) than those of the Am-SPAEKS membrane (TS: 31.5 MPa).[157] The cross-linked membranes showed higher oxidative stability than the pristine membrane, as the cross-linked membranes had a higher density, preventing peroxide radical attacks and enhancing oxidative stability.[157] The physical, mechanical, and oxidative properties of the pristine and cross-linked membranes are displayed in **Figure 8**.[157] Among all the cross-linked membranes, the SPAEKS-CL-QP5-7% showed the highest PC value (88.1 mS/cm at 80 ℃), illustrated in **Table 4** and exhibited high long-term stability by retaining more than 98% of its initial PC value after 144 h.[157] The SPAEKS-CL-QP5-7% displayed better single fuel cell performance (4.7 times higher PPD value) than the Am-SPAEKS at 80 ℃ and 100% RH.[157] This study reveals that the cross-linking improved the overall PEM properties and PEMFC results.

4.2.4 Poly(arylene thioether)s, PATEs

Hydrocarbon-based sulfonated poly(arylene thioether)s (SPATEs) are another essential high-performing polymer.[158] These sulfonated copolymers can serve as PEM materials similar to the SPAEs.[158-162] Like SPAEs, SPATEs also show high thermal, mechanical, and proton conductivity values.[158-163] Additionally, the inclusion of the thioether (-S-) groups in place of the ether (-O-) groups in the polymer backbone further improved the dimensional stability, oxidative stability, flame-retardancy properties, and refractive index in the thioester-based polymers compared to the ether-based analogues polymers.[161,162,164-168] Generally, the PATEs are prepared by the nucleophilic substitution polycondensation reaction between the activated aryl dihalo compounds with various types of aryl diphenthiol in polar aprotic solvents.[158-163] Whereas the SPATEs were prepared either by using sulfonated comonomers in polycondensation reactions or by the post-sulfonation process.[161,163] Herein, a few recently developed SPATEs for the PEMFC applications are discussed below.

Bai *et al.* synthesized a trifluoromethyl (-CF₃) groups-containing sulfonated poly(arylene thioether sulfone) [SPATES, 6F-SPTES-50] having 50 mol% of sulfonic acid content by the nucleophilic polycondensation reaction of 4,4-(hexafluoroisopropylidene)-diphenylthiol with two different difluorosulfones (3,3′-disulfonate-4,4′-difluorodiphenylsulfone and 4,4′-difluorodiphenylsulfone), which is shown in **Scheme 11**.[169] The η_inh and number-average molecular weight (M_n) of the 6F-SPTES-50 copolymers were 0.92 dL/g and 25800 g/mol.[169] The experimental NMR-based sulfonic acid content (46 mol%) was in close agreement with the theoretical value (50 mol%) of the 6F-SPTES-50 copolymer.[169] The 6F-SPTES-50 copolymer demonstrated high thermal stability (onset decomposition temperature was 450 ℃) in TGA analysis under synthetic air conditions (**Table 5**). The 6F-SPTES-50 copolymer exhibited lower WU values (20-30%) than the non-fluorinated analogues copolymer (SPTES-50).[169] The 6F-SPTES-50 copolymer showed a PC value of 120 mS/cm at 85 ℃ under 85% RH conditions.[169] The H₂/O₂ single fuel cell performance of the 6F-SPTES-50 membrane displayed a current density value of 750 mA/cm² at 80 ℃ with an OCV value of 0.988 V.[169]

Yan *et al.* synthesized a series of hexafluoroisopropylidene moiety-based sulfonated poly(arylene thioether phosphine oxide)s with various DS (sPTPOF-x) by the nucleophilic polycondensation reaction of 4,4'-(hexafluoroisopropylidene) diphenthiol with sulfonated

Table 5. *The IEC, M_w, T_d, TS, YM, EB, WU, τ, and σ values of the SPATs.*

Polymer	IEC (meq/g)[a]	M_w (kDa)[b]	T_d (℃)[c]	TS (MPa)	YM (GPa)	EB (%)	WU (%)[d]	τ (h)[e,f]	σ (mS/cm)[g]	Ref.
6F-SPTES-50	1.51	-	~450[h]	-	-	-	30	-	120[i]	169
PTPOF	-	157	509	57.8	1.28	4.8	-	-	-	170
sPTPOF-60	0.87	119	407	54.6	1.07	5.5	~9	17.5[e]	~5	170
sPTPOF-70	1.00	110	396	53.4	0.99	6.3	~12	15.5[e]	~17	170
sPTPOF-80	1.13	119	391	52.6	0.86	7.9	~16	5.2[e]	~40	170
sPTPOF-90	1.26	210	388	51.3	0.75	9.4	~22	2.2[e]	~55	170
sPTPOF-100	1.38	430	385	38.4	0.69	13	24.8	2.0[e]	90	170
tsPTPO-80	1.36	50.5	388	24.2	0.92	3.3	~32	80[f]	~34	158
tsPTPO-85	1.43	60.2	379	26.0	1.05	5.2	~34	55[f]	~45	158
tsPTPO-90	1.51	113	375	29.2	1.07	5.5	~36	21[f]	~54	158
tsPTPO-95	1.58	91.2	365	40.7	1.13	15	~38	18[f]	~60	158
tsPTPO-100	1.65	70.2	352	42.2	1.17	17	52	13[f]	87	158
msPTPO-100	1.65	134	376	28.9	0.82	18	180	3.0[f]	-	158
SPTES	1.647	-	446[j]	-	-	-	~98	2.4[f]	138	171
SPTES/Si-imP2.5	1.652	-	-	-	-	-	~11	2.7[f]	~150	171
SPTES/Si-imP5.0	1.579	-	456[j]	-	-	-	~115	3.1[f]	173	171
SPTES/Si-imP7.5	1.564	-	-	-	-	-	~95	3.3[f]	~140	171
SPTES/Si-imP10	1.543	-	-	-	-	-	~88	3.8[f]	~136	171
sPATPO-80	1.36	136[163]	412[163]	39.9	0.66	20	30[163]	35	~55[163]	172
sPATPO80/sPBI2	1.36	-	-	42.2	0.82	11	-	205	25	172
sPATPO-90	1.51	156[163]	408[163]	29.3	0.54	19	116[163]	20.5	95.4[163]	172
sPATPO90/sPBI2.5	1.50	-	-	31.4	0.57	31	52	110	~75	172
sPATPO90/sPBI3.0	1.50	-	-	32.9	0.73	30	-	200	67	172
sPATPO90/sPBI3.5	1.50	-	-	34.7	0.75	21	-	210	-	172
sPATPO-100	1.65	199[163]	405[163]	22.9	0.47	7.7	319[163]	6.5	120[163]	172
sPATPO100/sPBI5.5	1.63	-	-	34.0	0.51	28	-	120	84	172
sPATPO100/sPBI6.0	1.63	-	-	35.9	0.58	20	-	276	74	172
sPATPO100/sPBI6.5	1.62	-	-	36.6	0.62	12	34	>288	-	172

[a] Theoretical IEC value, [b] weight-average molecular weight, [c] 5% decomposition temperature obtained from TGA analysis, [d] WU values at 80 ℃, [e] starting fractured time in Fenton's reagent at 80 ℃, [f] complete dissolution time in Fenton's reagent at 80 ℃, [g] σ values under fully hydrated state at 80 ℃, [h] onset decomposition temperature, [i] σ values at 85 ℃ in 85% RH, [j] initial degradation temperature in TGA analysis.
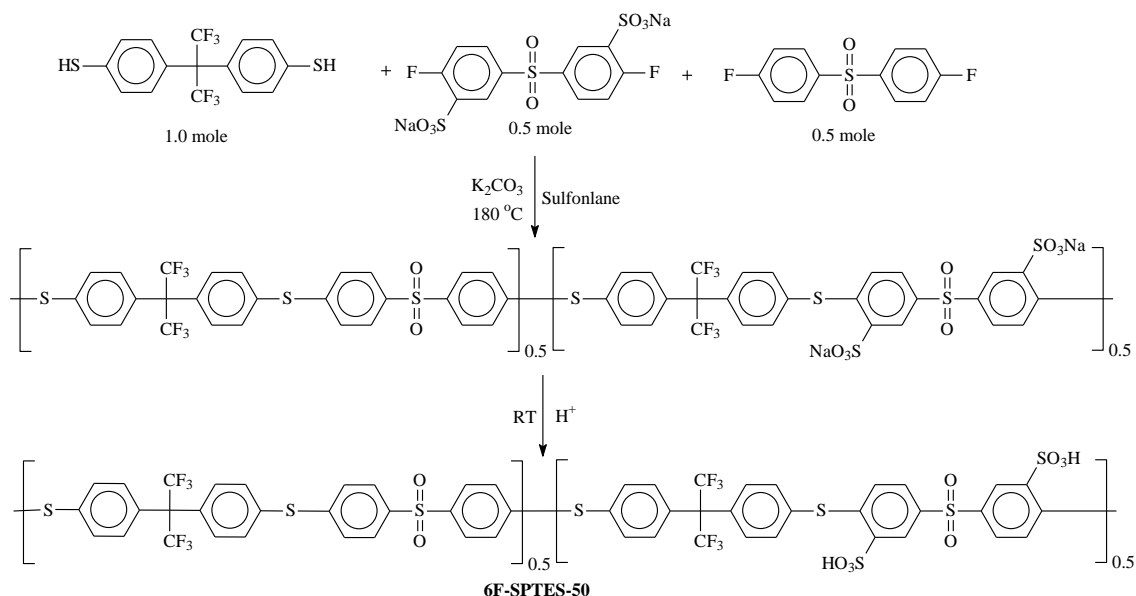
Scheme 11. The synthesis scheme of the fluoro-sulfonated poly(arylene thioether sulfone) copolymer (6F-SPTES-50).[169]

bis(4-fluorophenyl)phenyl phosphine oxide and bis(4-fluorophenyl)phenyl phosphine oxide, as depicted in **Scheme 12**.[170]

The non-sulfonated homopolymer (PTPOF) and sPTPOF-x copolymers showed high M_w (110-430 kg/mol) and PDI (1.57-2.00) values in GPC analysis.[170] The IEC values of the sPTPOF-x copolymers were calculated between 0.87-1.38 meq/g, as illustrated in **Table 5**. The sPTPOF-x copolymers exhibited high thermal ($T_{d5\%} \leq 385$ °C) and mechanical stabilities (TS: 48-55 MPa and YM: 695-1068 MPa), as tabulated in **Table 5**. Due to the presence of the hydrophobic hexafluoroisopropylidene unit, the sPTPOF-x copolymers demonstrated high dimensional stability (the SR value of the sPTPOF-100 membrane was 5.3% at 80 °C).[170] The morphological AFM phase images of the sPTPOF-x membranes exemplified a unique nano-scale phase-segregated morphology that favors the agile proton conduction and restricts the excessive swelling.[170] Out of all the membranes, the sPTPOF-100 membrane illustrated the highest σ value (90 mS/cm) at 80 °C (**Table 5**). As compiled in **Table 5**, the sPTPOF-x membranes showed oxidative stability (τ) values between 2.0 and 17.5 h.

Yao *et al.* synthesized a series of trisulfonated and monosulfonated poly(arylene thioether phosphine oxide)s [tsPTPO-x and msPTPO-100] with different sulfonic acid contents by the nucleophilic polycondensation reaction as depicted in **Scheme 13**.[158] The IEC values of the copolymers were calculated in the range of 1.36-1.65 meq/g (**Table 5**). The GPC results (M_w: 50-134 kg/mol and PDI: 1.52-1.71) of the copolymers confirmed the formation of the high molecular weight copolymers.[158] All the trisulfonated and monosulfonated copolymers exhibited high thermal and mechanical stability, as tabulated in **Table 5**. The tsPTPO-100 copolymer membrane showed moderate WU (52%) and SR (21%) values at 80 °C.[158] The tsPTPO-x membranes displayed excellent oxidative stability in Fenton's reagent at 80 °C, as provided in **Table 5**. The trisulfonated tsPTPO-100 membrane showed the highest proton conductivity value of 87 mS/cm at 80 °C, which is close to the Nafion-117.[158]

Ding *et al.* synthesized a series of phosphorylated nanocomposite membranes (SPTES/Si-imPx) for PEM applications.[171] The schematic illustration of the synthesis of imino-functionalized phosphorylated silica nanoparticles (Si-imP) is depicted in **Figure 9**. They prepared a series of nanocomposite membranes of sulfonated poly(arylene thioether sulfone), SPTES, of various wt% of nanoparticles loading (2.5, 5.0, 7.5, and 10 wt%).[171] The reaction scheme for synthesizing SPTES is provided in **Scheme 14**. The homogeneous and uniform distribution of the Si-imP nanoparticles in the SPTES/Si-imPx membranes was
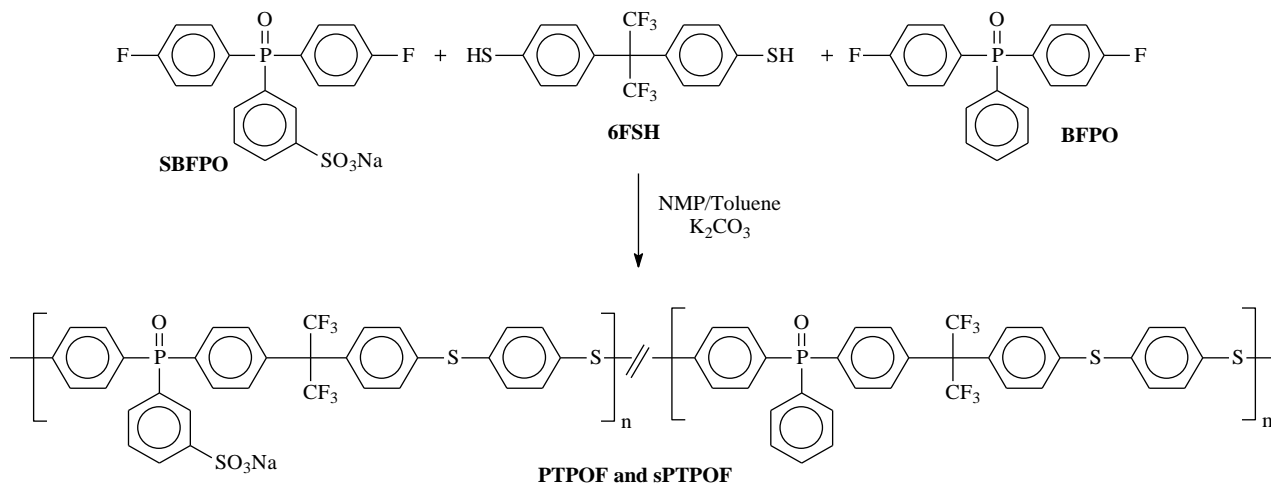
Scheme 12. The synthesis scheme of hexafluoroisopropylidene- and phosphine oxide-based PTPOF and sPTPOF copolymers.[170]

Banerjee and Ghanti

Innov. Chem. Mater. Sustain. **2025,** 2(1), 032-073
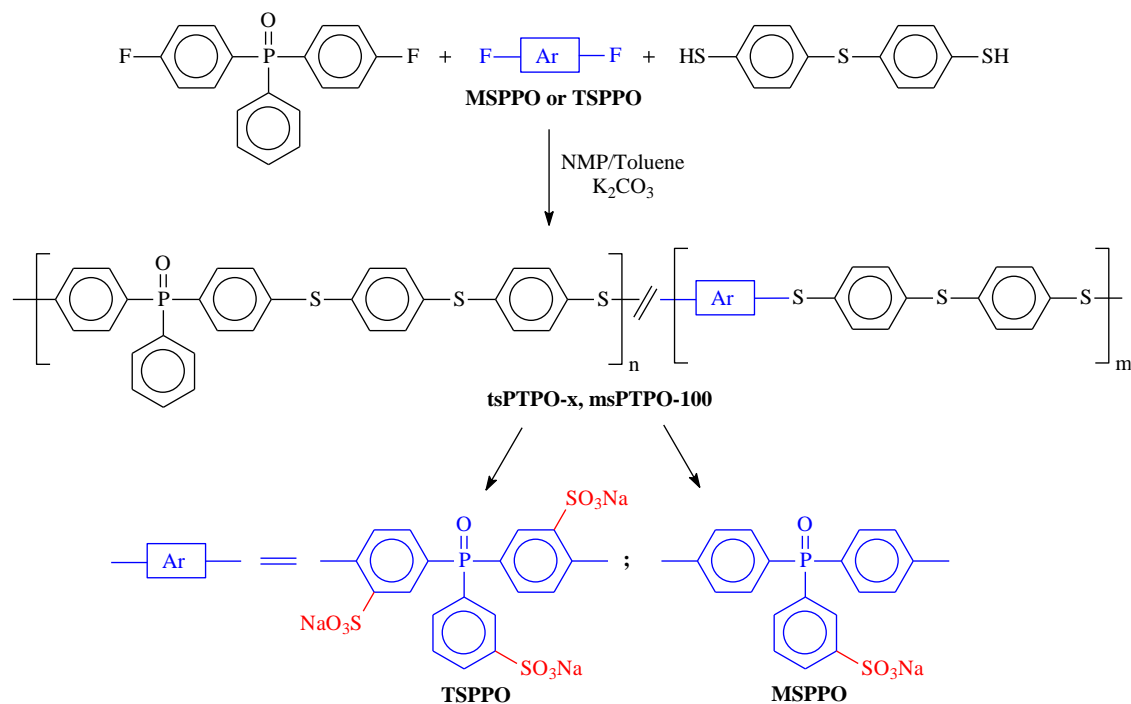
Scheme 13. Synthesis scheme of the phosphine oxide-based TSPPO and MSPPO copolymers [158]
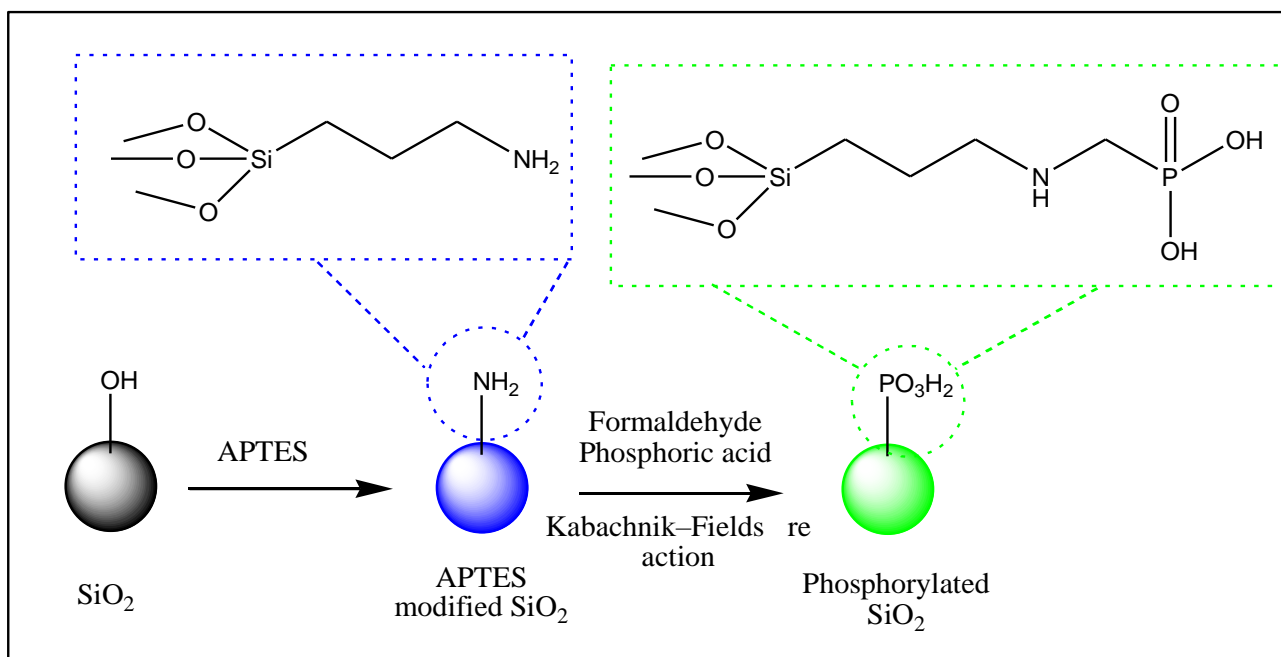
Figure 9. The schematic illustration of the synthesis of imino-containing phosphorylated silica particles (Si-imP).[171]

confirmed by FTIR, SEM, and EDX analysis.[171] The composite membranes demonstrated higher thermal stability than the SPTES membrane, which confirmed that the Si-imP fillers enhanced the thermos-oxidative stability of the composite membranes (**Table 5**). The SPTES/Si-imP5.0 showed the highest WU (~115%) and SR (~55) values among all the membranes.[171] The SPTES/Si-imP10 composite membrane 3.8 h in Fenton's reagent at 80 ℃ (**Table 5**). The SPTES/Si-imP5 composite membrane showed 26% higher proton conductivity (173 mS/cm) than the pristine SPTES membrane (138 mS/cm) at 80 ℃, as provided in **Table 5**. The predicted proton transportation mechanism in the composite membranes shows that the addition of Si-imP nanoparticles into the polymer matrix boosted the proton conduction process through

the additional electrostatic and intermolecular hydrogen bonding interactions.[171]

Yan *et al*. prepared a series of sulfonated blend membranes of sulfonated poly(arylene thioether phosphine oxide)s (sPATPOs) and sulfonated polybenzimidiazoles (sPBIs) to improve the dimensional stability.[172] The synthesis schemes of the sPATPOs and sPBIs are shown in **Schemes 15** and **16**. The theoretical and experimental IEC values of the blend membranes (sPATPOxx/sPBIy, where xx represents the DS value of sPATPO and y represents wt% of sPBI) were obtained between 1.36-1.63 meq/g and 1.28-1.61 meq/g, respectively.[172] The blend copolymers demonstrated higher thermal stability than the pristine sPATPO copolymers due to
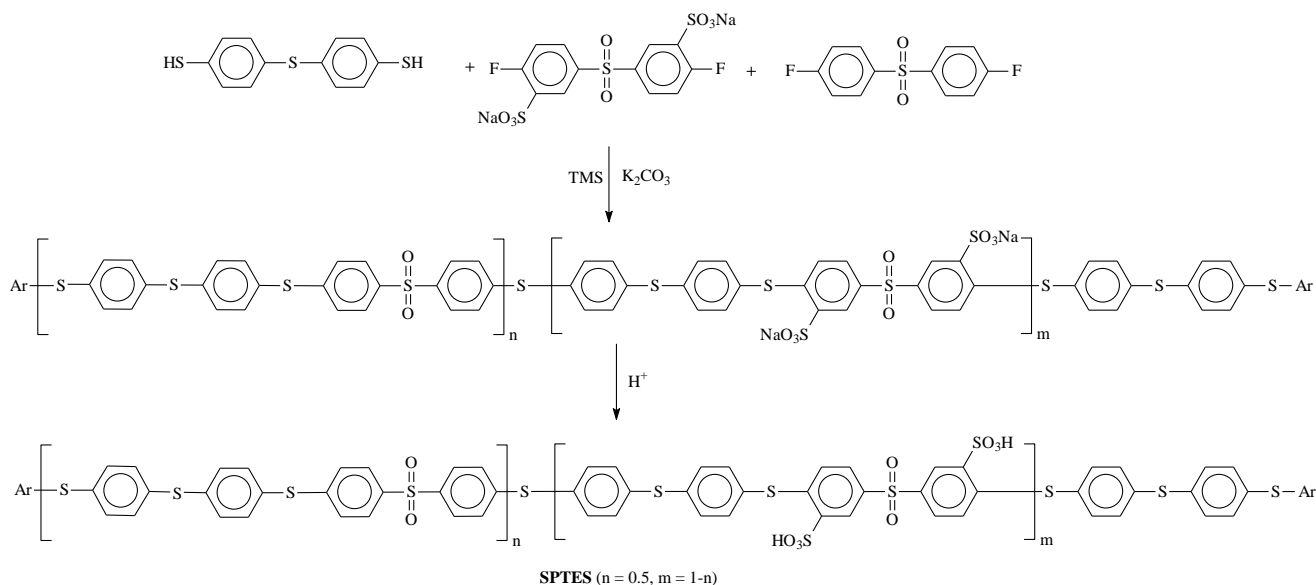
Scheme 14. The synthesis scheme of the sulfonated poly(arylene thioether sulfone), SPTES.[171]

the stronger acid-base interactions between sPATPO and sPBI.[172] The blend membranes (WU: 34-52% and SR: 7-18% at 80 ℃) showed higher dimensional stability than the pristine sPATPO membranes (WU: 30-319% and SR: 9-10% at 80 ℃).[163,172] The blend membranes exhibited higher mechanical stability than the pristine membranes due to the stronger intermolecular interactions, as compiled in **Table 5**. The AFM morphological investigation of the blend membranes revealed that the hydrophilic domains become more interconnected with the increase in wt% of the sPBI.[172] Among all the blend membranes, the sPATPO100/sPBI5.5 membrane showed the highest σ value of 84 mS/cm at 80 ℃, as illustrated in **Table 5**. The blend membranes exhibited outstanding oxidative stability in Fenton's reagent at 80 ℃, mainly due to the lower absorption properties of the blend membranes and the radical resistance property of the sPBIs backbone.[172]

4.2.5 Polybenzimidazoles, PBIs

Hydrocarbon-based aromatic polymers composed of heterocyclic moieties, especially the nitrogen-containing heterocyclic units such as PBIs, polybenzothiazoles (PBTs),

mechanical, dimensional, and oxidative stabilities, and high ion conduction abilities.[61,173-175] Among these, PBIs have gained much consideration in this century owing to their promising properties in the PEMFC applications.[173,176-180] The phosphoric acid (PA)-doped PBIs usually showed extremely high proton conductivity even at anhydrous conditions and a moderate to high-temperature range (up to 200 ℃).[173] The PC values of the PA-doped PBIs mainly depend on the PA-doping levels. However, recent studies revealed that the PA-doped sulfonated polybenzimidazoles (SPBIs) have gained particular interest due to their higher proton conductivity values than those of the non-sulfonated PA-doped PBIs.[179,181-184] Generally, the PBIs are synthesized by the polycondensation reaction between tetramine compounds with diacids or dianhydride in polyphosphoric acid (PPA) or phosphorus pentoxide-methanesulfonic acid (PPMA). As described earlier, the SPBIs are also synthesized by the direct sulfonation and post-sulfonation processes.[173,183,184] Herein, a few recently developed SPBIs for moderate or high-temperature PEMFC applications are described below.

Yan *et al.* synthesized a series of sPBIs with varying DS
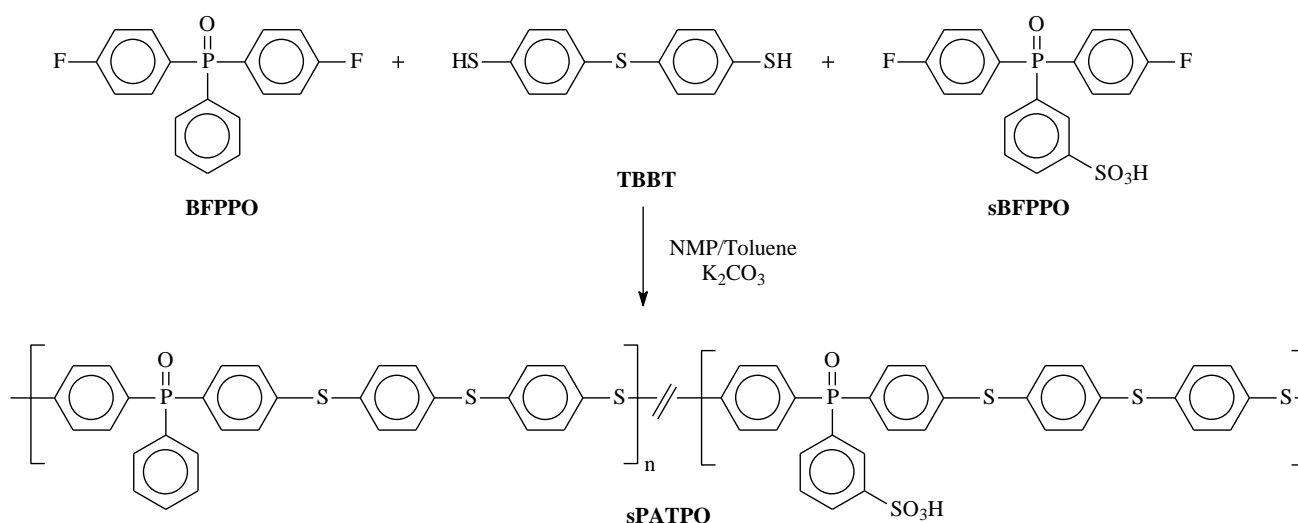
Scheme 15. The synthesis scheme of the sulfonated poly(arylene thioether phosphine oxide)s, sPATPOs.[172]

polybenzoxazoles (PBOs), polytriazoles (PTs), etc., have attracted remarkable attention due to their high thermal,

values by the direct polycondensation reaction of 3,3′-diaminobenzidine (DAB) with 3,3′-Disulfonate-4,4′-

Banerjee and Ghanti

Innov. Chem. Mater. Sustain. **2025**, 2(1), 032-073

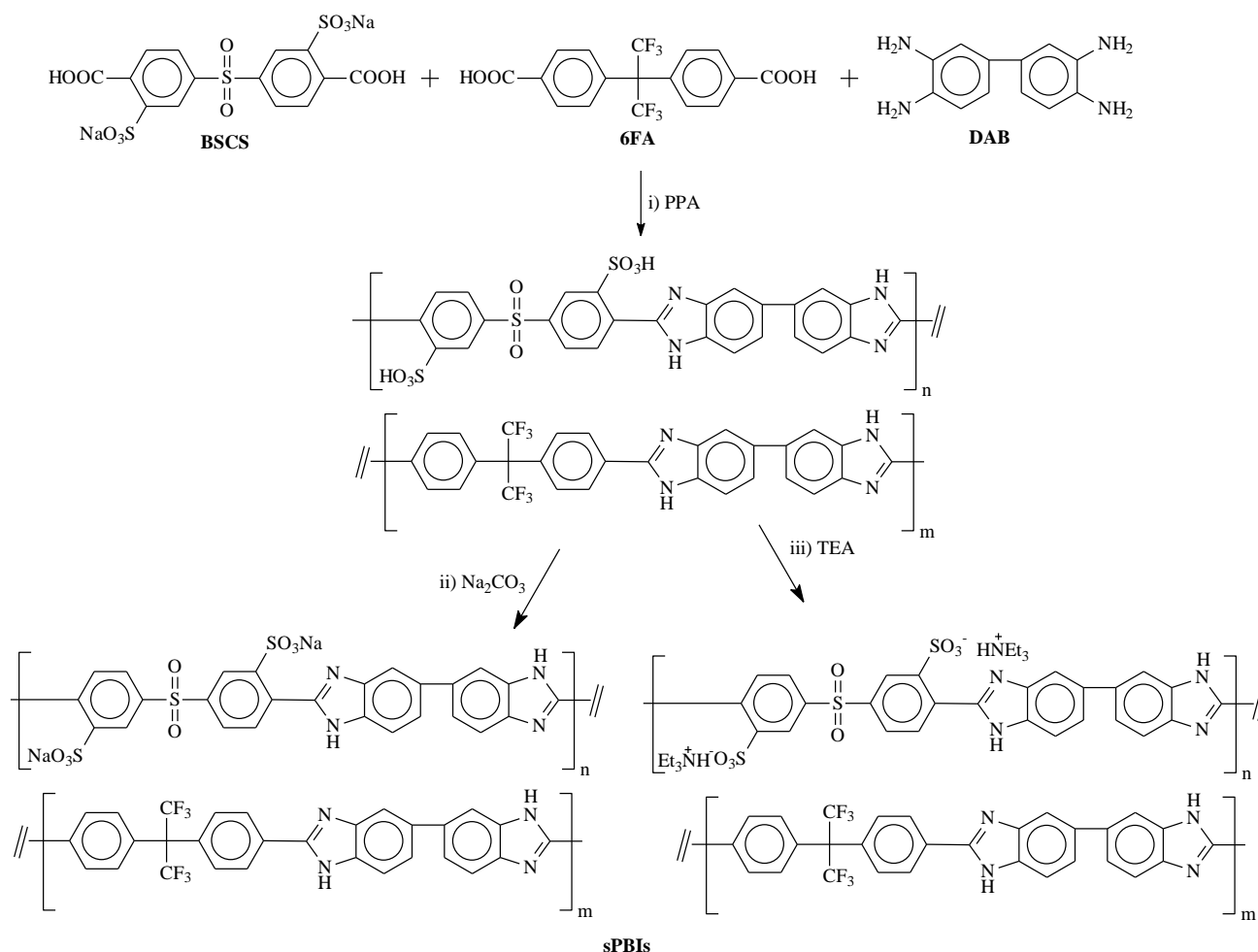dicarboxylbiphenyl (SCBP) and other non-sulfonated diacids, as depicted in **Scheme 17**.[185] The IEC values of sPBI-xx (xx: 30, 40, 50, 60, and 70) copolymers were between 1.12-2.59 meq/g, as compiled in **Table 6**. The GPC results (M_w: 147-248 kg/mol and PDI: 2.19-2.86) of the sPBI-xx copolymers confirmed the formation of high molecular weight polymers.[185] The sPBI-xx copolymers showed high thermal and viscoelastic properties.[185] All the sPBI-xx demonstrated anomalous water absorption properties, where both the WU and SR values initially increased up to 50 °C, then decreased between 50-70 °C, and again slightly increased between 70-90 °C.[185] The elapsed time (τ) of all the sPBI-xx membranes was more than 72 h (Table 3), which indicates the superior oxidative stability of those copolymers. Out of all the membranes, the sPBI-70 membrane demonstrated the highest PC value of 2.79 mS/cm at 80 °C.[185]

Chen *et al.* synthesized a series of phosphine oxide-based SPBIs (sPBI-PO) by the random co-polycondensation reaction of sulfonated bis(4-methylbenzoate)phenylphosphine oxide (sBMPO), bis(4-methylbenzoate)phenylphosphine oxide (BMPO), and 3,3′-diaminobenzidine (DAB) in PPA, as shown in **Scheme 18**.[186] The η$_{inh}$ values of the sPBI-POxx copolymers were found between 1.51-2.41dL/g, which confirms the formation of the high molecular weight copolymers by the random co-polycondensation reaction.[186] The sPBI-POxx copolymers exhibited high thermal and mechanical stabilities, as compiled in **Table 6**. All the copolymer membranes displayed higher oxidative stability (τ > 48 h and RW ≥ 95%).[186] The sPBI-POxx membranes showed WU values between 21.3-25.2% at 80 °C, as provided in **Table 6**. The AFM morphological investigation of the sPBI-POxx revealed that the ionic cluster becomes much closer and more prominent with the rise in the DS value of the copolymers.[186] The sPBI-PO90 membrane showed the highest PA uptake of 187.3%, with the lowest volume swelling (170.6%).[186] The undoped sPBI-POxx membranes showed a PC value of 4.6-7.1 mS/cm at 80 °C under a fully hydrated state (**Table 6**). Whereas the PA-doped sPBI-PO90 membranes showed 3.9 times higher PC value (27.6 mS/cm) compared to the undoped sample at 80 °C under 100% RH.[186]

Yan *et al.* synthesized a series of SPBIs (sPBI-x) with a controlled proportion of pendant sulfophenylsulfonyl groups by the direct polycondensation reaction of 3,3′-diaminobenzidine (DAB) with 4′-Sulfonate-2,5-dicarboxyphenyl sulfone (SCPS) and 2,5-dicarboxyphenyl sulfone (CPS) in PPA as shown in **Scheme 19**.[187] The high molecular weight (M_w: 111-143 kg/mol and PDI: 170-1.93) sPBI-x copolymers showed excellent solubility in commonly available polar aprotic solvents (DMF, DMSO, DMAc, and NMP).[187] The sPBI-x (x: 60, 70, 80, 90, 100) demonstrated high thermal ($T_{d5\%}$: 387-407 °C), mechanical (TS: 114-123 MPa; YM: 1.65-1.72 GPa; EB: 20-27%), hydrolytic (1% weight loss after 24 h of the hydrolytic stability in deionized water at 140 °C), and oxidative stabilities (τ > 168 h), as illustrated in **Table 6**.[187] The sPBI-100 membrane exhibited the highest water absorption properties (WU: 20.2% and SR: 8.2%) at 80 °C among the sPBI-x membranes.[187] The microstructural analysis of the sPBI-x membranes confirmed the formation of more interconnected ionic aggregation with increased sulfonic acid contents in the copolymer architecture.[187] The sPBI-100
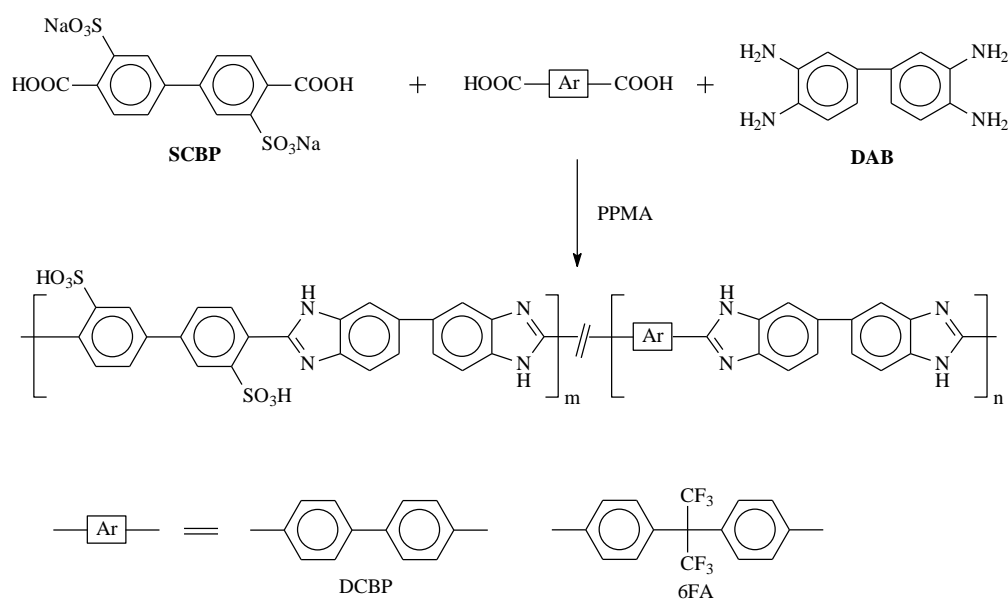

Scheme 16. The synthesis scheme of the sulfonated polybenzimidazoles, sPBIs.[172]

Banerjee and Ghanti

Innov. Chem. Mater. Sustain. **2025**, 2(1), 032-073

Table 6. *The IEC, M_w, T_d, TS, YM, EB, WU, τ, and σ values of the SPATs.*

Polymer	IEC (meq/g)[a]	M_w (kDa)[b]	T_d (℃)[c]	TS (MPa)	YM (GPa)	EB (%)	WU (%)[d]	τ (h)[e,f]	σ (mS/cm)[g]	Ref.
sPBI-30	1.12	239	480	-	-	-	~15	>72[e]	-	185
sPBI-40	1.49	179	475	-	-	-	~17	>72[e]	-	185
sPBI-50	1.85	248	463	-	-	-	~19	>72[e]	-	185
sPBI-60	2.22	196	461	-	-	-	~20	>72[e]	-	185
sPBI-70	2.59	167	459	-	-	-	~21	>72[e]	2.79	185
sPBI-PO60	1.10	-	491	60	1.56	16.2	21.3	>48[e]	4.6	186
sPBI-PO70	1.27	-	490	45	1.87	6.7	-	>48[e]	4.9	186
sPBI-PO80	1.43	-	488	43	1.81	4.9	-	>48[e]	6.5	186
sPBI-PO90	1.57	-	485	53	1.39	15.2	25.2	>48[e]	7.1	186
sPBI-PO100	-	-	480	-	-	-	-	-	-	186
sPBI-60	1.21	143	407	-	-	-	16.5	>168[f]	~0.9	187
sPBI-70	1.39	133	403	114	1.65	27	17.3	>168[f]	~1.0	187
sPBI-80	1.56	111	396	120	1.71	25	18.0	>168[f]	~1.4	187
sPBI-90	1.73	128	395	123	1.72	20	19.5	>168[f]	~1.7	187
sPBI-100	1.89	139	387	-	-	-	20.2	>168[f]	2.8	187
OPBI	-	-	-	0.50	-	81	11.7	-	67[h]	188
PSM 1-3%	-	-	-	0.76	-	134	13.3	-	202[h]	188
PSM 1-5%	-	-	-	1.55	-	176	16.1	-	233[h]	188
PSM 1-7%	-	-	-	1.51	-	285	18.9	-	266[h]	188
PSM 1-10%	-	-	-	1.31	-	360	19.8	-	290[h]	188
PSM 2-7%	-	-	-	1.45	-	274	18.9	-	277[h]	188
PSM 2-10%	-	-	-	1.18	-	350	20.9	-	308[h]	188
SHBPBI	-	-	259	-	-	-	-	-	-	189
oPBI-TAIC(5%)-SHBPBI(40%)	-	-	326	39.5	-	11.4	-	-	122[i]	189
oPBI-TAIC(10%)-SHBPBI(40%)	-	-		54.4	-	9.8	-	-	110[i]	189
oPBI-TAIC(5%)-SHBPBI(50%)	-	-	324	35.8	-	12.9	-	-	147[i]	189
oPBI-TAIC(10%)-SHBPBI(50%)	-	-	302	42.9	-	10.6	-	-	136[i]	189

[a] Theoretical IEC value, [b] weight-average molecular weight, [c] 5% decomposition temperature obtained from TGA analysis, [d] WU values at 80 ℃, [e] starting fractured time in Fenton's reagent at 80 ℃, [f] starting dissolution time in Fenton's reagent (30 ppm $FeSO_4$ in 30% H_2O_2) at 80 ℃, [g] σ values under fully hydrated state at 80 ℃, [h] σ values in anhydrous conditions at 160 ℃, [i] σ values in 100% RH at 180 ℃.

Scheme 17. The synthesis scheme of the SPBI copolymers (sPBI-XX).[185]

membrane demonstrated the highest σ value of 2.8 mS/cm at 80 ℃ in deionized water, as compiled in **Table 6**. The σ values of the sPBI-x membranes were lower than those in the studies performed without the PA-doping.

Das *et al.* synthesized a series of sulfonated MOF-based PBI composite membranes with different wt% of MOF (PSM 1 or PSM 2) loading.[188] The pristine PBI polymer was synthesized by the polycondensation reaction of 3,3',4,4'-tetraaminobiphenyl (TAB) and 4,4'-oxybis(benzoic acid) (OBA), as shown in **Scheme 20**.[188] The PSM 1 and PSM 2 MOFs were synthesized by the post-modification of the UiO-66-NH2 MOF with 1,3-propane sultone and 1,4-butane sultone, respectively.[188] A series of composite PBI membranes were fabricated by the solution blending method with various wt% of MOF loading; the fabrication of PBI composite

membranes is shown in **Figure 10**.[188] The nanocomposite membranes were doped with PA and utilized for the PEM properties evolution. The PA-doped nanocomposite membranes demonstrated higher thermal, mechanical, and oxidative stabilities than the pristine OPBI membrane.[188] The matrix membranes with higher wt% of MOF loading (7 and 10%) showed more fibrous-like networks and porous structures in cross-sectional FESEM analysis.[188] Among the nanocomposite membranes, the PSM 2-10% membranes showed the maximum σ value of 308 mS/cm at 160 ℃ under anhydrous conditions (**Table 6**). The PSM 2 loaded composite membrane showed enhanced proton conductivity due to the extensive interfacial H-bonding in the composite polymer.

Li *et al.* synthesized a series of highly sulfonated covalently cross-linked PBI membranes for high-temperature proton

Banerjee and Ghanti

Innov. Chem. Mater. Sustain. **2025**, 2(1), 032-073

Scheme 18. Synthesis scheme of the sPBI-PO.[186]

Scheme 19. The synthesis scheme of the pendant sulfophenylsulfonyl groups-containing SPBI copolymers (sPBI-x).[187]

Scheme 20. The synthesis scheme of the pristine OPBI polymer.[188]
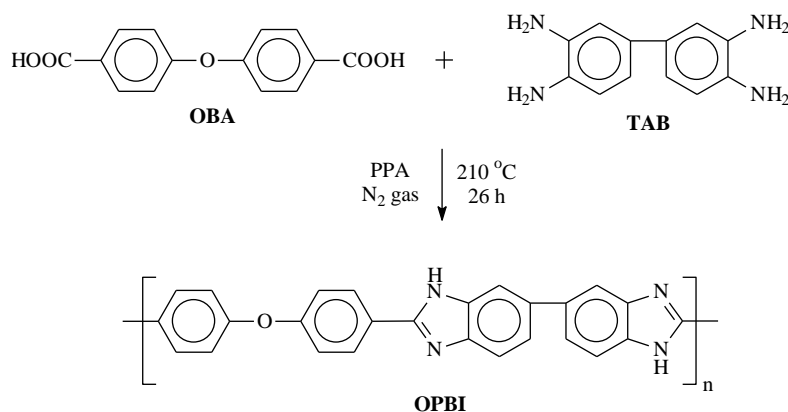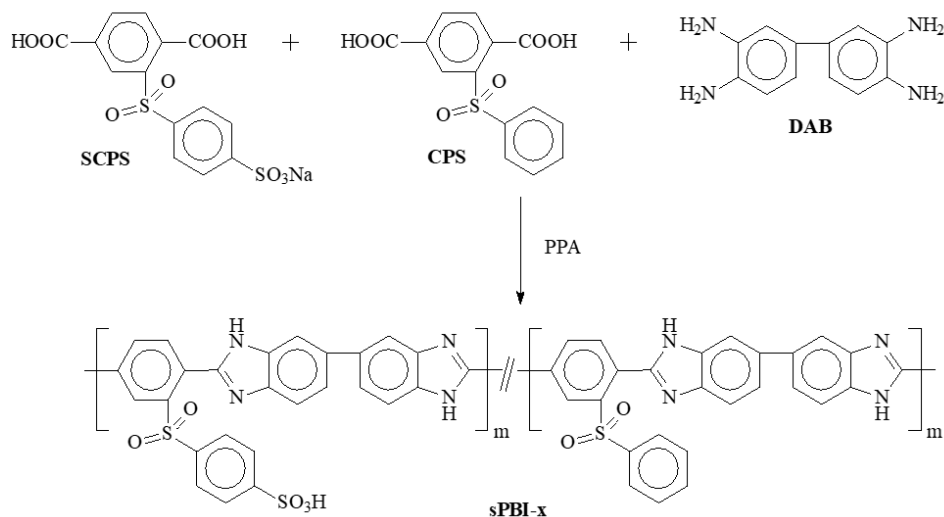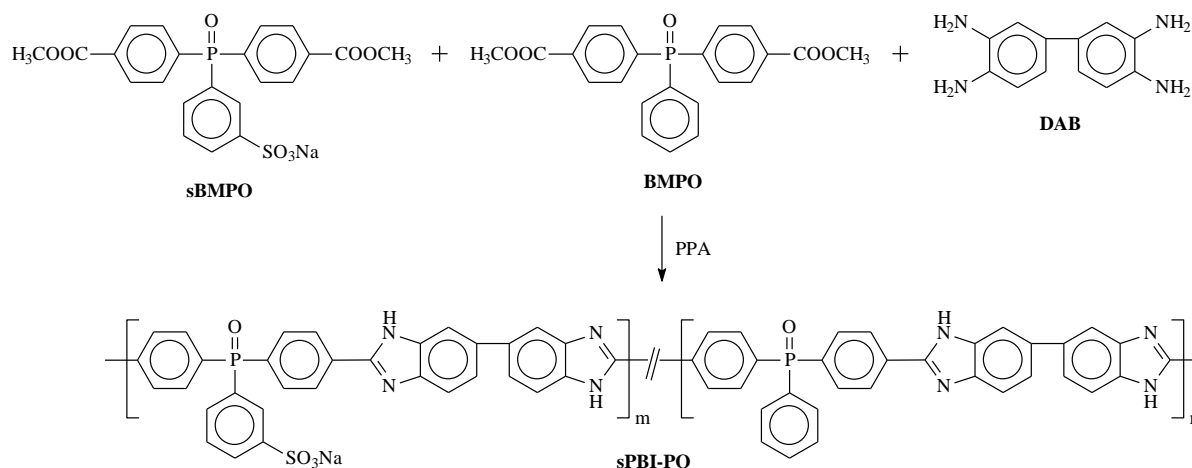
exchange membrane (HTPEM) applications[189] The hyperbranched polybenzimidazole (HBPBI) was synthesized by the polycondensation reaction of give 4,4',4''-((2,4,6-trioxo-1,3,5-triazinane-1,3,5-triyl)tris(oxy))tribenzoic acid (TTA) and 3,3'-diaminobenzidine (DAB) in presence of P$_2$O$_5$ and methane sulfonic acid (MSA), as shown in **Scheme 21**.[189] Then, the sulfonated hyperbranched polybenzimidazole (SHBPBI) was prepared by the reaction of HBPBI with 1,3-propane sultone in

DMAc, which is depicted in **Scheme 21**.[189] Finally, a series of highly sulfonated covalently cross-linked oPBI-TAIC-SHBPBI membranes were fabricated from the mixing the ether-containing polybenzimidazole (oPBI), triallyl isocyanurate (TAIC), and SHBPBI in DMAc at 160 °C, as shown in **Scheme 22**.[189] The schematic illustration of the fabrication of the oPBI-TAIC-SHBPBI membranes are provided in **Figure 11**.[189] The

Banerjee and Ghanti

Innov. Chem. Mater. Sustain. **2025**, 2(1), 032-073
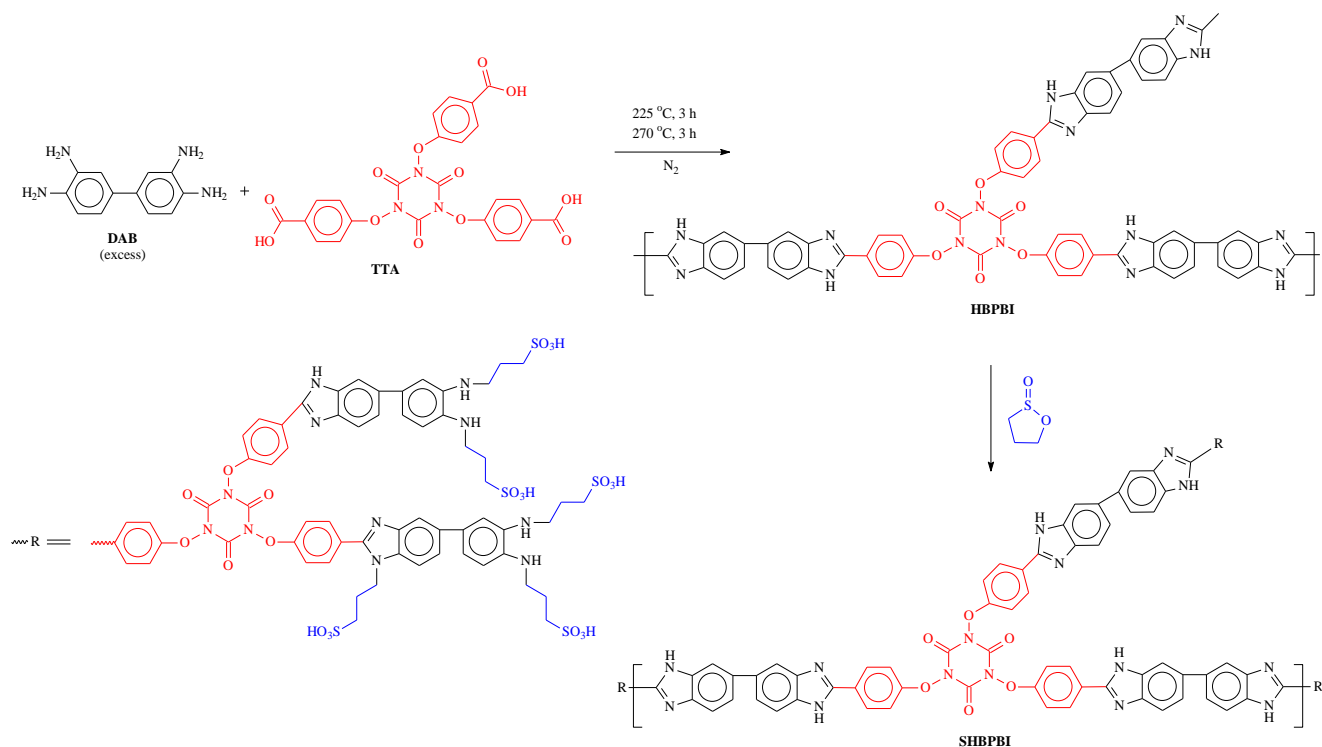
Scheme 21. The synthesis scheme of the sulfonated hyperbranched polybenzimidazole (SHBPBI).[189]
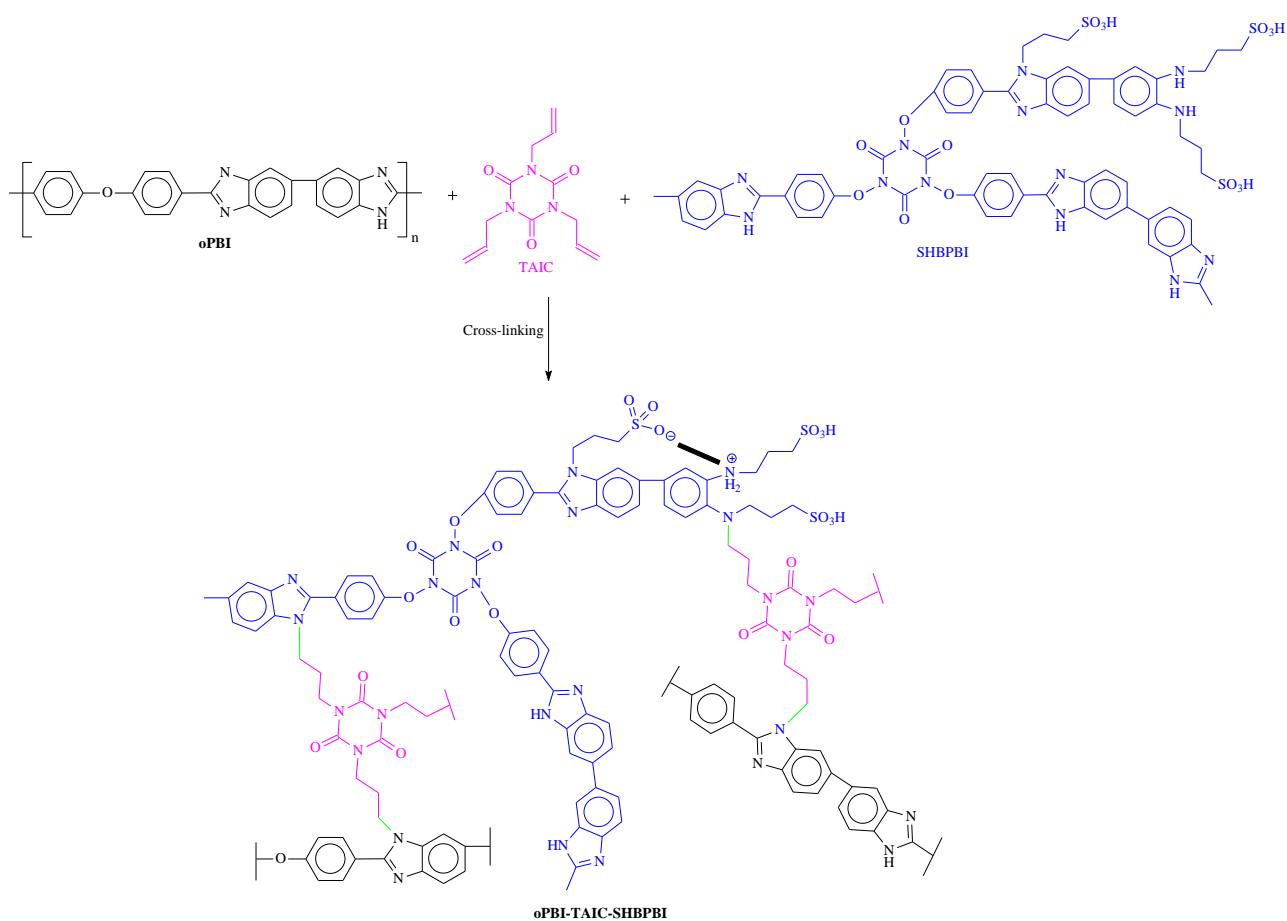
Scheme 22. The synthesis scheme of the highly sulfonated covalently cross-linked oPBI-TAIC-SHBPBI.[189]

covalently cross-linked oPBI-TAIC-SHBPBI showed higher thermal stability than the SHBPBI, as compiled in **Table 6**. The oPBI-TAIC-SHBPBI membranes' SEM analysis showed that the cross-section was homogeneous, dense, and defect-

free.[189] The stress-strain analysis of the oPBI-TAIC-SHBPBI membranes confirmed that the mechanical properties of the cross-linked membranes were increased with the increase in the cross-linking degree (CLD).[189] The membrane with the

Banerjee and Ghanti

Innov. Chem. Mater. Sustain. **2025**, 2(1), 032-073
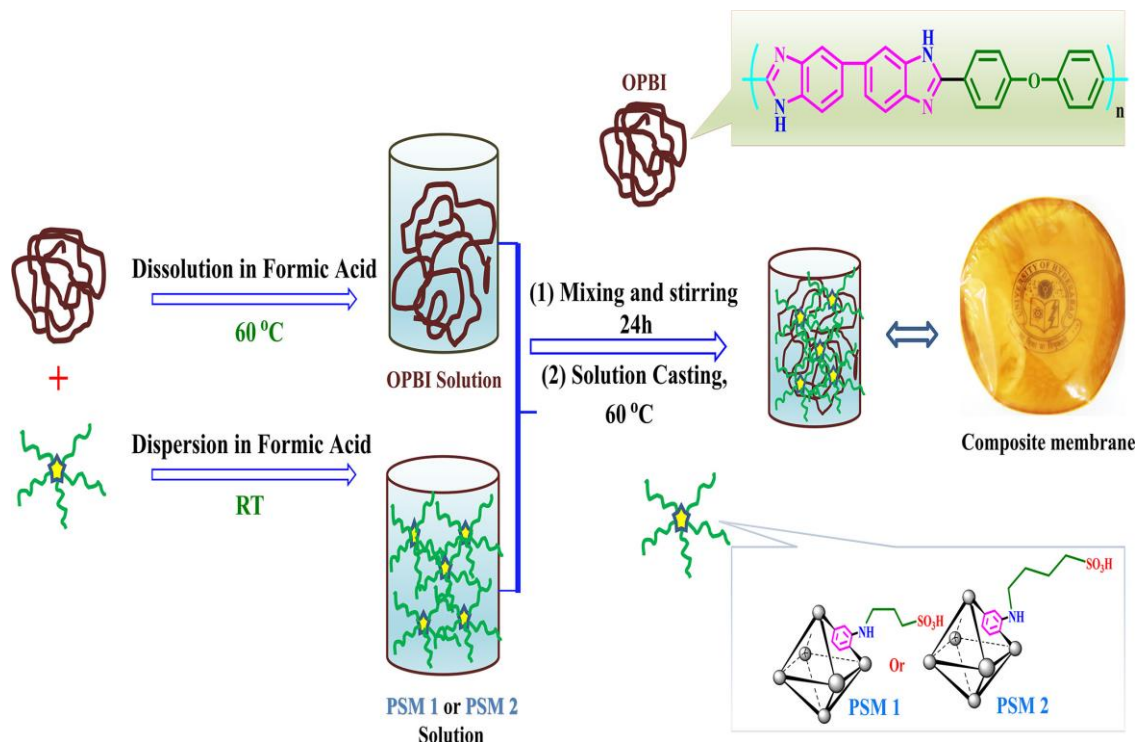
Figure 10. Schematic illustration of PSM 1 and PSM 2 loaded PBI composite membranes.[188] (Reprinted with permission from (188). Copyright (2020) American Chemical Society.)
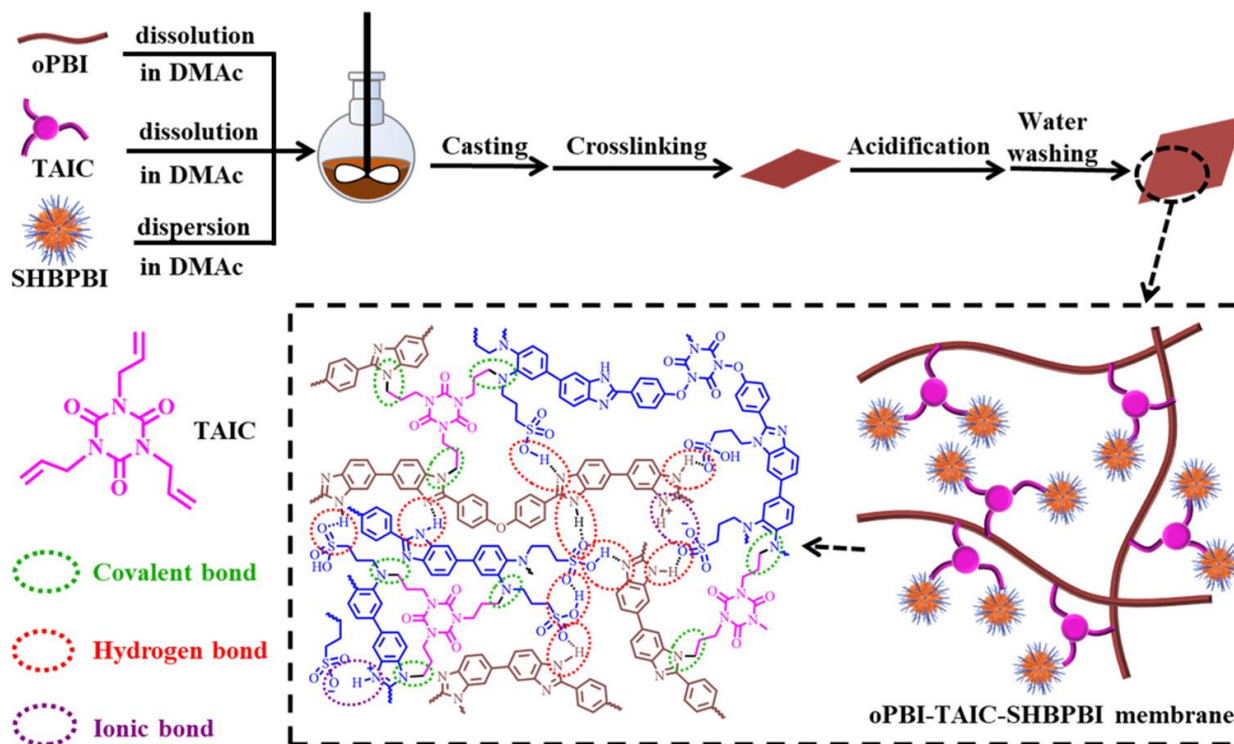
Figure 11. The schematic illustration of the fabrication of oPBI-TAIC-SHBPBI membranes.[189] (Reprinted with permission from (189). Copyright (2022) American Chemical Society.)

higher CLD demonstrated better dimensional stability (lower SR) than the membrane with lower CLD due to the increase in the covalent network with the increase in the CLD in the oPBI-TAIC-SHBPBI membrane.[189] Among all the covalently cross-

inked membranes, the oPBI-TAIC(10%)-SHBPBI(40%) membrane exhibited the highest oxidative stability (retaining 96.4% of weight after the Fenton's test) owing to its higher CLD

and lower proportion of sulfonated units.[189] The oPBI-TAIC(5%)-SHBPBI(50%) membrane demonstrated the maximum σ value of 147 mS/cm at 180 ℃ under 100% RH conditions (**Table 6**). The oPBI-TAIC(5%)-SHBPBI(50%) membrane retained 97.1% of its proton conductivity after washing with DI water for 96 h, which confirmed its durability

and low leaching ability of the cross-linked membrane that is superior for HTPEM applications.[189]

4.2.6 Polyimides, PIs

Hydrocarbon-based aromatic polyimides (PIs) are another special class of high-performing polymers known for their excellent thermal, mechanical, and electrochemical properties.[115,190-194] PIs are prepared by the polycondensation reaction of aromatic diamines with aromatic dianhydrides.[115,190-194] Generally, the polyimidization reaction proceeds through two steps; the first step is the formation of the polyamic acid (PAA) precursor, and the second step is the thermal or chemical cyclodehydration.[115,190-195] The chemical cyclodehydration of PAAs is mainly performed using acetic anhydride in the presence of a sodium acetate base.[115,190-195] Despite their excellent properties, they possessed limited applicability due to their high melting point, low processability, low solubility, and formation of various intermolecular charge transfer complexes (CTCs).[115,196,197] Thus, in recent years, several efforts have been employed to develop soluble, processable, and tractable PIs without compromising their high-performing properties. The sulfonated polyimides (SPIs) have gained remarkable attention as an alternative PFSA-based material due to the imide rings in the polymer backbone, which provide tremendous thermal stability, high mechanical characteristics, superior oxidative stability, and excellent proton conductivity.[96,198-200] Herein, a few recently developed SPI-based PEMs are discussed.
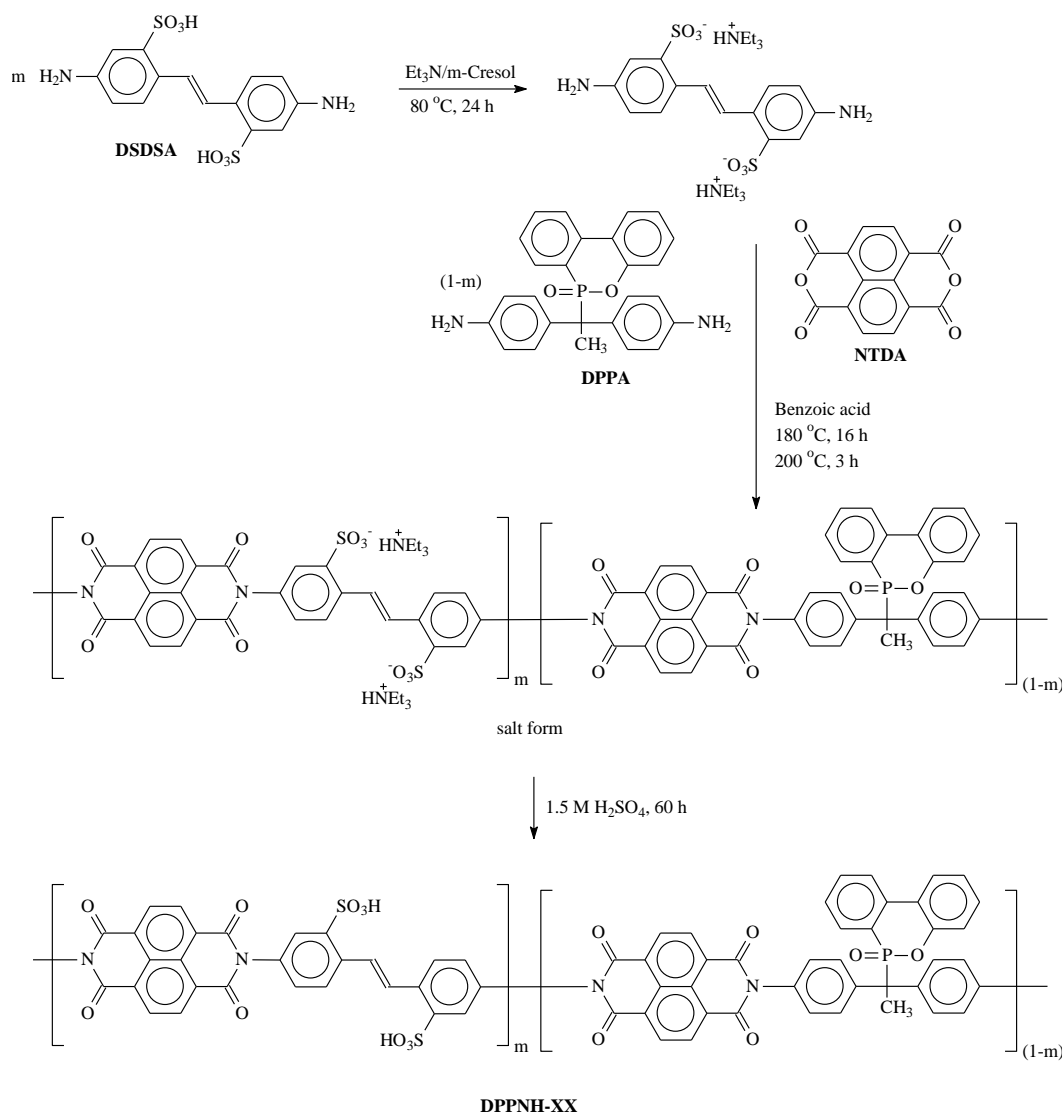
Banerjee *et al.* synthesized a series of 9,10-dihydro-9-oxa-10-phosphaphenanthrene 10-oxide (DOPO)-based SPIs (DPPNH-XX) having various DS values by the polycondensation reaction between 1,4,5,8-naphthalenetetracarboxylic dianhydride (NTDA) with 4,4′-diaminostilbene-2,2′-disulfonic acid (DSDSA) and 1,1-bis (4-aminophenyl)-1-(6-oxido-6H-dibenz <c, e> <1,2> oxaphosphorin-6-yl) ethane (DPPA), as shown in **Scheme 23**.[96] The DPPNH-XX copolyimides demonstrated high solubility in polar aprotic solvents.[96] The η_{inh} values of the DPPNH-XX copolymers were obtained between 1.01-1.22 dL/g.[96] The experimental IEC (IEC$_{NMR}$) values of the DPPNH-XX copolymers were calculated from the ^{1}H NMR spectra and obtained in close agreement with the theoretical IEC values.[96] The DPPNH-XX membranes showed high thermal and mechanical stabilities, as illustrated in **Table 7**. The DPPNH-XX membranes showed lowered SR values (in-plane SR: 6-10% at 80 °C) than the other literature-reported sulfonated PEMs, which indicates the higher dimensional stability of the DOPO-based DPPNH-XX copolymers.[96] The DPPNH-XX membranes showed τ values between 7.0-24 h in Fenton's reagent at 80 °C (**Table 7**). The microstructural analysis of the DPPNH-XX membranes revealed an interconnected and well-segregated phase morphology.[96] Among all the copolyimides, the DPPNH-90 membrane demonstrated the highest σ value of 235 mS/cm at 80 °C, as illustrated in **Table 7**. The proton conductivity-related E$_a$ values of the DPPNH-XX copolymers were found between 10.8-13.3 kJ/mol.[96]
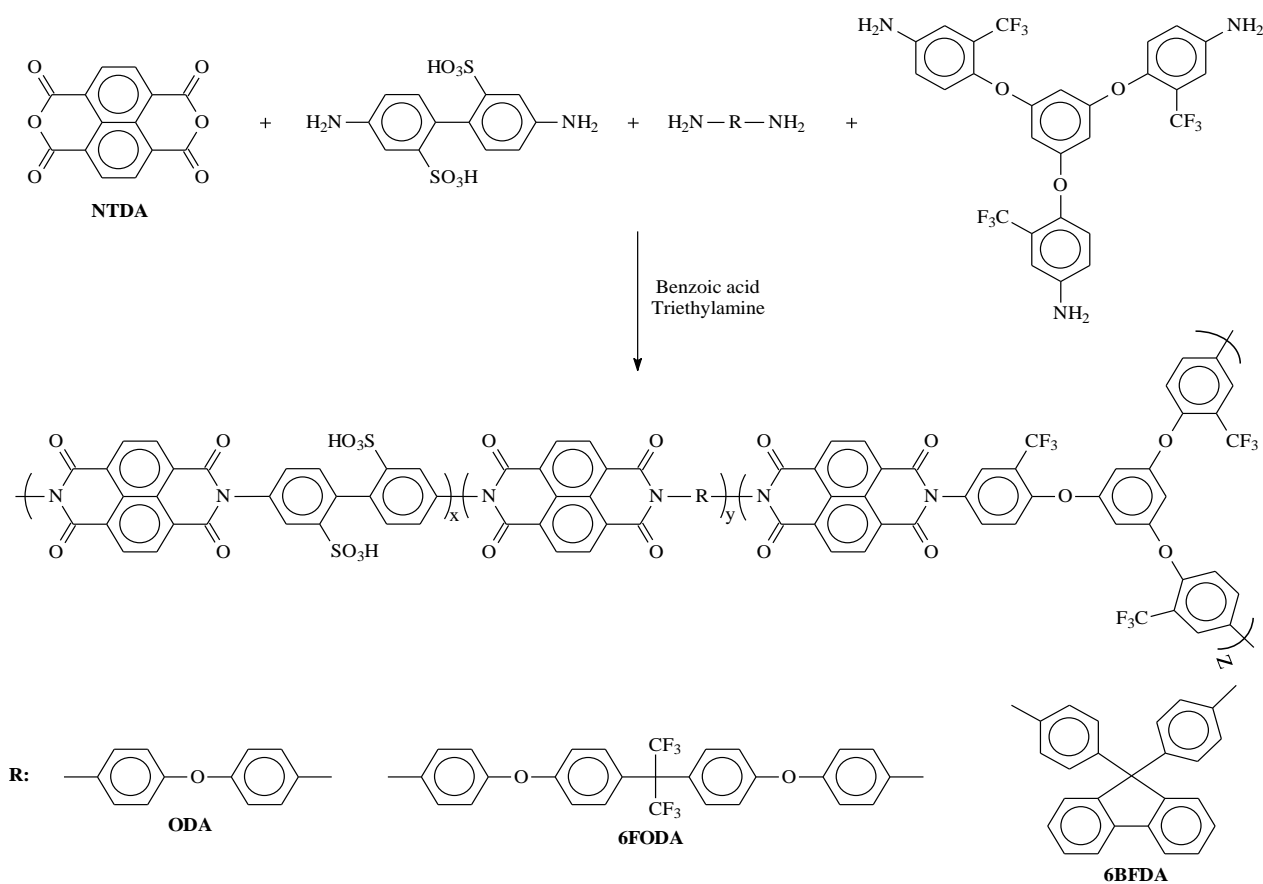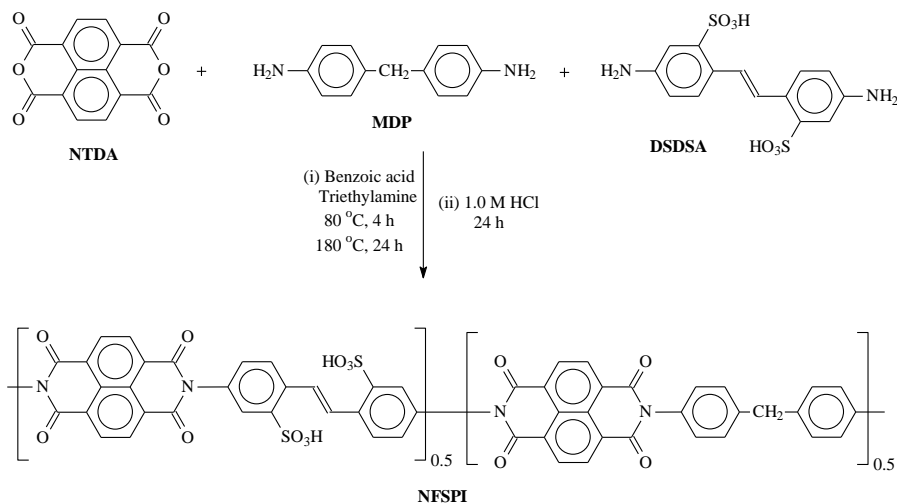

Scheme 23. The synthesis scheme of the sulfonated polyimides (DPPNH-XX).[96]

Banerjee and Ghanti

Innov. Chem. Mater. Sustain. **2025**, 2(1), 032-073

Table 7. *The IEC, Mw, η$_{inh}$, T$_d$, TS, YM, EB, WU, τ, and σ values of the SPIs*

Polymer	IEC (meq/g)[a]	η$_{inh}$ (dL/g)[b]	T$_d$ (°C)[c]	TS (MPa)	YM (GPa)	EB (%)	WU (%)[d]	τ (h)[e,f]	σ (mS/cm)[g]	Ref.
DPPNH-60	1.88	1.01	321	69	1.44	15	31	>24[f]	87	96
DPPNH-70	2.23	1.16	315	60	1.32	13[h]	36	>17[f]	104	96
DPPNH-80	2.58	1.17	301	52	1.22	10	46	>15[f]	202	96
DPPNH-90	2.95	1.22	295	45	1.02	7.0	64	>7[f]	235	96
SPI-ODA-0	-	-	-	62.1	-	-	-	2.3[e]	-	201
SPI-ODA-1	-	-	-	62.0	-	-	-	2.2[e]	-	201
SPI-ODA-2	-	-	-	50.7	-	-	-	2.5[e]	-	201
SPI-6FODA-0	2.01	0.83	-	71.7	1.72	-	-	>120[e]	-	201
SPI-6FODA-3	2.01	0.69	-	47.4	1.33	-	-	>120[e]	-	201
SPI-6FODA-5	1.99	0.72	-	41.7	1.22	-	-	>120[e]	-	201
SPI-6FODA-7	1.97	0.61	-	32.1	1.15	-	-	>120[e]	-	201
SPI-BFDA-0	2.38	0.54	-	62.3	-	-	-	3.5[e]	-	201
SPI-BFDA-1	2.36	-	-	66.4	-	-	-	4.8[e]	-	201
SPI-BFDA-3	2.33	0.46	-	46.2	-	-	-	4.5[e]	-	201
SPI-BFDA-5	2.31	0.49	-	41.2	-	-	-	4.0[e]	-	201
SPI-BFDA-7	2.29	0.31	-	38.2	-	-	-	4.3[e]	-	201
NFSPI	1.54	-	-	-	-	-	21.9[i]	42[f]	280	202
SPI-B20	1.77	-	-	88	-	18.7	47.2[i]	-	~100	203
SPI-B40	1.76	-	-	102	-	12.3	48.3[i]	24[j]	146	203
SPI-B60	1.77	-	-	92	-	16.2	47.8[i]	-	~130	203
SPI-1	1.24	2.46	-	-	-	-	28.4[i]	-	10.3[h]	204
SPI-1-1	1.40	-	-	-	-	-	23.7[i]	-	12.4[h]	204
SPI-1-1.5	1.55	-	-	-	-	-	34.2[i]	-	11.2[h]	204
SPI-2	1.77	1.82	-	74.9	-	-	47.9[i]	-	18.8[h]	204
SPI-2-0.8	1.79	-	-	-	-	-	64.5[i]	-	33.5[h]	204
SPI-2-1	1.81	-	-	67.9	-	-	96.9[i]	-	39.3[h]	204
SPI-2-1.2	1.72	-	-	-	-	-	64.4[i]	-	30.5[h]	204
SPI-2-1.5	1.87	-	-	-	-	-	73.5[i]	-	27.5[h]	204
SPI-3	1.95	1.39	-	73.3	-	-	63.1[i]	-	28.6[h]	204
SPI-3-0.5	1.80	-	-	-	-	-	54.5[i]	-	40.2[h]	204
SPI-3-0.8	1.80	-	-	56.2	-	-	62.3[i]	-	62.2[h]	204
SPI-3-1	1.87	-	-	-	-	-	69.3[i]	-	57.5[h]	204
SPI-3-1.2	1.72	-	-	-	-	-	54.1[i]	-	44.5[h]	204

[a] Theoretical IEC value, [b] inherent viscosity, [c] 10% decomposition temperature obtained from TGA analysis, [d] WU values at 80 °C, [e] starting fractured time in Fenton's reagent (30 ppm FeSO$_4$ in 30% H$_2$O$_2$) at 30 °C, [f] starting dissolution time in Fenton's reagent (30 ppm FeSO$_4$ in 30% H$_2$O$_2$) at 30 °C, [g] σ values under fully hydrated state at 80 °C, [h] through-plane σ value at 80 °C, [i] WU values after 24 h immersion in DI water [j] τ value in 3 ppm FeSO$_4$ in 10% H$_2$O$_2$ at 80 °C.

Scheme 24. Synthesis scheme of the sulfonated polynaphthylimides.[201]

NFSPI

Scheme 25. Synthesis scheme of the non-fluorinated SPI (NFSPI).[202]

SPI-Bn

n/m = 4/6; n = 20, 40, 60
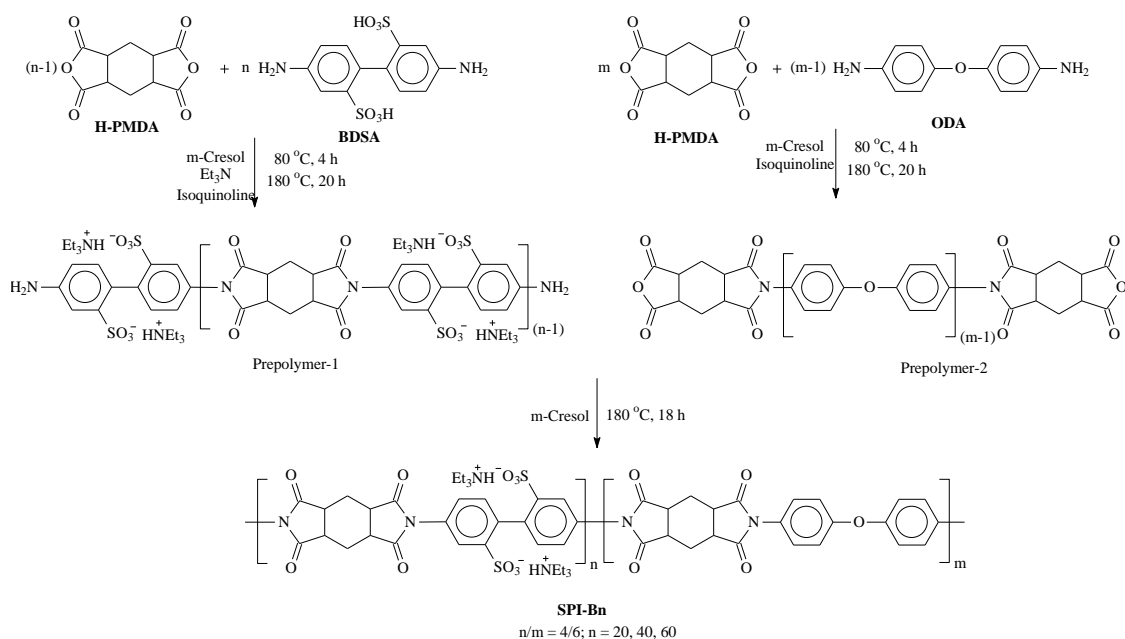
Scheme 26. The synthesis scheme of the sulfonated block copolyimides (SPI-Bn).[203]

SPI-x (Triethylamine salt form)
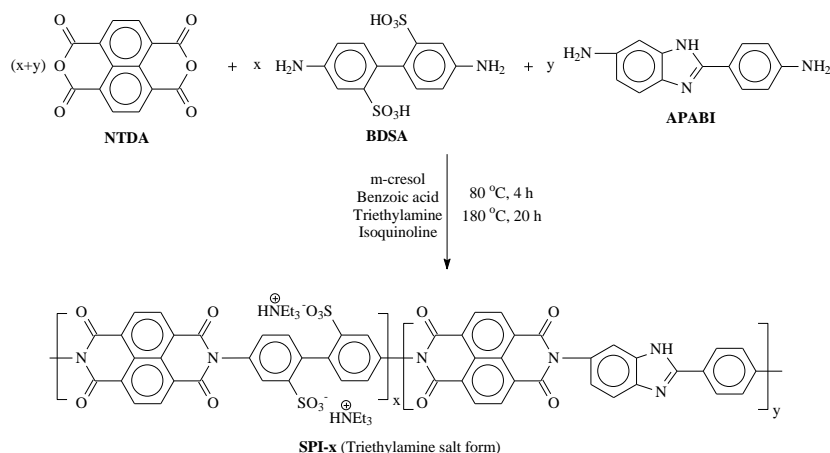
Scheme 27. Synthesis scheme of benzimidazole-containing SPI (SPI-x).[204]

Wang *et al*. synthesized a series of branched SPIs using NTDA as the dianhydride monomer, 4,4′-diamino-2,2′-biphenyldisulfonic acid (DAPS) as the sulfonated diamine monomer, 1,3,5-tris (2-trifluoromethyl-4-aminophenoxy)

benzene as the trifunctional branching monomer, and three other non-sulfonated diamine monomers [4,4′-oxydianiline (ODA), 2,2-bis[4-(4-aminophenoxy)phenyl]hexafluoropropane (6FODA), and 4,4′-(9-fluorenylidene)dianiline (BFDA)], as shown in **Scheme 24**.[201] The theoretical IEC values of the SPI-

Banerjee and Ghanti

Innov. Chem. Mater. Sustain. **2025**, 2(1), 032-073
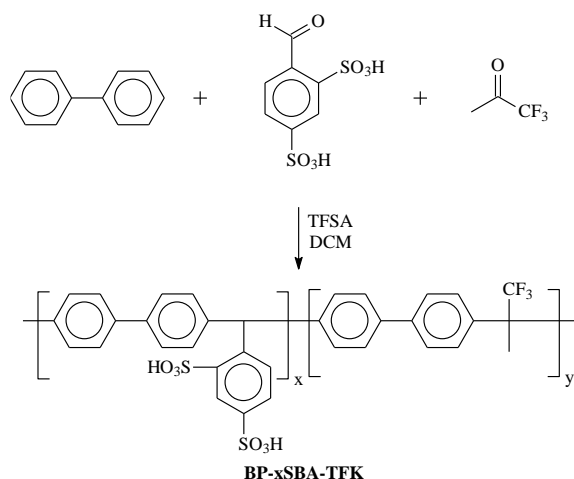
Scheme 28. The synthesis scheme of the SPPA copolymers [P(BP-xSBA-TFK)].[218]

6FODA-x and SPI-6BFDA were obtained between 1.97-2.01 mmol/g and 2.29-2.38 mmol/g, respectively (**Table 7**). The branched SPIs showed appropriate thermal stability and mechanical properties for PEMFC applications.[201] Among all the branched series SPI membranes, the SPI-6BFDA series membranes exhibited the highest WU values due to the more considerable steric hindrance of the side chain in the branched polyimide structures.[201] The SPI-6FODA series membranes demonstrated the highest oxidative stability in Fenton's reagent (20 ppm $FeSO_4$ in 30% H_2O_2) at 30 ℃, as tabulated in **Table 7**. The oxidative stability also increased with the increase in the degree of branching (DB) in the branched SPI membranes.[201] The SPI-6FDA series membranes showed the highest proton conductivity values in coordination with WU values.[201]

Mahajan *et al.* synthesized a non-fluorinated sulfonated polyimide (NFSI) by the polycondensation reaction of the dianhydride NTDA with sulfonated [4,4′-diamino stilbene-2,2-sulfonic acid (DSDSA)] and non-sulfonated [4,4′-diamino diphenyl methane (MDP)] diamines monomers in the presence of benzoic acid and triethylamine (TEA) in m-cresol, as provided in **Scheme 25**.[202] The theoretical IEC value of the NFSPI copolymer was 1.54 meq/g (**Table 7**). The NFSPI membrane showed appropriate water absorption properties (WU: 21.9% and hydration number value: 8).[202] The NFSPI membrane exhibited a σ value of 280 mS/cm at 80 ℃, as illustrated in **Table 7**. The non-fluorinated SPI membrane demonstrated high hydrolytic stability (51 h) and oxidative stability (42 h; 30 ppm $FeSO_4$ in 30% H_2O_2 at 30 ℃).[202] The open circuit potential (OCP) value of the NFSPI membrane in a single fuel cell test was 0.80 V at 80 ℃, whereas that of the Nafion was 0.85 V, which indicates that the NFSPI membrane demonstrated comparable PEMFC performance.[202]

Wang *et al.* synthesized a series of multiblock sulfonated polyimides (SPI-Bn) by the polycondensation reaction of a flexible aliphatic six-membered cyclic dianhydride monomer [1,2,4,5-cyclohexanetetracarboxylic Dianhydride (H-PMDA)] with sulfonated diamine [4,4'-diaminobiphenyl-2,2′-disulfonic acid hydrate (BDSA)] and non-sulfonated diamine [4,4'-oxydianiline (ODA)] monomers, as shown in **Scheme 26**.[203] The theoretical IEC value of the SPI-Bn block copolymers ranged between 1.76-1.77 meq/g (**Table 7**). The sulfonated block copolyimides displayed high thermal and mechanical stability (TS: 88-102 MPa and EB: 12.3-18.7%).[203] The SPI-Bn membranes exhibited WU values between 47.2-48.3%, as compiled in **Table 7**. The SPI-B40 membranes demonstrated the τ value of 24 h in Fenton's reagent (3 ppm $FeSO_4$ in 10% H_2O_2) at 80 ℃.[203] Among all the membranes, the SPI-B40 membrane displayed the highest σ value of 146 mS/cm at 80 ℃ (**Table 7**). In the hydrogen-oxygen (H_2-O_2) fuel

cell performance, the maximum peak power density order was SPI-B20 (641 mW/cm²) < SPI-B60 (727 mW/cm²) < SPI-B40 (869 mW/cm²) at 80 ℃ under 100% RH conditions.[203]

Ding et al. designed and fabricated a series of composite SPI membranes (SPI-x-y) by mixing the SPI and nano carbon sulfonic acid (NCSA) using the solution blending method.[204]
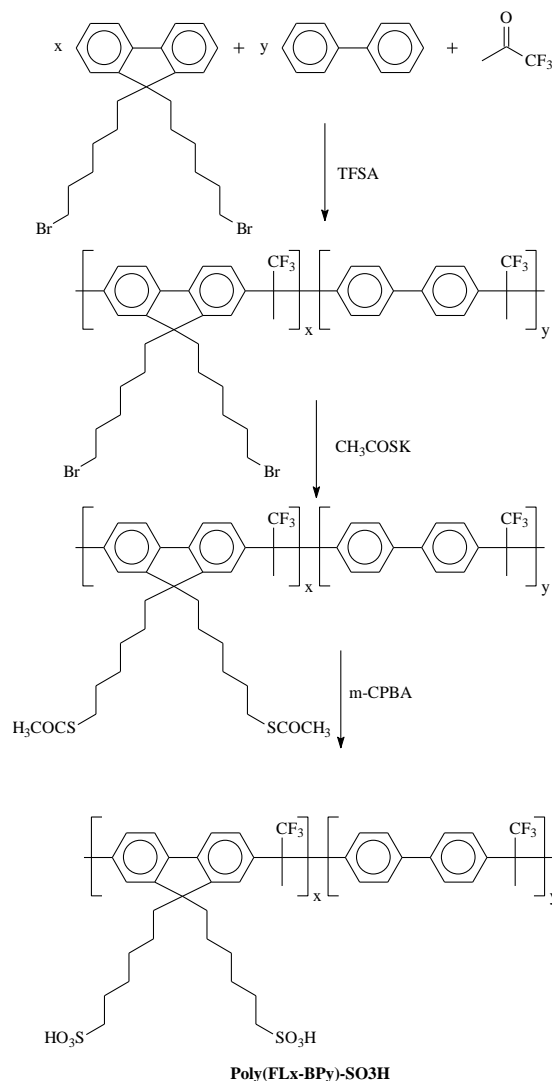
Poly(FLx-BPy)-SO3H
Scheme 29. The synthesis scheme of the poly(FLx-BPy)-SO₃H copolymers.[219]

The pristine SPI copolymer with various DS values is prepared

Banerjee and Ghanti

Innov. Chem. Mater. Sustain. **2025**, 2(1), 032-073

by the polycondensation reaction of NTDA with sulfonated diamine monomer [2,2′-benzidinedisulfonic acid (BDSA)] and benzimidazole-containing non-sulfonated diamine monomer [2-(4-aminophenyl)-5-aminobenzimidazole (APABI)], as depicted in **Scheme 27**.[204] The NCSA nanoparticle is prepared by the chemical reaction of nano carbon particles (NCPs) with benzenesulfonic acid.[204] The η_{inh} values of the pristine SPI-x copolymers were between 1.39-2.46 dL/g (**Table 7**). Among all the composite membranes, the SPI-2-1 composite membrane displayed the highest water absorption properties (WU: 96.9% and SR: 117.2%) after 24 h of immersion in DI water.[204] The SPI-3-0.8 composite membrane reached the maximum through-plane σ value of 136.8 mS/cm at 90 °C, which is twice that of the pristine SPI-3 membrane and 50% higher than that of the Nafion-117 membrane.[204] In the PEMFC test, the SPI-3-0.8 composite membrane-based MEA reached the maximum PPD value of 1.584 W/cm² at 80 °C without any backpressure, which is 20% higher than that of the pristine SPI-3 membrane-based MEA (1.312 W/cm²).[204] The OCV value of the SPI-3-0.8 composite membrane-based MEA was 0.97 V, whereas that value after one week was close to 0.90 V, which indicates the long-term stability of the SPI-3-0.8 composite membrane.[204]

4.2.7 Poly(phenylene alkane)s, PPAs

Poly(phenylene alkane)s, PPAs are an essential class of high-performing liner polymers, synthesized by the efficient superacid-catalyzed Friedel–Crafts (SACFC) polyhydroxyalkylations reaction of super electrophilic carbonyl compounds and electron-rich aromatic compounds (biphenyl, p-terphenyl, fluorene, carbazole, etc.) in the presence of the superacid, such as trifluoromethanesulfonic acid (TFSA), methanesulfonic acid (MSA), etc.[205-208] PPAs are known for their high thermal stability, good mechanical properties, excellent proton conductivity, and superior oxidative stability owing to the lack of radical attack-prone ether

linkages on the polymer backbone.[205,209-211] Sulfonated poly(phenylene alkane)s, SPPAs are usually prepared either by direct polyhydroxyalkylations reaction of sulfonated monomers or by the post-sulfonation grafting method of the polymers.[212-215] Generally, the SPPAs possessed high molecular weight, good solubility, excellent thermal and mechanical stability, high proton conductivity, and, more specifically, outstanding chemical or oxidative stability.[212-217] In this section, a few recently developed SPPAs for PEMFC applications are discussed below.

Zhang *et al.* synthesized a series of all-carbon backbone and dense SPPAs, designated as P(BP-xSBA-TFK) with various sulfonic acid contents by the SACFC polyhydroxyalkylations reaction of biphenyl (BP) with 1,3-disulfonic acid benzaldehyde (DFD) and 1,1,1-trifluoroacetone (TFK), as shown in **Scheme 28**.[218] The theoretical IEC values of the P(BP-xSBA-TFK) copolymer were between 1.3-4.1 meq/g, as provided in **Table 8**. The P(BP-xSBA-TFK) copolymer displayed η_{inh} values between 1.45-1.65 dL/g (**Table 8**), which confirms the formation of a high molecular weight copolymer by the SACFC polyhydroxyalkylations reaction. The P(BP-xSBA-TFK) copolymer demonstrated high thermal (decomposition

temperature up to 400 °C) and mechanical stability.[218] The P(BP-0.8SBA-TFK) membrane showed the highest water absorption (WU: 37.9% and SR: 16.9%) at 80 °C, as tabulated in **Table 8**. The morphological analysis of the P(BP-xSBA-TFK) copolymer displayed an interconnected phase morphology, which benefits the agile ion transportation process.[218] Out of all the SPPA membranes, the P(BP-0.8SBA-TFK) membrane reached the maximum σ value of 404.3 mS/cm at 80 °C, as illustrated in **Table 8**. The P(BP-0.6SBA-TFK) membrane retained more than 99.2% of its weight after an hour of the Fenton's test at 80 °C and reached the maximum
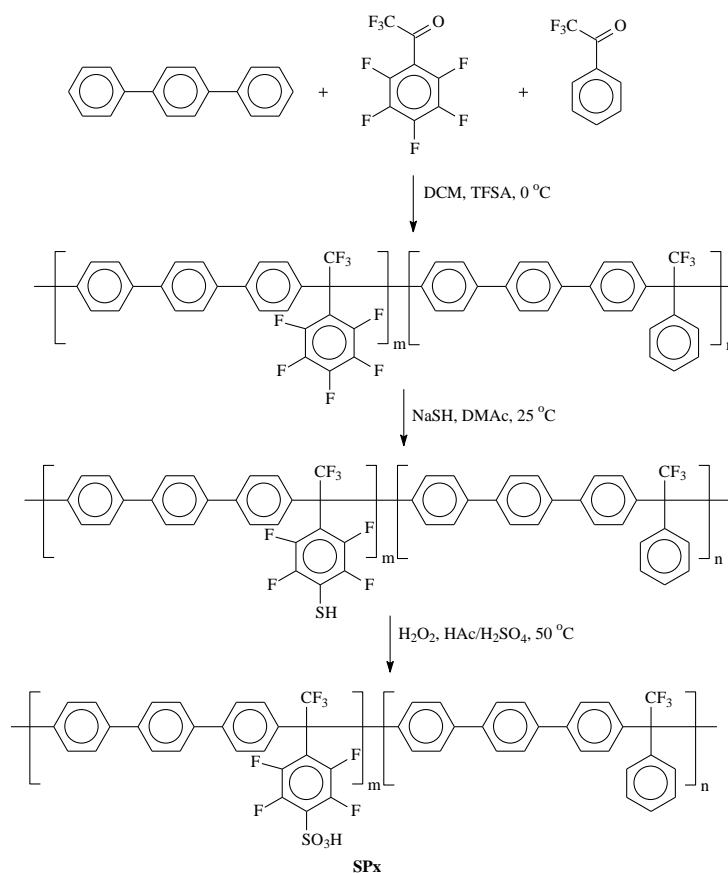
Scheme 30. The synthesis scheme of SPPA copolymers (SPx).[220]

Table 8. *The IEC, η$_{inh}$, T$_d$, TS, YM, EB, WU, τ, and σ values of the SPPAs*

Polymer	IEC (meq/g)[a]	η$_{inh}$ (dL/g)[b]	T$_d$ (°C)[c]	TS (MPa)	YM (GPa)	EB (%)	WU (%)[d]	τ (h)[e]	σ (mS/cm)[f]	Ref.
P(BP-0.8SBA-TFK)	4.1	1.45	-	28.2	-	15	37.9	-	404	218
P(BP-0.6SBA-TFK)	3.3	1.56	-	29.4	-	25	30.6	-	352	218
P(BP-0.4SBA-TFK)	2.4	1.61	-	54.0	-	19	15.0	-	231	218
P(BP-0.2SBA-TFK)	1.3	1.65	-	69.3	-	11	7.5	-	85	218
Poly(FL30-BP70)-SO3H	1.71	-	-	37.9	0.89	6.5	47	-	134	219
Poly(FL40-BP60)-SO3H	2.08	-	-	39.5	1.17	4.8	-	-	160	219
Poly(FL50-BP50)-SO3H	2.39	-	-	49.1	1.18	4.5	-	-	191	219
Poly(FL60-BP40)-SO3H	2.65	-	-	51.6	1.19	4.1	91	-	202	219
SP55	1.17	-	285	-	-	-	9.8	-	42	220
SP72	1.45	-	283	-	-	-	21	-	104	220
SP83	1.62	-	284	-	-	-	30	-	136	220
SP100	1.85	-	277	-	-	-	39	-	203	220
TSPHFTP-35	2.23	-	-	28.5	-	39.6	49.2	-	138	221
TSPHFTP-42	2.43	-	-	23.7	-	47.1	86.8	-	227	221
TSPHFTP-50	2.63	-	-	19.7	-	49.1	105	-	303	221
SP1	2.13	-	<300[g]	10.3	0.58	2.5	31.7	6.0	75	222
SP2	1.50	-	<300[g]	24.7	0.81	20.6	16	8.5	25	222
SP3	1.78	-	<300[g]	31.4	0.69	6.2	43.8	10	107	222

[a] Theoretical IEC value, [b] inherent viscosity, [c] onset decomposition temperature obtained from TGA analysis in N$_2$, [d] WU values at 80 °C, [e] starting fractured time in Fenton's reagent at 80 °C, [f] σ values at 80 °C and 100% RH, [g] 5% decomposition temperature obtained from TGA.

PPD value of 560 mW/cm^2 at 80 °C under 100% RH conditions.[218]

Yang *et al*. designed and synthesized a comb-like structure of SPPAs [Poly(FLx-BPy)-SO$_3$H] having an ether-free all-carbon backbone and flexible double sulfohexyl side chain, as depicted in **Scheme 29**.[219] The theoretical IEC values of the Poly(FLx-BPy)-SO$_3$H copolymers were between 1.71-2.65 meq/g, whereas the experimental IEC values were obtained between 1.64-2.54 meq/g.[219] The Poly(FLx-BPy)-SO$_3$H membranes showed appropriate mechanical stability (TS: 37-52 MPa, YM: 0.89-1.19 GPa, and EB: 6.5-4.1%) and superior oxidative stability (RW ≥ 99.4% after 4 h of the Fenton's test at 80 °C).[219] Among the Poly(FLx-BPy)-SO$_3$H membranes, the Poly(FL60-BP40)-SO$_3$H membranes reached the highest WU value of 91% at 80 °C in DI water, as tabulated in **Table 8**. The morphological investigation of the Poly(FLx-BPy)-SO$_3$H membranes demonstrated a phase-segregated microstructure.[219] The Poly(FLx-BPy)-SO$_3$H membranes exhibited the σ value between 134-202 mS/cm at 80 °C, as illustrated in **Table 8**. The Poly(FL50-BP50)-SO$_3$H-based MEA reached the maximum PPD value of 2.46 W/cm^2 in H$_2$/O$_2$ single fuel cell test at 80 °C under 100% RH conditions.[219]

Jannasch *et al*. synthesized a series of poly(p-terphenyl perfluorophenylsulfonic acid)s [SPx] by the metal-free SACFC polyhydroxyalkylations reaction of p-terphenyl with perfluoroacetophenone and acetophenone, followed by the selective post-sulfonation of the non-sulfonated copolymers by the thiol-oxidation method, as shown in **Scheme 30**.[220] The M$_w$ and PDI values of the non-sulfonated copolymers (Px, x: 55, 72, 83, 100) were between 50-162 kg/mol and 1.5-1.8, respectively.[220] The SPx copolymers showed high thermal stability (T$_{d,onset}$: 277-285 °C), as illustrated in **Table 8**. The SPx membranes exhibited WU values between 9.8-39% at 80 °C
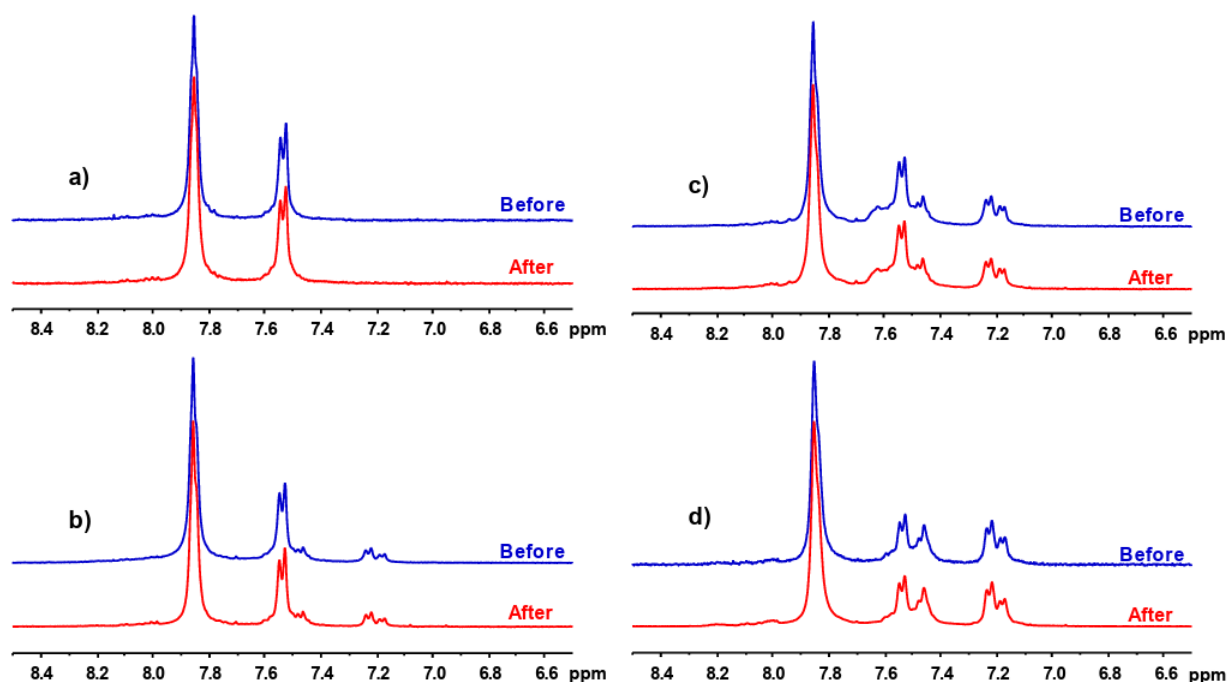

Figure 12. ^{1}H NMR spectra before and 1 h after the Fenton's test in DMSO-d$_6$ of (a) SP100, (b) SP83, (c) SP72, and (d) SP55 copolymers.[220] (Reprinted with permission from (220). Copyright (2019) American Chemical Society.)

Banerjee and Ghanti

Innov. Chem. Mater. Sustain. **2025**, 2(1), 032-073

(**Table 8**). The through-plane SR and hydration number (λ) values of the SPx membranes at 80 ℃ were 5.9-21% and 4.8-12.[220] Among the SPx membranes, the SP100 membrane reached the highest σ value of 203 mS/cm at 80 ℃ in fully hydrated conditions (**Table 8**). The SPx membranes displayed superior oxidative stability after an hour of the Fenton's test at 80 ℃, as no change in copolymer structures was observed in the ^{1}H NMR spectra (**Figure 12**).[220]

Zhu *et al.* designed and synthesized a series of graft-type pendant dual 1,2,3-triazole and disulfonated moieties-based ether-free all-carbon backbone SPPAs (TSPHFTP-x) copolymers for the PEMFC applications, as shown in **Scheme 31**.[221] The M_w and PDI values of the BPHFTP-x copolymers were between 144-176 kg/mol and 2.15-2.63, which confirms the formation of the high molecular weight copolymer by the SACFC polyhydroxyalkylations reaction.[221] The theoretical IEC values of the TSPHFTP-x copolymers ranged from 2.23-2.63 meq/g (**Table 8**). The TSPHFTP-x copolymers exhibited high thermal stability (5% weight loss temperature up to 300 ℃) and mechanical stability (TS: 19.7-28.5 MPa and EB: 39.6-49.1%).[221] The TSPHFTP-x membranes demonstrated high oxidative stability (RW ≥ 94%) after an hour of the Fenton test at 80 ℃.[221] The TSPHFTP-x membranes exhibited a high σ value (138-303 mS/cm) at 80 ℃ under 100% RH conditions (**Table 8**). In the H_2/O_2 single fuel cell test, the OCV, PPD, and current density values of the TSPHFTP-50 PEMs were 0.98 V, 1.013 W/cm^2, and 2.54 A/cm^2 at 60 ℃ and 100% RH.[221] The OCV value of the TSPHFTP-50 MEA dropped from 0.75 V to 0.67 V after 55 h of the durability test, which confirms the long-term durability of the TSPHFTP-50 PEMs.[221]

Liu *et al.* synthesized three all-carbone backbone PPAs (P1, P2, P3) by the SACFC polyhydroxyalkylations reaction of 2,3,4,5,6-pentafluorobenzaldehyde (PFBA) with three different commercially available aromatic compounds (1,4-dimethoxybenzene, 6,6′-dimethoxy-3,3,3′,3′-tetramethyl-1,1′-spirobisindane, and p-Terphenyl) in presence of the methanesulfonic acid (MSA) in DCM, as shown in **Scheme 32**.[222] The M_w and PDI values of the PPAs (Px) polymers were 115-888 kDa and 1.83-7.24, respectively.[222] Then, the SPPAs (SP1, SP2, and SP3) were prepared by the aromatic nucleophilic substitution reaction between para-aryl-F and sodium 4-oxybenzenesulfonate at 120 ℃ (**Scheme 32**). The theoretical and experimental NMR-based IEC values of the SPx copolymers were obtained between 1.78-2.13 and 1.25-1.78 meq/g, respectively.[222] The SPx copolymers exhibited high thermal and mechanical stability, as illustrated in **Table 8**. The SPx membranes displayed high dimensional stability (WU: 16-44% and SR: 4.9-12.9%) at 80 ℃.[222] Among the SPx membranes, the SP3 membranes showed the highest σ value of 107 mS/cm at 80 ℃ and 100% RH conditions, as compiled in **Table 8**. The all-carbon backbone SPx membranes demonstrated high oxidative stability (after 1 h of test, RW ≥ 96% and τ ≥ 6.0 h) in Fenton's reagent at 80 ℃.[222] In the H_2/Air single fuel cell test, the OCV, PPD, and current density values of the SP3 PEMs were 0.93 V, 532 mW/cm^2, and 1.2 A/cm^2 at 80 ℃ and 100% RH.[221] During the long-term durability test of SP3 MEA, the OCV value slowly decreased from 0.95 to 0.81 V after 108 h.[222]

4.2.8 Polytriazoles, PTs

PTs are another special type of high-performing polymer, well known for their diverse functionalities in various fields, such as heat resistivity, metal coordinator, and antimicrobial activities.[223-225] PTs are mainly synthesized by the metal-catalyzed (Cu, Ir, Ru, Ni) azide-alkyne cycloaddition (MCAAC) "click" polymerization reactions.[226-228] The Cu(I)-catalyzed azide-alkyne cycloaddition (CuAAC) reaction is the most employed due to its excellent yield, high selectivity, high specificity, outstanding efficiency, and simplistic synthesis procedure.[229-232] The CuAAC polymerization reaction mainly produced 1,4-substituted 1,2,3-triazole rings with high

selectivity and yield.[89,129,229-232] Sulfonated polytriazoles (SPTs) are also synthesized by the CuAAC "click" polymerization reaction, and they have gained remarkable consideration for their high thermal and mechanical stabilities, good solubility, high dimensional stability, excellent ionic conductivity, and better oxidative stability.[61,89,129,221,232] The presence of the 1,2,3-triazole rings in the SPT backbone improved the thermal
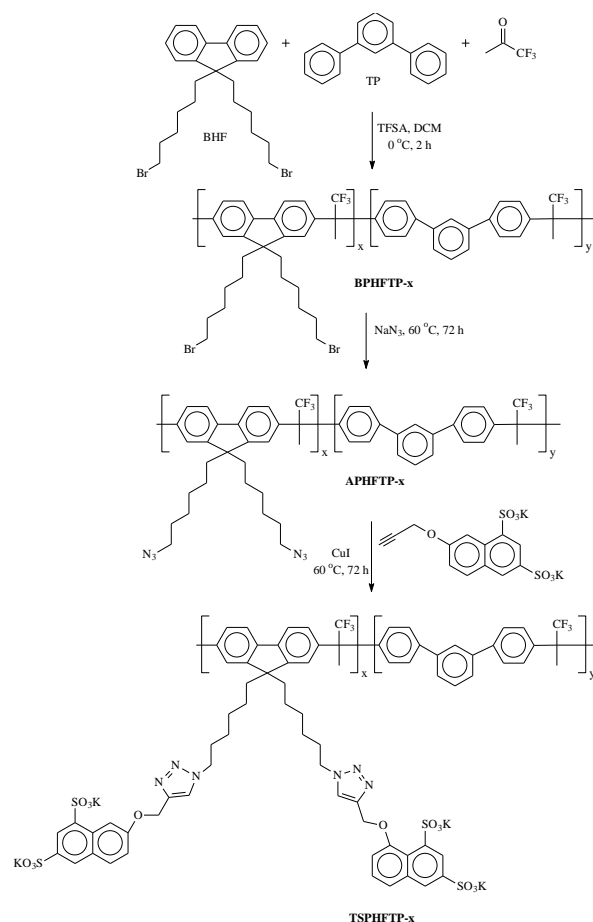
Scheme 31. The synthesis scheme of the pendant 1,2,3-triazole-based dual SPPAs (TSPHFTP-x) copolymers.[221]
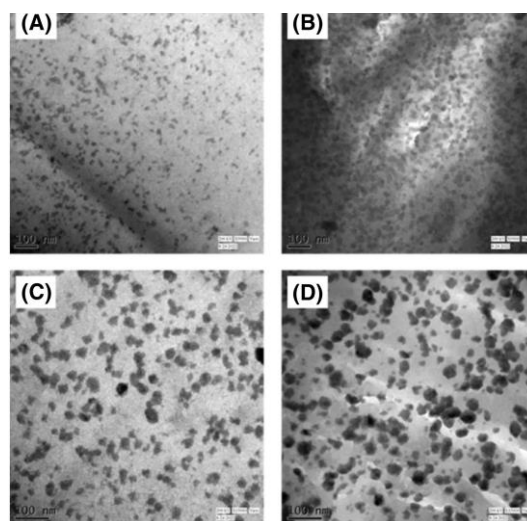

Figure 13. The lead acetate-stained TEM images of the (A) BABPSSH-60, (B) BABPSSH-70, (C) BABPSSH-80, and (D) BABPSSH-90.[80] (Copyright 2023, Adopted with permission from (80) John Wiley & Sons, Inc.)

Table 9. The IEC, M_w, T_d, TS, YM, EB, WU, τ, and σ values of the SPTs.

Polymer	IEC_w (meq/g)[a]	M_w (kDa)[b]	T_{d10} (°C)[c]	TS (MPa)	YM (GPa)	EB (%)	WU (%)[d]	τ (h)[e]	σ (mS/cm)[f]	Ref.
BABPSSH-60	1.60	-	271	33	1.47	13	11	>24	25.5	80
BABPSSH-70	1.88	-	269	27	1.45	26	15	>24	29.4	80
BABPSSH-80	2.17	-	265	24	1.28	11	23	13	53.7	80
BABPSSH-90	2.46	-	260	17	0.68	11	32	6	91.5	80
PTPFDSH-70	2.24	63.8	317	68	1.82	89	28	>24	91	233
PTPFDSH-80	2.67	71.4	279	56	1.66	66	33	>24	138	233
PTPFDSH-90	3.13	77.5	266	50	1.47	61	49	14.5	176	233
PYPYSH-70	2.28	451	350	65	2.37	13	26	48	95	100
PYPYSH-80	2.70	283	321	46	1.86	17	35	44	110	100
PYPYSH-90	3.15	222	312	40	1.53	14	53	30	155	100
PYPYSH-100	3.64	265	274	18	0.59	21	65	17	184	100
PYPOSSH-60	1.34	274	304	45	1.82	45	8.4	>48	20	99
PYPOSSH-70	1.61	230	287	41	1.66	42	11	>48	53	99
PYPOSSH-80	1.88	144	283	47	1.8	34	16	38	78	99
PYPOSSH-90	2.17	126	281	33	1.05	17	28	26	114	99
PTSF-FeS-3	-	-	-	31.3	1.2	40	21	27	66	234
PTSF-FeS-5	-	-	-	-	-	30	27	30	69	234
PTSF-FeS-7	-	-	-	-	-	28	31	31	80	234
PTSF-FeS-9	-	-	-	20.8	0.91	20	38	34	78	234

[a] Theoretical IEC value, [b] weight-average molecular weight, [c] 10% decomposition temperature obtained from TGA analysis, [d] WU values at 80 °C, [e] complete dissolution time in Fenton's reagent (2 ppm $FeSO_4$ in 3% H_2O_2) at 80 °C, [f] σ values under fully hydrated state at 80 °C.
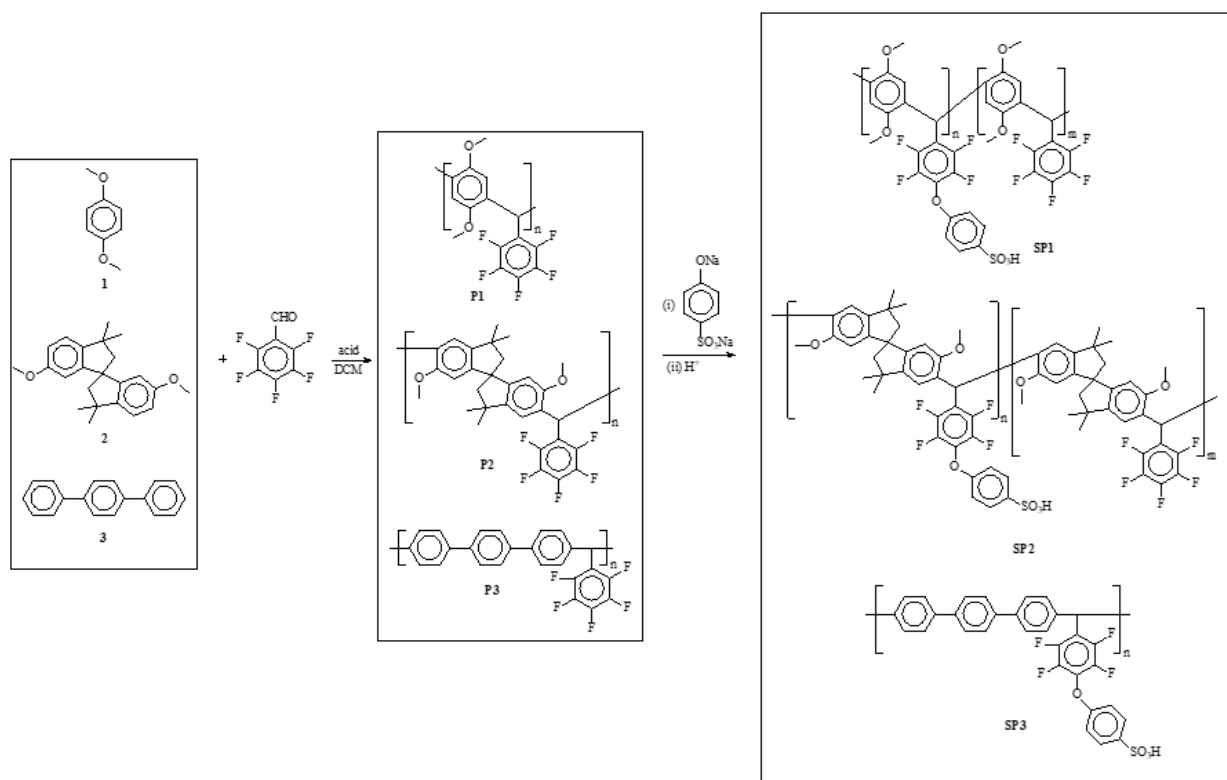
Scheme 32. The synthesis scheme of the PPAs (P1-P3) and SPPAs (SP1-SP3).[222]

and dimensional stability through its aromatic nature. It enhanced the proton conductivity by creating additional hydrogen bonding sites via its basic nitrogen atom of the 1,2,3-triazole rings.[61,89,129,221,232] Herein, a few recently developed SPTs for PEMFC applications are discussed below.

Banerjee *et al*. designed and synthesized a series of semi-fluorinated SPTs (BABPSSH-XX) with various DS values by the CuAAC "click" polymerization reaction of 4,4′-(propane-2,2′-diyl)bis((prop-2-ynyloxy)benzene) [BPAAL] with 1,4-bis(4-azido-2-(trifluoromethyl)phenoxy)benzene [BATFB] and 4,4′-diazido-2,2′-stilbenesulfonic acid disodium salt tetrahydrate [DASSA] in DMSO at 80 °C, as shown in **Scheme 33**.[80] The

η_{inh} values of the BABPSSH-XX copolymers were obtained between 1.15-1.35 dL/g.[80] The experimental NMR-based IEC values (IEC_{NMR}: 1.62-2.49 meq/g) match the theoretical IEC values (IEC_{theo}: 160-2.46 meq/g).[80] The BABPSSH-XX copolymers showed high thermal (T_{d10}: 260-271 °C) and mechanical stabilities (TS: 17-24 MPa, YM: 0.68-1.47 GPa), as provided in **Table 9**. All the copolymer membranes demonstrated high dimensional and oxidative stability owing to the presence of the semi-fluorinated unit in the copolymer architecture.[80] The TEM morphological investigation confirms the formation of the well-segregated and interconnected phase morphology (**Fig. 13**), which is beneficial for the facile proton transportation process. The BABPSSH-90 membrane
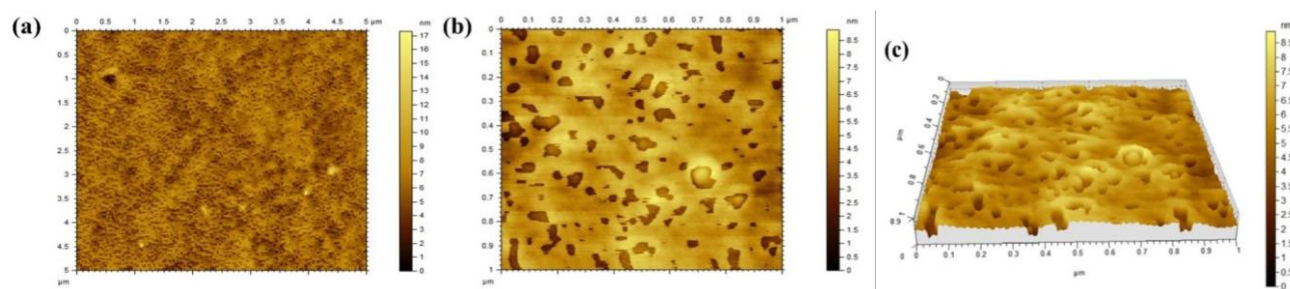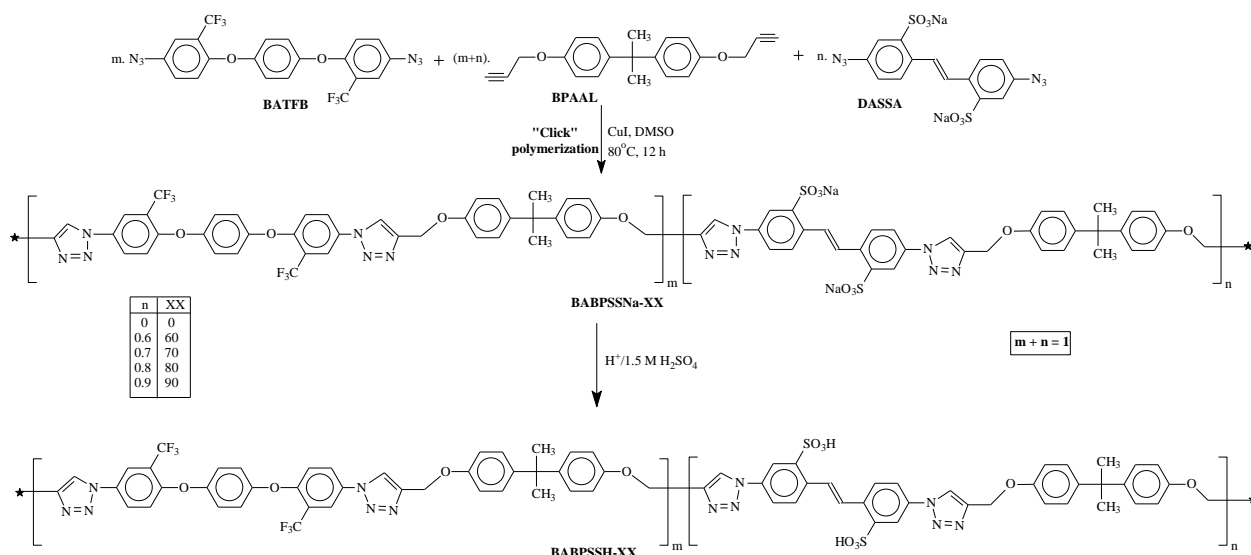
Figure 14. The TM surface images of the PYPYSH-80 membrane (a) 2D 5×5 µm², (b) 2D 1×1 µm², and (c) 3D 1×1 µm².[100] (Reprinted with permission from (100). Copyright (2022) American Chemical Society.)

Scheme 33. The synthesis scheme of the semi-fluorinated SPTs (BABPSSH-XX).[80]

demonstrated the highest σ value of 91.5 mS/cm at 80 °C in DI water, as compiled in **Table 9**.

Banerjee *et al.* designed and synthesized a series of phosphine oxide (P=O)-based SPTs (PTPFDSH-XX) with various sulfonic acid content utilizing 1,3-diethynylbenzene (DEB), bis[4-(4′-azidophenoxy)-3-trifluoromethylphenyl] phenylphosphine oxide (PFAZ), and 4,4'-diazido-2,2'-stilbenesulfonic acid disodium salt (DSAZ) by CuAAC "click" polymerization reaction, as depicted in **Scheme 34**.[233] The M_w
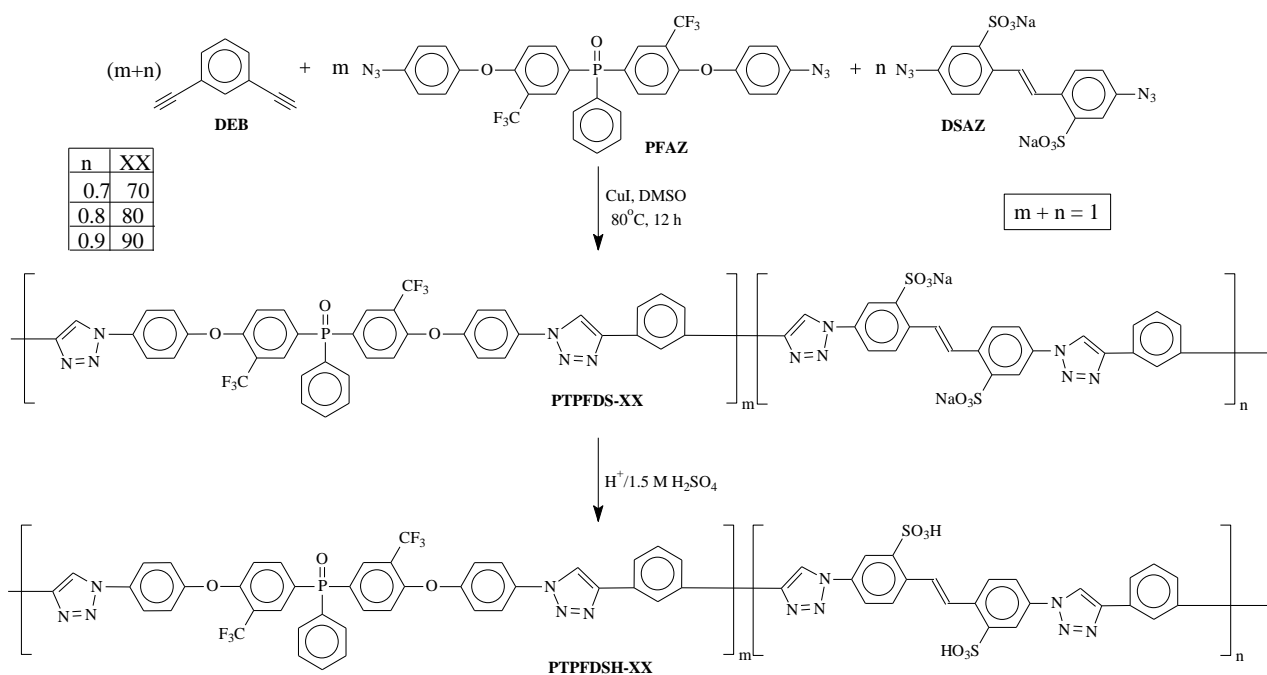
Scheme 34. The synthesis scheme of the phosphine oxide (P=O)-based semi-fluorinated SPTs (PTPFDSH-XX) copolymers.[233]

Banerjee and Ghanti

Innov. Chem. Mater. Sustain. **2025**, *2*(1), 032-073
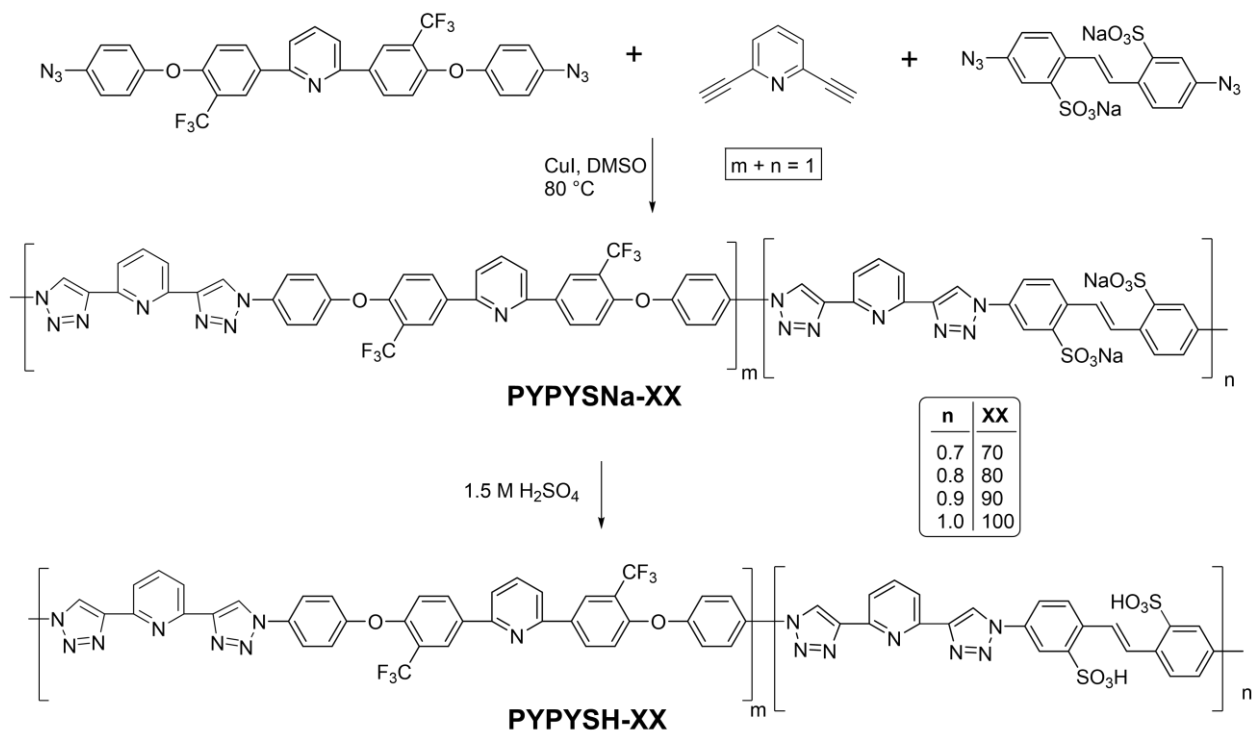
Scheme 35. The synthesis scheme of the 2,6-sterically hindered pyridinyl-based SPTs (PYPYSH-XX).[100]
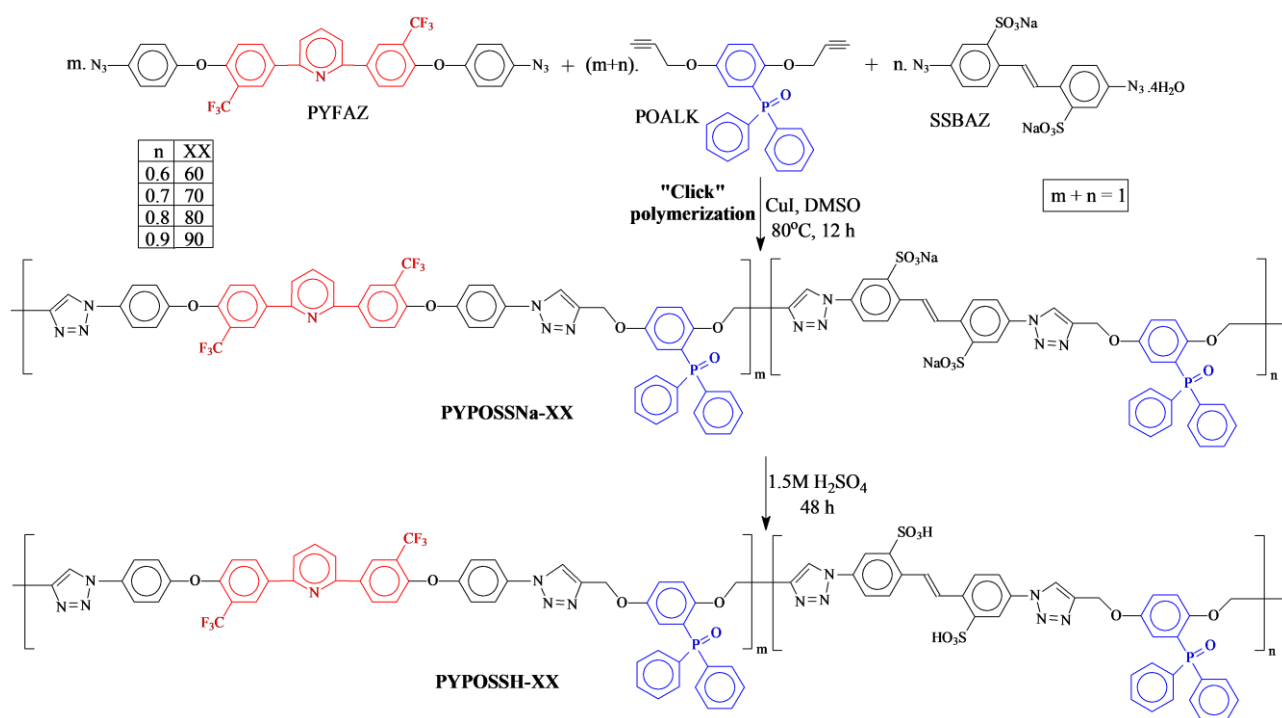
Scheme 36. The synthesis scheme of the pyridinyl- and P=O-based semi-fluorinated SPTs (PYPOSSH-XX).[99]

and PDI values of the PTPFDSH-XX copolymers were obtained between 63800-77500 g/mol and 1.71-2.29.[233] The theoretical IEC values of the SPTs were between 2.24-3.13 meq/g (**Table 9**). The PTPFDSH-70 to -90 copolymers exhibited desired thermal and mechanical stabilities, as illustrated in **Table 9**. The WU and in-plane SR values of the P=O-based semi-fluorinated SPT membranes were between 28-49% and 6.2-7.3% at 80 ℃, which revealed their high dimensional stability.[233] Among all the membranes, the PTPFDSH-90 membranes showed the highest σ value of 176 mS/cm at 80 ℃ (**Table 9**). The PTPFDSH-70 to -90

membranes showed superior oxidative stability in Fenton's reagent at 80 ℃, as tabulated in **Table 9**.

Banerjee *et al.* designed and synthesized a series of 2,6-sterically hindered pyridinyl-based SPTs (PYPYSH-XX) copolymers with DS values between 70-100% by the CuAAC "click" polymerization reaction in DMSO at 80 ℃, as reported in **Scheme 35**.[100] The theoretical IEC and M_w values of the PYPYSH-XX copolymers were obtained between 2.28-3.64 meq/g and 222000-451000 g/mol, respectively (**Table 9**). The pyridinyl-based SPT copolymers showed high thermal (Td10%: 274-350 ℃) and mechanical stabilities (TS: 18-65

Banerjee and Ghanti

Innov. Chem. Mater. Sustain. **2025**, 2(1), 032-073

Figure 15. The (a) ¹H NMR spectra and (b) HSQC spectrum of the aromatic C-H region of the PYPOSSH-XX copolymers in DMSO-d₆.[99] (Reprinted with permission from (99). Copyright (2024) American Chemical Society.)

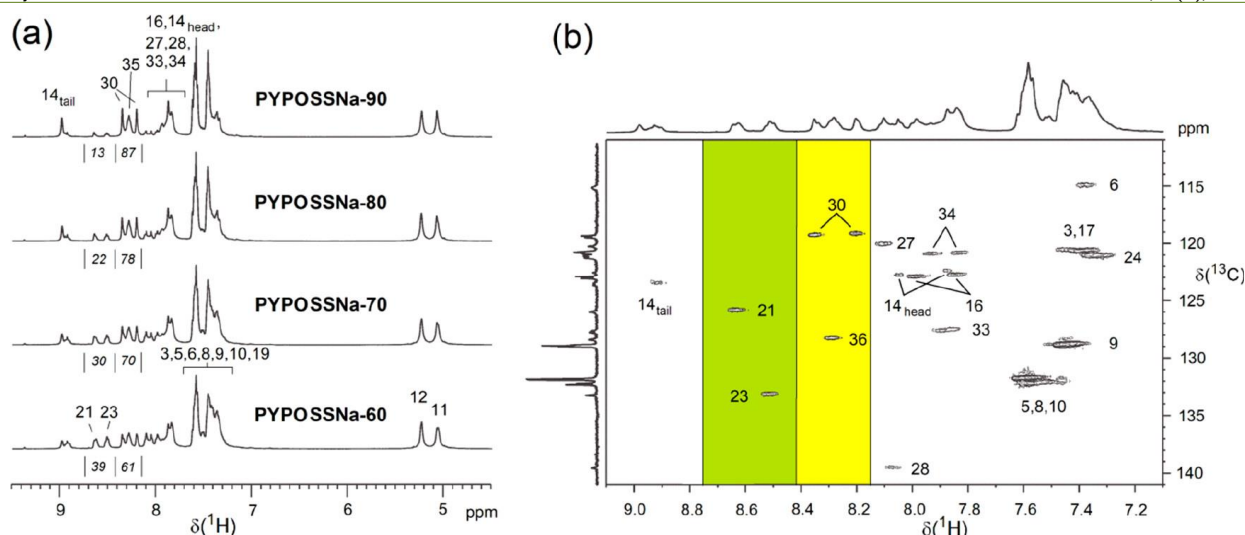MPa, YM: 0.59-2.37 GPa, EB: 13-21%), as illustrated in **Table 9**. The PYPYSH-XX membranes showed WU and through-plane SR values between 25-65% and 2.8-6.8% at 80 °C.[100] The AFM microstructural investigation reveals an interconnected and phase-segregated morphology, as depicted in **Figure 14**.[100] The PYPYSH-XX membranes exhibited excellent σ values (95-184 mS/cm) and superior oxidative stability (τ: 17-48 h) in Fenton's reagent at 80 °C, due to the presence of the H-bond propagating and radical scavenging pyridinyl units in both the hydrophobic and hydrophilic segments of the copolymer backbone (**Table 9**). In the H₂-O₂ single-cell experiment, the PYPYSH-100 MEA demonstrated the open circuit potential (OCP) and maximum PPD values of 0.75 V and 966 mW/cm² at 80 °C and 100% RH.[100]

Banerjee *et al.* designed and synthesized a series of pyridinyl- and P=O-moieties containing SPTs (PYPOSSH-XX) with sulfonic acid content values between 60 to 90% by the CuAAC reaction of the bisalkyyne monomer, 2,5-bis(prop-2′-ynyloxy)phenyl](diphenyl)phosphine oxide [POALK] with the semi-fluorinated bisazide monomer, 2,6-bis-[4′-(4″-azidophenoxy)-3′-(trifluoromethyl)phenyl]pyridine [PYFAZ] and sulfonated bisazide monomer, 4,4′-diazido-2,2′-stilbenesulfonic acid disodium salt [SSBAZ], as shown in **Scheme 36**.[99] The theoretical and NMR-based IEC values of the PYPOSSH-XX copolymers were obtained between 1.34-

2.17 and 1.37-2.10 meq/g.[99] The ¹H NMR spectra and HSQC correlation spectrum of the aromatic C-H of PYPOSSH-XX copolymers are provided in **Figure 15**. The PYPOSSH-60 to -90 copolymers showed high thermal and mechanical stabilities, as illustrated in **Table 9**. The maximum storage modulus values of the PYPOSSH-60 to -90 membranes ranged between 2027 and 7862 MPa.[99] The PYPOSSH-90 membrane exhibited the highest WU and SR values of 27.6% and 12.8% at 80 °C; this confirms the high dimensional stability of the PYPOSSH-XX copolymers.[99] Among the PYPOSSH-XX membranes, the PYPOSSH-90 membrane exhibited the highest σ value of 114 mS/cm at 80 °C in hydrated conditions (**Table 9**). The PYPOSSH-XX membranes demonstrated outstanding oxidative stability values (τ: ≥ 26 h and RW after 1 h: > 95%) in Fenton's reagent at 80 °C.[99] The extremely high oxidative stability of the PYPOSSH-XX membranes is due to the synergistic effect of pyridinyl and phosphine oxide moieties of the copolymer framework.[99]

Banerjee *et al.* fabricated a series of sulfonated Fe-MOF (Fe-S MOF)-containing SPT hybrid membranes (PTSF-FeS-X) for the PEMFC applications.[234] pristine PTSF-60 copolymer was synthesized by the CuAAC "click" polymerization reaction, as depicted in **Scheme 37**.[234] The Fe-S MOF was synthesized by the post-sulfonation process of the Fe-MIL-53-NH₂ MOF with 1,3-propane sultone, as shown in **Scheme 38**.[234] The microstructure of the FeS-MOF and PTSF-FeS-X composite
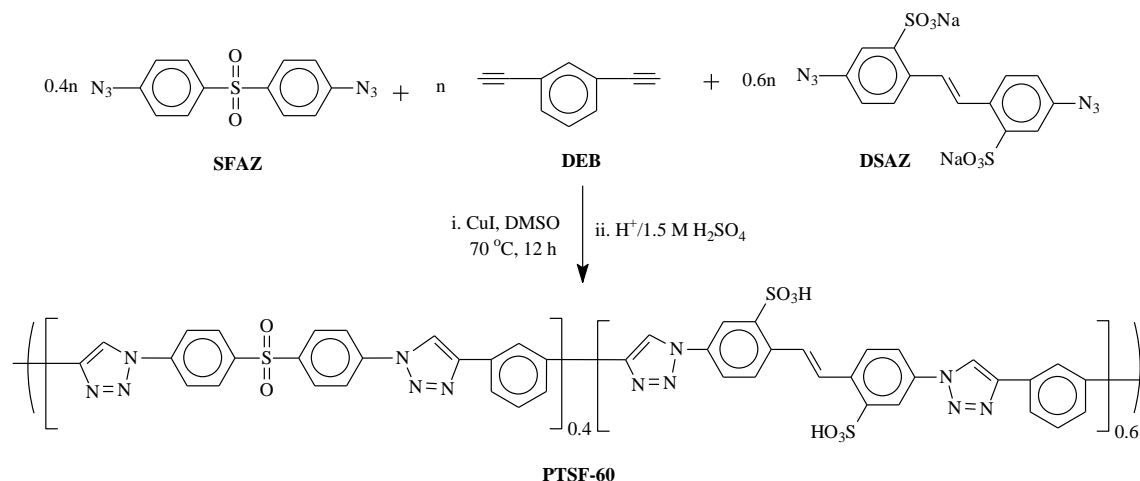
Scheme 37. The synthesis scheme of the pristine PTSF-60 copolymer.[234]

Banerjee and Ghanti

Innov. Chem. Mater. Sustain. **2025**, *2*(1), 032-073
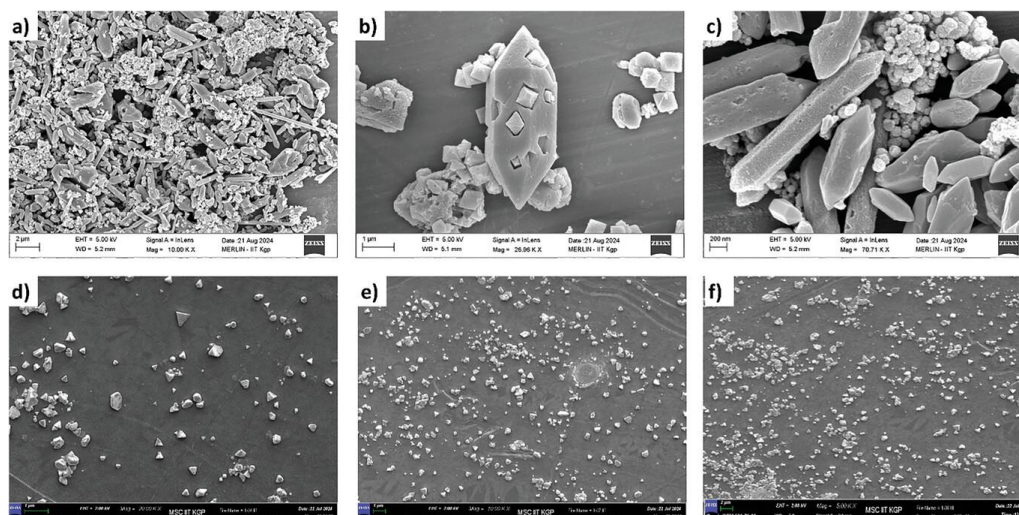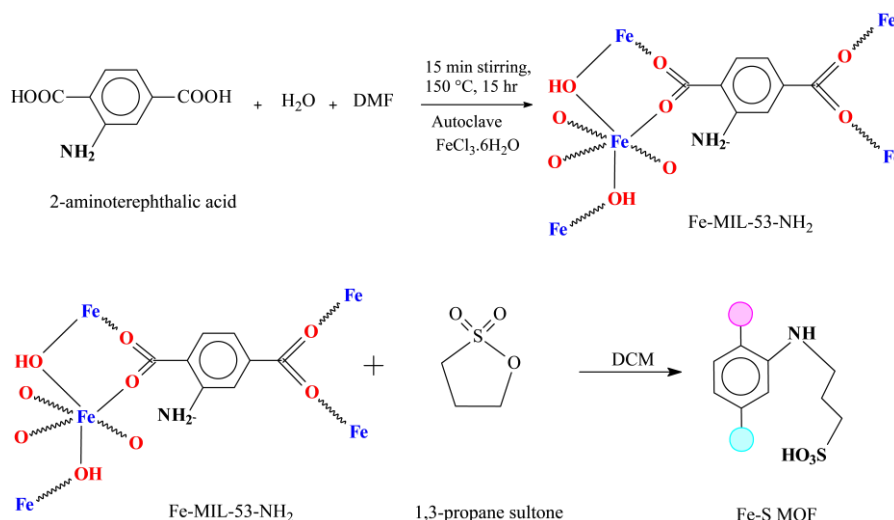

Figure 16. The FESEM surface images of (a-c) Fe-S MOF and (d-f) PTSF-FeS-3, -7, -9.[234] (Copyright 2025, Adopted with permission from (234) John Wiley & Sons, Inc.)

Scheme 38. The synthesis scheme of the sulfonated Fe-MOF (Fe-S MOF).[234]

membranes was investigated by the FESEM surface analysis, and the corresponding outcomes are depicted in **Figure 16**. The composite PTSF-FeS-X membranes demonstrated high thermal and mechanical stability values.[234] The WU values of the PTSF-FeS-X composite membranes were between 21-38% at 80 ℃, as compiled in **Table 9**. The PTSF-FeS-X composite membranes showed better oxidative stability (τ: 27-34 h) than the pristine SPT membrane in Fenton's reagent at 80 ℃, which is primarily due to the incorporation of the Fe-S MOF into the copolymer backbone.[234] Among all the composite membranes, the PTSF-FeS-7 membrane exhibited the highest σ value of 80 mS/cm at 80 ℃, as illustrated in **Table 9**. The proton conduction-related E_a values of the PTSF-FeS-X membranes were obtained between 9-13 kJ/mol.[234]

4.2.9 Others

Besides those mentioned above, sulfonated heteroaromatic polymeric backbones and a few other high-performing sulfonated heteroaromatic polymeric backbones have been employed for PEMFC applications. Those kinds of high-performing sulfonated heteroaromatic polymeric backbones are sulfonated polyoxadiazoles (SPODs), sulfonated polybenzoxazoles (SPBOs), sulfonated poly(phenylene oxide)s (SPPOs), sulfonated polybenzothiazoles (SPBTs), and sulfonated poly(oxindole

biphenylene)s (SPOBPs) etc.[235-239] These types of sulfonated heteroaromatic polymeric backbones also possess high thermal stability, mechanical properties, good solubility, high proton conductivity, and excellent oxidative stability. Still, there are a few studies that have been reported on those types of polymeric architecture.[235-239] Herein, the aforementioned types of sulfonated heteroaromatic PEMs are discussed below.

Abdolmaleki *et al*. synthesized two types of phenol-containing sulfonated polyoxadiazoles (SPPOD and SCDPPOD) by the one-spot high-temperature polycondensation reaction of dicarboxylic acid derivative and hydrazine sulfate in PPA medium, as depicted in **Scheme 39**.[235] The theoretical IEC values of the SPPOD and SCDPPOD were 3.0 and 2.4 meq/g, as illustrated in **Table 10**. The η_{inh} value of the SCDPPOD copolymer was 0.6 dL/g in DMSO, which confirms the formation of a high molecular weight copolymer (**Table 10**). The SCDPPOD copolymer showed high thermal stability ($T_{d5\%}$ value 320 ℃), as compiled in **Table 10**. The SCDPPOD membrane demonstrated a WU value of 38% in DI water at 25 ℃.[235] The SCDPPOD membrane showed the highest σ value of 65 mS/cm at 80 ℃ and 100% RH.[235] Thus, the phenol-containing sulfonated polyoxadiazoles exhibited good proton conductivity value, which is attributed to the presence of the various heteroatomic sites in the polymeric backbone and made them a potential candidate for PEMFC applications.[235]

Table 10. The IEC, η_{inh}, T_d, TS, YM, EB, WU, τ, and σ values of the SPODs, SPBOs, SPPOs, SPBTs, and SPOBPs.

Polymer	IEC_w (meq/g)[a]	η_{inh} (dL/g)[b]	T_d (°C)[c]	TS (MPa)	YM (GPa)	EB (%)	WU (%)[d]	τ (h)[e]	σ (mS/cm)[f]	Ref.
SPPOD	3.0	-	265	-	-	-	400	-	-	235
SCDPPOD	2.4	0.6	320	-	-	-	38	-	65	235
PTEBO	0	1.19	-	-	-	-	-	>200	-	236
SPTESBO-20	0.61	0.96	261[g]	-	-	-	~5	18.5	17[h]	236
SPTESBO-40	1.16	0.86	253[g]	-	-	-	~15	21.6	52[h]	236
SPTESBO-60	1.81	0.83	247[g]	-	-	-	~25	10	130[h]	236
PTEBO-HFB	0	1.89	-	-	-	-	-	>200	-	236
SPTESBO-HFB-20	0.65	1.46	263[g]	-	-	-	~7	30	24[h]	236
SPTESBO-HFB-40	1.36	1.47	257[g]	-	-	-	~12	25	78[h]	236
SPTESBO-HFB-60	1.56	1.67	248[g]	-	-	-	~30	18	130[h]	236
SNO40%-BPPO	0.93	-	-	35	-	24	16	-	38[h]	237
SNO65%-BPPO	1.42	-	-	26	-	20	22	-	~4h[i]	237
SNO80%-BPPO	1.55	-	-	21	-	13	25	-	~55[h]	237
SNO100%-BPPO	1.62	-	-	16	-	9	34	-	71[h]	237
sPBT-F70	2.32	-	361	-	-	-	30	6.0	110	238
sPBT-F72.5	2.38	-	350	-	-	-	32	5.6	-	238
sPBT-F75	2.45	-	340	-	-	-	37	5.2	-	238
sPBT-F77.5	2.51	-	317	-	-	-	41	4.8	~120	238
sPBT-F80	2.58	-	316	-	-	-	42	4.5	130	238
sPBT-F82.5	2.64	-	299	-	-	-	46	4.2	143	238
SPOBP100	2.75	-	-	54	1.11	13	366	5.5	203	239
SPOBP$_{50}$-FPOBP$_{50}$	1.50	-	-	82	1.87	24	33	>48	74	239
SPOBP$_{50}$-ClPOBP$_{50}$	1.47	-	-	84	2.12	15	-	>48	-	239
SPOBP$_{50}$-BrPOBP$_{50}$	1.38	-	-	82	1.93	12	-	>48	-	239
SPOBP$_{50}$-IPOBP$_{50}$	1.29	-	-	50	0.91	20	-	4.5	-	239
SPOBP$_{50}$-NO$_2$POBP$_{50}$	1.45	-	-	80	1.91	13	39	>48	76	239
SPOBP$_{50}$-CH$_3$OPOBP$_{50}$	2.64	-	-	47	0.66	22	-	5.0	-	239

[a] Theoretical IEC value, [b] inherent viscosity, [c] 5% decomposition temperature obtained from TGA analysis in N_2 flow, [d] WU values at 80 °C, [e] complete dissolution time in Fenton's reagent, [f] σ values at 80 °C and 100% RH, [g] decomposition temperature of the -SO_3H group obtained from TGA analysis, [h] σ values at room temperature under fully humidified condition.
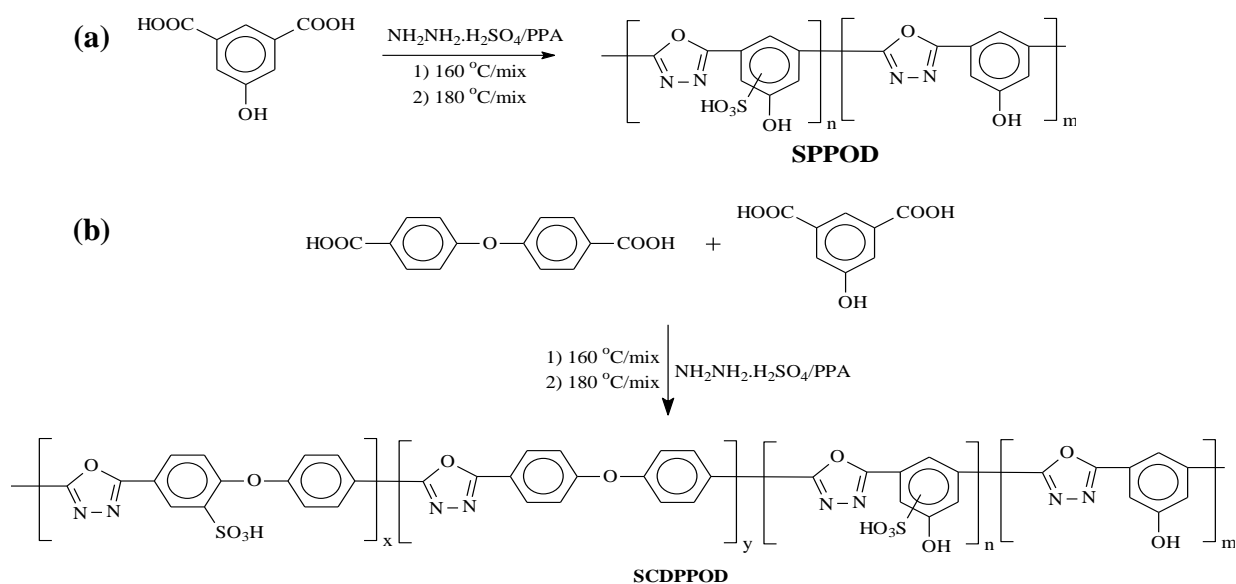
Scheme 39. The synthesis schemes of (a) SPPOD and (b) SCDPPOD copolymers.[235]

Liu *et al.* designed and synthesized a series of thioether-containing sulfonated polybenzoxazoles (SPTESBO-x) with various DS values, as depicted in **Scheme 42**.[236] Additionally, a series of end-capping thioether-containing sulfonated polybenzoxazoles (SPTESBO-HFB-x) were synthesized by the reaction of hexafluorobenzene (HFB) with PTESBO-x in DMAc at 80 °C to further enhance the oxidative stability of the sulfonated copolymers.[236] The theoretical IEC values of the SPTESBO-x and SPTESBO-HFB-x copolymers were obtained between 0.61-1.81 and 0.65-1.56 meq/g, respectively (**Table 10**). The end-capped SPTESBO-HFB-x copolymers showed higher η_{inh} values than the SPTESBO-x copolymers with the same DS values, which evidences the formation of high molecular weight copolymers during the end-capping polymerization reaction (**Table 10**). The end-capped

SPTESBO-HFB-x membranes demonstrated better τ values compared to the SPTESBO-x membranes in the accelerated Fenton test at 80 °C, which is associated with the elimination of the unstable end-groups for the end-capped SPTESBO-HFB-x copolymers.[236] The high DS value-containing sulfonated polybenzoxazole (SPTESBO-60 and SPTESBO-HFB-60) membranes exhibited an identical σ value of 0.13 S/cm at room temperature under fully humidified conditions, as compiled in **Table 10**. In the H_2-O_2 fuel cell test, the SPTESBO-HFB-60 MEA showed the maximum PPD value of 640 mW/cm^2 at 80 °C and 100% RH conditions.[236]

Xu *et al.* designed and synthesized a series of pendant naphthalene sulfonated poly(phenylene oxide)s (SPPOs; SNOx–BPPOs) via the etherification reaction of the bromomethylated PPO (BPPO) with Sodium 6-hydroxy-2-

Banerjee and Ghanti

Innov. Chem. Mater. Sustain. **2025**, *2*(1), 032-073

naphthalenesulfonate, as shown in **Scheme 41**.[237] The theoretical IEC values of the SNOx–BPPO copolymers were calculated between 0.93-1.62 mmol/g, as tabulated in **Table 10**. All the acidified SNOx–BPPO copolymers showed high thermal and mechanical (in the hydrated state, TS: 16-35 MPa and EB: 9-24%) stabilities, which is beneficial for PEMFC applications.[237] The SNOx–BPPO membranes demonstrated WU values between 15-28.2% and 16-34% at 25 and 80 ℃, respectively.[237] The SNOx–BPPO membranes exhibited lower water absorption properties due to incorporating the pendant naphthalene sulfonic acid group that restricts the excessive water intake.[237] The AFM morphological investigation revealed

that the hydrophilic ionic segments have become more significant in size and interconnected with the increase in the sulfonic acid contents of the SNOx–BPPO copolymers.[237] Among all the membranes, the SNO100%–BPPO membrane showed the highest σ value of 71 mS/cm at 25 ℃ and 100% RH conditions, as illustrated in **Table 10**.

Lee *et al.* synthesized a series of sulfonated polybenzothiazoles (sPBT-Fx) by the polycondensation reaction of 2,5-diamino-1,4-benzenedithiol dihydrochloride (DABDT) with the fluoro-sulfonated monomer 3,3′-disulfonate-2,2-bis(4-carboxyphenyl)hexafluoropropane (SCFA) and non-
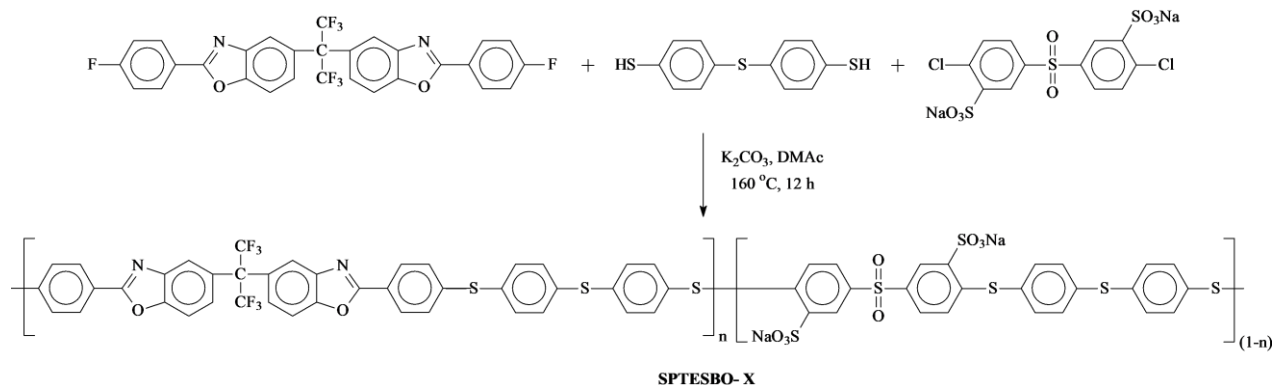
Scheme 40. The synthesis scheme of sulfonated poly(benzoxazole thioether sulfone)s (SPTESBO-x).[236]
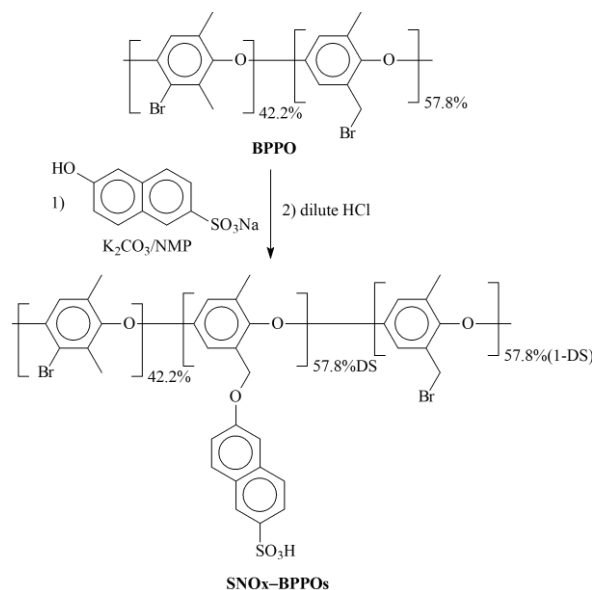
Scheme 41. The synthesis scheme of the pendant sulfonated poly(phenylene oxide) (SNOx–BPPOs) via the etherification reaction.[237]
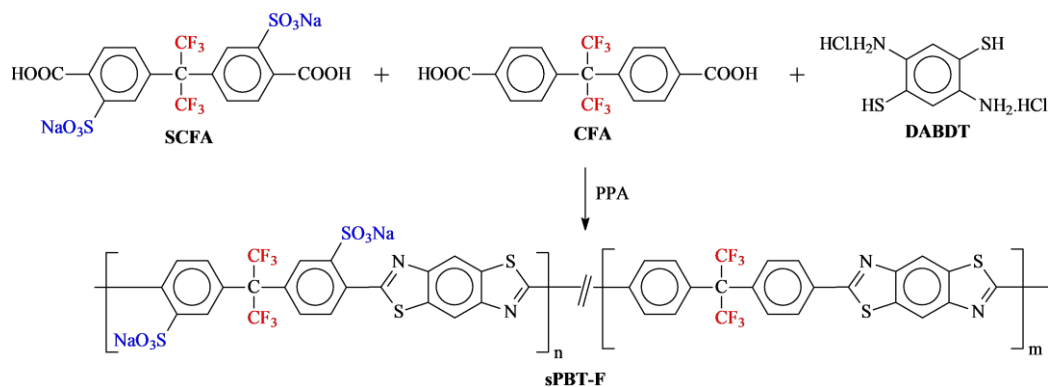
Scheme 42. The synthesis scheme of the semi-fluorinated sulfonated polybenzothiazoles (sPBT-F).[238]

Banerjee and Ghanti

Innov. Chem. Mater. Sustain. **2025,** 2(1), 032-073
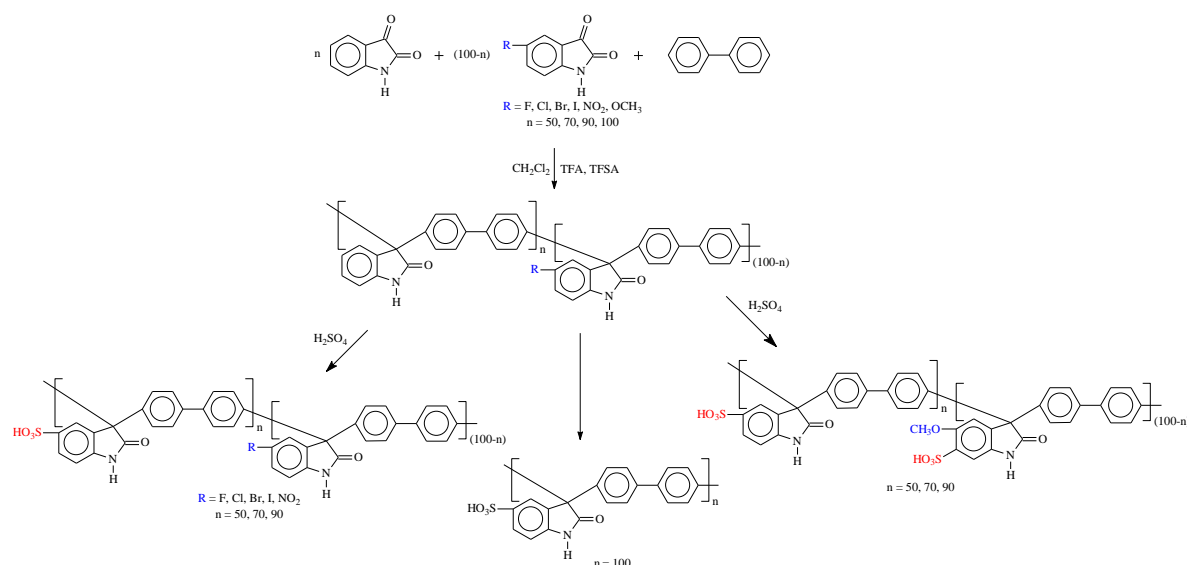
Scheme 43. The synthesis scheme of the sulfonated poly(oxindole biphenylene) copolymers [SPOBP$_n$-RPOBP$_{(100-n)}$, R = F, Cl, Br, I, NO$_2$, and OCH$_3$].[239]

sulfonated monomer 2,2-bis(4-carboxyphenyl)hexafluoropropane (CFA) in the presence of PPA, as depicted in **Scheme 42**.[238] The M$_w$ and PDI values of the sPBT-Fx copolymers were obtained between 327.9-337.5 kg/mol and 2.36-2.43.[238] The theoretical and titration-based experimental IEC values of the sPBT-Fx copolymers were found between 2.32-2.64 and 2.34-2.66 meq/g, respectively.[238] The sPBT-Fx copolymers showed excellent thermal stability (T$_{d5\%}$: 299-361 ℃ in TGA analysis under N$_2$ flow) and better oxidative stability (τ: 4.2-6.0 h) in Fenton's experiment at 80 ℃, as illustrated in **Table 10**. The sPBT-Fx membranes exhibited closer or better WU values (30-46%) than those of the Nafion (30%) at 80 ℃ (**Table 10**). Among all the sPBT-Fx membranes, the sPBT-F82.5 membrane showed the highest σ value of 143 mS/cm at 80 ℃ and 100% RH conditions, as compiled in **Table 10**. The proton conduction-related E$_a$ values of the sPBT-Fx membranes were obtained between 4.38-6.62 kJ/mol, which indicates the continuous and accelerated proton transportation in the sPBT-Fx membranes.[238]

Li *et al*. designed and synthesized a series of ether-free sulfonated poly(oxindole biphenylene) copolymers [SPOBP$_n$-RPOBP$_{(100-n)}$, R = F, Cl, Br, I, NO$_2$, and OCH$_3$] by the SACFC polyhydroxyalkylations reaction of isatin, various substituted isatin, and biphenyl, followed by the post-sulfonation method, as shown in **Scheme 43**.[239] The η$_{inh}$ values of the non-sulfonated copolymers [POBP$_n$-RPOBP$_{(100-n)}$] were obtained between 1.21-1.69 dL/g.[239] The theoretical IEC values of the [SPOBP$_{50}$-RPOBP$_{50}$, R = F, Cl, Br, I, NO$_2$, and OCH$_3$] copolymers were found between 1.29-2.64 meq/g, as tabulated in **Table 10**. Among all the substituted copolymers, the -F, -Cl, and -Br group-containing sulfonated copolymers showed improved thermal stability in the TGA analysis under N$_2$ flow.[239] The -F, -Cl, -Br, and -NO$_2$ group-containing sulfonated poly(oxindole biphenyl) [SPOBP$_{50}$-RPOBP$_{50}$] membranes showed higher mechanical characteristics in the dry state than the other substituted membranes, as compiled in **Table 10**. The SPOBP$_{50}$-RPOBP$_{50}$ (R = F, Cl, Br, and NO$_2$) membranes exhibited WU and SR values of 33-39% and 10-13% at 80 ℃.[239] The SPOBP$_{50}$-RPOBP$_{50}$ (R = F, Cl, Br, and NO$_2$) membranes demonstrated extremely higher oxidative stability compared to the SPOBP$_{50}$-RPOBP$_{50}$ (R = I and CH$_3$O) membranes in Fenton's experiment at 80 ℃, as compiled in **Table 10**. The SPOBP$_{50}$-RPOBP$_{50}$ (R = F, Cl, Br, and NO$_2$) membranes showed the σ value of 29-34 and 74-76 mS/cm at 20 and 80 ℃ in 100% RH conditions.[239] In the H$_2$/O$_2$ fuel cell test, the SPOBP$_{50}$-FPOBP$_{50}$ MEA demonstrated the maximum PPD value of 950 mW/cm^2 with an OCV value of 0.90 V at 80 ℃ and 100% RH conditions.[239]

5. Future Perspective

Despite the impressive design and development of alternative hydrocarbon-based PEM materials, there are still some challenges and endeavors in designing and developing new ionic polymer architectures for PEMFC applications:

- Despite the lower molecular weight and η$_{inh}$ values of the partially fluorinated sulfonated PEMs, they demonstrated higher thermal and dimensional (lower WU and SR values) stabilities than the analogous non-fluorinated sulfonated PEMs.[143] Thus, the design and synthesis of new partially fluorinated sulfonated PEMs may benefit PEMFC applications.

- The end-capped sulfonated copolymers showed superior oxidative or chemical stability and enhanced thermal stability compared to the non-end-capped sulfonated copolymers, along with identical proton conductivity values.[236] So, this approach might be fruitful for synthesizing alternative hydrocarbon-based sulfonated PEMs with improved oxidative stability.

- The filler-loaded (MOF, nano-particles, etc.) composite membranes exhibited improved thermal stability, oxidative stability, proton conductivity value, and single-cell performance.[171,204,234] However, there is a requirement for optimization of filler loading percentage in the composite membranes for future PEMFC applications, as some of the high filler-loaded hybrid membranes demonstrated low PEMFC performances.

- Usually, the cross-linkers often compromise the proton conductivity values of the PEMs by enhancing the dimensional and oxidative stabilities.[157] However, few multiterm covalently cross-linked PEMs showed enhanced proton conductivity values with higher mechanical, dimensional, and oxidative stability values.[157,189] Hence, the appropriate multiterm cross-linked PEMs design may benefit the PEMFC applications.

- The blend PEMs showed remarkably higher thermal stability, mechanical properties, oxidative stabilities, and proton conductivity values than the pristine PEMs.[79,119,172] Therefore, the designing and synthesis of blend sulfonated PEMs are also beneficial for future PEMFC applications.

- The hydrocarbon-based N-heterocyclic sulfonated polazoles, such as sulfonated polybenzimidazoles, sulfonated polytriazoles, sulfonated polybenzoxazoles, sulfonated polybenzothiazoles, sulfonated polyoxadiazoles, etc., have appeared as a promising candidate for PEMFC applications.[99,102,173-175,231,238] Among these sulfonated polyazoles, only sulfonated polybenzimidazoles and

Banerjee and Ghanti

Innov. Chem. Mater. Sustain. **2025**, *2*(1), 032-073

sulfonated polytriazoles have been well-studied for PEMFC applications. Thus, the other sulfonated polyazole types must be explored more for PEMFC applications in the future.

- The phosphonic acid-based PEMs are relatively less evaluated than the sulfonic acid-based PEMs for PEMFC applications due to the lower proton conductivity value of the phosphonic acid-based PEMs.[105-107] Recently, a few phosphonated sulfonated PEMs have been investigated for PEMFC applications, and those PEMs exhibited higher proton conductivity values.[240-242] Hence, the designing and synthesis of these types of phosphonated sulfonated PEMs should have been a beneficial route for future PEMFC applications.

- Some of the alternative sulfonated PEMs demonstrated better fuel cell performances than the commercially available PFSA-based PEMs.[156,204,219,221] However, they have faced substantial challenges in their commercial market growth due to their primary challenges in large-scale production, long-term chemical durability, and economic restrictions. Therefore, continuous rational design and innovation of extended chemical durability, efficient power density, and more economical and environmentally friendly alternative sulfonated PEMs will be substantial for replacing PFSA-based PEMs.

6. Conclusion

FC technologies are on the verge of creating a massive evolution in the energy and automobile sectors for their sustainable energy generation capabilities. This review article provides a brief history of the FC and the various advantages, disadvantages, and limitations of FC technologies. The classifications of FCs based on the electrolyte types are summarized in this article, along with their limitations and particular applications. The working principle and essential components of a PEMFC are also described. The PEM of the PEMFCs is a solid polymer electrolyte membrane that allows the passage of protons but not electrons. Various factors that influence the performance of the PEM in PEMFC are also summarized. The PFSA-based membranes have been the most employed PEM materials in the PEMFC application due to their excellent proton conductivity and superior chemical stability. However, PFSA-based PEM materials are expensive, and their PEM characteristics are deuterated at higher temperatures and low RH levels. This review article beheld a variety of novel hydrocarbon-based sulfonated PEMs (such as SPAs, SPAEs, SPATEs, SPBIs, SPIs, SPTs, SPPAs, SPODs, SPBOs, SPBOs, SPPOs, SPBTs, and SPOBPs) that might be utilized as an alternative to the PFSA-based membranes in PEMFC applications. The synthetic methodologies, various PEM properties (thermal stability, mechanical properties, WU, proton conductivity, and oxidative stability values), H_2-O_2 fuel cell performance, and benefits of those novel hydrocarbon-based alternative PEMs are summarized.

Author Contribution Declaration

Bholanath Ghanti: Conceptualization, Data curation, Writing – original draft. **Susanta Banerjee:** Supervision, Conceptualization, Review and Editing of the manuscript, Funding acquisition.

Data Availability Declaration

There are no new data were created, hence data sharing is not applicable.

Declaration of Conflicts of Interest

The authors declare no competing financial interest.

References

1. A. E. Léodé, F. H. Agnimonhan, G. K. n'Gobi, B. Glinma, C. A. Kouchadé, B. Kounouhéwa. Review on the Proton Exchange Membrane Fuel Cell (PEMFC) in Benin Republic (West Africa). *Res. J. Physical Sci.*, **2024**, *12*, 1. ISSN.;2320:4796.
2. A. Ajanovic, R. Haas. Prospects and impediments for hydrogen and fuel cell vehicles in the transport sector. *Int. J. Hydrogen Energy*, **2021**, *46*, 10049. https://doi.org/10.1016/j.ijhydene.2020.03.122
3. A. B. Ali, A. K. Nemah, Y. A. Al Bahadli. Principles and performance and types, advantages and disadvantages of fuel cells: A review. Case Stud. Chem. Environ. Eng., **2024**, *10*, 100920. https://doi.org/10.1016/j.cscee.2024.100920
4. B. P. Statistical Review of World Energy, 69th ed.; BP p.l.c.: London, UK, 2020; Available online: https://www.bp.com/en/global/corporate/energy-economics/statistical-review-of-world-energy.html (accessed on 30 August **2021**)
5. B. Su, Y. Wang, Z. Xu, W. Han, H. Jin, H. Wang. Novel ways for hydrogen production based on methane steam and dry reforming integrated with carbon capture. *Energy Convers. Manag.*, **2022**, *270*, 116199. https://doi.org/10.1016/j.enconman.2022.116199
6. Y. Yang, X. Yu, W. Zhu, C. Xie, B. Zhao, L. Zhang, Y. Shi, L. Huang, R. Zhang. Degradation prediction of proton exchange membrane fuel cells with model uncertainty quantification, *Renew. Energy*, **2023**, *219*, 119525. https://doi.org/10.1016/j.renene.2023.119525
7. Z. Xu, W. Xu, E. Stephens, B. Koeppel. Mechanical reliability and life prediction of coated metallic interconnects within solid oxide fuel cells. Renew. Energy, **2017**, 113, 1472. https://doi.org/10.1016/j.renene.2017.06.103
8. Y. Zhou, R. Li, Z. Lv, J. Liu, H. Zhou, C. Xu. Green hydrogen: A promising way to the carbon-free society. *Chin. J. Chem. Eng.*, **2022**, 43, 2. https://doi.org/10.1016/j.cjche.2022.02.001
9. S. S. Kumar, H. Lim. An overview of water electrolysis technologies for green hydrogen production. *Energy Rep.*, **2022**, *8*, 13793. https://doi.org/10.1016/j.egyr.2022.10.127
10. S. Li, M. Tabatabaei, F. Li, S.-H. Ho. A review of green biohydrogen production using anoxygenic photosynthetic bacteria for hydrogen economy: Challenges and opportunities. *Int. J. Hydrogen Energy*, **2024**, *54*, 218. https://doi.org/10.1016/j.ijhydene.2022.11.014
11. L. A. Omeiza, A. M. Abdalla, B. Wei, A. Dhanasekaran, Y. Subramanian, S. Afroze, M. S. Reza, S. A. Bakar, A. K. Azad. Nanostructured Electrocatalysts for Advanced Applications in Fuel Cells. *Energies* (Basel), **2023**, *16*, 1876. https://doi.org/10.3390/en16041876
12. M. C. Heller, G. A. Keoleian. Greenhouse Gas Emission Estimates of U.S. Dietary Choices and Food Loss. *J. Ind. Ecol.*, **2015**, *19*, 391. https://doi.org/10.1111/jiec.12174
13. S. Li, X. Li, S.-H. Ho. How to enhance carbon capture by evolution of microalgal photosynthesis? *Sep. Purif. Technol.*, **2022**, *291*, 120951. https://doi.org/10.1016/j.seppur.2022.120951
14. R. V. Vardhan, R. Mahalakshmi, R. Anand, A. Mohanty. A Review on Green Hydrogen: Future of Green Hydrogen in India, in: 2022 6th International Conference on Devices, Circuits and Systems (ICDCS), IEEE, **2022**, 303. https://doi.org/10.1109/ICDCS54290.2022.9780805
15. A. Bajoria, J. Kanpariya, A. Bera. Greenhouse gases and global warming. In Advances and Technology Development in Greenhouse Gases: Emission, Capture and Conversion, Elsevier, **2024**, 121. https://doi.org/10.1016/B978-0-443-19066-7.00006-0
16. M. Zavala-Méndez, A. Vargas, J. Carrillo-Reyes. Maximization of bio-hydrogen production from winery vinasses using on-line feedback control. *Int. J. Hydrogen Energy*, **2022**, *47*, 33259. https://doi.org/10.1016/j.ijhydene.2022.07.196
17. P. P. Edwards, V. L. Kuznetsov, W. I. F. David, N. P. Brandon. Hydrogen and fuel cells: Towards a sustainable energy future. *Energy Policy*, **2008**, *36*, 4356. https://doi.org/10.1016/j.enpol.2008.09.036
18. S. J. C. Cleghorn, D. K. Mayfield, D. A. Moore, J. C. Moore, G. Rusch, T. W. Sherman, N. T. Sisofo, U. Beuscher. A polymer electrolyte fuel cell life test: 3 years of continuous operation. *J. Power Sources*, **2006**, *158*, 446. https://doi.org/10.1016/j.jpowsour.2005.09.062
19. T. K. Maiti, J. Singh, P. Dixit, J. Majhi, S. Bhushan, A. Bandyopadhyay, S. Chattopadhyay. Advances in perfluorosulfonic acid-based proton exchange membranes for fuel cell applications: A review. *Chem. Eng. J. Adv.*, **2022**, *12*, 100372. https://doi.org/10.1016/j.ceja.2022.100372
20. J. You, L. Dou, K. Yoshimura, T. Kato, K. Ohya, T. Moriarty, K. Emery, C. C. Chen, J. Gao, G. Li, Y. Yang. A polymer tandem solar cell with 10.6% power conversion efficiency. *Nat. Commun.*, **2013**, *4*, 1446. https://doi.org/10.1038/ncomms2411

Banerjee and Ghanti

Innov. Chem. Mater. Sustain. **2025**, *2*(1), 032-073

21.   J. R. Kim, S. W. Choi, S. M. Jo, W.S. Lee, B. C. Kim. Electrospun PVdF-based fibrous polymer electrolytes for lithium-ion polymer batteries. *Electrochim. Acta.*, **2004**, *50*, 69. https://doi.org/10.1016/j.electacta.2004.07.014

22.   J. Xi, Z. Wu, X. Qiu, L. Chen. Nafion/SiO₂ hybrid membrane for vanadium redox flow battery. *J. Power Sources*, **2007**, *166*, 531. https://doi.org/10.1016/j.jpowsour.2007.01.069

23.   N. S. Rathore, N. L. Panwar. Renewable energy sources for sustainable development. New Delhi, India: New India Publishing Agency, **1996**.

24.   A. Hussain, S. M. Arif, M. Aslam. Emerging renewable and sustainable energy technologies: State of the art. Renew. Sustain. Energy Rev., **2017**, *71*, 12. https://doi.org/10.1016/j.rser.2016.12.033

25.   N. L. Panwara, S. C. Kaushik, K. Surendra. Role of renewable energy sources in environmental protection: a review. *Renew. Sustain. Energy Rev.*, **2011**, *15*, 1513. https://doi.org/10.1016/j.rser.2010.11.037

26.   N. H. Ravindranath, D. O. Hall. Biomass, energy, and environment: a developing country perspective from India. Oxford, United Kingdom, Oxford University Press, **1995**. https://doi.org/10.1093/oso/9780198564362.001.0001

27.   H. Zhang, P. K. Shen. Advances in the high performance polymer electrolyte membranes for fuel cells. *Chem. Soc. Rev.*, **2012**, *41*, 2382. https://doi.org/10.1039/c2cs15269j

28.   O. M. Babatunde, B. D. Akintayo, M. U. Emezirinwune, O. A. Olanrewaju. Environmental impact assessment of a 1 kW proton-exchange membrane fuel cell: a mid-point and end-point analysis. *Hydrogen*, **2024**, *5*, 352. https://doi.org/10.3390/hydrogen5020020

29.   O. Sel, A. Soules, B. Améduri, B. Boutevin, C. Laberty-Robert, G. Gebel, C. Sanchez. Original fuel-cell membranes from crosslinked terpolymers via a "sol–gel" strategy. *Adv. Funct. Mater.*, **2010**, *20*, 1090. https://doi.org/10.1002/adfm.200902210

30.   K. Jiao, J. Xuan, Q. Du, Z. Bao, B. Xie, B. Wang, Y. Zhao, L. Fan, H. Wang, Z. Hou, S. Huo, N.P. Brandon, Y. Yin, M. D. Guiver. Designing the next Generation of Proton-Exchange Membrane Fuel Cells. *Nature*, **2021**, *595*, 361. https://doi.org/10.1038/s41586-021-03482-7

31.   W. Li, W. Liu, W. Jia, J. Zhang, Q. Zhang, Z. Zhang, J. Zhang, Y. Li, Y. Liu, H. Wang, Y. Xiang, S. Lu. Dual-Proton Conductor for Fuel Cells with Flexible Operational Temperature. *Adv. Mater.*, **2024**, *36*, 2310584. https://doi.org/10.1002/adma.202310584

32.   U. Lucia. Overview on fuel cells. *Renew. Sustain. Energy Rev.*, **2014**, *30*, 164. https://doi.org/10.1016/j.rser.2013.09.025

33.   W. Vielstich, H. Gasteiger, A. Lamm. Handbook of Fuel cells—fundamentals, technology, applications. New York, Wiley, ISBN: 978-0-471-49926-8, **2003**, 2720.

34.   H. Davy. The collected works of Sir Humphry Davy...: Discourses delivered before the Royal society. Elements of agricultural chemistry, pt. I. Smith, Elder and Company, **1840**.

35.   R. Meldola, S. C. Friedrich. Ein Blatt zur Geschichte des 19 Jahrhunderts. *Nature*, **1900**, *62*, 97. https://doi.org/10.1038/062097a0

36.   W. R. Grove. On a new voltaic combination. London and Edinburgh Philosophical Magazine, **1838**, *13*, 430.

37.   W. R. Grove. On a new voltaic combination of gasses by platinum. London and Edinburgh Philosophical Magazine, **1839**, *14*, 127. https://doi.org/10.1080/14786443908649684

38.   J. M. Andújar, F. Segura. Fuel cells: history and updating. A walk along two centuries. *Renew. Sustain. Energy Rev.*, **2009**, *13*, 2309. https://doi.org/10.1016/j.rser.2009.03.015

39.   P. Grimes. Historical pathways for fuel cells. The new electric century. *Proc. Annu. Batter. Conf. Appl. Adv.*, **2000**, 41. https://doi.org/10.1109/BCAA.2000.838369

40.   C. Spiegel. Designing and Building Fuel Cells, McGraw-Hill, New York, **2007**.

41.   M. L. Perry, T. F. Fuller. A Historical Perspective of Fuel Cell Technology in the 20th Century. *J. Electrochem. Soc.*, **2002**, *149*, S59. https://doi.org/10.1149/1.1488651

42.   S. Shamim, K. Sudhakar, B. Choudhary, J. Anwar. A review on recent advances in proton exchange membrane fuel cells: materials, technology and applications. *Adv. Appl. Sci. Res.*, **2015**, *6*, 89, ISSN: 0976-8610.

43.   B. C. H. Steele. Material science and engineering: The enabling technology for the commercialisation of fuel cell systems. *J. Mater. Sci.*, **2001**, *36*, 1053. https://doi.org/10.1023/A:1004853019349

44.   L. Mond, C. Langer. A new form of gas battery, communicated by Lord R.S. Rayleigihs. Proceedings of the Royal Society of London XLVI, **1889**, 296–304.

45.   A. Kirubakaran, S. Jain, R. K. Nema. A review on fuel cell technologies and power electronic interface. *Renew. Sustain. Energy Rev.*, **2009**, *13*, 2430. https://doi.org/10.1016/j.rser.2009.04.004

46.   H. Morikawa, H. Kikuchi, N. Saito. Development and advances of a V-flow FC tack for FCX clarity. SAE Tech. Pap., **2009**, *2*, 955. https://doi.org/10.4271/2009-01-1010

47.   N. A. Qasem, G. A. Abdulrahman. A recent comprehensive review of fuel cells: history, types, and applications. *Int. J. Energy Res.*, **2024**, *2024*, 7271748. https://doi.org/10.1155/2024/7271748

48.   J. M. Andújar, F. Segura. Fuel cells: history and updating. A walk along two centuries. *Renew. Sustain. Energy Rev.*, **2009**, *13*, 2309. https://doi.org/10.1016/j.rser.2009.03.015

49.   L. Carrette, K. A. Friedrich, U. Stimming. Fuel cells: principles, types, fuels, and applications. *ChemPhysChem*, **2000**, *1*, 162. https://doi.org/10.1002/1439-7641(20001215)1:4<162::AIDCPHC162>3.0.CO;2-Z

50.   R. E. Rosli, A. B. Sulong, W. R. W. Daud, M. A. Zulkifley, T. Husaini, M. I. Rosli, E. H. Majlan, M. A. Haque. A Review of High-Temperature Proton Exchange Membrane Fuel Cell (HTPEMFC) System. *Int. J. Hydrogen Energy*, **2017**, *42*, 9293. https://doi.org/10.1016/j.ijhydene.2016.06.211

51.   S. Mekhilef, R. Saidur, A. Safari. Comparative study of different fuel cell technologies. *Renew. Sustain. Energy Rev.*, **2012**, *16*, 981. https://doi.org/10.1016/j.rser.2011.09.020

52.   R. Rath, P. Kumar, S. Mohanty, S. K. Nayak. Recent advances, unsolved deficiencies, and future perspectives of hydrogen fuel cells in transportation and portable sectors. *Int. J. Energy Res.*, **2019**, *43*, 8931. https://doi.org/10.1002/er.4795

53.   A. Javed, P. P. Gonzalez, V. Thangadurai. A critical review of electrolytes for advanced low-and high-temperature polymer electrolyte membrane fuel cells. *ACS Appl. Mater. Interfaces*, **2023**, *15*, 29674. https://doi.org/10.1021/acsami.3c02635

54.   S. Bose, T. Kuila, T. X. Nguyen, N. H. Kim, K. T. Lau, J. H. Lee. Polymer membranes for high temperature proton exchange membrane fuel cell: Recent advances and challenges. *Prog. Polym. Sci.*, **2011**, *36*, 813. https://doi.org/10.1016/j.progpolymsci.2011.01.003

55.   J. Wang, B. Wang, C. Tongsh, T. Miao, P. Cheng, Z. Wang, Q. Du, K. Jiao. Combining proton and anion exchange membrane fuel cells for enhancing the overall performance and self-humidification. *Chem. Eng. J.*, **2022**, *428*, 131969. https://doi.org/10.1016/j.cej.2021.131969

56.   J. H. Wee. Applications of proton exchange membrane fuel cell systems. *Renew. Sustain. Energy Rev.*, **2007**, *11*, 1720. https://doi.org/10.1016/j.rser.2006.01.005

57.   L. Zhang, S. R. Chae, Z. Hendren, J. S. Park, M. R. Wiesner. Recent advances in proton exchange membranes for fuel cell applications. *Chem. Eng. J.*, **2012**, *204*, 87. https://doi.org/10.1016/j.cej.2012.07.103

58.   Z. Shang, R. Wycisk, P. Pintauro. Electrospun composite proton-exchange and anion-exchange membranes for fuel cells. *Energies*, **2021**, *14*, 6709. https://doi.org/10.3390/en14206709

59.   A. K. Mohanty, E. A. Mistri, A. Ghosh, S. Banerjee. Synthesis and characterization of novel fluorinated poly (arylene ether sulfone)s containing pendant sulfonic acid groups for proton exchange membrane materials. *J. Membr. Sci.*, **2012**, *409*, 145. https://doi.org/10.1016/j.memsci.2012.03.048

60.   E. A. Mistri, A. K. Mohanty, S. Banerjee. Synthesis and characterization of new fluorinated poly(ether imide) copolymers with controlled degree of sulfonation for proton exchange membranes. *J. Membr. Sci.*, **2012**, *411*, 117. https://doi.org/10.1016/j.memsci.2012.04.023

61.   A. Singh, R. Mukherjee, S. Banerjee, H. Komber, B. Voit. Sulfonated polytriazoles from a new fluorinated diazide monomer and investigation of their proton exchange properties. *J. Membr. Sci.*, **2014**, *469*, 225. https://doi.org/10.1016/j.memsci.2014.06.043

62.   D. R. Dekel. Review of Cell Performance in Anion Exchange Membrane Fuel Cells. *J. Power Sources*, **2018**, *375*, 158. https://doi.org/10.1016/j.jpowsour.2017.07.117

63.   M. M. Hossain, Z. Yang, L. Wu, X. Liang, T. Xu. Introducing a New Generation of Anion Conducting Membrane Using Swelling Induced Fabrication of Covalent Methanol Barrier Layer. *J. Membr. Sci.*, **2021**, *620*, 118840. https://doi.org/10.1016/j.memsci.2020.118840

64.   Y. Zha, M. L. Disabb-Miller, Z. D. Johnson, M. A. Hickner, G. N. Tew. Metal-Cation-Based Anion Exchange Membranes. *J. Am. Chem. Soc.*, **2012**, *134*, 4493. https://doi.org/10.1021/ja211365r

65.   R. Mukherjee, S. Banerjee, H. Komber, B. Voit. Carboxylic acid functionalized fluorinated sulfonated poly (arylene ether sulfone) copolymers with enhanced oxidative stability. *J. Membr. Sci.*, **2016**, *510*, 497. https://doi.org/10.1016/j.memsci.2016.03.028

66.   Y. Xue, L. Shi, X. Liu, J. Fang, X. Wang, B. P. Setzler, W. Zhu, Y. Yan, Z. Zhuang. A highly active, stable, and low-cost platinum-free anode catalyst based on RuNi for hydroxide exchange membrane fuel cells. *Nat. Commun.*, **2020**, *11*, 5651. https://doi.org/10.1038/s41467-020-19413-5

67.   D. Henkensmeier, M. Najibah, C. Harms, J. Žitka, J. Hnát, K. Bouzek. Overview: State-of-the-Art Commercial Membranes for Anion Exchange Membrane Water Electrolysis. *J. Electrochem. Energy Convers. Storage*, **2020**, *18*, 024001. https://doi.org/10.1115/1.4047963

68.   J. R. Varcoe, P. Atanassov, D. R. Dekel, A. M. Herring, M. A. Hickner, P. A. Kohl, A. R. Kucernak, W. E. Mustain, K. Nijmeijer, K. Scott, T. Xu. Anion-Exchange Membranes in Electrochemical Energy Systems. *Energy Environ. Sci.*, **2014**, *7*, 3135. https://doi.org/10.1039/C4EE01303D

69.   Amel, A.; Smedley, S.B.; Dekel, D.R.; Hickner, M.A.; Ein-Eli, Y. Characterization and Chemical Stability of Anion Exchange Membranes Cross-Linked with Polar Electron-Donating Linkers. *J. Electrochem. Soc.*, **2015**, *162*, F1047. https://doi.org/10.1149/2.0891509jes

70.   D. R. Dekel, M. Amar, S. Willdorf, M. Kosa, S. Dhara, C. E. Diesendruck. Effect of Water on the Stability of Quaternary Ammonium Groups for Anion Exchange Membrane Fuel Cell Applications. *Chem. Mater.*, **2017**, *29*, 4425. https://doi.org/10.1021/acs.chemmater.7b00958

71.   Z. Tao, C. Wang, X. Zhao, J. Li, M. D. Guiver. Progress in high-performance anion exchange membranes based on the design of stable cations for alkaline fuel cells. *Adv. Mater. Technol.*, **2021**, *6*, 2001220. https://doi.org/10.1002/admt.202001220

Banerjee and Ghanti

Innov. Chem. Mater. Sustain. **2025**, *2*(1), 032-073

72. G. Couture, A. Alaaeddine, F. Boschet, B. Ameduri. Polymeric materials as anion-exchange membranes for alkaline fuel cells. *Prog. Polym. Sci.*, **2011**, *36*, 1521. https://doi.org/10.1016/j.progpolymsci.2011.04.004

73. W. E. Mustain, M. Chatenet, M. Page, Y. S. Kim. Durability challenges of anion exchange membrane fuel cells. *Energy Environ. Sci.*, **2020**, *13*, 2805. https://doi.org/10.1039/D0EE01133A

74. Y. Prykhodko, K. Fatyeyeva, L. Hespel, S. Marais. Nafion®-based membranes for proton exchange fuel cell application. *Chem. Eng. J.*, **2021**, *409*, 127329. https://doi.org/10.1016/j.cej.2020.127329

75. M. J. Workman, A. Serov, L. Tsui, P. Atanassov, K. Artyushkova. Fe–N–C Catalyst Graphitic Layer Structure and Fuel Cell Performance. *ACS Energy Lett.*, **2017**, *2*, 1489. https://doi.org/10.1021/acsenergylett.7b00391

76. J. Wang, Y. Zhao, B. P. Setzler, S. Rojas-Carbonell, C. B. Yehuda, A. Amel, M. Page, L. Wang, K. Hu, L. Shi, S. Gottesfeld, B. Xu, Y. Yan. Poly(aryl piperidinium) membranes and ionomers for hydroxide exchange membrane fuel cells. *Nat. Energy*, **2019**, *4*, 392. https://doi.org/10.1038/s41560-019-0372-8

77. X. Wu, S. Xing, J. Luo, H. Wang, F. Huang, C. Zhao. Progress and Challenges on Air-cooled Open-cathode Proton Exchange Membrane Fuel Cells: Materials, Structures, and Systems. *Energy Rev.*, **2025**, *4*, 100130. https://doi.org/10.1016/j.enrev.2025.100130

78. A. Singh, S. Banerjee, H. Komber, B. Voit. Synthesis and characterization of highly fluorinated sulfonated polytriazoles for proton exchange membrane application. *RSC advances*, **2016**, *6*, 13478. https://doi.org/10.1039/C5RA26821D

79. B. Campagne, G. David, B. Améduri, D. J. Jones, J. Rozière, I. Roche. Novel blend membranes of partially fluorinated copolymers bearing azole functions with sulfonated PEEK for PEMFC operating at low relative humidity: influence of the nature of the N-heterocycle. *Macromolecules*, **2013**, *46*, 3046. https://doi.org/10.1021/ma400239f

80. B. Ghanti, R. Kamble, S. Roy, S. Banerjee. Synthesis and characterization of sulfonated polytriazoles utilizing 1, 4-bis (4-azido-2-(trifluoromethyl) phenoxy) benzene for the proton exchange membrane applications. *J. Polym. Sci.*, **2023**, *61*, 1792. https://doi.org/10.1002/pol.20220769

81. H. Pourrahmani, C. M. Bernier, J. Van Herle. The application of fuel-cell and battery technologies in unmanned aerial vehicles (UAVs): a dynamic study. *Batteries*, **2022**, *8*, 73. https://doi.org/10.3390/batteries8070073

82. Y. Liu, H. Ma, Y. Tong, A. Uma, Y. Luo, S. Zhao. Progress of Polyhedral Oligomeric Silsesquioxanes in Proton Exchange Membrane Fuel Cells: A Review. *Process. Saf. Environ. Prot.*, **2024**, *187*, 1322. https://doi.org/10.1016/j.psep.2024.05.057

83. X. Z. Yuan, C. Nayoze-Coynel, N. Shaigan, D. Fisher, N. Zhao, N. Zamel, P. Gazdzicki, M. Ulsh, K. A. Friedrich, F. Girard, U. Groos. A review of functions, attributes, properties and measurements for the quality control of proton exchange membrane fuel cell components. *J. Power Sources*, **2021**, *491*, 229540. https://doi.org/10.1016/j.jpowsour.2021.229540

84. Y. Wang, D. F. Ruiz Diaz, K. S. Chen, Z. Wang, X. C. Adroher. Materials, Technological Status, and Fundamentals of PEM Fuel Cells – A Review. *Mater. Today*, **2020**, *32*, 178. https://doi.org/10.1016/j.mattod.2019.06.005

85. Y. Sun, S. Polani, F. Luo, S. Ott, P. Strasser, F. Dionigi. Advancements in cathode catalyst and cathode layer design for proton exchange membrane fuel cells. *Nat. Commun.*, **2021**, *12*, 5984. https://doi.org/10.1038/s41467-021-25911-x

86. D. Wu, C. Peng, C. Yin, H. Tang. Review of system integration and control of proton exchange membrane fuel cells. *Electrochem. Energy Rev.*, **2020**, *3*, 466. https://doi.org/10.1007/s41918-020-00068-1

87. B. Smitha, S. Sridhar, A. A. Khan. Solid polymer electrolyte membranes for fuel cell applications—a review. *J. Membr. Sci.*, **2005**, *259*, 10. https://doi.org/10.1016/j.memsci.2005.01.035

88. A. G. Kumar, A. Singh, H. Komber, B. Voit, B. R. Tiwari, M. T. Noori, M. M. Ghangrekar, S. Banerjee. Novel sulfonated Co-poly(ether imide)s containing trifluoromethyl, fluorenyl and hydroxyl groups for enhanced proton exchange membrane properties: Application in microbial fuel cell. *ACS Appl. Mater. Interfaces*, **2018**, *10*, 14803. https://doi.org/10.1021/acsami.8b03452

89. A. Ghorai, S. Banerjee. Phosphorus-containing aromatic polymers: Synthesis, structure, properties and membrane-based applications. *Prog. Polym. Sci.*, **2023**, *138*, 101646. https://doi.org/10.1016/j.progpolymsci.2023.101646

90. E. Qu, X. Hao, M. Xiao, D. Han, S. Huang, Z. Huang, S. Wang, Y. Meng. Proton exchange membranes for high temperature proton exchange membrane fuel cells: Challenges and perspectives. *J. Power Sources*, **2022**, *533*, 231386. https://doi.org/10.1016/j.jpowsour.2022.231386

91. H. Pourrahmani, A. Yavarinasab, M. Siavashi, M. Matian. Progress in the proton exchange membrane fuel cells (PEMFCs) water/thermal management: From theory to the current challenges and real-time fault diagnosis methods. *Energy Rev.*, **2022**, *1*, 100002. https://doi.org/10.1016/j.enrev.2022.100002

92. J. Fan, M. Chen, Z. Zhao, Z. Zhang, S. Ye, S. Xu, H. Wang, H. Li. Bridging the gap between highly active oxygen reduction reaction catalysts and effective catalyst layers for proton exchange membrane fuel cells. *Nat. Energy*, **2021**, *6*, 475. https://doi.org/10.1038/s41560-021-00824-7

93. A. Kusoglu, A. Z. Weber. New insights into perfluorinated sulfonic-acid ionomers. *Chem. Rev.*, **2017**, *117*, 987. https://doi.org/10.1021/acs.chemrev.6b00159

94. B. Ghanti, R. Kamble, H. Komber, B. Voit, S. Banerjee. High proton-conducting phosphine oxide-and pyridinyl-based fluoro-sulfonated proton exchange membranes with enhanced chemical stability. *J. Power Sources*, **2025**, *631*, 236201. https://doi.org/10.1016/j.jpowsour.2025.236201

95. Z. Li, Y. Wang, Y. Mu, B. Wu, Y. Jiang, L. Zeng, T. Zhao. Recent advances in the anode catalyst layer for proton exchange membrane fuel cells. *Renew. Sustain. Energy Rev.*, **2023**, *176*, 113182. https://doi.org/10.1016/j.rser.2023.113182

96. A. K. Mandal, S. Bisoi, S. Banerjee. Effect of phosphaphenanthrene skeleton in sulfonated polyimides for proton exchange membrane application. *ACS Appl. Polym. Mater.*, **2019**, *1*, 893. https://doi.org/10.1021/acsapm.9b00128

97. B. Ghanti, S. Banerjee. Fluorine-Free Sulfonated Poly (sulfone triazole) s with a Pendant Phosphaphenanthrene Moiety for Proton Exchange Membrane Applications. *Macromolecules*, **2025**. https://doi.org/10.1021/acs.macromol.5c00277

98. Z. Rui, J. Liu. Understanding of free radical scavengers used in highly durable proton exchange membranes. *Prog. Nat. Sci.: Mater. Int.*, **2020**, *30*, 732. https://doi.org/10.1016/j.pnsc.2020.08.013

99. B. Ghanti, R. Kamble, H. Komber, B. Voit, S. Banerjee. Synergistically Functionalized Pyridinyl-and Phosphine-Oxide-Based Semifluoro-Sulfonated Copolytriazole Membrane Preparation via "Click" Polymerization for Proton Exchange Membrane Applications. *Macromolecules*, **2024**, *57*, 4584. https://doi.org/10.1021/acs.macromol.4c00050

100. S. Roy, B. Ghanti, D. Ghosh, D. Pradhan, B. Voit, S. Banerjee. Sterically Hindered Pyridine-Linked Sulfonated Polytriazoles: Fabrication of Membranes and Investigation of Single Fuel Cell Performance. *ACS Appl. Polym. Mater.*, **2022**, *4*, 7450. https://doi.org/10.1021/acsapm.2c01189

101. B. Date, J. Han, S. Park, E. J. Park, D. Shin, C. Y. Ryu, C. Bae. Synthesis and morphology study of SEBS triblock copolymers functionalized with sulfonate and phosphonate groups for proton exchange membrane fuel cells. *Macromolecules*, **2018**, *51*, 1020. https://doi.org/10.1021/acs.macromol.7b01848

102. A. Abdolmaleki, K. Eskandari, M. R. Molavian. Sulfonated or phosphonated membranes? DFT investigation of proton exchange in poly (oxadiazole) membranes. *Polymer*, **2016**, *87*, 181. https://doi.org/10.1016/j.polymer.2016.02.011

103. S. Bano, Y. S. Negi, K. Ramya. Studies on new highly phosphonated poly (ether ketone) based promising proton conducting membranes for high temperature fuel cell. *Int. J. Hydrogen Energy*, **2019**, *44*, 28968. https://doi.org/10.1016/j.ijhydene.2019.09.067

104. T. Wei, Y. Zhao, Z. Ren, Y. Han, H. Zhang, Z. Shao. Facile and affordable synthesis of sulfonated and phosphonated poly (p-terphenyl perfluorophenyl) s for proton exchange membrane fuel cells. *Next Sustainability*, **2024**, *3*, 100021. https://doi.org/10.1016/j.nxsust.2023.100021

105. J. Parvole, P. Jannasch. Polysulfones grafted with poly (vinylphosphonic acid) for highly proton conducting fuel cell membranes in the hydrated and nominally dry state. *Macromolecules*, **2008**, *41*, 3893. https://doi.org/10.1021/ma800042m

106. N. Y. Abu-Thabit, S. A. Ali, S. J. Zaidi. New highly phosphonated polysulfone membranes for PEM fuel cells. *J. Membr. Sci.*, **2010**, *360*, 26. https://doi.org/10.1016/j.memsci.2010.04.041

107. H. Tang, K. Geng, Y. Hu, N. Li. Synthesis and properties of phosphonated polysulfones for durable high-temperature proton exchange membranes fuel cell. *J. Membr. Sci.*, **2020**, *605*, 118107. https://doi.org/10.1016/j.memsci.2020.118107

108. M. A. Hickner, H. Ghassemi, Y. S. Kim, B. R. Einsla, J. E. McGrath. Alternative polymer systems for proton exchange membranes (PEMs). *Chem. Rev.*, **2004**, *104*, 4587. https://doi.org/10.1021/cr020711a

109. A. Ghorai, S. Roy, S. Das, H. Komber, M. M. Ghangrekar, B. Voit, S. Banerjee. Chemically stable sulfonated polytriazoles containing trifluoromethyl and phosphine oxide moieties for proton exchange membranes. *ACS Appl. Polym. Mater.*, **2020**, *2*, 2967. https://doi.org/10.1021/acsapm.0c00443

110. T. Higashihara, K. Matsumoto, M. Ueda. Sulfonated aromatic hydrocarbon polymers as proton exchange membranes for fuel cells. *Polymer*, **2009**, *50*, 5341. https://doi.org/10.1016/j.polymer.2009.09.001

111. S. M. Ibrahim, E. H. Price, R. A. Smith. EI duPont de Nemours. *Proc. Electrochem. Soc.*, **1983**, 83.

112. R. Kamble, A. Ghorai, B. Ghanti, D. Pradhan, S. Banerjee. Fabrication of high proton conducting composite membranes from amino group functionalized MOF and semi-fluorinated sulfonated poly (arylene ether sulfone)s. *Eur. Polym. J.*, **2022**, *179*, 111574. https://doi.org/10.1016/j.eurpolymj.2022.111574

113. Z. Cui, E. Drioli, Y. M. Lee. Recent progress in fluoropolymers for membranes. *Prog. Polym. Sci.*, **2014**, *39*, 164. https://doi.org/10.1016/j.progpolymsci.2013.07.008

114. K. D. Kreuer. Ion conducting membranes for fuel cells and other electrochemical devices. *Chem. Mater.*, **2014**, *26*, 361. https://doi.org/10.1021/cm402742u

115. M. G. Dhara, S. Banerjee. Fluorinated high-performance polymers: Poly(arylene ether)s and aromatic polyimides containing trifluoromethyl

Banerjee and Ghanti

Innov. Chem. Mater. Sustain. **2025**, *2*(1), 032-073

groups. *Prog. Polym. Sci.*, **2010**, *35*, 1022. https://doi.org/10.1016/j.progpolymsci.2010.04.003

116. K. H. Lee, J. Y. Chu, A. R. Kim, D. J. Yoo. Facile fabrication and characterization of improved proton conducting sulfonated poly (arylene biphenylether sulfone) blocks containing fluorinated hydrophobic units for proton exchange membrane fuel cell applications. *Polymers*, **2018**, *10*, 1367. https://doi.org/10.3390/polym10121367

117. R. Devanathan. Recent developments in proton exchange membranes for fuel cells. *Energy Environ. Sci.*, **2008**, *1*, 101. https://doi.org/10.1039/b808149m

118. M. Kim, H. Ko, S. Y. Nam, K. Kim. Study on control of polymeric architecture of sulfonated hydrocarbon-based polymers for high-performance polymer electrolyte membranes in fuel cell applications. *Polymers*, **2021**, *13*, 3520. https://doi.org/10.3390/polym13203520

119. S. H. Mirfarsi, M. J. Parnian, S. Rowshanzamir, E. Kjeang. Current status of cross-linking and blending approaches for durability improvement of hydrocarbon-based fuel cell membranes. *Int. J. Hydrogen Energy*, **2022**, *47*, 13460. https://doi.org/10.1016/j.ijhydene.2022.02.077

120. C. H. Park, C. H. Lee, M. D. Guiver, Y. M. Lee. Sulfonated hydrocarbon membranes for medium-temperature and low-humidity proton exchange membrane fuel cells (PEMFCs). *Prog. Polym. Sci.*, **2011**, *36*, 1443. https://doi.org/10.1016/j.progpolymsci.2011.06.001

121. H. Hou, M. L. Di Vona, P. Knauth. Durability of sulfonated aromatic polymers for proton-exchange-membrane fuel cells. *ChemSusChem*, **2011**, *4*, 1526. https://doi.org/1002/cssc.201000415

122. L. Fu, G. Xiao, D. Yan. Sulfonated poly(arylene ether sulfone) s with phosphine oxide moieties: a promising material for proton exchange membranes. *ACS Appl. Mater. Interfaces*, **2010**, *2*, 1601. https://doi.org/10.1021/am1000739

123. J. Miyake, M. Watanabe, K. Miyatake. Sulfonated poly (arylene ether phosphine oxide ketone) block copolymers as oxidatively stable proton conductive membranes. *ACS Appl. Mater. Interfaces*, **2013**, *5*, 5903. https://doi.org/10.1021/am401625j

124. K. Umezawa, T. Oshima, M. Yoshizawa-Fujita, Y. Takeoka, M. Rikukawa. Synthesis of hydrophilic–hydrophobic block copolymer ionomers based on polyphenylenes. *ACS Macro. Lett.*, **2012**, *1*, 969. https://doi.org/10.1021/mz300290x

125. K. Si, R. Wycisk, D. Dong, K. Cooper, M. Rodgers, P. Brooker, D. Slattery, M. Litt. Rigid-rod poly (phenylenesulfonic acid) proton exchange membranes with cross-linkable biphenyl groups for fuel cell applications. *Macromolecules*, **2013**, *46*, 422. https://doi.org/10.1021/ma301875n

126. A. K. Mandal, A. Ghorai, S. Banerjee. Sulphonated polysilsesquioxane–polyimide composite membranes: proton exchange membrane properties. *Bull. Mater. Sci.*, **2020**, *43*, 1. https://doi.org/10.1007/s12034-020-02158-8

127. J. L. Jespersen, E. Schaltz, S. K. Kær. Electrochemical characterization of a polybenzimidazole-based high temperature proton exchange membrane unit cell. *J. Power Sources*, **2009**, *191*, 289. https://doi.org/10.1016/j.jpowsour.2009.02.025

128. J. Yang, H. Jiang, L. Gao, J. Wang, Y. Xu, R. He. Fabrication of crosslinked polybenzimidazole membranes by trifunctional crosslinkers for high temperature proton exchange membrane fuel cells. *Int. J. Hydrogen Energy*, **2018**, *43*, 3299. https://doi.org/10.1016/j.ijhydene.2017.12.141

129. Y. J. Huang, Y. S. Ye, Y. C. Yen, L. D. Tsai, B. J. Hwang, F. C. Chang. Synthesis and characterization of new sulfonated polytriazole proton exchange membrane by click reaction for direct methanol fuel cells (DMFCs). *Int. J. Hydrogen Energy*, **2011**, *36*, 15333. https://doi.org/10.1016/j.ijhydene.2011.08.093

130. S. Saha, S. Banerjee, H. Komber, B. Voit. Flexible diazide based sulfonated polytriazoles and their proton exchange membrane properties. *Macromol. Chem. Phys.*, **2017**, *218*, 1700070. https://doi.org/10.1002/macp.201700070

131. F. Liu, D. M. Knauss. Sulfonated poly (meta-phenylene isophthalamide)s as proton exchange membranes. *J. Polym. Sci. Part A: Polym. Chem.*, **2016**, *54*, 2582. https://doi.org/10.1002/pola.28136

132. Q. Yuan, P. Liu, G. L. Baker. Sulfonated polyimide and PVDF-based blend proton exchange membranes for fuel cell applications. *J. Mater. Chem. A*, **2015**, *3*, 3847. https://doi.org/10.1039/C4TA04910A

133. J. Fang, X. Guo, S. Harada, T. Watari, K. Tanaka, H. Kita, K. I. Okamoto. Novel sulfonated polyimides as polyelectrolytes for fuel cell application. 1. Synthesis, proton conductivity, and water stability of polyimides from 4, 4 '-diaminodiphenyl ether-2, 2'-disulfonic acid. *Macromolecules*, **2002**, *35*, 9022. https://doi.org/10.1021/ma020005b

134. J. M. García, F. C. García, F. Serna, J. L. de la Peña. High-performance aromatic polyamides. *Prog. Polym. Sci.*, **2010**, *35*, 623. https://doi.org/10.1016/j.progpolymsci.2009.09.002

135. P. W. Morgan. Synthesis and properties of aromatic and extended chain polyamides. *Macromolecules*, **1977**, *10*, 1381. https://doi.org/10.1021/ma60060a040

136. C. C. Lin, W. F. Lien, Y. Z. Wang, H. W. Shiu, C. H. Lee. Preparation and performance of sulfonated polyimide/Nafion multilayer membrane for proton exchange membrane fuel cell. *J. Power Sources*, **2012**, *200*, 1. https://doi.org/10.1016/j.jpowsour.2011.10.001

137. A. Ghosh, S. K. Sen, S. Banerjee, B. Voit. Solubility improvements in aromatic polyimides by macromolecular engineering. *RSC advances*, **2012**, *2*, 5900. https://doi.org/10.1039/C2RA20175E

138. S. Maji, S. Banerjee. Synthesis, characterization, and properties of novel fluorine containing aromatic polyamides. *J. Appl. Polym. Sci.*, **2008**, *108*, 1356. https://doi.org/10.1002/app.27831

139. N. Yamazaki, F. Higashi. Studies on reactions of the N-phosphonium salts of pyridines—VII: Preparation of peptides and active esters of amino acids by means of diphenyl and triphenyl phosphites in the presence of tertiary amines. *Tetrahedron*, **1974**, *30*, 1323. https://doi.org/10.1016/S0040-4020(01)97242-4

140. T. S. Jo, C. H. Ozawa, B. R. Eagar, L. V. Brownell, D. Han, C. Bae. Synthesis of sulfonated aromatic poly (ether amide)s and their application to proton exchange membrane fuel cells. *J. Polym. Sci. Part A: Polym. Chem.*, **2009**, *47*, 485. https://doi.org/10.1002/pola.23165

141. H. A. Every, G. J. Janssen, E. F. Sitters, E. Mendes, S. J. Picken. Performance analysis of sulfonated PPTA polymers as potential fuel cell membranes. *J. Power Sources*, **2006**, *162*, 380. https://doi.org/10.1016/j.jpowsour.2006.07.002

142. Y. Pérez-Padilla, M. A. Smit, M. J. Aguilar-Vega. Preparation and characterization of sulfonated copolyamides based on poly (hexafluoroisopropylidene) isophthalamides for polymer electrolytic membranes. *Ind. Eng. Chem. Res.*, **2011**, *50*, 9617. https://doi.org/10.1021/ie102409d

143. Y. Chang, Y. B. Lee, C. Bae. Partially fluorinated sulfonated poly (ether amide) fuel cell membranes: influence of chemical structure on membrane properties. *Polymers*, **2011**, *3*, 222. https://doi.org/10.3390/polym3010222

144. C. Wang, B. Shen, Y. Zhou, C. Xu, W. Chen, X. Zhao, J. Li. Sulfonated aromatic polyamides containing nitrile groups as proton exchange fuel cell membranes. *Int. J. Hydrogen Energy*, **2015**, *40*, 6422. https://doi.org/10.1016/j.ijhydene.2015.03.078

145. R. Sulub-Sulub, M. I. Loría-Bastarrachea, M. O. González-Díaz, M. Aguilar-Vega. Synthesis and characterization of block sulfonated amphiphilic aromatic copolyamides for cation conductive membranes. *Polym. Bull.*, **2023**, *80*, 429. https://doi.org/10.1007/s00289-022-04093-6

146. D. S. Kim, G. P. Robertson, Y. S. Kim, M. D. Guiver. Copoly(arylene ether)s containing pendant sulfonic acid groups as proton exchange membranes. *Macromolecules*, **2009**, *42*, 957. https://doi.org/10.1021/ma802192y

147. R. Mukherjee, S. Banerjee, H. Komber, B. Voit. Highly proton conducting fluorinated sulfonated poly (arylene ether sulfone) copolymers with side chain grafting. *RSC Advances*, **2014**, *4*, 46723. https://doi.org/10.1039/C4RA07291J

148. N. Li, D. W. Shin, D. S. Hwang, Y. M. Lee, M. D. Guiver. Polymer electrolyte membranes derived from new sulfone monomers with pendent sulfonic acid groups. *Macromolecules*, **2010**, *43*, 9810. https://doi.org/10.1021/ma102107a

149. R. N. Johnson, A. G. Farnham, R. A. Clendinning, W. F. Hale, C. N. Merriam. Poly(aryl ethers) by nucleophilic aromatic substitution. I. Synthesis and properties. *J. Polym. Sci. Part A: Polym. Chem.*, **1967**, *5*, 2375. https://doi.org/10.1002/pol.1967.150050916

150. F. Wang, M. Hickner, Q. Ji, W. Harrison, J. Mecham, T. A. Zawodzinski, J. E. McGrath. Synthesis of highly sulfonated poly(arylene ether sulfone) random (statistical) copolymers via direct polymerization. *Macromol. Symp.*, **2001**, *175*, 387. https://doi.org/10.1002/1521-3900(200110)175:1<387::AID-MASY387>3.0.CO;2-1

151. F. Wang, M. Hickner, Y. S. Kim, T. A. Zawodzinski, J. E. McGrath. Direct polymerization of sulfonated poly(arylene ether sulfone) random (statistical) copolymers: candidates for new proton exchange membranes. *J. Membr. Sci.*, **2002**, *197*, 231. https://doi.org/10.1016/S0376-7388(01)00620-2

152. C. Wang, D. W. Shin, S. Y. Lee, N. R. Kang, Y. M. Lee, M. D. Guiver. Poly(arylene ether sulfone) proton exchange membranes with flexible acid side chains. *J. Membr. Sci.*, **2012**, *405*, 68. https://doi.org/10.1016/j.memsci.2012.02.045

153. M. Oroujzadeh, S. Mehdipour-Ataei. Highly fluorinated poly(arylene ether)s containing sulfonated naphthol pendants with improved proton conductivity as a polymer electrolyte for proton exchange membrane fuel cells. *Renew. Energy*, **2025**, *240*, 122298. https://doi.org/10.1016/j.renene.2024.122298

154. L. Meng, M. Ju, J. Xu, X. Chen, P. Zhao, J. Lei, T. Lan, F. Chen, Z. Hu, Z. Wang. Achieving high efficient proton transport in sulfonated poly(arylene ether ketone sulfone)s containing fluorenyl groups by introducing bifunctionalized metal-organic frameworks. *Int. J. Hydrogen Energy*, **2023**, *48*, 40000. https://doi.org/10.1016/j.ijhydene.2023.07.148

155. J. Lei, L. Meng, P. Zhao, J. Wang, T. Lan, J. Xu. A simple strategy for synthesis of side-chain sulfonated poly(arylene ether ketone sulfone) constructing hydrophilic/hydrophobic phase separation structure. *J. Polym. Res.*, **2024**, *31*, 52. https://doi.org/10.1007/s10965-024-03894-9

156. Z. Zhao, D. Liu, J. Zhong, J. Li, Z. Lin, Z. Zhao, J. Pang. Poly(aryl ether sulfone ketone) with densely sulfonated structural units facilitate microphase separation to promote proton transport. *J. Membr. Sci.*, **2024**, *693*, 122319. https://doi.org/10.1016/j.memsci.2023.122319

157. X. Dong, H. Li, J. Xu, X. Wang, S. Wang, Y. Yin, C. L. Song, T. Lan, Z. Wang, Y. W. Yang. Cross-Linking of Bromo-Pillar-[5]-arenes and Sulfonated Poly(Aryl Ether Ketone Sulfone) Enhances Proton Conductivity of Membranes at Low Ion Exchange Capacity. *ACS mater. lett.*, **2024**, *6*, 4962. https://doi.org/10.1021/acsmaterialslett.4c01980

158. Y. Tan, K. Zhang, H. Liao, G. Xiao, Y. Yao, G. Sun, D. Yan. Trisulfonation approach: To improve the properties of poly (arylene thioether

Banerjee and Ghanti

Innov. Chem. Mater. Sustain. **2025**, *2*(1), 032-073

phosphine oxide)s based proton exchange membranes. *J. Membr. Sci.*, **2016**, *508*, 32. https://doi.org/10.1016/j.memsci.2016.02.020

159. C. Allam, K. J. Liu, J. E. McGrath, D. K. Mohanty. Preparation and properties of novel aromatic poly (thioethers) derived from 4, 4′-thiobisbenzenethiol. *Macromol. Chem. Phys.*, **1999**, *200*, 1854. https://doi.org/10.1002/(SICI)1521-3935(19990801)200:8<1854::AID-MACP1854>3.0.CO;2-9

160. S. J. Rodrigues, T. L. Reitz, T. D. Dang, Z. Bai, K. Bardua. Polyarylenethioethersulfone membranes for fuel cells. *J. Electrochem. Soc.*, **2007**, *154*, B960. https://doi.org/10.1149/1.2755881

161. Z. Bai, M. F. Durstock, T. D. Dang. Proton conductivity and properties of sulfonated polyarylenethioether sulfones as proton exchange membranes in fuel cells. *J. Membr. Sci.*, **2006**, *281*, 508. https://doi.org/10.1016/j.memsci.2006.04.021

162. K. B. Wiles, F. Wang, J. E. McGrath. Directly copolymerized poly(arylene sulfide sulfone) disulfonated copolymers for PEM-based fuel cell systems. I. Synthesis and characterization. *J. Polym. Sci. Part A: Polym. Chem.*, **2005**, *43*, 2964. https://doi.org/10.1002/pola.20744

163. X. Ma, L. Shen, C. Zhang, G. Xiao, D. Yan, G. Sun. Sulfonated poly(arylene thioether phosphine oxide)s copolymers for proton exchange membrane fuel cells. *J. Membr. Sci.*, **2008**, *310*, 303. https://doi.org/10.1016/j.memsci.2007.11.003

164. A. Kausar, S. Zulfiqar, M. I. Sarwar. Recent developments in sulfur-containing polymers. *Polym. Rev.*, **2014**, *54*, 185. https://doi.org/10.1080/15583724.2013.863209

165. S. J. Wang, Y. Z. Meng, A. R. Hlil, A. S. Hay. Synthesis and characterization of phthalazinone containing poly(arylene ether)s, poly(arylene thioether)s, and poly(arylene sulfone)s via a novel N− C coupling reaction. *Macromolecules*, **2004**, *37*, 60. https://doi.org/10.1021/ma030246z

166. J. P. Kim, W. Y. Lee, J. W. Kang, S. K. Kwon, J. J. Kim, J. S. Lee. Fluorinated poly (arylene ether sulfide) for polymeric optical waveguide devices. *Macromolecules*, **2001**, *34*, 7817. https://doi.org/10.1021/ma010439r

167. H. S. Chan, S. C. Ng. Synthesis, characterization and applications of thiophene-based functional polymers. *Prog. Polym. Sci.*, **1998**, *23*, 1167. https://doi.org/10.1016/S0079-6700(97)00032-4

168. S. Matsumura, N. Kihara, T. Takata. Properties of a few aromatic poly (thioether ketones) as sulfur-containing high-performance polymers. *J. Appl. Polym. Sci.*, **2004**, *92*, 1869. https://doi.org/10.1002/app.20169

169. Z. Bai, J. A. Shumaker, M. D. Houtz, P. A. Mirau, T. D. Dang. Fluorinated poly(arylenethioethersulfone) copolymers containing pendant sulfonic acid groups for proton exchange membrane materials. *Polymer*, **2009**, *50*, 1463. https://doi.org/10.1016/j.polymer.2009.01.028

170. L. Gui, C. Zhang, S. Kang, N. Tan, G. Xiao, D. Yan. Synthesis and properties of hexafluoroisopropylidene-containing sulfonated poly(arylene thioether phosphine oxide)s for proton exchange membranes. *Int. J. Hydrogen Energy*, **2010**, *35*, 2436. https://doi.org/10.1016/j.ijhydene.2009.12.137

171. J. Hou, S. Liu, X. Sun, Z. Xiao, H. Ding. Preparation and characterization of sulfonated poly (arylene thioether sulfone)/imino-containing phosphorylated silica particle composite proton exchange membranes. *High Perform. Polym.*, **2019**, *31*, 753. https://doi.org/10.1177/0954008318793932

172. D. Liu, H. Liao, N. Tan, G. Xiao, D. Yan. Sulfonated poly(arylene thioether phosphine oxide)/sulfonated benzimidazole blends for proton exchange membranes. *J. Membr. Sci.*, **2011**, *372*, 125. https://doi.org/10.1016/j.memsci.2011.01.057

173. H. Xu, K. Chen, X. Guo, J. Fang, J. Yin. Synthesis of novel sulfonated polybenzimidazole and preparation of cross-linked membranes for fuel cell application. *Polymer*, **2007**, *48*, 5556. https://doi.org/10.1016/j.polymer.2007.07.029

174. N. Tan, Y. Chen, G. Xiao, D. Yan. Synthesis and properties of sulfonated polybenzothiazoles with benzimidazole moieties as proton exchange membranes. *J. Membr. Sci.*, **2010**, *356*, 70. https://doi.org/10.1016/j.memsci.2010.03.028

175. H. Maekawa, K. Nakamura, H. Kudo. Synthesis and properties of highly thermally stable ultrathin films of fluorine-containing hyperbranched polybenzoxazoles. *J. Polym. Sci.*, **2024**, *62*, 1731. https://doi.org/10.1002/pol.20230659

176. R. Bouchet, E. Siebert. Proton conduction in acid doped polybenzimidazole. *Solid State Ion.*, **1999**, *118*, 287. https://doi.org/10.1016/S0167-2738(98)00466-4

177. R. He, Q. Li, G. Xiao, N. J. Bjerrum. Proton conductivity of phosphoric acid doped polybenzimidazole and its composites with inorganic proton conductors. *J. Membr. Sci.*, **2003**, *226*, 169. https://doi.org/10.1016/j.memsci.2003.09.002

178. J. A. Asensio, P. Gómez-Romero. Recent Developments on Proton Conduc-ting Poly (2, 5-benzimidazole)(ABPBI) Membranes for High Temperature Poly-mer Electrolyte Membrane Fuel Cells. *Fuel Cells*, **2005**, *5*, 336. https://doi.org/10.1002/fuce.200400081

179. S. Qing, W. Huang, D. Yan. Synthesis and characterization of thermally stable sulfonated polybenzimidazoles. *Eur. Polym. J.*, **2005**, *41*, 1589. https://doi.org/10.1016/j.eurpolymj.2005.02.001

180. S. Qing, W. Huang, D. Yan. Synthesis and properties of soluble sulfonated polybenzimidazoles. *React. Funct. Polym.*, **2006**, *66*, 219. https://doi.org/10.1016/j.reactfunctpolym.2005.07.020

181. J. A. Asensio, S. Borrós, P. Gómez-Romero. Sulfonated poly (2, 5-benzimidazole)(SABPBI) impregnated with phosphoric acid as proton conducting membranes for polymer electrolyte fuel cells. *Electrochim. Acta*, **2004**, *49*, 4461. https://doi.org/10.1016/j.electacta.2004.05.002

182. M. J. Ariza, D. J. Jones, J. Rozière. Role of post-sulfonation thermal treatment in conducting and thermal properties of sulfuric acid sulfonated poly(benzimidazole) membranes. *Desalination*, **2002**, *147*, 183. https://doi.org/10.1016/S0011-9164(02)00532-5

183. P. Staiti, F. Lufrano, A. S. Arico, E. Passalacqua, V. Antonucci. Sulfonated polybenzimidazole membranes—preparation and physico-chemical characterization. *J. Membr. Sci.*, **2001**, *188*, 71. https://doi.org/10.1016/S0376-7388(01)00359-3

184. X. Glipa, M. El Haddad, D. J. Jones, J. Rozière. Synthesis and characterisation of sulfonated polybenzimidazole: a highly conducting proton exchange polymer. *Solid State Ion.*, **1997**, *97*, 323. https://doi.org/10.1016/S0167-2738(97)00032-5

185. S. Kang, C. Zhang, G. Xiao, D. Yan, G. Sun. Synthesis and properties of soluble sulfonated polybenzimidazoles from 3, 3′-disulfonate-4, 4′-dicarboxylbiphenyl as proton exchange membranes. *J. Membr. Sci.*, **2009**, *334*, 91. https://doi.org/10.1016/j.memsci.2009.02.021

186. G. Wang, S. Yang, B. Y. Hua, M. X. Lu, J. Q. Kang, W. S. Tang, H. L. Wei, X. X. Liu, L. F. Cui, X. D. Chen. Soluble sulfonated polybenzimidazoles containing phosphine oxide units as proton exchange membranes. *New J. Chem.*, **2023**, *47*, 10613. https://doi.org/10.1039/d3nj00796k

187. N. Tan, G. Xiao, D. Yan, G. Su. Preparation and properties of polybenzimidazoles with sulfophenylsulfonyl pendant groups for proton exchange membranes. *J. Membr. Sci.*, **2010**, *353*, 51. https://doi.org/10.1016/j.memsci.2010.02.029

188. S. Mukhopadhyay, A. Das, T. Jana, S. K. Das. Fabricating a MOF material with polybenzimidazole into an efficient proton exchange membrane. *ACS Appl. Energy Mater.*, **2020**, *3*, 7964. https://doi.org/10.1021/acsaem.0c01322

189. Y. Wang, P. Sun, Z. Xia, Z. Li, H. Ding, Z. Fan, H. Guo. Anchoring highly sulfonated hyperbranched PBI onto oPBI: fast proton conduction with low leaching. *ACS Appl. Energy Mater.*, **2022**, *5*, 10802. https://doi.org/10.1021/acsaem.2c01491

190. S. Banerjee, M. K. Madhra, A. K. Salunke, G. Maier. Synthesis and properties of fluorinated polyimides. 1. Derived from novel 4, 4 ″-bis (aminophenoxy)-3, 3 ″-trifluoromethyl terphenyl. *J. Polym. Sci. Part A: Polym. Chem.*, **2002**, *40*, 1016. https://doi.org/10.1002/pola.10189

191. M. K. Madhra, A. K. Salunke, S. Banerjee, S. Prabha. Synthesis and properties of fluorinated polyimides, 2. Derived from novel 2,6-bis(3′-trifluoromethyl-p-aminobiphenyl ether)pyridine and 2,5-bis (3′-trifluoromethyl-p-aminobiphenyl ether) thiophene. *Macromol. Chem. Phys.*, **2002**, *203*, 1238. https://doi.org/10.1002/1521-3935(200206)203:9<1238::AID-MACP1238>3.0.CO;2-R

192. E. A. Mistri, A. K. Mohanty, S. Banerjee, H. Komber, B. Voit. Naphthalene dianhydride based semifluorinated sulfonated copoly (ether imide)s: Synthesis, characterization and proton exchange properties. *J. Membr. Sci.*, **2013**, *441*, 168. https://doi.org/10.1016/j.memsci.2013.03.015

193. S. K. Sen, S. Banerjee. Gas transport properties of fluorinated poly (ether imide) films containing phthalimidine moiety in the main chain. *J. Membr. Sci.*, **2010**, *350*, 53. https://doi.org/10.1016/j.memsci.2009.12.011

194. B. Dasgupta, S. K. Sen, S. Banerjee. Aminoethylaminopropylisobutyl POSS—Polyimide nanocomposite membranes and their gas transport properties. *Mater. Sci. Eng. B*, **2010**, *168*, 30. https://doi.org/10.1016/j.mseb.2009.10.006

195. V. Kute, S. Banerjee. Novel semi-fluorinated poly (ether imide) s derived from 4-(p-aminophenoxy)-3-trifluoromethyl-4'-aminobiphenyl. *Macromol. Chem. Phys.*, **2003**, *204*, 2105. https://doi.org/10.1002/macp.200350070

196. M. Ding. Isomeric polyimides. *Prog. Polym. Sci.*, **2007**, *32*, 623. https://doi.org/10.1016/j.progpolymsci.2007.01.007

197. K. Xie, J. G. Liu, H. W. Zhou, S. Y. Zhang, M. H. He, S. Y. Yang. Soluble fluoro-polyimides derived from 1,3-bis(4-amino-2-trifluoromethyl-phenoxy)benzene and dianhydrides. *Polymer*, **2001**, *42*, 7267. https://doi.org/10.1016/S0032-3861(01)00138-0

198. A. Ganeshkumar, D. Bera, E. A. Mistri, S. Banerjee. Triphenyl amine containing sulfonated aromatic polyimide proton exchange membranes. *Eur. Polym. J.*, **2014**, *60*, 235. https://doi.org/10.1016/j.eurpolymj.2014.09.009

199. A. K. Mandal, S. Bisoi, S. Banerjee, H. Komber, B. Voit. Sulfonated copolyimides containing trifluoromethyl and phosphine oxide moieties: synergistic effect towards proton exchange membrane properties. *Eur. Polym. J.*, **2017**, *95*, 581. https://doi.org/10.1016/j.eurpolymj.2017.08.050

200. A. G. Kumar, D. Bera, S. Banerjee, R. Veerubhotla, D. Das. Sulfonated poly(ether imide) with fluorenyl and trifluoromethyl groups: Application in microbial fuel cell (MFC). *Eur. Polym. J.*, **2016**, *83*, 114. https://doi.org/10.1016/j.eurpolymj.2016.08.009

201. C. Gao, J. Chen, B. Zhang, L. Wang. Effect of chemical structure and degree of branching on the stability of proton exchange membranes based on sulfonated polynaphthylimides. *Polymers*, **2020**, *12*, 652. https://doi.org/10.3390/polym12030652

202. T. Rohilla, A. Husain, N. Singh, D. K. Mahajan. Atomistic simulation and synthesis of novel sulfonated Polyimide polymer electrolyte membranes with facile proton transport. *Chem. Eng. J.*, **2023**, *474*, 145727. https://doi.org/10.1016/j.cej.2023.145727

203. J. Yang, Y. Guo, L. Liu, L. Guo, Z. Sun, C. Wang. Preparation of proton exchange membrane with intrinsic micropores constructing efficient ion transport channels based on segmented copolymer (sulfonated polyimide). *J. Energy Storage*, **2023**, *72*, 108407. https://doi.org/10.1016/j.est.2023.108407

204. X. Wang, S. Zhao, S. Wang, X. Hou, J. Yang, C. Liang, Y. Zhao, L. Wang, C. Shen, N. Gao, L. Jia. Facile preparation of high-performance sulfonated polyimide proton exchange membrane by doping nano carbon sulfonic acid. *J. Membr. Sci.*, **2025**, *717*, 123605. https://doi.org/10.1016/j.memsci.2024.123605

205. E. J. Park, P. Jannasch, K. Miyatake, C. Bae, K. Noonan, C. Fujimoto, S. Holdcrof, J. R. Varcoe, D. Henkensmeier, M. D. Guiver, Y. S. Kim. Aryl ether-free polymer electrolytes for electrochemical and energy devices. *Chem. Soc. Rev.*, **2024**, *53*, 5704. https://doi.org/10.1039/D3CS00186E

206. G. A. Olah. Superelectrophiles. *Angew. Chem., Int. Ed. Engl.*, **1993**, *32*, 767. https://doi.org/10.1002/anie.199307673

207. G. A. Olah, G. Rasul, C. York, G. S. Prakash. Superacid-catalyzed condensation of benzaldehyde with benzene. Study of protonated benzaldehydes and the role of superelectrophilic activation. *J. Am. Chem. Soc.*, **1995**, *117*, 11211. https://doi.org/10.1021/ja00150a018

208. O. Hernández-Cruz, M. G. Zolotukhin, S. Fomine, L. Alexandrova, C. Aguilar-Lugo, F. A. Ruiz-Treviño, G. Ramos-Ortíz, J. L. Maldonado, G. Cadenas-Pliego. High-Tg functional aromatic polymers. *Macromolecules*, **2015**, *48*, 1026. https://doi.org/10.1021/ma502288d

209. M. K. Pagels, S. Adhikari, R. C. Walgama, A. Singh, J. Han, D. Shin, C. Bae. One-pot synthesis of proton exchange membranes from anion exchange membrane precursors. *ACS Macro Lett.*, **2020**, *9*, 1489. https://doi.org/10.1021/acsmacrolett.0c00550

210. M. R. Hibbs, C. H. Fujimoto, C. J. Cornelius. Synthesis and characterization of poly (phenylene)-based anion exchange membranes for alkaline fuel cells. *Macromolecules*, **2009**, *42*, 8316. https://doi.org/10.1021/ma901538c

211. J. Ahn, R. Shimizu, K. Miyatake. Sulfonated aromatic polymers containing hexafluoroisopropylidene groups: a simple but effective structure for fuel cell membranes. *J. Mater. Chem. A*, **2018**, *6*, 24625. https://doi.org/10.1039/C8TA09587F

212. Q. Wang, L. Sang, L. Huang, J. Guan, H. Yu, J. Zheng, Q. Zhang, G. Qin, S. Li, S. Zhang. Design and synthesis of comb-like bisulfonic acid proton exchange membrane with regulated microstructure. *Adv. Funct. Mater.*, **2024**, *34*, 2316506. https://doi.org/10.1002/adfm.202316506

213. C. Ba, S. Xu, C. G. Arges, J. H. Park, J. Park, M. Urgun-Demirtas. Design of non-fluorinated proton exchange membranes from Poly(Terphenyl fluorenyl isatin) with fluorene-linked sulfonate groups and microblock structures. *J. Membr. Sci.*, **2025**, *717*, 123551. https://doi.org/10.1016/j.memsci.2024.123551

214. T. Ryu, H. Jang, F. Ahmed, N. S. Lopa, H. Yang, S. Yoon, I. Choi, W. Kim. Synthesis and characterization of polymer electrolyte membrane containing methylisatin moiety by polyhydroalkylation for fuel cell. *Int. J. Hydrogen Energy*, **2018**, *43*, 5398. https://doi.org/10.1016/j.ijhydene.2017.12.164

215. H. Nederstedt, P. Jannasch. Poly(p-terphenyl alkylene)s grafted with highly acidic sulfonated polypentafluorostyrene side chains for proton exchange membranes. *J. Membr. Sci.*, **2022**, *647*, 120270. https://doi.org/10.1016/j.memsci.2022.120270

216. X. Yan, H. Zhang, Z. Hu, L. Li, L. Hu, Z. A. Li, L. Gao, Y. Dai, X. Jian, G. He. Amphoteric-side-chain-functionalized "ether-free" poly(arylene piperidinium) membrane for advanced redox flow battery. *ACS Appl. Mater. Interfaces*, **2019**, *11*, 44315. https://doi.org/10.1021/acsami.9b15872

217. H. Bai, H. Peng, Y. Xiang, J. Zhang, H. Wang, S. Lu, L. Zhuang. Poly(arylene piperidine)s with phosphoric acid doping as high temperature polymer electrolyte membrane for durable, high-performance fuel cells. *J. Power Sources*, **2019**, *443*, 227219. https://doi.org/10.1016/j.jpowsour.2019.227219

218. J. Guan, X. Sun, H. Yu, J. Zheng, Y. Sun, S. Li, G. Qin, S. Zhang. High conductive and dimensional stability proton exchange membranes with an all-carbon main chain and densely sulfonated structure. *J. Membr. Sci.*, **2024**, *700*, 122664. https://doi.org/10.1016/j.memsci.2024.122664

219. W. Li, R. Zhang, X. Zhao, Z. Yue, H. Qian, H. Yang. Highly proton conductive and stable sulfonated poly(arylene-alkane) for fuel cells with performance over 2.46 W cm^{-2}. *J. Mater. Chem. A*, **2023**, *11*, 4547. https://doi.org/10.1039/D2TA08911D

220. N. R. Kang, T. H. Pham, P. Jannasch. Polyaromatic perfluorophenylsulfonic acids with high radical resistance and proton conductivity. *ACS Macro Lett.*, **2019**, *8*, 1247. https://doi.org/10.1021/acsmacrolett.9b00615

221. Y. Liang, Z. Liu, K. Lin, W. Yin, Y. Zhu. High-performance poly(m-terphenyl fluorenyl)s containing long flexible side chains with dual 1,2,3-triazole and disulfonated units for proton exchange membranes. *J. Membr. Sci.*, **2025**, *718*, 123691. https://doi.org/10.1016/j.memsci.2025.123691

222. B. Xue, M. Z. Zhu, S. Q. Fu, P. P. Huang, H. Qian, P. N. Liu. Facile synthesis of sulfonated poly (phenyl-alkane) s for proton exchange membrane fuel cells. *J. Membr. Sci.*, **2023**, *673*, 121263. https://doi.org/10.1016/j.memsci.2022.121263

223. R. X. Yao, L. Kong, Z. S. Yin, F. L. Qing. Synthesis of novel aromatic ether polymers containing perfluorocyclobutyl and triazole units via click chemistry. *J. Fluor. Chem.*, **2008**, *129*, 1003. https://doi.org/10.1016/j.jfluchem.2008.04.012

224. G. Qiu, P. Nava, A. Martinez, C. Colomban. A tris(benzyltriazolemethyl)amine-based cage as a CuAAC ligand tolerant to exogenous bulky nucleophiles. *Chem. Commun.*, **2021**, *57*, 2281. https://doi.org/10.1039/D0CC08005E

225. M. C. Floros, J. F. Bortolatto, Jr O. B. Oliveira, S. L. Salvador, S. S. Narine. Antimicrobial activity of amphiphilic triazole-linked polymers derived from renewable sources. *ACS Biomater. Sci. Eng.*, **2016**, *2*, 336. https://doi.org/10.1021/acsbiomaterials.5b00412

226. X. Wang, X. Zhang, Y. Wang, S. Ding. IrAAC-based construction of dual sequence-defined polytriazoles. *Polym. Chem.*, **2021**, *12*, 3825. https://doi.org/10.1039/D1PY00718A

227. D. Huang, Y. Liu, A. Qin, B. Z. Tang. Nickel-Catalyzed Azide–Alkyne Click Polymerization toward 1, 5-Regioregular Polytriazoles. *Macromolecules*, **2023**, *56*, 10092. https://doi.org/10.1021/acs.macromol.3c02000

228. M. Li, X. Duan, Y. Jiang, X. Sun, X. Xu, Y. Zheng, W. Song, N. Zheng. Multicomponent polymerization of azides, alkynes, and electrophiles toward 1,4,5-trisubstituted polytriazoles. *Macromolecules*, **2022**, *55*, 7240. https://doi.org/10.1021/acs.macromol.2c00966

229. V. V. Rostovtsev, L. G. Green, V. V. Fokin, K. B. Sharpless. A stepwise huisgen cycloaddition process: copper (I)-catalyzed regioselective "ligation" of azides and terminal alkynes. *Angew. Chem., Int. Ed.*, **2002**, *41*, 2596. https://doi.org/10.1002/1521-3773(20020715)41:14<2596::AID-ANIE2596>3.0.CO;2-4

230. A. Ghosh, S. Banerjee. Sulfonated fluorinated-aromatic polymers as proton exchange membranes. *e-Polymers*, **2014**, *14*, 227. https://doi.org/10.1515/epoly-2014-0049

231. A. Ghorai, S. Roy, S. Das, H. Komber, M. M. Ghangrekar, B. Voit, S. Banerjee. Preparation of sulfonated polytriazoles with a phosphaphenanthrene unit via click polymerization: fabrication of membranes and properties thereof. *ACS Appl. Polym. Mater.*, **2021**, *3*, 4127. https://doi.org/10.1021/acsapm.1c00600

232. A. Ghorai, A. K. Mandal, S. Banerjee. Synthesis and characterization of new phosphorus containing sulfonated polytriazoles for proton exchange membrane application. *J. Polym. Sci.*, **2020**, *58*, 263. https://doi.org/10.1002/pol.20190030

233. A. Ghorai, S. Banerjee. Phosphorus-Containing Fluoro-Sulfonated Polytriazole Membranes with High Proton Conductivity: Understanding Microstructural and Thermomechanical Behaviors as a Function of Degree of Sulfonation. *Macromol. Chem. Phys.*, **2023**, *224*, 2200031. https://doi.org/10.1002/macp.202200031

234. R. Kamble, B. Ghanti, D. Pradhan, S. Banerjee. Fabrication of a High Proton-Conducting Sulfonated Fe-Metal Organic Framework-Polytriazole Composite Membranes: Study of Proton Exchange Membrane Properties. *Macromol. Rapid Commun.*, **2025**, 2401026. https://doi.org/10.1002/marc.202401026

235. A. Abdolmaleki, M. Zhiani, M. Maleki, S. Borandeh, K. Firouz. Preparation and evaluation of sulfonated polyoxadiazole membrane containing phenol moiety for PEMFC application. *Polymer*, **2015**, *75*, 17. https://doi.org/10.1016/j.polymer.2015.08.021

236. D. Zhao, J. Li, M. K. Song, B. Yi, H. Zhang, M. Liu. A durable alternative for proton-exchange membranes: Sulfonated poly(benzoxazole thioether sulfone)s. *Adv. Energy Mater.*, **2011**, *1*, 203. https://doi.org/10.1002/aenm.201000062

237. Z. Zhang, L. Wu, T. Xu. Synthesis and properties of side-chain-type sulfonated poly (phenylene oxide) for proton exchange membranes. *J. Membr. Sci.*, **2011**, *373*, 160. https://doi.org/10.1016/j.memsci.2011.03.002

238. G. Wang, S. Yang, N. Y. Kang, B. Hua, M. Lu, H. Wei, J. Kang, W. Tang, Y. M. Lee. Sulfonated polybenzothiazoles containing hexafluoroisopropyl units for proton exchange membrane fuel cells. *Macromolecules*, **2023**, *56*, 5546. https://doi.org/10.1021/acs.macromol.3c00301

239. G. Chao, Z. Zhang, Z. Lv, E. Yang, R. Gao, Q. Ju, H. Gao, C. Niu, H. Qian, K. Geng, N. Li. Copolymerized sulfonated poly (oxindole biphenylene) polymer electrolyte for proton exchange membrane fuel cells. *J. Membr. Sci.*, **2024**, *700*, 122674. https://doi.org/10.1016/j.memsci.2024.122674

240. K. F. Tadavani, A. Abdolmaleki, M. R. Molavian, S. Borandeh, E. Sorvand, M. Zhiani. Synergistic behavior of phosphonated and sulfonated groups on proton conductivity and their performance for high-temperature proton exchange membrane fuel cells (PEMFCs). *Energy Fuels*, **2017**, *31*, 11460. https://doi.org/10.1021/acs.energyfuels.7b01065

241. N. Y. Abu-Thabit, S. A. Ali, S. J. Zaidi, K. Mezghani. Novel sulfonated poly (ether ketone)/phosphonated polysulfone polymer blends for proton conducting membranes. *J. Mater. Res.*, **2012**, *27*, 1958. https://doi.org/10.1557/jmr.2012.145

242. B. Xue, S. Zhou, J. Yao, F. Wang, J. Zheng, S. Li, S. Zhang. Novel proton exchange membranes based on sulfonated-phosphonated poly(p-phenylene-co-aryl ether ketone) terpolymers with microblock structures for passive direct methanol fuel cells. *J. Membr. Sci.*, **2020**, *594*, 117466. https://doi.org/10.1016/j.memsci.2019.117466

RESEARCH ARTICLE

# Rational Design of Pt Supported Catalysts for Hydrosilylation: Influence of Support and Calcination Temperature

Kazu Okumura [a]* ![ORCID], Shinsaku Aikawa[a], Yuki Aoki[a], Anas Abdullahi[a], and Mustapha G. Mohammed[b]

[a] *Department of Applied Chemistry, School of Advanced Engineering, Kogakuin University, 2665-1 Nakano-machi Hachioji-city, 192-0015, Tokyo, Japan.*
[b] *Department of Chemical Engineering, Faculty of Engineering, Universiti Malaya, 50603, Kuala Lumpur, Malaysia*
Correspondence: okmr@cc.kogakuin.ac.jp (K. Okumura)

Abstract: The hydrosilylation reaction plays a significant role in organosilicon chemistry, enabling the formation of silicon-carbon bonds crucial for industrial and specialty chemical production. While homogeneous platinum catalysts are incredibly efficient, they come with drawbacks like limited recyclability and high Pt consumption, necessitating researchers to develop more durable, heterogeneous alternatives. By harnessing the synergies of support materials and thermal treatment, this study aims to develop highly active heterogeneous platinum-supported catalysts for the hydrosilylation reaction. We synthesized Pt-supported catalysts on nine different metal oxide supports using impregnation and heat treatment at 500 – 1000 °C. Among them, Pt/CeO_2 900H, prepared by calcining Pt-supported CeO_2 at 900 °C, followed by reducing it with hydrogen at 500 °C, emerged as the most effective catalyst for alkene hydrosilylation, achieving a turnover number (TON) of 6.9×10^6, comparable to the widely used Karstedt catalyst. For alkyne hydrosilylation, Pt/CeO_2 600C and Pt/ZrO_2 500C demonstrated outstanding performance. These catalysts, prepared by calcining Pt-impregnated CeO_2 at 600 °C and ZrO_2 at 500 °C, respectively, exhibited remarkable activity and stability, maintaining high performance over 10 reaction cycles. These findings highlight how the right combination of support material and thermal treatment can fine-tune Pt catalysts for more sustainable hydrosilylation processes. By providing a scalable and cost-effective alternative to traditional homogeneous catalysts, this work connects fundamental research with industrial applications, advancing greener and more efficient approaches to organosilicon synthesis.
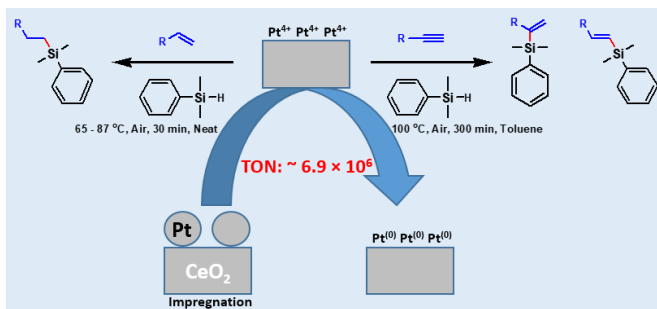
Keywords: *Hydrosilylation, alkene, alkyne, platinum catalyst, cerium oxide*

Introduction

The hydrosilylation reaction, a key hydrometallation process, is pivotal in the silicone industry. This reaction entails the addition of hydrosilane compounds H_nSiR_{4-n}, (where n = 1 or 2, and R = alkyl, aryl, or alkoxy groups) to unsaturated hydrocarbons such as olefins, dienes, and acetylenes, resulting in the formation of alkyl silanes.[1] The origins of modern hydrosilylation chemistry trace back to 1947, when Sommer published his groundbreaking report on the trichlorosilane addition to 1-octene catalyzed by peroxide, established a foundational milestone for subsequent advancements in the field.[2] Since then, hydrosilylation has evolved into a cornerstone of organosilicon chemistry, with its industrial and academic significance driving continuous innovation in catalyst design and reaction optimization. The profound significance of this reaction stems from its ability to efficiently construct silicon-carbon bonds, which are fundamental to the properties of numerous industrial materials.[3]

Beyond its indispensable role in the silicone industry, hydrosilylation finds extensive application in the synthesis of fine chemicals.[4] Its remarkable versatility is highlighted by its ability to proceed efficiently even in the existence of sensitive functional groups like epoxides. This property is valuable in a variety of applications, ranging from the formulation of silicon-containing paints to the precise functionalization of polymers bearing unsaturated bonds. For instance, dimethylpolysiloxane, a ubiquitous silicone rubber, can be tailored through cross-linking with vinyl silicone reagents, demonstrating the reaction's capacity to impart specific properties to polymeric materials.

Transition metals from group 9 and 10, particularly platinum-based catalysts like the Speier catalyst (H_2PtCl_6) and Karstedt catalyst ($O[Si(CH_3)_2CH=CH_2]_2Pt$), are highly effective for hydrosilylation. These homogeneous catalysts achieve remarkable efficiency, often requiring as little as 0.1 mol% Pt. However, their recovery and reuse remain challenging, leading to significant Pt consumption with approximately 5.6 tons of Pt used in the organosilicon industry. This has spurred efforts to develop heterogeneous catalysts that can be recycled to reduce Pt usage. Additionally, research has explored cheaper and more abundant transition metals (Co^5, Fe^6, etc.) based catalysts, though these have yet to find industrial application.[7]

Nevertheless, the unparalleled catalytic activity of platinum-based systems continues to anchor industrial hydrosilylation processes.[8] Among these, Karstedt's catalyst remains the most widely used and versatile, acting as the benchmark for assessing new catalyst. The mechanistic intricacies of hydrosilylation over homogeneous catalysts have been meticulously dissected, revealing two primary pathways: the Chalk-Harrod mechanism and its improved variant. Both pathways initiate with oxidative addition to the metal center. However, they diverge in the subsequent steps. The Chalk-Harrod mechanism posits hydride insertion and subsequent reductive elimination as the rate-determining step, while the modified mechanism favors silyl insertion, followed by isomerization to form Z-alkenyl silanes, thereby mitigating steric repulsion. This modified mechanism better explains the behaviors of Ru, Rh, and Ir catalyzed systems.[9] Despite their undeniable efficacy and mechanistic insights, the drawbacks of homogeneous catalysts, including limited recyclability and sensitivity to reaction conditions, have spurred the development of robust, heterogeneous alternatives.[10]

Recent advancements in heterogeneous catalysis have opened new avenues for addressing these challenges. Supported platinum catalysts, in particular, have emerged as promising alternatives, offering enhanced stability, recyclability, and tunable activity through rational design of the support material and optimization of catalyst preparation parameters.[11] The selection of support materials, ranging

from metal oxides (e.g., Al_2O_3, SiO_2) to carbon-based substrates, is crucial in tailoring the electronic and geometric properties of Pt nanoparticles, directly impacting their catalytic performance.[12] Furthermore, calcination temperature critically influences dispersion, oxidation state, and stability of Pt species, which are essential for maximizing activity and selectivity in hydrosilylation.[13]

The influence of these electronic and geometric properties can be found in literature. For instance, single-site Pt catalysts supported on Al_2O_3 or TiO_2 have demonstrated remarkable activity in hydrosilylation reactions.[14] Beller *et al.* reported that Pt/NR-Al_2O_3-IP, prepared by impregnating alumina nanorods with $H_2PtCl_6 \cdot H_2O$, achieved six reuse cycles and a maximum turnover number (TON) of 300,000 even in the presence of highly reactive functional groups.[15] Similarly, Wang et al. developed a single-site Pt catalyst ($Pt^{\delta+}/TiO_2$) using electrostatic induced ion exchange and a two-dimensional confinement strategy. This catalyst was successfully reused five times, with density functional theory (DFT) calculations attributing its high activity to the atomic dispersion of the active species and the electronic structure of the partially positively charged $Pt^{\delta+}$, which is not present in conventional nanocatalysts.[16]

In another study, Gupton *et al.* utilized solvent-free microwave irradiation of graphene loaded with Pt as a precursor of $PtCl_4^{2-}$ which leads to the reduction of $PtCl_4^-$ and the formation of graphene defects or holes that strongly anchor Pt nanoparticles. The resulting catalyst exhibited turnover frequency (TOF) of 4.8×10^6 h^{-1} and a TON of 9.4×10^6, enabling continuous hydrosilylation in a packed-bed reactor.[17]

In our laboratory, we reported that Pt supported on MgO and heat-treated at high temperature can control Pt dispersion through solid solution formation and re-deposition, suggesting that the behavior of Pt changes with thermal treatment and serves as the foundation for further optimization.[18] Building on these insights, this study explores the hydrosilylation of alkenes and alkynes using Pt catalysts supported on various oxides and subjected to high-temperature treatments. The highly active catalysts are characterized through advanced techniques such as X-ray absorption fine structure (XAFS) spectroscopy, and their reusability is assessed in alkyne hydrosilylation. This work seeks to advance the design of efficient and recoverable heterogeneous catalysts for sustainable hydrosilylation processes.

This study marks a significant advancement toward sustainable and efficient catalytic systems, effectively bridging fundamental research with industrial application. By overcoming the limitations of existing catalysts and presenting a scalable, cost-effective alternative, our approach holds the potential to transform organosilicon compound synthesis, fostering greener and more efficient chemical processes.

The catalysts are designated as Pt/Support xC or Pt/Support xH, where x represents the calcination temperature in degrees Celsius, C and H represent pre- and post-reduction, respectively. For example, platinum supported on Al_2O_3, calcined at 500 °C and reduced is labeled as Pt/Al_2O_3 500H.

Results and Discussion

Reactions using alkenes as substrates

To study the effect of support and thermal treatment temperature on the hydrosilylation reaction using alkenes as the substrates, the reaction was conducted using Pt supported on nine different metal oxides and calcined at different temperatures (500 – 1000 °C). Figure 1(a) and (b) illustrate the relationship between heat treatment temperature

and reaction yield for Pt catalysts supported on different metal oxides, comparing those subjected to heat treatment alone and those further reduced, respectively. Among the pre-reduced catalysts, Pt/ZrO_2 700C exhibited the highest activity. At higher temperatures, Pt/MgO and Pt/CeO_2 also demonstrated significant activity, with the yield of Pt/CeO_2 progressively increasing as the calcination temperature rose.

Notably, catalysts that underwent reduction generally exhibited enhanced activity compared to their heat-treated counterparts, with Pt/CeO_2 900H displaying the highest performance (Figure 1(b)). At lower temperatures, Pt/ZrO_2 500H and Pt/TiO_2 500H also showed considerable activity; however, their performance declined upon heat treatment at higher temperatures. In contrast, catalysts supported on CeO_2 exhibited improved activity with increasing temperature.
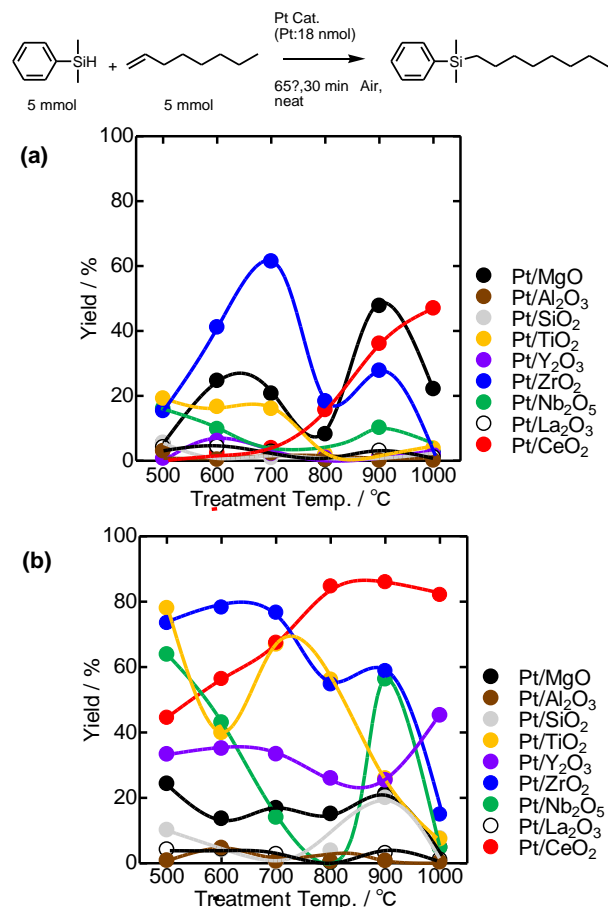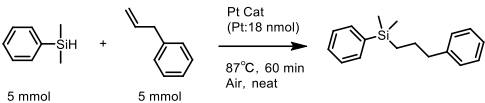

Figure 1. *(a) The relationship between thermal treatment temperature and yield in the reaction of alkenes with catalysts prior to reduction treatment. (b) The relationship between thermal treatment temperature and yield in the reaction of alkenes with catalysts after the reduction treatment with hydrogen.*

Figure S1 (a) shows the change over time of the reaction catalyzed by Pt/CeO_2 900H at 47 and 65 °C. The yield obtained after 2 h at 47 °C was 80%, while the yield obtained after 1 h at 65 °C reached 92%. Next, the reaction was performed at 65 °C using Pt/CeO_2 500H-1000H. The highest activity was obtained with Pt/CeO_2 800H and 900H; the yield reached over 90% in 1 h using these catalysts (Figure S1(b)). These results indicate that the hydrosilylation of dimethylphenylsilane with 1-octene should be performed at 65 °C for 1 h to obtain yields higher than 90% using Pt/CeO_2 800H or 900H catalysts. The catalytic performance of Pt/CeO_2 900H was particularly interesting because the activity of metal-supported catalysts usually decreases with increasing temperature as the particle size increases, which not only reduces the number of accessible atoms for adsorption but also reduces the surface energy of the atoms due to the coordination effects.
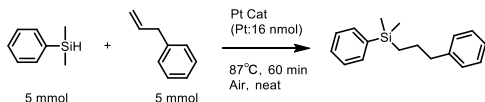
Table 1. *Influence of Pt precursors on the reaction in Pt/CeO₂*

Catalyst	Time (h)	Yield (%)	TON
Ptnp/CeO₂ 900H	1	85	2.4×10^5
Pt(acac)₂/CeO₂ 900H	1	78	2.2×10^5

To assess the impact of the Pt precursor on catalytic activity, Pt(acac)₂/CeO₂ 900H was prepared using Pt(acac)₂ as the precursor and compared with Ptnp/CeO₂ 900H, which was synthesized using a Pt nanoparticle solution (Table 1). Time-course change in the yield over time is shown in Figure S2. When Pt(acac)₂ was used as the precursor, the reaction yield decreased by approximately 8% at 60 min, and the turnover number (TON) declined by about 2×10^4. However, no significant overall changes were observed, suggesting that the choice of Pt precursor had a limited impact on the catalytic performance of Pt/CeO₂.

To investigate the potential role of basic sites on CeO₂ in the catalytic reaction over Pt/CeO₂, catalytic tests were conducted under different gas circulation conditions following heat treatment and reduction. Allylbenzene was used as the alkene substrate, with the results summarized in Table 2. The overall variations in activity were minimal. Notably, the yield remained largely unchanged even after O₂ distribution, indicating that air oxidation of the reduced catalyst had little to no impact on its catalytic performance. These findings suggest that the reaction atmosphere does not significantly influence the reaction.

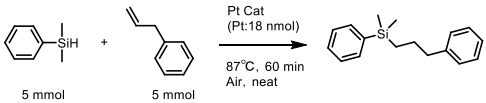**Table 2.** *Effect of gas reaction atmosphere on the reaction for Pt/CeO₂ 900H*

Catalyst	Flow gas	Yield (%)	TON
Pt/CeO₂ 900H	None (air)	87	2.2×10^5
Pt/CeO₂ 900H	N₂	82	2.2×10^5
Pt/CeO₂ 900H	O₂	86	2.4×10^5
Pt/CeO₂ 900H	CO₂	85	2.3×10^5

To investigate the effect of temperature on the reaction during the reduction process following heat treatment, experiments were carried out using Pt/CeO₂ 900H catalysts reduced at varying temperatures. Allylbenzene was used as the alkene substrate, and the results are presented in Table 3. High catalytic activity was observed at reduction temperatures above 200 °C, with no significant change in activity between 200 °C and 700 °C.

However, at 600 °C and 700 °C, a decline in yield was noted after the reaction. Based on these findings, a reduction temperature of 500 °C was selected to maintain consistency across different catalyst supports. To assess the dispersion of Pt in the prepared catalysts, CO chemisorption measurements were performed. Figure 2 illustrates the relationship between heat treatment temperature and dispersion of Pt on the various supports, revealing a bimodal distribution for MgO, Y₂O₃, and La₂O₃, with distinct peaks at

ca. 600 and 900 °C. The dispersion can be correlated with the electronegativity of support cations, as discussed in the reference.[18]
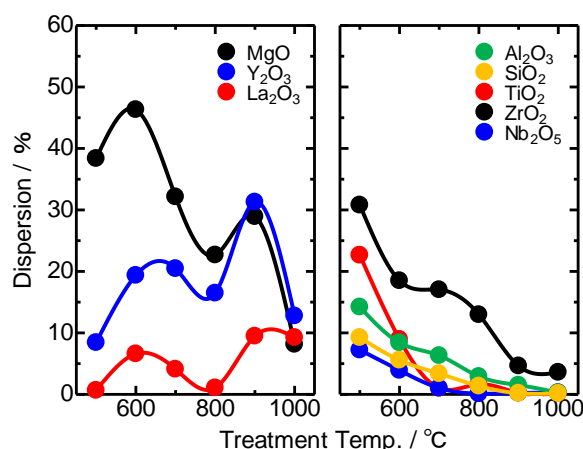
Figure 2. *Relationship between heat treatment temperature and dispersion of Pt on various supports measured with CO adsorption.*

Table 3. *Effect of reduction temperature on reaction for Pt/CeO₂*

Catalyst	Reduction Temp. (°C)	Yield (%)	TON
Pt/CeO₂ 900H	100	22	6.0×10^4
Pt/CeO₂ 900H	200	75	2.1×10^5
Pt/CeO₂ 900H	300	82	2.3×10^5
Pt/CeO₂ 900H	400	81	2.4×10^5
Pt/CeO₂ 900H	500	85	2.2×10^5
Pt/CeO₂ 900H	600	72	2.3×10^5
Pt/CeO₂ 900H	700	79	2.1×10^5

STEM-HAADF imaging and EDS mapping were performed to investigate the dispersion and distribution of Pt in highly active Pt/CeO₂ catalysts. In Pt/CeO₂ 500C (Figure S3), Pt particles were observed in the EDS mapping, whereas no distinct Pt particles were detected in Pt/CeO₂ heat-treated above 600 °C using STEM-HAADF (Figure S4). Figure S5(a) and (b) present the STEM-HAADF images of Pt/CeO₂ 900C and Pt /CeO₂ 900H, respectively, revealing that no Pt particles were observable before reduction treatment (Pt/CeO₂ 900C); however, after reduction treatment (Pt/CeO₂ 900H), finely dispersed Pt particles were deposited as observed in the EDS mapping (Figure S5(c)). These Pt particles are considered to contribute significantly to the high catalytic activity observed in the reaction.

Figure S6 illustrates the relationship between reduction temperature, lattice distortion and crystallite size of Pt/CeO₂ 900H, as determined by temperature-programmed XRD measurements. The analysis was conducted at temperatures of 100, 200, 300, 400, 500, 700, and 900 °C, starting from room temperature and finally cooling back to room temperature. The CeO₂(111) diffraction peak was used to calculate lattice distortion and crystallite size. Lattice distortion increased from room temperature to 300 °C before subsequently decreased, whereas the crystallite size remained relatively unchanged up to 500 °C but exhibited a significant increase at higher temperatures. These findings suggest that up to 300 °C, Pt remains in a solid solution or is surface-dispersed, resulting in a structurally disordered state with high strain. However, at higher temperatures, the structure becomes well-defined, with reduced strain and increased crystallite size, likely due to thermal effect.
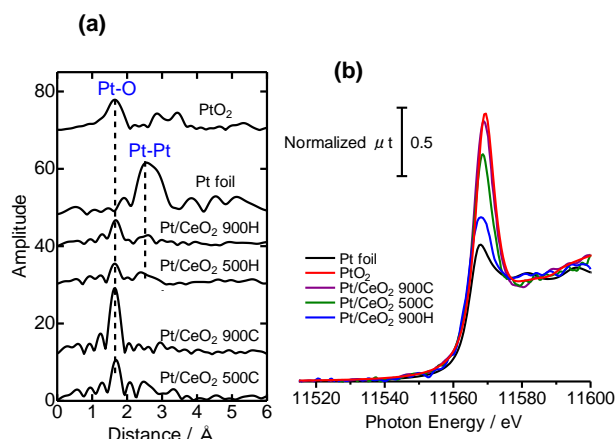
Figure 3. *Pt L₃-edge (a) EXAFS radial distribution function and (b) XANES of Pt/CeO₂.*

Figure 3(a) and (b) presents Pt L₃-edge EXAFS and XANES spectra for Pt/CeO₂ 500C, Pt/CeO₂ 900C, and Pt/CeO₂ 900H, together with reference ones, respectively. In Pt/CeO₂ 900C, the EXAFS spectra in Figure 3(a) are dominated by Pt–O interactions, with almost no Pt–Pt interactions, indicating a high dispersion of Pt in the oxidized state. In contrast, Pt/CeO₂ 500H and Pt/CeO₂ 900H exhibit reduced Pt–O signals compared to their pre-reduction states, along with the appearance of a Pt–Pt peak, confirming the presence of Pt(0) in Pt/CeO₂ 900H. This suggests that Pt, initially well-dispersed during high-temperature heat treatment, precipitates as metallic Pt(0) on the surface following reduction. The formation of Pd(0) in Pt/CeO2 500H and Pt/CeO2 900H is consistent with the reduced white line intensity at 11568 eV in XANES (Figure 3(b)).

Figure 4 illustrates in situ CO adsorption FT-IR spectra of Pt/CeO₂, the plot represents the difference between spectra measured before and after CO adsorption. Peaks at 2070 and 1600 - 1000 cm⁻¹ are attributed to CO adsorption, with the 2070 cm⁻¹ peak specifically assigned to CO adsorbed on Pt(0). The intensity of CO adsorption peaks is relatively low at heat treatment temperatures of 500 to 700 °C but increases significantly at 800 to 1000 °C. These trends correlate with the yield of alkyne hydrosilylation reactions using Pt/CeO₂ after reduction treatment, as shown in Figure 1(b). The increase in the yield in parallel with the higher CO peak intensity at calcination temperatures 800 - 1000 °C suggests that temperatures above 800 °C facilitate the formation of Pt(0) species upon reduction, leading to a higher number of active sites and thereby increasing the reaction yields.

Table 4 and 5 summarizes the results of reactions using various alkenes and hydrosilanes catalyzed by Pt/CeO₂

900H, respectively. Notably, all reactions exhibited TON of 5.3×10⁴ (Table 5, entry 5) or higher, demonstrating the effectiveness of the catalyst across diverse substrates. To further evaluate the catalytic efficiency of Pt/CeO₂ 900H, its performance was compared with that of the industrially used homogeneous Karstedt catalyst. The substrate and reaction conditions are presented in Table 6, where Pt/CeO₂ 900H exhibited high activity almost comparable to the
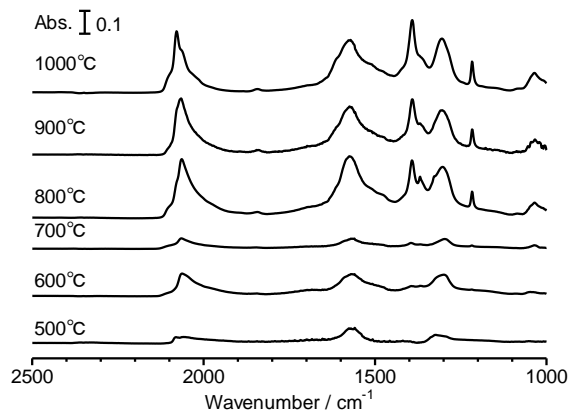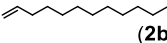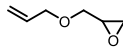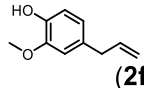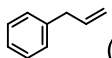

Figure 4. *In situ FT-IR spectra of adsorbed CO on Pt/CeO₂.*

homogeneous system, underscoring its industrial potential. The plausible mechanism for the high activity of Pt/CeO₂ in the reaction using alkenes as substrates is illustrated in Figure 5, inferred from STEM-HAADF and XAFS analyses. The high activity of Pt on CeO₂ is attributed to the dispersion of Pt on the surface during high temperature heat treatment, followed by its dissolution into the substrate. Subsequent hydrogen reduction treatment leads to the re-deposition of Pt as finely dispersed particles on the surface. This reversible redispersion and deposition process likely contributed to the sustained high activity of the Pt/CeO₂ catalyst.

Table 4. *Reaction scope of the Pt/CeO₂ catalyst with various alkenes*

Entry	Substrate	Time (h)	T (°C)	Yield (%)	TON (10⁵)
1	(**2b**)	2	87	92	2.6
2	(**2c**)	2	108	89	2.5
3	(**2d**)	4	87	99	0.64
4	(**2e**)	2	87	84	2.4
5	(**2f**)	4	108	96	0.69
6	(**2g**)	4	87	87	2.4

Okumura *et al.*

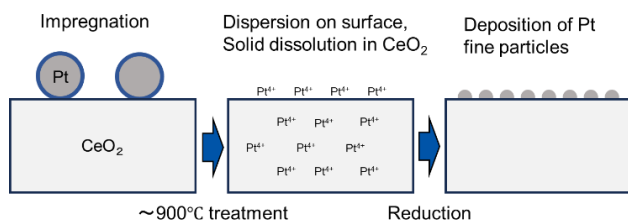*Innov. Chem. Mater. Sustain.* **2025**, 2(1), 074-082

Figure 5. *Proposed mechanism of high activity of Pt/CeO₂ in reactions using alkenes as substrates.*

Table 5. *Reaction scope of the Pt/CeO₂ catalyst with various hydrosilanes*

Entry	Substrate	Time (h)	T (°C)	Yield (%)	TON (10^5)
1	PhMe₂SiH (**1a**)	2	87	97	2.8
2	Me(EtO)₂SiH (**1b**)	2	70	91	2.5
3	HSi(Me)₂OSi(Me)₃ (**1C**)	2	87	90	1.6
4	Si(Me)₃OSiH(Me)₂OSi(Me)₃ (**1d**)	4	87	97	0.66
5	(EtO)₃SiH (**1e**)	4	87	81	0.53

Table 6. *Comparison with industrially used homogeneous Karstedt catalyst.*

Catalyst	Time (h)	Yield (%)	TON
Pt/CeO₂ 900H	2	62	5.2×10^6
Pt/CeO₂ 900H	4	71	6.4×10^6
Pt/CeO₂ 900H	6	77	6.9×10^6
Karstedt Cat.	2	78	7.3×10^6
Karstedt Cat.	4	82	7.7×10^6
Karstedt Cat.	6	85	7.9×10^6

Reactions using alkynes as substrates

Figure 6(a) and (b) illustrate the relationship between heat treatment temperature and reaction yield for Pt catalysts supported on different metal oxides, comparing those subjected to heat treatment alone and those further reduced, respectively. Most Pt-supported oxides exhibited high activity when the catalysts were heat treated at lower temperatures, with a decline in activity observed at higher heat treatment temperatures. However, Pt/CeO₂ catalysts maintained high activity without a significant decrease in yield, even at elevated heat treatment temperatures, particularly in the reactions where the catalyst was reduced with hydrogen prior to the reaction (Figure 6(b)). Since some of the catalysts had yields greater than 90% at 1 h, the catalysts were selected based on yields greater than 40% at 1 h. Figure S7 shows the
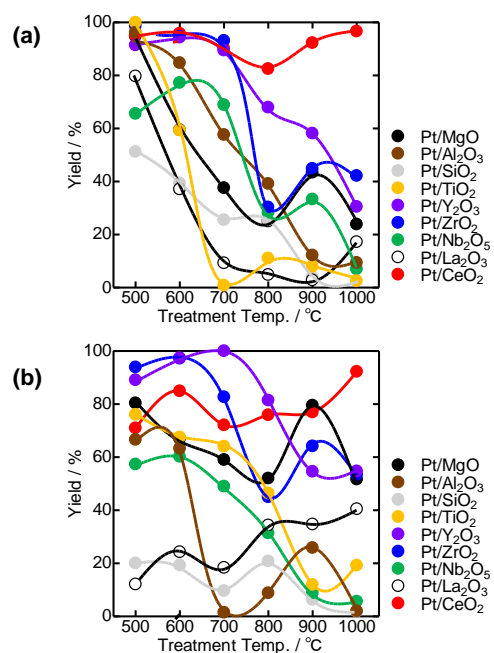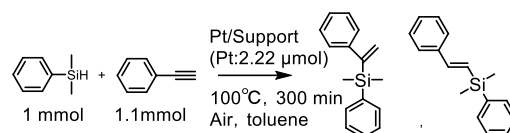

Figure 6. *(a) The relationship between thermal treatment temperature and yield in the reaction of the alkyne (phenylacetylene) with catalysts prior to reduction treatment. (b) The relationship between thermal treatment temperature and yield in the reaction of the alkyne (phenylacetylene) with catalysts after the reduction treatment with hydrogen.*
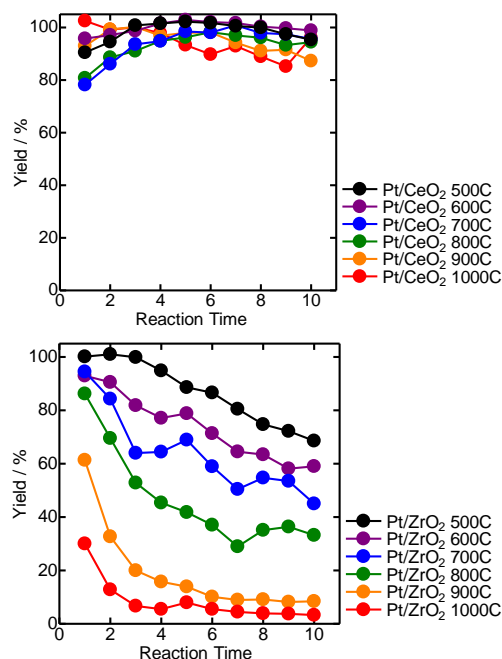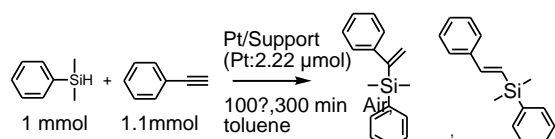

Figure 7. *Catalyst reuse in the hydrosilylation of the alkyne (phenylacetylene) with (a) Pt/CeO₂ and (b) Pt/ZrO₂ heat-treated at Various Temperatures.*

change of yield over time for each catalyst. Among the tested catalysts, Pt/Al₂O₃ 500C, Pt/TiO₂ 500C, Pt/Y₂O₃ 600C, Pt/Y₂O₃ 600H Pt/ZrO₂ 500C, and, Pt/CeO₂ 600C achieved yields above 40%, with Pt/ZrO₂ 500C exhibiting the highest activity.

Figure S8 highlights the recycling performance of highly active catalysts in the hydrosilylation of alkynes. Pt/CeO₂ 600C demonstrated exceptional reusability, whereas Pt/ZrO₂ 500C and Pt/TiO₂ 500C, despite high initial activity, experienced a significant decline in yield after three cycles. The comparative recycling study of Pt/CeO₂ and Pt/ZrO₂ (Figure 7) further confirms that Pt/CeO₂ maintains superior reusability across all heat treatment temperatures. In contrast, the activity and reusability of Pt/ZrO₂ progressively declined with increasing heat treatment temperatures, suggesting that Pt/CeO₂ offers a more robust and durable catalytic system for alkyne hydrosilylation reactions.
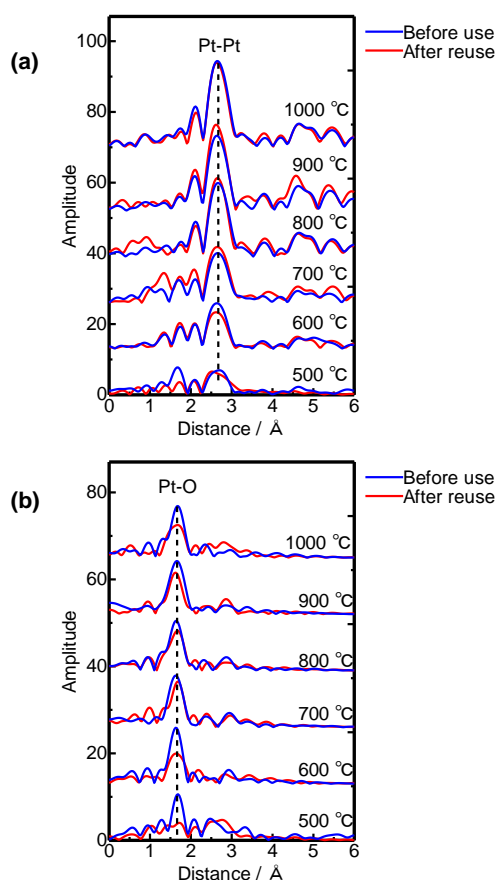

Figure 8. *Pt L₃-edge EXAFS radial distribution function. (a) Pt/ZrO₂ 500-1000C and (b) Pt/CeO₂ 500-1000C before and after the recycling test.*

Since hydrosilylation reactions are usually performed under N₂ atmosphere, catalyst recycling tests were conducted in N₂, and the results are presented in Figure S9. Interestingly, Pt loaded on ZrO₂ and CeO₂ supports exhibited comparable or even higher reusability in air compared to nitrogen. This suggests that the reoxidation of the catalysts by oxygen in air may play a crucial role in maintaining the high activity of the Pt loaded on ZrO₂ and CeO₂ supports. XAFS measurements were conducted on Pt/CeO₂ and Pt/ZrO₂ catalysts after heat treatment and recycling (Figure 8). For Pt/ZrO₂, the Pt-Pt coordination peak was prominent following heat treatment, with its intensity increasing at higher

treatment temperature, indicating progressive Pt agglomeration (Figure 8(a)). In contrast, Pt/CeO₂ exhibited a dominant Pt-O peak even after heat treatment, with no detectable Pt-Pt peak at higher temperatures, indicating that Pt remains well-dispersed on the CeO₂ support under these conditions (Figure 8(b)). Comparing the catalysts before and after recycling, Pt/ZrO₂ showed no change or an increase in the Pt-Pt peak after recycling (except for the 600 °C heat treatment), implying further Pt agglomeration during the reaction. Figure S10 and S11 present Pt-L₃ edge EXAFS radial distribution functions and XANES spectra before and after recycling in air and N₂ atmosphere for highly active catalysts, respectively. A common characteristic of the ZrO₂ and CeO₂ supports that showed relatively high activity is that they have basic character. However, if the basicity is too strong, as in the case of MgO, Pt forms a solid solution with MgO.[18] Similar solid solution formation has been observed in Pt-TiO₂ calcined at 900 and 1000 °C.[19]

The Pt⁴⁺ fraction, derived from XANES analysis (Figure 9), reveals that Pt aggregation occurred to form Pt(0) in all catalysts except Pt/CeO₂ treated at 600 °C. Notably, the Pt/CeO₂ 600C catalyst retained a Pt⁴⁺ content exceeding 70% after recycling, indicating that Pt remains predominantly in a dispersed, oxidized state rather than aggregating into zero-valent Pt particles. This exceptional stability suggests that Pt/CeO₂ 600C maintains its oxidation state and prevents the formation of large Pt clusters, contributing to its sustained catalytic performance.
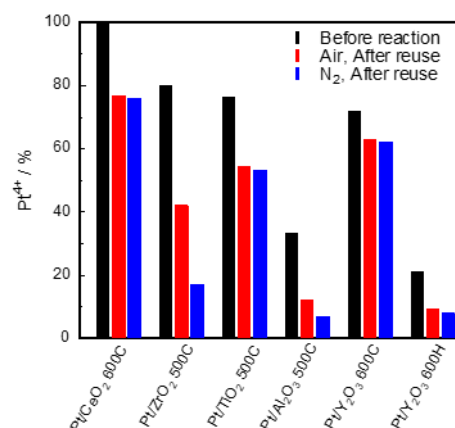

Figure 9. *Pt⁴⁺ fraction determined from Pt-L₃ edge XANES before and after recycling in Air and N₂ atmospheres of active catalysts.*

Figure 10 presents the expanded XRD pattern focusing on the Pt(111) peak for Pt/ZrO₂ and Pt/CeO₂. The unenlarged XRD is given in Figure S12. In the XRD of Pt/ZrO₂, distinct Pt diffraction peaks are observed at heat treatment temperatures ranging from 800 to 1000 °C, indicating Pt agglomeration at these high temperatures. In contrast, Pt/CeO₂ exhibits no detectable Pt peaks across all treatment temperatures, suggesting that Pt remains highly dispersed on the CeO₂ support, even at elevated temperatures. These results further reinforce the contrasting thermal ability of Pt on ZrO₂ and CeO₂. While high-temperature treatment promotes Pt/ZrO₂, leading to loss of active surface area, Pt/CeO₂ effectively prevents agglomeration, maintaining a finely dispersed Pt state. This enhanced dispersion likely contributes to the superior catalytic performance and durability of Pt/CeO₂ in the reaction.

Okumura *et al.*

Innov. Chem. Mater. Sustain. **2025**, 2(1), 074-082

Figure 11(a) illustrates the relationship between the Pt^{4+} fraction (from XANES analysis) and the reaction yield for Pt/CeO_2 catalyst as function of the thermal treatment temperature. The data reveals a similar trend, indicating that the presence of Pt in a higher oxidation state (Pt^{4+}) is associated with enhanced catalytic activity. Figure 11(b) further supports this trend, demonstrating a consistent
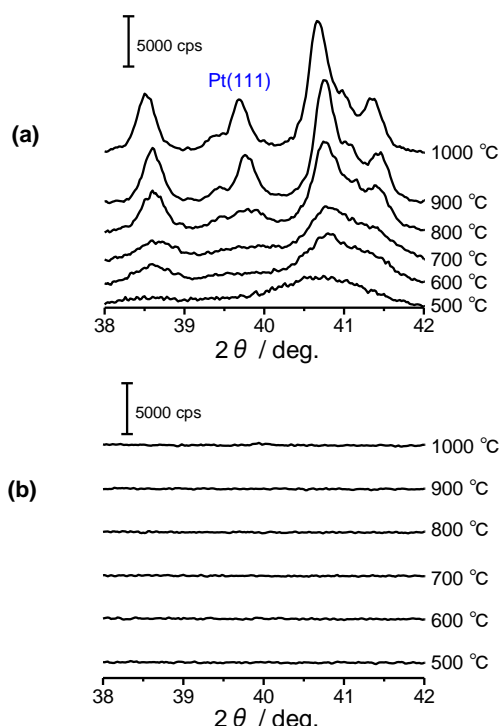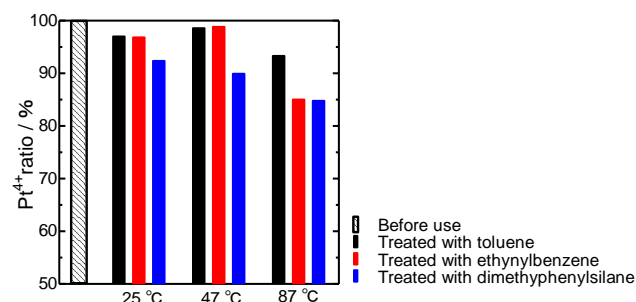

Figure 12. *Pt^{4+} fraction determined from XANES in Pt/CeO_2 600C pretreated with substrate and solvent.*

relationship between the Pt^{4+} fraction and yield for Pt/CeO_2 catalysts. An exception is observed for Pt/CeO_2 500C, where catalytic performance deviates from the expected trend. STEM-HAADF analysis confirms significant Pt agglomeration in this catalyst as displayed in Figure S3, suggesting that the loss of dispersion diminishes the number of accessible active sites, thereby reducing the overall activity. These findings highlight the crucial role of Pt dispersion and oxidation state in maintaining high catalytic efficiency, with Pt/CeO_2 effectively stabilizing Pt^{4+} species and sustaining superior reactivity.

Figure S13(a) and (b) show the N_2 adsorption isotherms of Pt/CeO_2 catalysts and the relationship between the specific surface area and heat treatment temperature for Pt/supports, respectively. As the heat treatment temperature increased, the specific surface area of Pt/CeO_2 decreased, with a notable reduction observed between 600 and 700 °C. This reduction in surface area at higher temperatures may contribute to the observed catalytic behavior of Pt/CeO_2. The superior activity of Pt/CeO_2 treated at 600 °C can be attributed, in part, to the retention of sufficient surface area to maintain a high density of accessible active sites. Above 700 °C, further decreases in surface area likely led to reduced exposure of active Pt species, diminishing catalytic performance. The significant decrease in activity when reusing Pt catalysts with TiO_2, Y_2O_3, Nb_2O_5, and La_2O_3 supports may be due to their low surface area.

To confirm whether Pt^{4+} dispersed on the surface of Pt/CeO_2 600C is reduced by the reactants and solvent (toluene) after heat treatment, XAFS measurements were conducted on Pt/CeO_2 600C pretreated with the reactants, and the Pt^{4+} fraction was determined from XANES analysis. The treatment involved stirring the catalyst at 25, 47 and 87 °C for 3 h at 600 rpm in either 5 mL of toluene solvent or a solution containing 1 mmol of ethynylbenzene and 1 mmol of dimethylphenylsilane in 5 ml of toluene. The results at 87 °C (Figure 12) revealed that Pt^{4+} is reduced to Pt(0) in the presence of the reactants, as evidenced by 8% increase in Pt(0) when dimethylphenylsilane and ethynylbenzene were used compared to toluene alone. This suggests that the reactants actively participate in the reduction of Pt^{4+} to Pt(0) during the reaction.

The H_2-temperature-programmed reduction (H_2-TPR) profile of CeO_2 and Pt/CeO_2 catalysts heat-treated at various temperatures is shown in Figure 13. A progressive decrease in the reduction peak intensity was observed in the H_2-TPR curves of CeO_2 with increasing heat treatment temperature, which may be attributed to sintering of CeO_2. In Pt/CeO_2, it has been reported that the peaks observed up to 350 °C correspond to the reduction of oxygen species adsorbed on the surface, as well as Pt-O-Pt and Pt-O-Ce interactions.[20] For Pt/CeO_2 500C the exposed surface CeO_2 contributes to these reduction peaks. However, in Pt/CeO_2 catalysts heat-treated between 600 and 800 °C, these peaks disappeared, suggesting that the surface CeO_2 becomes covered by dispersed Pt particles, which alters the reduction behavior.

Figure 10. *XRD patterns of (a) Pt/ZrO_2 500-1000C and (b) Pt/CeO_2 500 – 1000C treated at different temperatures.*
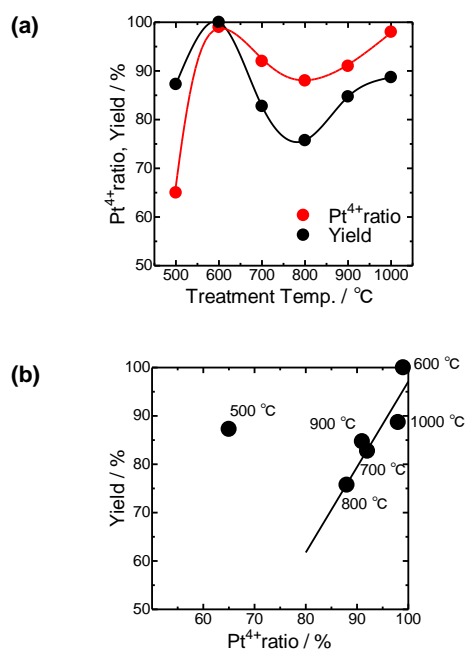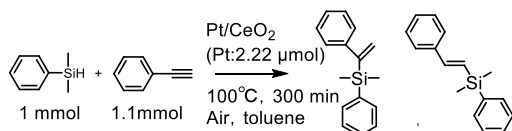

Figure 11. *(a) Dependence of Pt^{4+} fraction and yield on thermal treatment temperature in Pt/CeO_2 500 – 1000C. (b) Correlation between Pt^{4+} fraction and yield of Pt/CeO_2 500 – 1000C.*

This indicates that the dispersion of Pt on the surface plays a critical role in influencing the reducibility and surface properties of Pt/CeO$_2$ catalysts.
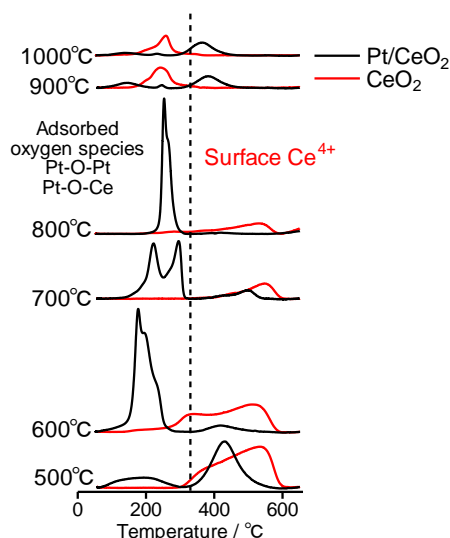

Figure 13. *H$_2$-TPR curves of CeO$_2$ and Pt/CeO$_2$ heat-treated at various temperatures.*

Figure 14 illustrates that Pt/CeO$_2$ 600C exhibited the highest catalytic activity in the alkyne reaction. This high activity is attributed to the Pt^{4+} species dispersed on the surface after heat treatment at 600°C, which are partially reduced to Pt(0) by the substrate, potentially forming high active single-site catalytic centers. This transformation likely enhances catalytic efficiency by facilitating optimal metal-support interactions and electronic modifications, thereby improving the overall reaction performance.
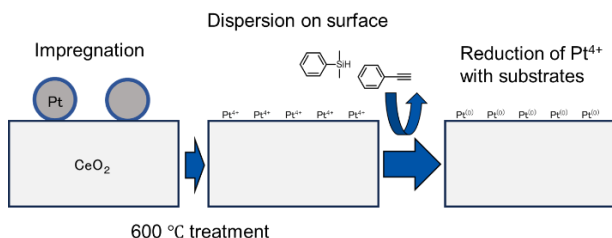

Figure 14. *Proposed mechanism for the formation of high activity of Pt/CeO$_2$ 600C in reaction with alkyne.*

Detailed characterization of all reaction products and the NMR data are given in the Supporting Information.

Conclusion

In this study, we aimed to develop heterogeneous catalysts as viable alternatives to homogeneous systems for the hydrosilylation of alkenes and alkynes. The choice of support and thermal treatment can significantly influence the structure, electronic properties, and catalytic behavior of supported Pt catalysts. To explore these effects, we prepared Pt catalysts on nine distinct metal oxide supports via impregnation and heat treatment, evaluating their performance in alkene and alkyne hydrosilylation. Among the tested catalysts, Pt/CeO$_2$ 900H, prepared by supporting Pt on CeO$_2$, heat-treated at 900 °C, and reduced at 500 °C under a hydrogen stream, demonstrated the highest activity for alkene hydrosilylation. Its performance was comparable to the industrially used Karstedt catalyst, achieving a maximum turnover number (TON) of 6.9 × 10^6. Notably, all catalysts exhibited TONs exceeding 5.3 × 10^4 across various substrates. Characterization of Pt/CeO$_2$ 900H revealed that Pt, initially dispersed or dissolved within the CeO$_2$ matrix during heat treatment, was deposited as Pt nanoparticles

upon reduction, contributing to its exceptional catalytic activity. For alkyne hydrosilylation, Pt/ZrO$_2$ 500C and Pt/CeO$_2$ 600C exhibited high activity and were successfully reused for up to 10 cycles particularly in Pt/CeO$_2$ 600C. A correlation was observed between reaction yield and the proportion of Pt^{4+} species, as determined by Pt L$_3$-edge XANES analysis at different heat treatment temperatures. Post-reaction XAFS measurements indicated that Pt was partially reduced during the reaction, suggesting that single-site Pt(0) species, generated in situ, plays a key role in catalytic activity and reusability. These findings highlight the critical role of support selection and thermal treatment in controlling Pt dispersion and oxidation states, enabling the design of highly active and reusable heterogeneous catalysts for hydrosilylation reactions.

Experimental Section

Catalyst preparation: Pt was loaded on nine metal oxide supports (MgO, Al$_2$O$_3$, SiO$_2$, TiO$_2$, Y$_2$O$_3$, ZrO$_2$, Nb$_2$O$_5$, La$_2$O$_3$, and CeO$_2$) by an impregnation method of Pt nanoparticles solution precursors (Renaissance Energy Research) on the supports. The list of oxides used as Pt support is shown in Table 7. The Pt nanoparticle solution was mixed with 100 mL of solvent (H$_2$O: EtOH = 9: 1) and 2 g of metal oxide support. The Pt loading of was 0.7 wt%. The solvent was then removed using a rotary evaporator. The resulting powder was ground in an agate mortar and heat-treated in air at temperatures ranging from 500 to 1000 °C, with a heating rate of 10 K min^{-1} and a holding time of 3 h. After natural cooling, the heat-treated samples were crushed in an agate mortar. Finally, the catalysts were obtained by reducing the heat-treated powder in a hydrogen gas flow at 500 °C. The prepared catalyst was used for the hydrosilylation reaction in the liquid phase.

Table 7. *List of Oxides used as the support for Pt*

Oxide Support	Sample Name	Source
MgO	500A	Ube Material Industries Co.
Al$_2$O$_3$	JRC-ALO-6	Reference Catalyst, Catalysis Society of Japan
SiO$_2$	CARiACT-Q10	Fuji Silysia Co.
TiO$_2$	P90	Evonik Co.
Y$_2$O$_3$	250-00442	Fujifilm-Wako Pure Chemical Co.
ZrO$_2$	JRC-ZRO-9	Reference Catalyst, Catalysis Society of Japan
Nb$_2$O$_5$	HY-340	CBMM
La$_2$O$_3$	La$_2$O$_3$	Prepared according to the literature[21]
CeO$_2$	JRC-CEO-6	Reference Catalyst, Catalysis Society of Japan

Catalytic reaction and analysis: Alkenes, alkynes, and hydrosilanes were purchased from Tokyo Chemical Industry Co. Hydrosilylation reactions were performed using the prepared catalysts. The reaction mixture, comprising alkene or alkyne, silane, and tridecane as an internal standard, was added to a pressure-resistant tube along with a 4 × 10 mm stirrer. The tube was then heated to a predetermined temperature while stirring at 600 rpm. Product analysis was conducted using GC-FID or ^{1}H NMR. For GC-FID, 2–3 drops of the reaction solution were periodically sampled, diluted with acetone, and analyzed with GC-FID (Shimadzu Co, GC-2025) equipped with a capillary column (GL Science Co, InertCap 1). The yield was calculated by the internal standard method using tridecane as the internal standard. For NMR, the sample was diluted with chloroform-d$_1$, spiked with 3,4,5-trichloropyridine as an internal standard, and analyzed accordingly. ^{1}H (400 MHz) and ^{13}C (100 MHz) NMR spectra were recorded on a JEOL ECZ-500 spectrometer (JEOL) in CDCl$_3$ using tetramethylsilane (TMS) as an internal reference

standard. High resolution mass spectra (HRMS) were obtained with a JEOL JMS-GC MATEII GC-MS system.

For recycle use, the catalyst was recovered by cooling the reaction mixture on ice, centrifuging, and carefully removing the supernatant without disturbing the catalyst. The test tubes containing the catalyst were flushed with N_2 gas and stored. The reaction was then repeated under a continuous N_2 flow at a rate of 10 mL min^{-1}.

Catalyst characterization: X-ray diffraction (XRD) patterns were acquired under ambient conditions using a MiniFlex X-ray diffractometer (Rigaku Co.). The measurements were performed in the 2θ range of 20 to 90° (10 deg. min^{-1}) with Cu Kα radiation. N_2 adsorption/desorption isotherms were measured using a BELSORP mini-X instrument (Microtrac Bel Co.). Prior to analysis, the samples were degassed at 300 °C. XAFS measurements were performed to investigate the local structure of supported Pt species. Measurements were performed at KEK-PF (High Energy Accelerator Research Organization Photon Factory) BL-9A and BL-9C (spectroscopic crystal: Si(111)) with a proposal number: 2024G563 using the fluorescence method. Approximately 50 mg of the sample was formed into 7.0 mm-diameter pellets for measurement. The X-ray fluorescence was detected with a 7-element silicon drift detector at 298 K in a step-scan mode. The data obtained were analyzed using REX2000 (Rigaku Co.). A Talos F200X G2 microscope (Thermo Fisher Scientific Co.) equipped with an EDX analyzer (Super-X) was used to take STEM-HAADF images of the Pt/CeO$_2$ samples, which was operated at 200 kV. *In situ* CO adsorption FT-IR measurements were conducted using a IRSpirit spectrometer (Shimadzu Co.) to investigate the CO adsorption characteristics of the samples. The experimental procedure was as follows: First, the empty cell was evacuated to a vacuum for background measurement. The sample was then introduced into the cell, heated to 400 °C, and subjected to hydrogen reduction at 100 Torr for 10 min. Afterward, the sample was evacuated again and cooled to below 40 °C in a vacuum before the first measurement. Subsequently, 10% CO/He was introduced at 100 Torr for the second measurement. Finally, the cell was evacuated to create a vacuum, and a third measurement was performed. H_2-TPR measurements were conducted to investigate the reduction characteristics of the samples using BELCAT II (Microtrac Bell Inc.). Samples (0.2–0.5 g) were pretreated in an N_2 gas flow for 15 min, followed by heating from 100 °C to 650 °C at 10 K min^{-1} under an 5%-H_2/Ar flow. Following the H_2-TPR analysis, Pt dispersion was evaluated using CO pulse adsorption. The Pt/CO ratio was assumed to be 1 for the dispersion measurement. For this analysis, samples were reduced at 500 °C for 30 min under hydrogen flow as pretreatment.

Supporting Information

Detailed Characterization of all reaction products and the NMR data are given in the Supporting Information.

Author Contribution Declaration

Declare the author contribution in brief here. e.g., 1st, 2nd and 3rd authors design the article, conceived the review/research plan and experimental strategy. 4th author synthesized the molecules, prepared draft manuscript. Last author confirmed the manuscript preparation and assist in daily laboratory supervision, design the research, analyzed the results, wrote manuscript.

Data Availability Declaration

The authors declare that the data supporting the findings are available within the article and its Supplementary Information file.

Notes

The authors declare no competing financial interest.

References

1. B. Marciniec. Catalysis by transition metal complexes of alkene silylation–recent progress mechanistic implications. *Coord. Chem. Rev.*, **2005**, *249*, 2374. https://doi.org/10.1016/j.ccr.2005.02.025
2. L. H. Sommer, E. W. Pietrusza, F. C. Whitmore. Peroxide-Catalyzed Addition of Trichlorosilane to 1-Octene. *J. Am. Chem. Soc.*, **1947**, *69*, 188. https://doi.org/doi:10.1021/ja01193a508
3. Z. T. Ball, 10.17 - C–E Bond Formation through Hydrosilylation of Alkynes and Related Reactions, *Comprehensive Organometallic Chemistry III*, Vol. 10 (Eds.: D. M. P. Mingos, R. H. Crabtree). Elsevier Science, **2007**, 789-813. https://doi.org/10.1016/B0-08-045047-4/00139-4
4. G. Pan, C. Hu, S. Hong, H. Li, D. Yu, C. Cui, Q. Li, N. Liang, Y. Jiang, L. Zheng, L. Jiang. Biomimetic caged platinum catalyst for hydrosilylation reaction with high site selectivity. *Nat. Commun.*, **2021**, *12*, 64. https://doi.org/10.1038/s41467-020-20233-w
5. L. D. de Almeida, H. Wang, K. Junge, X. Cui, M. Beller. Recent Advances in Catalytic Hydrosilylations: Developments beyond Traditional Platinum Catalysts. *Angew. Chem. Int. Ed. Engl.*, **2021**, *60*, 550. https://doi.org/10.1002/anie.202008729
6. K. Kamata, A. Suzuki, Y. Nakai, H. Nakazawa. Catalytic hydrosilylation of alkenes by iron complexes containing terpyridine derivatives as ancillary ligs. *Organometallics*, **2012**, *31*, 3825. https://pubs.acs.org/doi/10.1021/om300279t
7. I. K. Goncharova, R. A. Novikov, I. P. Beletskaya, A. V. Arzumanyan. Recyclable convenient-to-hle Pt/ethylene glycol catalytic system – an approach to sustainable hydrosilylation. *J. Catal.*, **2023**, *418*, 70. https://doi.org/10.1016/j.jcat.2023.01.004
8. T. K. Meister, K. Riener, P. Gigler, J. Stohrer, W. A. Herrmann, F. E. Kühn. Platinum Catalysis Revisited—Unraveling Principles of Catalytic Olefin Hydrosilylation. *ACS Catal.*, **2016**, *6*, 1274. https://doi.org/10.1021/acscatal.5b02624
9. L. W. Chung, Y.-D. Wu, B. M. Trost, Z. T. Ball. A Theoretical Study on the Mechanism, Regiochemistry, and Stereochemistry of Hydrosilylation Catalyzed by Cationic Ruthenium Complexes. *J. Am. Chem. Soc.*, **2003**, *125*, 11578. https://doi.org/10.1021/ja034833
10. J. Heveling. Heterogeneous catalytic chemistry by example of industrial applications. *J. Chem. Edu.*, **2012**, *89*, 1530. https://doi.org/10.1021/ed200816g
11. Y. Watanabe, Catalysis of Pt Clusters on Metal Oxide, in Encyclopedia of Interfacial Chemistry, K. Welt Ed. Oxford: Elsevier, **2018**, 398-405. https://doi.org/10.1016/B978-0-12-409547-2.12983-X
12. T. W. veelen, C. Hernández Mejía, K. P. de Jong. Control of metal-support interactions in heterogeneous catalysts to enhance activity selectivity. *Nat. Catal.*, **2019**, *2*, 955. https://doi.org/10.1038/s41929-019-0364-x
13. Y. Nakajima, S. Shimada. Hydrosilylation reaction of olefins: recent advances perspectives. *RSC Adv.*, **2015**, *5*, 20603. https://doi.org/10.1039/c4ra17281g
14. L. Zhang, M. Zhou, A. Wang, T. Zhang. Selective Hydrogenation over Supported Metal Catalysts: From Nanoparticles to Single Atoms. *Chem. Rev.*, **2020**, *120*, 683. https://doi.org/10.1021/acs.chemrev.9b00230
15. X. Cui, K. Junge, X. Dai, C. Kreyenschulte, M. M. Pohl, S. Wohlrab, F. Shi, A. Bru¨ckner, M. Beller. Synthesis of Single Atom Based Heterogeneous Platinum Catalysts: High Selectivity Activity for Hydrosilylation Reactions. *ACS Cent. Sci.*, **2017**, *3*, 580. https://doi.org/10.1021/acscentsci.7b00105
16. Y. Chen, S. Ji, W. Sun, W. Chen, J. Dong, J. Wen, J. Zhang, Z. Li, L. Zheng, C. Chen, Q. Peng, D. Wang, Y. Li. Discovering Partially Charged Single-Atom Pt for Enhanced Anti-Markovnikov Alkene Hydrosilylation. *J. Am. Chem. Soc.*, **2018**, *140*, 7407. https://doi.org/10.1021/jacs.8b03121
17. C. J. Kong, S. E. Gillil, B. R. Clark, B. F. Gupton. Highly-active, graphene-supported platinum catalyst for the solventless hydrosilylation of olefins. *Chem. Commun.*, **2018**, *54*, 13343. https://doi.org/10.1039/c8cc07641c
18. K. Okumura, H. Hoshi, H. Iiyoshi, H. Takaba. Formation of a Pt-MgO Solid Solution: Analysis by X-ray Absorption Fine Structure Spectroscopy, *ACS Omega*, **2022**, *7*, 27458. https://doi.org/10.1021/acsomega.2c02486
19. M. Hatanaka, N. Takahashi, T. Tanabe, Y. Nagai, Y. Aoki, T. Yoshida H. Shinjoh. Ideal Pt loading for a Pt/CeO$_2$-based catalyst stabilized by a Pt–O–Ce bond. *Appl. Catal. B*, **2010**, *99*, 336. https://doi.org/10.1016/j.apcatb.2010.07.003
20. K. Okumura, R. Chihara, A. Abdullahi, M. Kato. Characterization of the active species in the aerobic oxidation of benzyl alcohol catalyzed by Ru/ZrO$_2$. *Mol. Catal. B*, **2025**, *573*, 114820. https://doi.org/10.1016/j.mcat.2025.114820
21. H. Chuanqing, Y. Yingzhi, Y. Yue, W. Dashan, H. Feiyang, W. Xuewen, Z. Rongbin, F. Gang, Y. Jinmei. Ru/La$_2$O$_3$ catalyst for ammonia decomposition to hydrogen. *Appl. Surf. Sci.*, **2019**, *476*, 928. https://doi.org/10.1016/j.apsusc.2019.01.112

RESEARCH ARTICLE

Effects of Incorporation of Multicomponent Active Agents in Chitosan Biopolymer: A Simple Method for Sustainable Food Packaging

Srasti Yadav[#], Gopal Krishna Mehrotra, and Pradip Kumar Dutta*

Polymer Research Laboratory, Department of Chemistry, Motilal Nehru National Institute of Technology Allahabad, Prayagraj- 211004, India
[#]Present address: Division of Chemistry, School of Basic and Applied Sciences, Galgotias University, Greater Noida-203201, India
*Correspondence: pkd@mnnit.ac.in (P. K. Dutta)

Abstract: Chitosan-gelatin (Ch-ge) based transparent films containing gallic-acid (GA) grafted starch nanoparticles (GA-SNPs) namely, Ch-ge-GA-SNP-1 and Ch-ge-GA-SNP-2 with different amounts of GA-SNPs have been synthesized by solution casting method and characterized. The incorporation of multicomponents showed effective properties of chitosan films. Scanning Electron Microscopy (SEM), XRD and FTIR analysis revealed a homogenous and transparent nature and uniform distribution of the newly synthesized films respectively. The antibacterial activity of the films against both gram-positive and gram-negative bacteria (*B. substilis* and *E. coli*) indicated that Ch-ge-GA-SNP-2 films had pronounced antibacterial activity. The antioxidant activity of Ch-ge-GA-SNP-2 films was determined by DPPH and ABTS methods and results corresponded to 80.9% of DPPH and 84.9% of ABTS free radicals scavenging activities. The results indicated that Ch-ge-GA-SNP-2 films present a definitive advantage in terms of their barrier properties, mechanical strength as well as antibacterial and anti-oxidant activity compared to pristine chitosan-gelatin films.
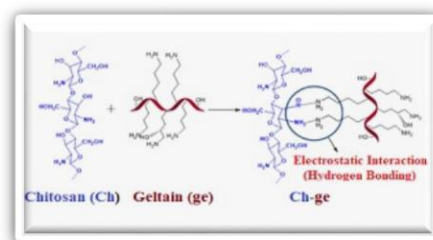
Keywords: *Gallic-acid loaded starch nanoparticles, chitosan-gelatin films, antioxidant activity, antibacterial activity*

1. Introduction

Sustainable bioactive food packaging systems of composite films or membranes and blends synthesized from natural polysaccharides in combination with other functional biomolecules such as proteins and plant extracts have extensively been studied in recent times as viable alternatives to unsustainable synthetic polymers.[1-4] At the forefront of this research, two naturally most abundant biopolymers chitosan, a deacetylated derivative of chitin, and starch-based biocomposite films have been found most promising in terms of their suitability for the intended purpose i.e., food packaging. The important attributes of these bio-based films and blends rely on their ease of access, biocompatibility, and biodegradability apart from exemplary moisture and oxygen barrier and antimicrobial properties which are very vital requirements in food safety and storage.[5-8] A profound challenge in fabricating these films lies in attaining the desired mechanical strength and plasticity which has so far precluded their mass production and use. This problem has, to a greater extent, been addressed by incorporating gelatin, a purified animal protein with exceptional film-forming capacity, into the chitosan and/or starch blends which compensates latter's shortcomings of brittleness, hydrophilicity, and inadequate tensile strength etc..[9-11] Biocomposites of chitosan-gelatin (Ch-ge) with proven antioxidant additives such as gallic-acid (GA, 3,4,5,-trihydroxy benzoic acid) represent a new class of 'green packaging system' having great future development potential.[12-16] The excellent biocompatibility of gelatin molecules results from the presence of biologically important functional groups such as carboxyl, hydroxyl and amino which help it blend with other natural bio-entities as potential film forming material. Films based on chitosan/gelatin have shown improved mechanical and barrier properties against water vapor and UV light[17] and veggies such as red bell pepper

treated with the above edible chitosan/gelatin coatings showed a lowering in microbial decay and longer storability.[18]

Moreno et al. have reported the synthesis of starch/gelatin films in order to promote polymer cross-linking between two bio-macromolecules through interactions between the starch carbonyl and gelatin amino groups which ultimately improved the desired properties (Schematic representation is shown in Supplementary).[19,20]

Conjugates combining chitosan and/or starch and gelatin remain little investigated in terms of the optimum macromolecular ratio of constituting biopolymers which can provide the best synergistic effect in improving these composites' mechanical and barrier properties.[21-24] Saldaña et al. have developed antimicrobial films based on chitosan, starch, and GA using subcritical water technology and evaluated the physicochemical and antimicrobial properties of the films whereas maximum elongation value of 100 percent and a decrease in water vapor permeability has been reported.[25]

It has been shown that nanoparticles of bioactive polysaccharides can be used as potential nanocarriers for the delivery of active ingredients to desired functional tasks.[26,27] Grafting of gallic-acid (GA) onto chitosan is reported to enhance antioxidant activities and favorably alter the rheological properties of the resulting conjugates. Starch nanoparticles (SNPs) score above all other natural alternatives as they can impart crucial physical attributes as inner reinforcement in polymer matrices.[28-30] Owing to the reactive nature of starch, SNP surface can be modified by grafting or cross-linking using potential bioactive compounds (e.g., flavonoids, vitamins, and gallic acid) rendering them more readily dispersible in the polymer matrix for their functional release as antioxidants or scavengers of free radicals.[31-33]

Table 1: *The relative amounts of chitosan, gelatin and GA-SNPs in the resultant films with reaction molar ratio*

S. No.	Samples	Samples Designation	Reaction Ratio	Molar Ratio (Chitosan : Gelatin : GA-SNPs)
1.	Chitosan	Chitosan film	2 g Chitosan	0.124 M
2.	Chitosan: Gelatin	Ch-ge film	2 g Chitosan / 50 mg gelatin	0.124 : 1.67x10^{-6} M
3.	Chitosan: Gelatin: GA-SNPs	Ch-ge-GA-SNP-1	2 g Chitosan / 50 mg gelatin / 30 mg GA-SNPs	0.124 : 1.67x10^{-6} : 0.0176 M
4.	Chitosan: Gelatin: GA-SNPs	Ch-ge-GA-SNP-2	2 g Chitosan / 50 mg gelatin / 50 mg GA-SNPs	0.124 : 1.67x10^{-6} : 0.0294 M

In the above context to fulfil the gap by using the active agents, GA and SNP both on this study motivated us to investigate the effects of incorporation of multicomponent active agents in the form of gallic acid-loaded starch nanoparticles (GA-SNPs) in chitosan-gelatin (Ch-ge) biopolymer films for food packaging applications so that it becomes easy to understand the film qualities such as opacity, crystallinity, tensile strength, solubility, and water vapor permeability. SEM was used to examine the films microstructure. The antimicrobial and antioxidant properties of the synthesized composite films, hereafter named as Ch-ge-GA-SNP-1 and Ch-ge-GA-SNP-2, have also been evaluated.

2. Experimental Section

2.1 Materials

Gallic acid was purchased from CDH, India. Nutrient agar and nutrient broth were obtained from Himedia, Mumbai, India. Chitosan of higher molecular weight (>350 kDa and 79% deacetylated) was taken from CIFT, Cochin (Central Institute of Fisheries Technology). Glacial acetic acid and ethanol were obtained from Merck, India. Tween-80, starch and gelatin were purchased from CDH, India. The test strains *Escherichia coli* (gram -ve) and *Bacillus subtilis* (gram +ve) were purchased from IMTECH, Chandigarh, India. Milli-Q was used as solvent obtained from our laboratory during the research.

2.2 Methods

Preparation of chitosan-gelatin (Ch-ge) based films containing (GA-SNPs) gallic-acid loaded Starch nanoparticles

The modified chitosan-gelatin (Ch-ge) based films containing gallic-acid loaded starch nanoparticles (GA-SNPs) were prepared by solution casting method.[34] Table 1 presents the relative amounts of the chitosan, gelatin, and GA-SNPs in the resultant films with designation. The detailed preparation methods are shown in supplementary.

2.3 Evaluation of chitosan-gelatin-based films in aspects of physicochemical and biological properties

2.3.1 FTIR

FTIR was used to analysis of the structural interactions of chitosan-based films. To obtain the dehydrated chitosan film samples, placed in a desiccator containing silica gel at room temperature for 2 weeks. FTIR spectra were measured in the range of 400-4000 cm^{-1} at a resolution of 8 cm^{-1} using KBr pellets and a Nicolet 170 SXFT-IR spectrophotometer.

2.3.2 XRD

The XRD spectra of the films were analyzed in the range of 5°–80° and 4° min^{-1} on Rigaku Smart lab diffractometer. The film specimens were cut into rectangles and mounted on a slide of glass. Cu-Ka radiation with a nickel monochromator filtering wave at 40 kV and 30 mA has been used to record the spectra.

2.3.3 Scanning Electron Microscope (SEM) Technique

SEM technique used to examine the morphology of the synthesized films on instrument (Carl Zeiss EVO 50, Germany) in Materials Science and Technology Department, IIT Kanpur, Kanpur. Double-sided tape was used to stick the film samples to cylindrical aluminum stubs. The surface morphology of the stub supporting film was investigated with a thin layer of gold in an ion sputter coater and placed into a scanning electron microscope. The other characterization techniques as well as biological evaluation like light transmittance, solubility in water and swelling degree of the films, water vapor permeability (WVP) and mechanical properties, antibacterial activity and antioxidant activity by DPPH and ABTS$^{.+}$ assay methods of chitosan based films are described.

3. Results and Discussion

3.1 FTIR spectra of films

The FTIR spectra of the GA-SNPs (gallic-acid loaded starch nanoparticles), chitosan, Ch-ge, Ch-ge-GA-SNP-1 and Ch-ge-GA-SNP-2 films shown in Fig. 1. From the FTIR spectra the major bands of GA-SNPs at 3296 cm^{-1} of O-H stretching and 2814 cm^{-1} is attributed to the N-H stretching.[35] And the bands at 1634 cm^{-1} is ascribed to C=O stretch of conjugated acid, 1341 cm^{-1} (O-H of the phenol alcohol) and 1006 cm^{-1} (C-O-H bending). The absorption bands around 1400-1650 cm^{-1} relates to the C=C stretching of gallic-acid.[36]

The characteristics peaks of pure chitosan film in the range of 3200-3300 cm^{-1} were ascribed to the O-H stretching related to the intermolecular H-bonding and the peak at 2900 cm^{-1} was attributed to the symmetric and antisymmetric –CH$_2$ stretching. The peaks at 1536 cm^{-1} and 1403 cm^{-1} were attributed to the N-H (amide II), and H-NC=O (amide III) stretching vibrations respectively and also the peaks around 1000-1100 cm^{-1} ascribed to the C-O-C stretching and C-O stretching which is easily view in the Fig. 1 (b).[37,38] In the Fig. 1, the band at 1544 cm^{-1} (amide-II) related to the combination band of the N-H bending vibrations and C–N stretching and band around 2905 cm^{-1} ascribed to the C-H stretching which
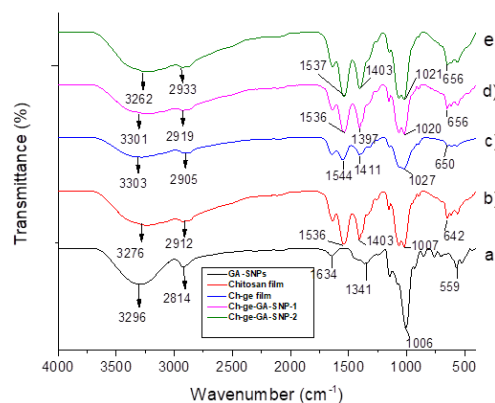

Figure 1: *FTIR spectra for (a) GA-SNPs (b) Chitosan film (c) Ch-ge film (d) Ch-ge-GA-SNP-1 (e) Ch-ge-GA-SNP-2*

Table 2: *Solubility in water, Absorbance and Opacity values of the chitosan based films*

Samples	Absorbance (A_{600})	Opacity (O) = A_{600}/X (X= film thickness in mm)	Solubility in water (%)
Chitosan film	0.059	0.4916 mm^{-1}	31.420 ± 0.437[a]
Ch-ge film	0.070	0.5998 mm^{-1}	30.480 ± 0.266[b]
Ch-ge-GA-SNP-1	0.089	0.7989 mm^{-1}	29.403 ± 0.140[c]
Ch-ge-GA-SNP-2	0.083	0.7255 mm^{-1}	27.320 ± 0.121[d]

a,b,c,d different letters in the same column indicate significant differences among formulations (p < 0.05).

suggested the presence of alkane. The peak around 3000 cm^{-1} was associated to the hydrogen-bonding of OH/NH stretching.[32,39] From FTIR spectra the results obtained of Ch-ge film and earlier reported papers are in good agreement.[40,41]

In the Fig. 1 (d) and (e) the addition of GA-SNPs into Ch-ge film, increased the peak intensity of Ch-ge-GA-SNP-1 and Ch-ge-GA-SNP-2 films which shown in figure. The FTIR spectra display a broad peak at around 3100-3300 cm^{-1} which could be ascribed to -NH$_2$ and -OH stretching. The peaks at 2900-2950 cm^{-1} represented C-H stretching, whereas the band at 1631 cm^{-1} could be attributed to C=O stretching. The peak at 1500-1550 cm^{-1} could be ascribed to NH$_2$ (Amide-II) and at 1400 cm^{-1} signifies C-N stretching and our results of FTIR spectra are in good agreement with the report of.[17] The interactions of gallic acid-starch nanoparticles (GA-SNPs) and gallic acid-starch nanoparticles (GA-SNPs) through Ch-Ge electrostatic interaction is shown in Supplementary which gives the clarity to the role of GA-SNPs in enhancing the film's properties.
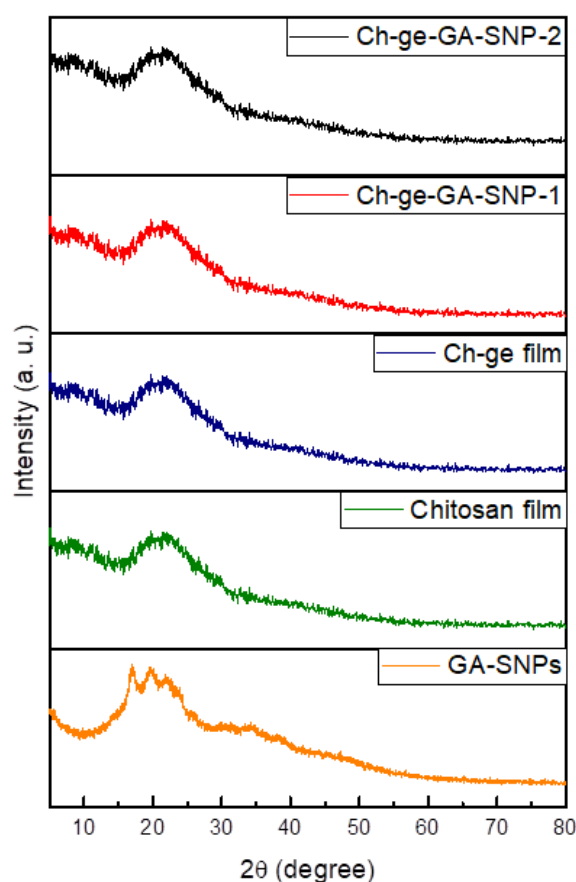

Figure 3: *XRD spectra for (a) GA-SNPs (b) Chitosan film (c) Ch-ge film (d) Ch-ge-GA-SNP-1 (e) Ch-ge-GA-SNP-2*

3.2 XRD

GA-SNPs peaks showed diffraction peaks at (2θ = 15.43°, 16.45°, 25.33°, 27.79° and 32.30°) which is appeared in its X-ray diffraction peaks and also indicates crystalline nature (in the Fig. 2). The crystallinity is the main important factor of the films to design specific application in the field of packaging industries. According to the previous study the XRD spectra of the pure chitosan films showing semi-crystalline state at 2θ =11.9° and 22.95°.[41] According to the literature Ahmed et al., [42], the chitosan and gelatin both biopolymers having lower compatibility i.e. in the blend films, each biopolymer having its own crystal region. But in diffraction pattern of the Ch-ge film, the spectrum of chitosan approximately disappears and become broader, exhibiting that the protein (gelatin) present in Ch-ge decreases the crystallinity of chitosan film. The Ch-ge film ascribed diffraction pattern at (2θ = 7.58° and 20.81°) and the results discussed in a line according to the literature.[40,43] In the XRD pattern of the Ch-ge films containing GA-SNPs the presence of GA-SNPs enhances the crystallinity of Ch-ge film and diffraction pattern at (2θ = 8.88°, 11.7° and 22.56°) which is shown in figure. The results of XRD spectra indicate the semi-crystalline state of Ch-ge-GA-SNP-1 and of Ch-ge-GA-SNP-2 film. These results of films suggested that the compatibility and interaction between different components in the films are good.

3.3 SEM

SEM images of chitosan, Ch-ge, Ch-ge-GA-SNP-1 and Ch-ge-GA-SNP-2 films shows in the Fig 3. The surface morphology of the only chitosan film shows a rough surface and compact texture, which is also explain in reported paper[44] and Ch-ge film shows a smooth and homogeneous surface in comparison of only chitosan film and when the incorporation of GA-SNPs to the Ch-ge film the roughness of films decreases and exhibits a smooth surface texture which is shown in figure. From the SEM analysis it is revealed that the surface of all biopolymer films apparent no presence of pores that might be effect on the WVP and tensile strength values. In general, we can say that the incorporation of GA-SNPs the morphology of the films improved.

3.4 Light transmission and transparency:

The transparency and light transmission of the newly synthesized films are shown in Table 2. Transparent film samples suggest that the films are homogeneous, i.e. there is no phase variation between the various components found in films. Because of light reflection or dispersion at the two-phase interface, if the compatibility between various constituents of the films is poor, the light transmission of the films is lower or the opacity of the films is higher, as reported.[40]

Since prepared chitosan-based films have strong UV barrier properties, chitosan/gelatin-based films containing GA-SNPs effectively blocked UV light, as according to these studies. This is due to the presence of protein (gelatin), which contains a high concentration of aromatic amino acids that absorb UV light and lead to improved UV barrier properties.[45]

3.5 Solubility in water and Swelling degree of the films

The Swelling Property of the films shows the material's hydrophilicity capability in the presence of appropriate water, showing that it is a water-retaining indicator. The swelling degree of the chitosan films largely depends upon the hydrophilic group presence in chitosan and biomacromolecules, in addition to the chemical interaction among the molecules.[46] Pure chitosan films without adding GA-SNPs it was found that highly hydrophilic in nature and more swelled to their original weight, similar results have been reported by Jafari.[47] However, the addition of gelatin and GA-SNPs into the chitosan films was found to extensively increment the film's hydrophobicity character with a significant decrease in the swelling property of the film, and also when increased the concentration of GA-SNPs the swelling property decreased, which is shown in Fig. 5 (A). This may be caused by the interaction between GA-SNPs, gelatin, and chitosan, as
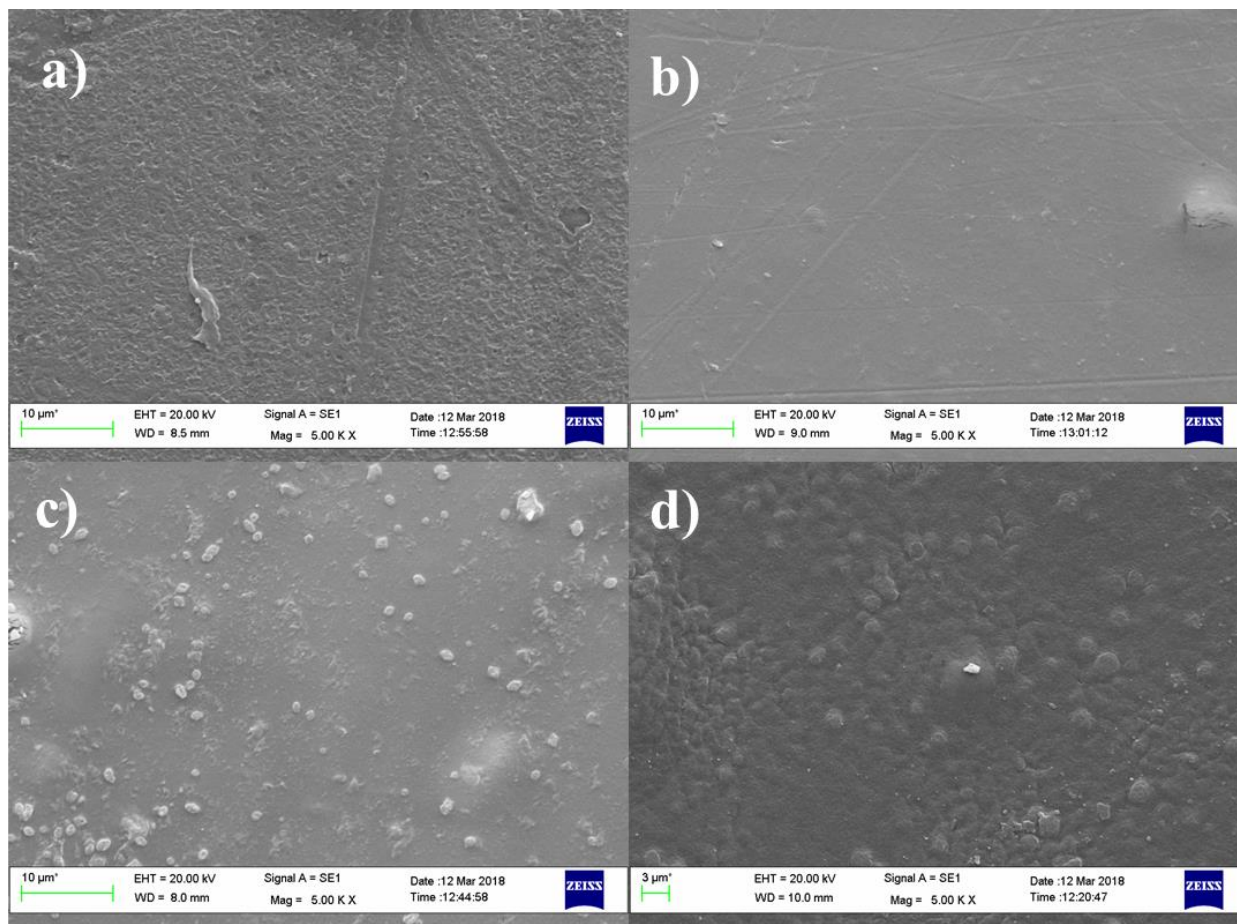

Figure 3: *SEM images for (a) Chitosan film (b) Ch-ge film (c) Ch-ge-GA-SNP-1 (d) Ch-ge-GA-SNP-2*
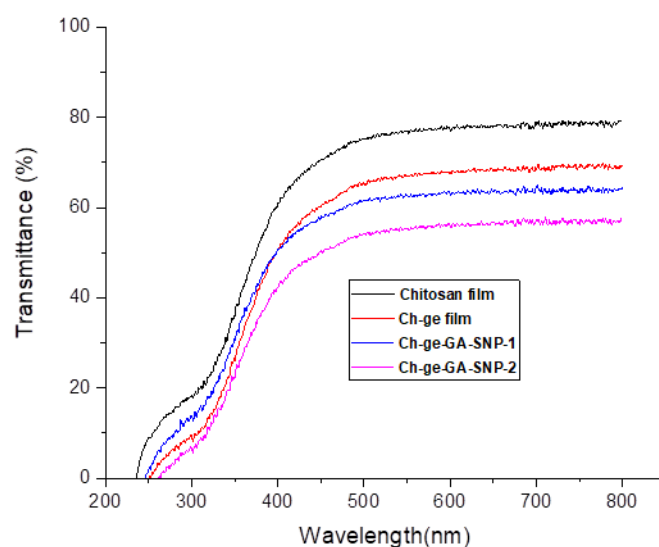

Figure 4: *Transmittance for (a) Chitosan film (b) Ch-ge film (c) Ch-ge-GA-SNP-1 (d) Ch-ge-GA-SNP-2*

Dutta *et al.*

Innov. Chem. Mater. Sustain. **2025**, 2(1), 083-091

well as the strong intermolecular hydrogen bonding interaction, which limited the amount of groups available in the network capable of forming hydrogen bonds with water molecules, decreasing the swelling property.[48] Furthermore, water

gallic-acid which influence the film structure.[54] The concentration of polyphenols and type of chitosan had positive effects on the results of tensile strength; explicitly, when the concentration of polyphenols increased the resulted in tensile

Table 3: *Mechanical Properties and WVP of the chitosan-based films*

Samples	Thickness	Tensile Strength	Elongation at break (EAB) (%)	WVP X 10^{-10} (g m^{-1} s^{-1} Pa^{-1})
Chitosan film	0.121 ± 0.002^a	9.187 ± 0.127^a	28.600 ± 0.304^a	7.290 ± 0.171^a
Ch-ge film	0.113 ± 0.003^b	12.460 ± 0.105^b	21.397 ± 0.468^b	3.164 ± 0.125^b
Ch-ge-GA-SNP-1	0.122 ± 0.002^a	18.343 ± 0.262^c	19.437 ± 0.273^c	2.085 ± 0.109^c
Ch-ge-GA-SNP-2	0.115 ± 0.003^b	23.737 ± 0.231^d	22.453 ± 0.236^d	1.540 ± 0.024^d

a, b, c, d different letters in the same column indicate significant differences among formulations ($p < 0.05$).

solubility was chosen as an indicator for evaluating water resistance and film stability because it reflected resistance to external moisture. At room temperature, the solubility of prepared films in water was examined as a percentage, which was showing in Table 2 and less solubility in water of chitosan films was found with a value of 31.420 ± 0.437 % approx, similar result was also described by Jara and team.[49] However, when gelatin and GA-SNPs were added to the chitosan films, the solubility in water was decreased by 29.403 ± 0.140 % and 27.320 ± 0.121 % of Ch-ge-GA-SNP-1 and Ch-ge-GA-SNP-2 respectively, mainly because gelatin and GA-SNPs also effectively responded to the chitosan matrix, making it very difficult for water molecules to penetrate the matrix and reducing the number of hydrophilic groups. Due to this reason, when increased the concentration of GA-SNPs into Ch-ge film, more hydrophilic groups were reduced and decreased the water solubility of the films. This explanation is supported by the reported paper on olive oil by Akyuz and co-worker.[50]

In conclusion, more hydrophobic molecules in GA-SNPs were found to inhibit with a water attack the destruction of hydrogen bonding between molecules of films, which was useful for waterproofing and producing integrity, and these findings were described in previously published reports.[51,52]

3.6 Mechanical Properties

The mechanical properties of the films indicate the lastingness and also their capability to sustain food integrity during handling, sailing and storage.[53] The mechanical properties of chitosan, Ch-ge and Ch-ge containing GA-SNPs films were measured by Tinius Olsen Testing Machine and summarized in Table 3. In this study, Tensile strength (TS) is defined as the form of maximum stress which is imposed against a film that it can be subjected to before break, while elongation at break (EAB) is a measure of capacity of a film to stress. Wu et al. reported the enhancement in tensile strength of the films were ascribed to compliant physical cross-linking due to the hydrogen bonding between the chitosan chain and

strength values due to this reason the value of the tensile strength of Ch-ge-GA-SNP-2 is more than Ch-ge-GA-SNP-1. The lowest value swelling index of Ch-ge-GA-SNP-2 can be ascribed to the interaction between polyphenols and biopolymers that the inner gaps, decreased the water sorption, this type of interaction can be responsible for the significant enhancement in tensile strength of the films which is reported in the paper and also indicated that different type of cross-linking amid the cassava starch and chitosan, improvement in the tensile strength but decreased EAB, and also a contribution to the decrease of the film solubility in water and WVP.[25]

3.7 WVP

The WVP is an essential factor for food packaging films because its primary purpose is to prevent moisture of transferring from the prepared film to the external environment. In compared with the only chitosan film, the resultant films had lower WVP values. The Table 3 shows the WVP of the resulting films. The WVP values of chitosan films containing GA-SNPs are lower in comparison to chitosan films. As shown in Table 3, the WVP values decrease after the addition of GA-SNPs, and also higher WVP value of Ch-ge-GA-SNP-1 in comparison to the Ch-ge-GA-SNP-2 ranged between 2.085 ± 0.109 X 10^{-10} g m^{-1} s^{-1} Pa^{-1} and 1.540 ± 0.024 X 10^{-10} g m^{-1} s^{-1} Pa^{-1}. Similar results of WVP were reported by working on wheat starch-chitosan edible films[55] and chitosan-tapioca starch.[56] As usual, the chitosan and Ch-ge films both showed the higher the WVP value and the addition of GA-SNPs into the Ch-ge films significantly WVP value reduced. The lowest WVP value for the Ch-ge-GA-SNP-2 film was obtained. However, introducing polyphenols to the synthesized films improved their barrier properties. As previously stated that the presence of polyphenols in biopolymer edible films can form hydrogen bonds and hydrophobic interactions with the polar groups in the biopolymers, restricting the number of free OH groups that can interact with water.[57] The presence of higher concentration values of GA-SNPs into the structural matrix of the Ch-ge film
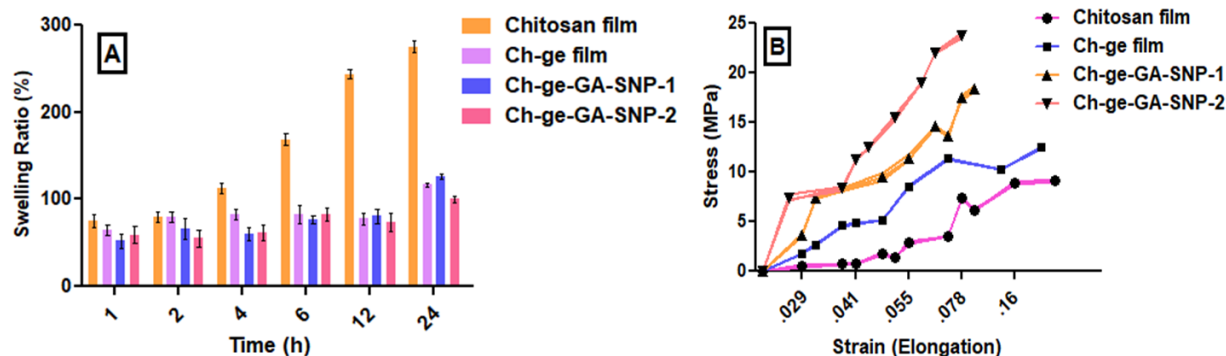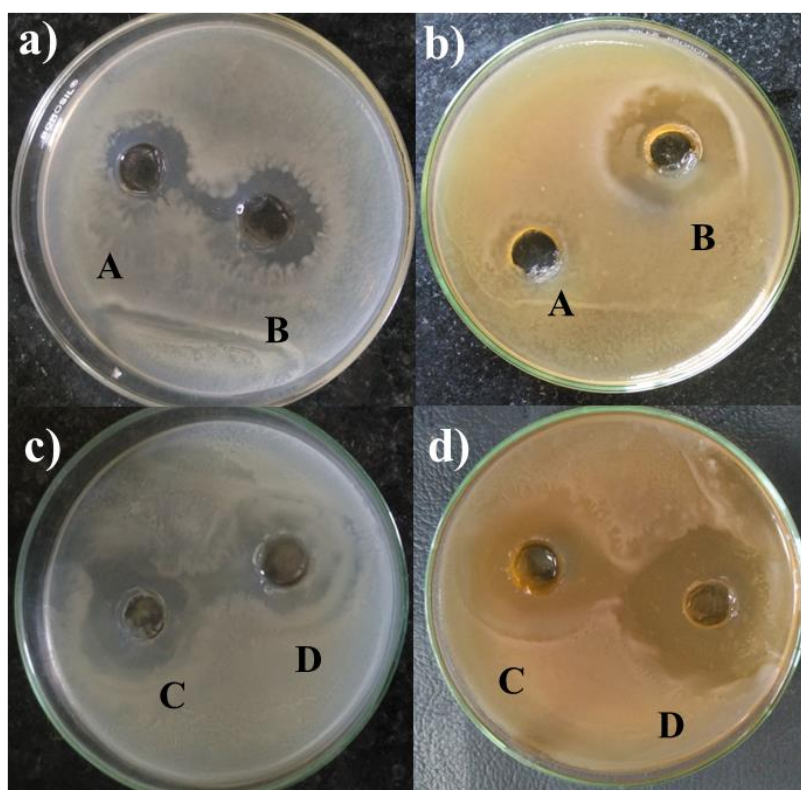

Figure 5: *(A) Swelling property for chitosan based films (B) Stress-strain curve of chitosan based films.*

Table 4: *Table for Inhibition zone of chitosan, Ch-ge Ch-ge-GA-SNP-1 and Ch-ge-GA-SNP-2 films*

Test Cultures	Chitosan film (mm)	Ch-ge film (mm)	Ch-ge-GA-SNP-1 (mm)	Ch-ge-GA-SNP-2 (mm)
Gram Positive *(B. subtilis)*	20±2	22±2	25±2	29±2
Gram Negative *(E. coli)*	22±2	26±2	27±2	32±2

Figure 6: *Inhibition zone of (A) Chitosan film (B) Ch-ge film (C) Ch-ge-GA-SNP-1 (D) Ch-ge-GA-SNP-2 films against (a, c) B. subtilis and (b, d) E. coli*

stimulates internally rearrangement and restricts water permeability; this may be because the form of chitosan and concentration of polyphenols had a reliable impact on the WVP value. Similar results have also been reported by Liu and co-worker.[58] The films with higher concentration values of GA-SNPs have strong mechanical strength and lower water vapor permeability, according to the different studies of the crosslinked films.

3.8 Antibacterial activity

The result of the antibacterial effect of chitosan-based films was evaluated against bacterial strain *B. subtilis* (Gram-positive bacteria) and *E. coli.* (Gram-negative bacteria) using agar well diffusion method and the concentration of films were 20 mg/mL in 1% acetic acid. A significant increment in the zone of inhibition (ZOI) of the synthesized Ch-ge-GA-SNP-1 and Ch-ge-GA-SNP-2 films as compared to that of chitosan and Ch-ge films due to the presence of GA-SNPs. As reported papers related gallic-acid and SNPs to have significant antibacterial properties.[20] In Table 4, the ZOI (mm) of chitosan-based films against bacterial strain are presented (Fig. 6).

3.9 The result of antioxidant property of chitosan, Ch-ge, Ch-ge-GA-SNPs-1 and Ch-ge-GA-SNPs-2 films

Two methods for determining antioxidant activity were used in this study: the DPPH assay and the ABTS assay.

(A). DPPH assay:

The DPPH (2,2-diphenyl-1-picrylhydrazyl) assay was used to analyze the scavenging activities of Ch-ge films and Ch-ge films containing GA-SNPs in our study. The absorbance value at wavelength 517 nm was used to evaluate the reducing potential of all samples. The resultant absorbance value decreases as the sample concentration increases. The % scavenging activity of DPPH radical as seen in Fig. 8(A). At a concentration of 1 mg/mL, the DPPH radical scavenging activity of Ch-ge-GA-SNP-1 and Ch-ge-GA-SNP-2 films are 73.34% and 80.9% respectively.[14] In comparison to chitosan and Ch-ge films, the antioxidant ability of Ch-ge-GA-SNP-1 and Ch-ge-GA-SNP-2 films increased after GA-SNPs were added to the film.

(B) ABTS.+ assay

A blue-green compound of ABTS (2,2'-azino-bis(3-ethylbenzothiazoline-6-sulfonic acid) is used to evaluate antioxidant activity in the food industry. The stabilization of unstable free radicals in the ABTS assay was found to be slightly faster than in the DPPH assay in this report. At a concentration of 1 mg/mL the result of radical scavenging activity of Ch-ge-GA-SNP-1 and Ch-ge-GA-SNP-2 films was estimated to be 79.3% and 84.9% respectively, as shown in Fig. 8(B). The antioxidant activities of Ch-ge-GA-SNP-1 and Ch-ge-GA-SNP-2 films improved after GA-SNPs were added to the film, compared to chitosan and Ch-ge films, indicating that the antioxidant ability of Ch-ge-GA-SNP-2 film was improved. The antioxidant ability of the ABTS assay was
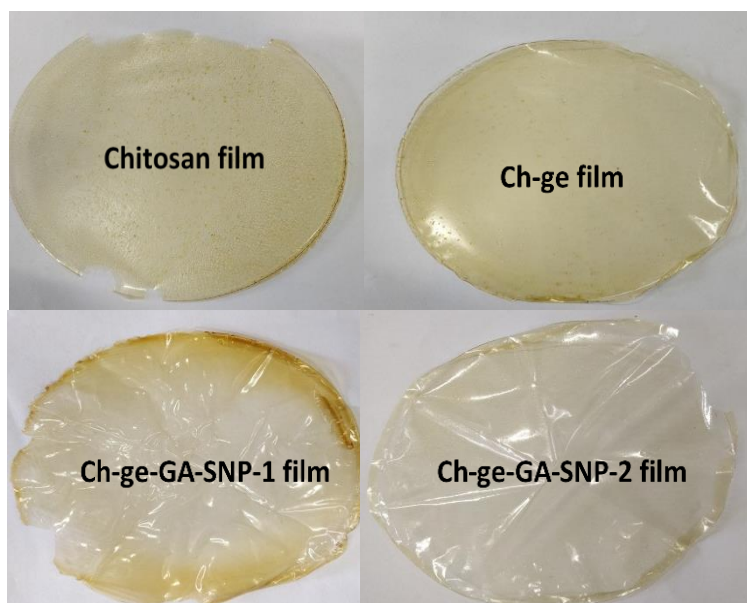
Figure 7: *Photographs of synthesized chitosan films*

shown to be faster than that of the DPPH assay, which can be seen in Table 5.

4. Conclusion

In the present study, gallic-acid grafted starch nanoparticles (GA-SNPs) have been synthesized by a modified facile method. Their effect on the physicochemical and biological properties of chitosan-gelatin (Ch-ge) bioactive film has been studied in the GA-SNPs incorporated nano biocomposite Ch-ge-GA-SNPs films produced by simple solution casting technique. The newly fabricated films have been characterized by UV-vis, XRD, FTIR, and morphology is evaluated by SEM techniques. The results indicate that non-covalent interactions and hydrogen bonding between chitosan-gelatin and GA-SNPs which intensifies with increasing starch nanoparticles' concentration might have contributed in decreased WVP and swelling properties of the films. The Ch-ge-GA-SNP-2 films have also shown considerable enhancement in other properties such as water solubility, transparency, tensile strength, and resistance to UV

absorption as well as antioxidant and antibacterial properties. Although the results are promising, several challenges remain to be addressed in the future. These include determining the optimal amount of nanoparticles to maintain both the strength and bioactivity of the film, understanding the durability and biodegradability of the films under different food storage conditions, and ensuring their compatibility with various types of food. Additionally, large-scale production and obtaining regulatory approval are essential steps for their use in food packaging.

Overall, the incorporation of multicomponent active agents into chitosan biopolymer matrices presents a promising and sustainable alternative to conventional plastic packaging, with significant potential to improve food safety, extend shelf life, and promote environmental sustainability

Author Contribution Declaration

The authors have no conflicts of interest regarding this investigation. Sristi conceptualized the idea of the study, data

Table 5: *Antioxidant activity of chitosan, Ch-ge, Ch-ge-GA-SNP-1 and Ch-ge-GA-SNP-2 films*

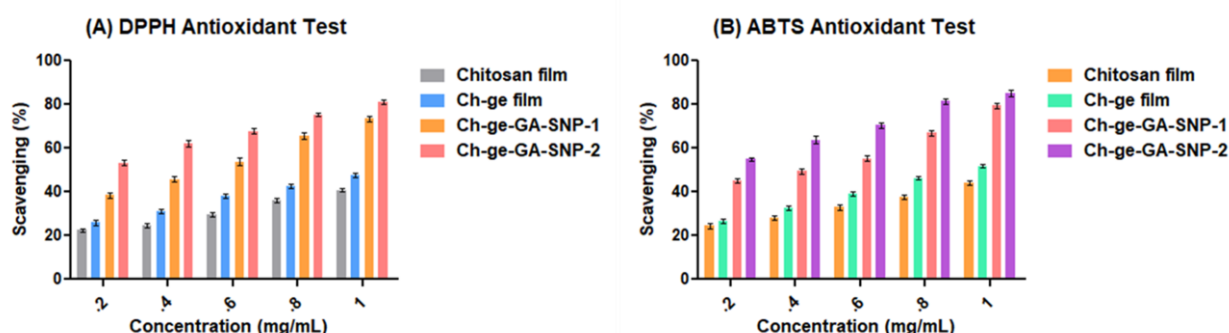| Test Cultures	Chitosan film	Ch-ge film	Ch-ge-GA-SNP-1	Ch-ge-GA-SNP-2
DPPH* scavenging activity (%) (A)	40.6	47.7	74.0	80.9
ABTS*+ scavenging activity (%) (B)	43.9	51.7	79.3	84.9

Figure 8: *(A) DPPH radical scavenging activity of chitosan based films (B) ABTS radical scavenging activity of chitosan based films*

Dutta *et al.*

Innov. Chem. Mater. Sustain. **2025**, *2*(1), 083-091

analysis, manuscript writing and reviewing. Mehrotra confirmed the manuscript writing and reviewing. Dutta involved in data validation and manuscript reviewing and acquired funding.

Attention: The authors have no financial conflicts of interest to disclose.

Funding sources

No funding source.

Data Availability Declaration

The newly generated and analysed data are available within the article and its supporting information.

Supporting Information

The details preparation of chitosan-gelatin (Ch-ge) based films containing (GA-SNPs) gallic-acid loaded starch nanoparticles are given in the supporting information.
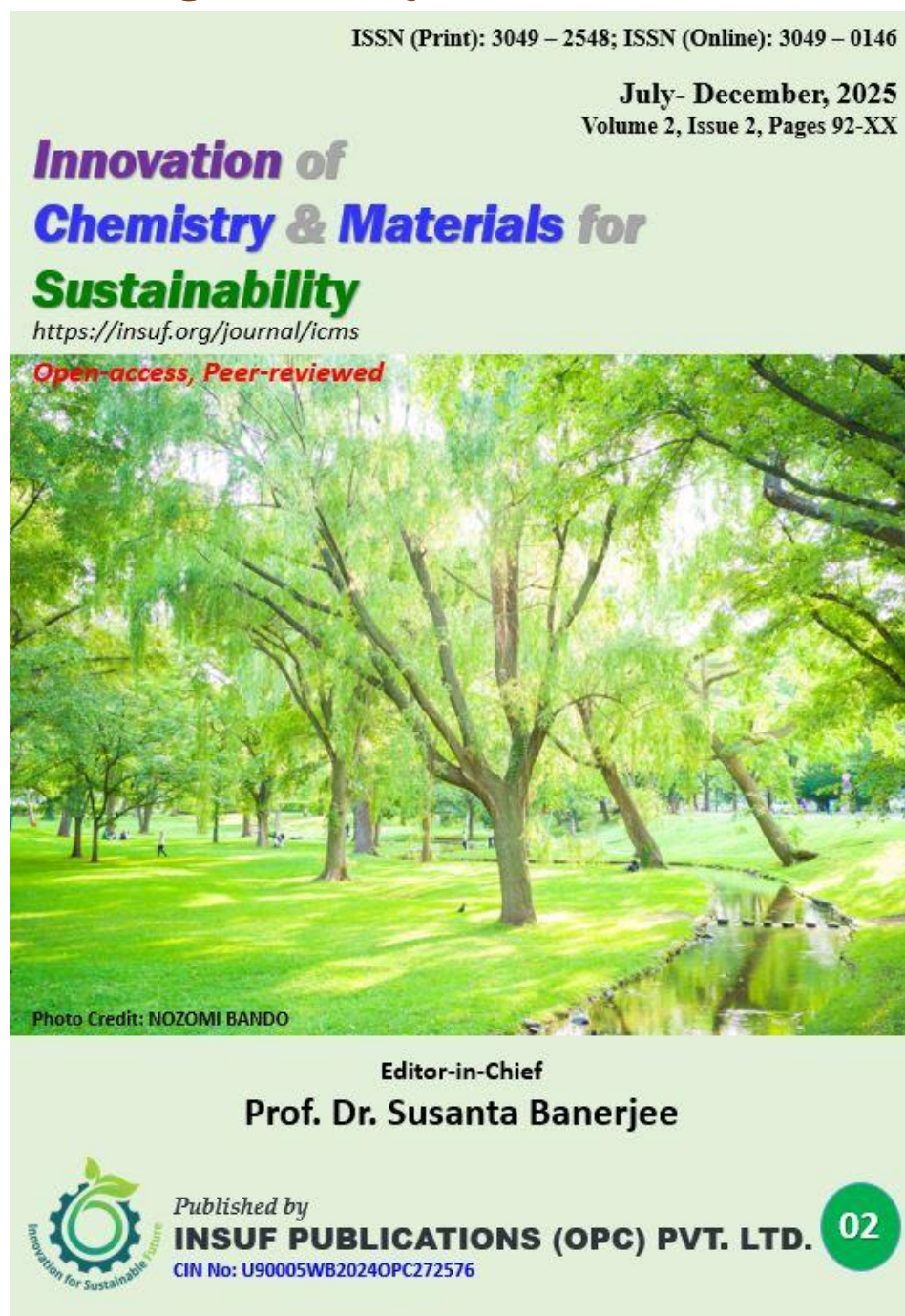
Acknowledgements

References

1. H. Wang, J. Qian, F. Ding. Emerging Chitosan-Based Films for Food Packaging Applications. *J. Agric. Food Chem.*, **2018**, *66*, 395. https://doi.org/10.1021/acs.jafc.7b04528

2. R. Sharma, S. Mahdi, S. Sharma. Antimicrobial bio-nanocomposites and their potential applications in food packaging. *Food Control*, **2020**, *112*, 107086. https://doi.org/10.1016/j.foodcont.2020.107086

3. P. Cazón, G. Velazquez, J. A. Ramírez, M. Vázquez. Polysaccharide-based films and coatings for food packaging: A review. *Food Hydrocoll.*, **2017**, *68*, 136. https://doi.org/10.1016/j.foodhyd.2016.09.009

4. S. Ali, X. Chen, S. Ahmad, W. Shah, M. Shafique, P. Chaubey, G. Mustafa, A. Alrashidi, S. Alharthi. Advancements and challenges in phytochemical-mediated silver nanoparticles for food packaging: Recent review (2021–2023). *Trends Food Sci Technol.*, **2023**, *141*, 104197. https://doi.org/10.1016/j.tifs.2023.104197

5. G. F. Mehyar, A. A. Al Nabulsi, M. Saleh, A. N. Olaimat, R. A. Holley. Effects of chitosan coating containing lysozyme or natamycin on shelf-life, microbial quality, and sensory properties of Halloumi cheese brined in normal and reduced salt solutions. *J. Food Process. Preserv.*, **2018**, *42*,1. https://doi.org/10.1111/jfpp.13324

6. L. A. M. Van Den Broek, R. J. I. Knoop, F. H. J. Kappen, C. G. Boeriu. Chitosan films and blends for packaging material. *Carbohydr. Polym.*, **2015**, *116*, 237. https://doi.org/10.1016/j.carbpol.2014.07.039

7. I. R. S. Vieira, A. P. A. de Carvalho, C.A. Conte-Junior. Recent advances in biobased and biodegradable polymer nanocomposites, nanoparticles, and natural antioxidants for antibacterial and antioxidant food packaging applications. *Compr Rev Food Sci Food Saf.*, **2022**, *21* 3673. https://doi.org/10.1111/1541-4337.12990

8. A. Jiang, R. Patel, B. Padhan, S. Palimkar, P. Galgali, A. Adhikari, I. Varga, M. Patel. Chitosan Based Biodegradable Composite for Antibacterial Food Packaging Application. *Polymers*, **2023**, *15*, 2235. https://doi.org/10.3390/polym15102235

9. X. Yang, Q. Yu, W. Gao, X. Tang, H. Yi, X. Tang. The mechanism of metal-based antibacterial materials and the progress of food packaging applications: A review. *Ceram. Int.*, **2022**, *48*, 34148. https://doi.org/10.1016/j.ceramint.2022.08.249

10. X. Hu, C. Lu, H. Tang, H. Pouri, E. Joulin, J. Zhang. Active Food Packaging Made of Biopolymer-Based Composites. *Materials*, **2023**, *16*, 279. https://doi.org/10.3390/ma16010279

11. M. Wang, Z. Wei, Z. Zhang. Antimicrobial Edible Films for Food Preservation: Recent Advances and Future Trends. *Food Bioprocess Technol*, **2024**, *17*, 1391. https://doi.org/10.1007/s11947-023-03178-y

12. L. Cai, H. Shi, A. Cao, J. Jia. Characterization of gelatin/chitosan polymer films integrated with docosahexaenoic acids fabricated by different methods. *Sci Rep*, **2019**, *9*, 1. https://doi.org/10.1038/s41598-019-44807-x

13. L. Rui, M. Xie, B. Hu, L. Zhou, D. Yin, X. Zeng. A comparative study on chitosan/gelatin composite films with conjugated or incorporated gallic

14. acid. *Carbohydr. Polym.*, **2017**, *173*, 473. https://doi.org/10.1016/j.carbpol.2017.05.072

14. A. G. Sagdicoglu Celep, A. Demirkaya, E. K. Solak. Antioxidant and anticancer activities of gallic acid loaded sodium alginate microspheres on colon cancer. *Curr. Appl. Phys.*, **2022**, *40*, 30. https://doi.org/10.1016/j.cap.2020.06.002

15. I. Zarandona, A. I. Puertas, M. T. Dueñas, P. Guerrero, K. de la Caba. Assessment of active chitosan films incorporated with gallic acid. *Food Hydrocoll.*, **2020**, *101*, 105486. https://doi.org/10.1016/j.foodhyd.2019.105486

16. Y. Zhang, C. Pu, W. Tang, S. Wang, Q. Sun. Gallic acid liposomes decorated with lactoferrin: Characterization, in vitro digestion and antibacterial activity. *Food Chem.*, **2019**, *293*, 315. https://doi.org/10.1016/j.foodchem.2019.04.116

17. S. F. Hosseini, M. Rezaei, M. Zandi, F. Farahmandghavi. Development of bioactive fish gelatin/chitosan nanoparticles composite films with antimicrobial properties. *Food Chem.*, **2016**, *194*, 1266. https://doi.org/10.1016/j.foodchem.2015.09.004

18. E. Poverenov, Y. Zaitsev, H. Arnon, R. Granit, S. Alkalai-Tuvia, Y. Perzelan, T. Weinberg, E. Fallik. Effects of a composite chitosan-gelatin edible coating on postharvest quality and storability of red bell peppers. *Postharvest Biol. Technol.*, **2014**, *96*, 106. https://doi.org/10.1016/j.postharvbio.2014.05.015

19. O. Moreno, J. Cárdenas, L. Atarés, A. Chiralt. Influence of starch oxidation on the functionality of starch-gelatin based active films. *Carbohydr. Polym.*, **2017**, *178*, 147. https://doi.org/10.1016/j.carbpol.2017.08.128

20. R. A. Shapi'i, S. H. Othman, N. Nordin, R. Kadir Basha, M. Nazli Naim. Antimicrobial properties of starch films incorporated with chitosan nanoparticles: In vitro and in vivo evaluation. *Carbohydr. Polym.*, **2020**, *230*, 115602. https://doi.org/10.1016/j.carbpol.2019.115602

21. R. A. Shapi'i, S. H. Othman, M. N. Naim, R. K. Basha. Mechanical properties of tapioca starch-based film incorporated with bulk chitosan and chitosan nanoparticle: A comparative study. *Pertanika J. Sci. & Technol.*, **2019**, *27*, 95.

22. Y. Qin, P. Li. Antimicrobial chitosan conjugates: Current synthetic strategies and potential applications. *Int. J. Mol. Sci.*, **2020**, *21*, 499. https://doi.org/10.3390/ijms21020499

23. D. Merino, A. Y. Mansilla, T. J. Gutiérrez, C. A. Casalongué, V. A. Alvarez. Chitosan coated-phosphorylated starch films: Water interaction, transparency and antibacterial properties. React. *Funct. Polym.*, **2018**, *131*, 445. https://doi.org/10.1016/j.reactfunctpolym.2018.08.012

24. J. F. Mendes, R. T. Paschoalin, V. B. Carmona, A. R. Sena Neto, A. C. P. Marques, J. M. Marconcini, L. H. C. Mattoso, E. S. Medeiros, J. E. Oliveira. Biodegradable polymer blends based on corn starch and thermoplastic chitosan processed by extrusion. *Carbohydr. Polym.*, **2016**, *137*, 452. https://doi.org/10.1016/j.carbpol.2015.10.093

25. Y. Zhao, J. S. Teixeira, M. M. Gänzle, M. D. A. Saldaña. Development of antimicrobial films based on cassava starch, chitosan and gallic acid using subcritical water technology. *J. Supercrit. Fluids*, **2018**, *137*, 101. https://doi.org/10.1016/j.supflu.2018.03.010

26. Y. Qin, L. Xiong, M. Li, J. Liu, H. Wu, H. Qiu, H. Mu, X. Xu, Q. Sun. Preparation of Bioactive Polysaccharide Nanoparticles with Enhanced Radical Scavenging Activity and Antimicrobial Activity. *J. Agric. Food Chem.*, **2018**, *66* 4373. https://doi.org/10.1021/acs.jafc.8b00388

27. J. Liu, H. Yong, Y. Liu, R. Bai. Recent advances in the preparation, structural characteristics, biological properties and applications of gallic acid grafted polysaccharides. *Int. J. Biol. Macromol.*, **2020**, *156*, 1539. https://doi.org/10.1016/j.ijbiomac.2019.11.202

28. B. Duan, P. Sun, X. Wang, C. Yang. Preparation and properties of starch nanocrystals/carboxymethyl chitosan nanocomposite films. *Starch – Stärke*, **2011**, *63*, 528. https://doi.org/10.1002/star.201000136

29. X. Zhang, J. Liu, C. Qian, J. Kan, C. Jin. Effect of grafting method on the physical property and antioxidant potential of chitosan film functionalized with gallic acid. *Food Hydrocoll.*, **2019**, *89*, 1. https://doi.org/10.1016/j.foodhyd.2018.10.023

30. U.G. Spizzirri, F. Iemma, F. Puoci, G. Cirillo, M. Curcio, O.I. Parisi, N. Picci. Synthesis of Antioxidant Polymers by Grafting of Gallic Acid and Catechin on Gelatin. *Biomacromolecules*, **2009**, *10*, 1923. https://doi.org/10.1021/bm900325t

31. Y. Qin, J. Wang, C. Qiu, Y. Hu, X. Xu, Z. Jin. Self-Assembly of Metal-Phenolic Networks as Functional Coatings for Preparation of Antioxidant, Antimicrobial, and pH-Sensitive-Modified Starch Nanoparticles. *ACS Sustain. Chem. Eng.*, **2019**, *7*, 17379. https://doi.org/10.1021/acssuschemeng.9b04332

32. N. Hari, S. Francis, A. G. Rajendran Nair, A. J. Nair. Synthesis, characterization and biological evaluation of chitosan film incorporated with β-Carotene loaded starch nanocrystals. *Food Packag. Shelf Life*, **2018**, *16*, 69. https://doi.org/10.1016/j.fpsl.2018.02.003

33. C. Chi, X. Li, Y. Zhang, L. Chen, L. Li, Z. Wang. Digestibility and supramolecular structural changes of maize starch by non-covalent interactions with gallic acid. *Food Funct.*, **2017**, *8*, 720. https://doi.org/10.1039/c6fo01468b

34. R. Priyadarshi, Y. S. Negi. Effect of Varying Filler Concentration on Zinc Oxide Nanoparticle Embedded Chitosan Films as Potential Food

Packaging Material, *J. Polym. Environ.*, **2016**, *25*, 1087. https://doi.org/10.1007/s10924-016-0890-4

35. A. P. M. Silva, A. V. Oliveira, S. M. A. Pontes, A. L. S. Pereira, M. de sá M. Souza Filho, M. F. Rosa, H. M. C. Azeredo. Mango kernel starch films as affected by starch nanocrystals and cellulose nanocrystals. *Carbohydr. Polym.*, **2019**, *211*, 209. https://doi.org/10.1016/j.carbpol.2019.02.013

36. F. Acevedo, J. Hermosilla, C. Sanhueza, B. Mora-Lagos, I. Fuentes, M. Rubilar, A. Concheiro, C. Alvarez-Lorenzo. Gallic acid loaded PEO-core/zein-shell nanofibers for chemopreventive action on gallbladder cancer cells. *Eur. J. Pharm. Sci.*, **2018**, *119*, 49. https://doi.org/10.1016/j.ejps.2018.04.009

37. H. Chen, X. Hu, E. Chen, S. Wu, D. J. McClements, S. Liu, B. Li, Y. Li. Preparation, characterization, and properties of chitosan films with cinnamaldehyde nanoemulsions, *Food Hydrocoll.*, **2016**, *61*, 662. https://doi.org/10.1016/j.foodhyd.2016.06.034

38. K. Ziani, J. Oses, V. Coma, J. I. Maté. Effect of the presence of glycerol and Tween 20 on the chemical and physical properties of films based on chitosan with different degree of deacetylation. *LWT*, **2008**, *41*, 2159. https://doi.org/10.1016/j.lwt.2007.11.023

39. H. Haghighi, S. Biard, F. Bigi, R. De Leo, E. Bedin, F. Pfeifer, H. W. Siesler, F. Licciardello, A. Pulvirenti. Comprehensive characterization of active chitosan-gelatin blend films enriched with different essential oils. *Food Hydrocoll.*, **2019**, *95*, 33. https://doi.org/10.1016/j.foodhyd.2019.04.019

40. J. T. Martins, M. A. Cerqueira, A. A. Vicente. Influence of α-tocopherol on physicochemical properties of chitosan-based films. *Food Hydrocoll.*, **2012**, *27*, 220. https://doi.org/10.1016/j.foodhyd.2011.06.011

41. M. Pereda, A. G. Ponce, N. E. Marcovich, R. A. Ruseckaite, J. F. Martucci. Chitosan-gelatin composites and bi-layer films with potential antimicrobial activity. *Food Hydrocoll.*, **2011**, *25*, 1372. https://doi.org/10.1016/j.foodhyd.2011.01.001

42. S. Ahmed, S. Ikram. Chitosan and gelatin based biodegradable packaging films with UV-light protection, *J. Photochem. Photobiol. B: Biol.*, **2016**, *163*, 115. https://doi.org/10.1016/j.jphotobiol.2016.08.023

43. C.H. Chen, F. Y. Wang, C. F. Mao, W. T. Liao, C. D. Hsieh. Studies of chitosan: II. Preparation and characterization of chitosan/poly(vinyl alcohol)/gelatin ternary blend films. *Int. J. Biol. Macromol.*, **2008**, *43*, 37. https://doi.org/10.1016/j.ijbiomac.2007.09.005

44. Y. Peng, Y. Li. Combined effects of two kinds of essential oils on physical, mechanical and structural properties of chitosan films. *Food Hydrocoll.*, **2014**, *36*, 287. https://doi.org/10.1016/j.foodhyd.2013.10.013

45. R. J. B. Pinto, S. C. M. Fernandes, C. S. R. Freire, P. Sadocco, J. Causio, C. P. Neto, T. Trindade. Antibacterial activity of optically transparent nanocomposite films based on chitosan or its derivatives and silver nanoparticles. *Carbohydr. Res.*, **2012**, *348*, 77. https://doi.org/10.1016/j.carres.2011.11.009

46. A. Ghosh, M. Azam Ali, R. Walls. Modification of microstructural morphology and physical performance of chitosan films. *Int. J. Biol. Macromol.*, **2010**, *46*, 179. https://doi.org/10.1016/j.ijbiomac.2009.11.006

47. H. Jafari, M. K. Pirouzifard, M. A. Khaledabad, H. Almasi. Effect of chitin nanofiber on the morphological and physical properties of

chitosan/silver nanoparticle bionanocomposite films. *Int. J. Biol. Macromol.*, **2016**, *92*, 461. https://doi.org/10.1016/j.ijbiomac.2016.07.051

48. G. Sun, X. Z. Zhang, C. C. Chu. Formulation and characterization of chitosan-based hydrogel films having both temperature and pH sensitivity. *J. Mater. Sci.: Mater. Med.*, **2007**, *18*, 1563. https://doi.org/10.1007/s10856-007-3030-9

49. A. Homez-Jara, L. D. Daza, D. M. Aguirre, J. A. Muñoz, J. F. Solanilla, H. A. Váquiro. Characterization of chitosan edible films obtained with various polymer concentrations and drying temperatures. *Int. J. Biol. Macromol.*, **2018**, *113*, 1233. https://doi.org/10.1016/j.ijbiomac.2018.03.057

50. L. Akyuz, M. Kaya, S. Ilk, Y. S. Cakmak, A. M. Salaberria, J. Labidi, B. A. Yılmaz, I. Sargin. Effect of different animal fat and plant oil additives on physicochemical, mechanical, antimicrobial and antioxidant properties of chitosan films, *Int. J. Biol. Macromol.*, **2018**, *111*, 475. https://doi.org/10.1016/j.ijbiomac.2018.01.045

51. M. Pérez-Mateos, P. Montero, M.C. Gómez-Guillén. Formulation and stability of biodegradable films made from cod gelatin and sunflower oil blends. *Food Hydrocoll.*, **2009**, *23*, 53. https://doi.org/10.1016/j.foodhyd.2007.11.011

52. S. Sanuja, A. Agalya, M. J. Umapathy. Synthesis and characterization of zinc oxide-neem oil-chitosan bionanocomposite for food packaging application. *Int. J. Biol. Macromol.*, **2015**, *74*, 76. https://doi.org/10.1016/j.ijbiomac.2014.11.036

53. S. Tanpichai, S. Witayakran, J. Wootthikanokkhan, Y. Srimarut, W. Woraprayote, Y. Malila. Mechanical and antibacterial properties of the chitosan coated cellulose paper for packaging applications: Effects of molecular weight types and concentrations of chitosan. *Int. J. Biol. Macromol.*, **2020**, *155*, 1510. https://doi.org/10.1016/j.ijbiomac.2019.11.128

54. C. Wu, J. Tian, S. Li, T. Wu, Y. Hu, S. Chen, T. Sugawara, X. Ye. Structural properties of films and rheology of film-forming solutions of chitosan gallate for food packaging, *Carbohydr. Polym.*, **2016**, *146*, 10. https://doi.org/10.1016/j.carbpol.2016.03.027

55. M.B. Vásconez, S.K. Flores, C.A. Campos, J. Alvarado, L.N. Gerschenson. Antimicrobial activity and physical properties of chitosan-tapioca starch based edible films and coatings. *Food Res Int.*, **2009**, *42*, 762. https://doi.org/10.1016/j.foodres.2009.02.026

56. J. Bonilla, L. Atarés, M. Vargas, A. Chiralt. Properties of wheat starch film-forming dispersions and films as affected by chitosan addition. *J. Food Eng.*, **2013**, *114*, 303. https://doi.org/10.1016/j.jfoodeng.2012.08.005

57. M. J. Fabra, I. Falcó, W. Randazzo, G. Sánchez, A. López-Rubio. Antiviral and antioxidant properties of active alginate edible films containing phenolic extracts. *Food Hydrocoll.*, **2018**, *81*, 96. https://doi.org/10.1016/j.foodhyd.2018.02.026

58. J. Liu, S. Liu, Y. Chen, L. Zhang, J. Kan, C. Jin. Physical, mechanical and antioxidant properties of chitosan films grafted with different hydroxybenzoic acids. *Food Hydrocoll.*, **2017**, *71*, 176. https://doi.org/10.1016/j.foodhyd.2017.05.019

Innovation of **Chemistry & Materials** for **Sustainability**

Cover Page of July-December 2025 issue

Innovation of
Chemistry & Materials for
Sustainability
https://insuf.org/journal/icms
Open-access, Peer-reviewed

Photo Credit: NOZOMI BANDO

Editor-in-Chief
Prof. Dr. Susanta Banerjee

Published by
INSUF PUBLICATIONS (OPC) PVT. LTD. 02
CIN No: U90005WB2024OPC272576

About the Cover page

As the summer sun begins its gentle descent, the cover captures a fleeting, serene moment bathed in soft, golden light. The intensity of the day gives way to a calm hush, where warm rays filter through a canopy of leaves, illuminating their tender green with a quiet brilliance. This tranquil scene mirrors the journal's vision—where innovation in chemistry and sustainable materials meets the elegance and balance of nature. The softened sunlight symbolizes a shift toward gentler, more harmonious technologies, echoing our commitment to a sustainable future inspired by the subtleties of the natural world.

Photo Credit: Nozomi Bando; Location: Hokkaido, Japan

About the Editor-in-Chief

Prof. Dr. Susanta Banerjee has been associated with the Indian Institute of Technology Kharagpur, India, for over 19 years. He previously served as the head of the Materials Science Centre (May 2014 to May 2017) and is currently the Institute Chair Professor and Chairperson of Central Research Facility. Before joining IIT Kharagpur, he served 14 years as Scientist at DRDO and GE India Technology Centre, Bangalore. He is the recipient of the prestigious AvH fellowship from Germany and a fellow of the WAST. Prof. Banerjee has supervised over 30 doctoral and 45 master's theses in polymer and materials science and engineering. He has completed many exciting projects at DRDO, GEITC, and IIT-Kharagpur, driven by his passion for advocating future sustainability. He is the founding Editor-in-Chief of the journal Innovation of Chemistry & Materials for Sustainability.

Innovate Today, Sustain Tomorrow

Compound –Target Network of Caesalpinia bonduc seeds

Articles are open access and can be found at:
https://insuf.org/journal/icms